

https://dspace.org/

The application of the attainable region concept to the oxidative dehyrogenation of N-butanes in inert porous membrane reactors

Milne, Alan David

2009-04-02T13:10:48Z
http://hdl.handle.net/10539/6871

Downloaded from a DSpace repository. https://dspace.org/

THE APPLICATION OF THE ATTAINABLE REGION CONCEPT TO THE OXIDATIVE DEHYDROGENATION OF *N*–BUTANES IN INERT POROUS MEMBRANE REACTORS

ALAN DAVID MILNE

A thesis submitted to the Faculty of Engineering and the Built Environment, University of the Witwatersrand, Johannesburg, in fulfilment of the requirements for the degree of Doctor of Philosophy.

Johannesburg, 2008

I declare that this thesis is my own unaided work. It is being submitted for the Degree of Doctor of Philosophy in the University of the Witwatersrand, Johannesburg. It has not been submitted before for any degree or examination in any other University.

Alan David Milne

23rd day of July 2008

ABSTRACT

The availability of kinetic data for the oxidative dehydrogenation (ODH) of *n*-butane from Téllez *et al*. (1999a and 1999b) and Assabumrungrat *et al*. (2002) presented an opportunity to submit a chemical process of industrial significance to Attainable Region (AR) analysis.

The process thermodynamics for the ODH of *n*-butane and *1*-butene have been reviewed. The addition of oxygen in less than the stoichiometric ratios was found to be essential to prevent deep oxidation of hydrocarbon products {Milne *et al*. (2004 and 2006c)}.

The AR concept has been used to determine the maximum product yields from the ODH of *n*-butane and *1*-butene under two control régimes, one where the partial pressure of oxygen along the length of the reactor was maintained at a constant level and the second where the oxygen partial pressure was allowed to wane. Theoretical maxima under the first régime were associated with very large and impractical residence times.

The Recursive Convex Control policy {Seodigeng (2006)} and the second régime were applied to confirm these maxima {Milne *et al*. (2008)}. Lower and more practical residence times ensued. A differential side-stream reactor was the preferred reactor configuration as was postulated by Feinberg (2000a).

The maximum yield of hydrocarbon product, the associated residence time and the required reactor configuration as functions of oxygen partial pressure were investigated for the series combinations of an inert porous membrane reactor and a fixed-bed reactor. The range of oxygen partial pressures was from 85 kPa to 0.25 kPa. The geometric profile for hydrocarbon reactant and product influences the residence times for the series reactors.

The concept of a residence time ratio is introduced to identify the operating circumstances under which it becomes advantageous to select an inert membrane reactor in preference to a continuously stirred tank reactor and *vice versa* from the perspective of minimising the overall residence time for a reaction {Milne *et al*. (2006b)}.

A two-dimensional graphical analytical technique is advocated to examine and balance the interplay between feed conditions, required product yields and residence times in the design of a reactor {Milne *et al*. (2006a)}..

A simple graphical technique is demonstrated to identify the point in a reaction at which the selectivity of the feed relative to a product is a maximum {Milne *et al*. (2006a)}.

Literature Cited

Assabumrungrat, S. Rienchalanusarn, T. Praserthdam, P. and Goto, S. (2002) Theoretical study of the application of porous membrane reactor to

oxidative dehydrogenation of *n*-butane, *Chemical Engineering Journal*, vol. 85, pp. 69-79.

Feinberg, M. (2000a) Optimal reactor design from a geometric viewpoint – Part II. Critical side stream reactors, *Chemical Engineering Science*, vol. 55, pp. 2455-2479.

Milne, D., Glasser, D., Hildebrandt, D., Hausberger, B., (2004), Application of the Attainable Region Concept to the Oxidative Dehydrogenation of *1*-Butene in Inert Porous Membrane Reactors, *Industrial and. Engineering Chemistry Research*, vol. 43, pp. 1827-1831 with corrections subsequently published in *Industrial and Engineering Chemistry Research*, vol. 43, p. 7208.

Milne, D., Glasser, D., Hildebrandt, D., Hausberger, B., (2006a), Graphical Technique for Assessing a Reactor's Characteristics, *Chemical Engineering Progress,* vol. 102, no. 3, pp. 46-51.

Milne, D., Glasser, D., Hildebrandt, D., Hausberger, B., (2006b), Reactor Selection : Plug Flow or Continuously Stirred Tank?, *Chemical Engineering Progress*. vol. 102, no. 4, pp. 34-37.

Milne, D., Glasser, D., Hildebrandt, D., Hausberger, B., (2006c), The Oxidative Dehydrogenation of *n*-Butane in a Fixed Bed Reactor and in an Inert Porous Membrane Reactor - Maximising the Production of Butenes and Butadiene, *Industrial and Engineering Chemistry Research* vol. 45, pp. 2661-2671.

Milne, D., Seodigeng, T., Glasser, D., Hildebrandt, D., Hausberger, B., (2008), The Application of the Recursive Convex Control (RCC) policy to the Oxidative Dehydrogenation of *n*-Butane and *1*-Butene, *Industrial and Engineering Chemistry Research,* (submitted for publication).

Seodigeng, T.G. (2006), Numerical Formulations for Attainable Region Analysis, Ph.D. thesis, University of the Witwatersrand, Johannesburg, South Africa.

Téllez, C. Menéndez, M. Santamaría, J. (1999a) Kinetic study of the oxidative dehydrogenation of butane on V/MgO catalysts, *Journal of Catalysis*, vol. 183, pp. 210-221.

Téllez, C. Menéndez, M. Santamaría, J. (1999b) Simulation of an inert membrane reactor for the oxidative dehydrogenation of butane, *Chemical Engineering Science*, vol. 54, pp. 2917-2925.

DEDICATION

I dedicate this thesis to four persons. To my wife, Anne, thank you for your support and encouragement during the four years of my research work. To my sons, Richard and Nicholas, whose assistance in easing the transition of their father from the slide rule age to the Matlab age was both invaluable, necessary and deeply appreciated and, finally, to the memory of my late professor of chemical engineering at University College, Dublin, John O'Donnell. John O'Donnell was an inspired teacher who inculcated in me a deep love for my profession and I regard my time as his student in the late 1950s as some of the most stimulating years of my life.

ACKNOWLEDGEMENTS

I should like to express my appreciation to Professor David Glasser, Professor Diane Hildebrandt and Dr. Brendon Hausberger of the Centre for Material Processing and Synthesis at the University of the Witwatersrand for their guidance, helpful suggestions and encouragement during this research.

In particular, I am indebted to the University of the Witwatersrand for its indulging my long-term goal of studying purely for pleasure once I had retired from corporate life and had the time to do so. My sojourn at the Centre for Material Processing and Synthesis as a part-time student has been most stimulating and I regret its coming now to a close.

TABLE OF CONTENTS

DECLARATION 2
ABSTRACT 3
DEDICATION 7
ACKNOWLEDGEMENTS 8
TABLE OF CONTENTS 9
LIST OF FIGURES 17
LIST OF TABLES 28
LIST OF SYMBOLS 31
NOMENCLATURE 33

Chapter 1 : INTRODUCTION 34

1.1 Preamble 34
1.2 Background to the Thesis 35

1.2.1 Process Thermodynamics 36
1.2.2 Attainable Regions 42
1.2.3 Oxidative Dehydrogenation (ODH) 52
1.2.4 Reactor Designs and Structures 60
1.2.5 Reaction Kinetics 67

1.3 Objective of the Thesis 76
1.4 Outline of the Thesis 78
1.5 Numerical and Integration Methods 89
1.6 Literature Cited 90

Chapter 2 : The Application of the Attainable Region Concept to the Oxidative Dehydrogenation of *1*-Butene to Butadiene in Inert Porous Membrane Reactors 103

2.1 Introduction 103
2.2 Background Literature 104
2.3 Results 107

2.3.1 Scenario 1 – Depletion of Oxygen in a FBR. 109
2.3.2 Scenario 2 – Replenishment of Oxygen in an IMR 112
2.3.3 Effect of the Temperature 120

2.4 Conclusions 122
2.5 Nomenclature 123
2.6 Literature Cited 124

Chapter 3 : The Oxidative Dehydrogenation of *n*-Butane in a Fixed Bed Reactor and in an Inert Porous Membrane Reactor - Maximising the Production of Butenes and Butadiene 125

3.1 Abstract 125
3.2 Introduction 126
3.3 Results 129

3.3.1 Scenario 1, Case 1 : Depletion of Oxygen in a FBR – Production of Butenes 130
3.3.2 Scenario 1, Case 2 : Depletion of Oxygen in a FBR – Production of Butadiene 136
3.3.3 Scenario 2, Case 3 : Replenishment of Oxygen in an IMR – Production of Butenes. 140

3.4 Butenes Yields 148

3.4.1 Effect of the Temperature upon the Yield of Butenes 149
3.4.2 Scenario 2, Case 4 : Replenishment of Oxygen in an IMR – Production of Butadiene..... 153
3.4.3 Butadiene Yields 162
3.4.4 Effect of the Temperature upon the Yields of Butadiene .. 163
3.4.5 Scenario 2, Case 5 : Replenishment of Oxygen in an IMR – Production of Butenes and Butadiene. 165
3.4.6 Scenario 3 : Extension of the Attainable Region – Two IMRs in Series. 169

3.5 Conclusions 171
3.6 Nomenclature 172
3.7 Literature Cited 172

Chapter 4 : Graphical Technique for Assessing a Reactor's Characteristics 174

4.1 Abstract 174
4.2 Introduction 175
4.3 Results 176

4.3.1 Step 1. Evaluate the Yield of C as a function of A 177
4.3.2 Step 2. Step off the Various Residence Times 178
4.3.3 Step 3. Repeat Step 1 and Step 2 178

4.4 Interpretation of Graphs 181
4.5 Maximum Selectivity of a Reactant 186
4.6 Conclusions 193
4.7 Nomenclature 194

4.8 Literature Cited. 194

Chapter 5 : Graphical Technique for deciding when to switch from a Plug Flow Reactor to a Continuously Stirred Tank Reactor (and v*ice versa*) to reduce Residence Time. 196

5.1 Abstract 196
5.2 Introduction 197
5.3 Results 198

5.3.1 Step 1. Evaluate the Yield of C as a function of A 198
5.3.2 Step 2. Add the Yields of C for Other Molar Values of A. 199
5.3.3 Step 3. Draw Tangents to the Profiles..... 200
5.3.4 Step 4. Calculate the CSTR Residence Times 201
5.3.5 Step 5. Calculate the PFR Residence Times 202
5.3.6 Step 6. Plot the Residence Times as Functions of Species A and C. 203
5.3.7 Step 7. Plot the Ratio of PFR to CSTR Residence Times as Functions of Species A and C. 203

5.4 Conclusions 211
5.5 Nomenclature 211
5.6 Footnote 212
5.7 Literature Cited 214

Chapter 6 : The Application of the Recursive Convex Control (RCC) policy to the Oxidative Dehydrogenation of *n*-Butane and *1*-Butene 216

6.1 Abstract 217

6.2 Introduction. 218
6.3 Recursive Convex Control Policy Tool 223
6.4 Results 228

6.4.1 Case 1 – ODH of *n*-butane to form butenes. 233
6.4.2 Case 2 – ODH of *n*-butane to form butadiene 240
6.4.3 Case 3 – ODH of *1*-butene to form butadiene 248

6.5 Discussion of Results 253
6.6 Conclusions 255
6.7 List of Symbols 257

6.7.1 Abbreviations 257
6.7.2 Symbols 257

6.8 Literature Cited 258

Chapter 7 : Practical Implementation of Reactors for the Oxidative Dehydrogenation of *n*-Butane to Butadiene 262

7.1 Introduction 262
7.2 Two Reactors in Series 264

7.2.1 Reduction of Oxygen Partial Pressure in Feed to Second Reactor 276

7.3 Three Reactors in Series 278

7.3.1 Reduction of Oxygen Partial Pressure in Feed to Third Reactor 290

7.4 Conclusions 294
7.5 Literature Cited 295

Chapter 8 : Two Reactors in Series – The Effect of Oxygen Partial Pressure and Configuration upon Yield 297

8.1 Introduction 297
8.2 Background Discussion 299

8.2.1 The ODH of *n*-butane to butadiene in an IMR. 301
8.2.2 The ODH of *n*-butane to butadiene in a FBR. 304
8.2.3 The ODH of *n*-butane to butenes in an IMR. 307
8.2.4 The ODH of *n*-butane to butenes in an FBR. 309
8.2.5 The ODH of *1*-butene to butadiene in an IMR. 312
8.2.6 The ODH of *1*-butene to butadiene in a FBR. 314
8.2.7 Conclusions 317

8.3 Results 318

8.3.1 Case 1 - The ODH of *n*-butane to butadiene; an IMR followed by a FBR 319
Conclusions. 333
8.3.2 Case 2 – The ODH of *n*-butane to butadiene; a FBR followed by an IMR 335
Conclusions. 350
8.3.3 Case 3 – The ODH of *n*-butane to butenes; an IMR followed by a FBR 352
Conclusions. 360
8.3.4 Case 4 – The ODH of *n*-butane to butenes; a FBR followed by an IMR 361
Conclusions 374

8.3.5 Case 5 – The ODH of *1*-butene to butadiene; an IMR followed by a FBR 376
Conclusions 383
8.3.6 Case 6 – The ODH of *1*-butene to butadiene; a FBR followed by an IMR 385
Conclusions. 398
8.3.7 Overall Conclusions. 399

Chapter 9 : Conclusions of this Thesis 402

9.1 Yields of Hydrocarbons 402

9.1.1 The ODH of *n*-Butane to Butenes in an IMR. 403
9.1.2 The ODH of *n*-Butane to Butenes in a PFR. 404
9.1.3 The ODH of *1*-Butene to Butadiene in an IMR. 404
9.1.4 The ODH of *1*-Butene to Butadiene in a PFR. 405
9.1.5 The ODH of *n*-Butane to Butadiene in an IMR. 406
9.1.6 The ODH of *n*-Butane to Butadiene in a PFR. 407

9.2 Graphical Technique for Assessing a Reactor's Characteristics 408
9.3 Maximum Selectivity of a Reactant 408
9.4 Residence Time Ratio 409
9.5 Recursive Convex Control Policy 410
9.6 Practical Application of Reactors 411
9.7 Two Reactors in Series 412

Chapter 10 : Recommendations for Future Research 414

10.1 Relevance of Kinetic Expressions 414

10.2 Ratio of Butene Isomers 414
10.3 The Residence Time Ratio and the Levenspiel Concept ... 415
10.4 Application of the Residence Time Ratio to Other Chemical Reactions 415
10.5 The Recursive Convex Control Policy 416
10.6 Graphical Technique for assessing a Reactor's Characteristics 416

REFERENCES 418
PUBLICATIONS 430

LIST OF FIGURES

Figure 1.1. Reaction mechanism for the oxidation of ethane to ethylene and acetaldehyde from Oyama et al. (1990). 72
Figure 1.2. Reaction mechanism for the oxidative dehydrogenation of *n*-butane to butene and butadiene. 79

Figure 2.1. Reaction scheme for the ODH of butene to butadiene. 106
Figure 2.2. FBR Configuration. 109
Figure 2.3. Profiles of butene and butadiene at oxygen partial pressures of 15, 25, 45, 65 and 85 kPa in a FBR. 110
Figure 2.4. Residence times for butadiene at oxygen partial pressures of 15, 25, 45, 65 and 85 kPa in a FBR. 111
Figure 2.5. Residence times for butene at oxygen partial pressures of 15, 25, 45, 65 and 85 kPa in a FBR. 112
Figure 2.6. IMR Configuration. 113
Figure 2.7. Profiles of butene and butadiene at constant oxygen partial pressures from 85 to 0.25 kPa in an IMR. 113
Figure 2.8. Residence times for butadiene at constant oxygen partial pressures from 85 to 0.25 kPa in an IMR. 114
Figure 2.9. Residence times for the ODH of *1*-butene at constant oxygen partial pressures from 85 kPa to 0.25 kPa in an IMR. 115
Figure 2.10. Profile of butene and butadiene at a very low constant oxygen partial pressure and in a very large IMR. 117
Figure 2.11. Butadiene residence times at a very low constant oxygen partial pressure and in a very large IMR. 118
Figure 2.12. Profiles of butene and butadiene at different oxygen partial pressures for an IMR and for a FBR. 119
Figure 2.13. Effect of the temperature upon theoretical maximum yield of butadiene. 121

Figure 3.1. Reaction scheme for the oxidative dehydrogenation of butane to butenes and butadiene. 128
Figure 3.2. FBR Configuration. 130
Figure 3.3. Profiles of butane and butenes at various oxygen partial pressures in a FBR. 131
Figure 3.4. Residence times for butenes at various oxygen partial pressures in a FBR. 133
Figure 3.5. Selectivity of butane to butenes in a FBR as a function of initial oxygen partial pressure for conditions of maximum yield of butenes. 134
Figure 3.6. Profiles of butane and butadiene at various oxygen partial pressures in a FBR. 136
Figure 3.7. Residence times for butadiene at various oxygen partial pressures in a FBR. 138
Figure 3.8. Selectivity of butane to butadiene in a FBR as a function of initial oxygen partial pressure for conditions of maximum yield of butadiene. 139
Figure 3.9. IMR Configuration 140
Figure 3.10. Profiles of butane and butenes at constant oxygen partial pressures from 85 kPa to 0.25 kPa in an IMR. 141
Figure 3.11. Residence times as a function of mass fraction of butenes at constant oxygen partial pressures from 85 kPa to 0.25 kPa in an IMR. 142
Figure 3.12. Residence times for maximum yield of butenes at constant oxygen partial pressures from 95 kPa to 0.25 kPa in an IMR. 143
Figure 3.13. Profile of butenes and butane at a very low oxygen partial pressure and in a very large IMR. 145
Figure 3.14. Residence time as a function of butenes concentrations at a very low oxygen partial pressure and in a very large IMR. . 146
Figure 3.15. Profiles of butane and butenes at different oxygen partial pressures for an IMR and for a FBR. 147

Figure 3.16. Effect of temperature upon theoretical maximum yield of butenes. 150
Figure 3.17. Magnified section of Figure 3.16. 151
Figure 3.18. Profiles of butane and butadiene at constant oxygen partial pressures from 85 kPa to 0.25 kPa in an IMR. 153
Figure 3.19. Residence times for butadiene at constant oxygen partial pressures from 85 kPa to 0.25 kPa in an IMR. 154
Figure 3.20. Residence times for maximum yield of butadiene at constant oxygen partial pressures from 85 kPa to 0.25 kPa in an IMR. 155
Figure 3.21. Selectivity of butane to butadiene in an IMR as a function of oxygen partial pressure for conditions of maximum yield of butadiene. 156
Figure 3.22. Profile of butane and butadiene at a very low oxygen partial pressure and in a very large IMR. 158
Figure 3.23. Residence times for butadiene production at a very low oxygen partial pressure and in a very large IMR. 159
Figure 3.24. Profiles of butane and butadiene at different oxygen partial pressures for an IMR and for a FBR. 160
Figure 3.25. Profile of candidate AR for the system sub-space butane-butadiene. 161
Figure 3.26. Effect of temperature upon theoretical maximum yield of butadiene 163
Figure 3.27. Profiles of butenes, butadiene and butenes plus butadiene against butane at a constant oxygen partial pressure of 85 kPa in an IMR. 165
Figure 3.28. IMR residence times for butenes, butadiene and butenes plus butadiene at a constant oxygen partial pressure of 85 kPa... 166
Figure 3.29. IMR profiles for butenes plus butadiene against butane at constant oxygen partial pressures..... 167
Figure 3.30. IMR residence times butenes plus butadiene at constant oxygen partial pressures. 168

Figure 3.31. IMR Series Configuration. 169
Figure 3.32. Butane-butadiene profiles from two IMRs in series. 170

Figure 4.1. Yield of species C as a function of species A. 177
Figure 4.2. Concentrations of A and C at various values of residence time, τ. 178
Figure 4.3. Concentrations of A and C at various initial molar values of A. 179
Figure 4.4. Reaction scheme for the ODH of *n*-butane to butene and butadiene. 180
Figure 4.5. IMR Configuration. 181
Figure 4.6. Topography of *n*-butane to butadiene at an oxygen partial pressure of 65 kPa (simplified diagram). 182
Figure 4.7. Topography of ODH of *n*-butane to butadiene at an oxygen partial pressure of 65 kPa. 184
Figure 4.8. Topography of *n*-butane to butadiene at an oxygen partial pressure of 65 kPa Tangent AB drawn from the feed point to the concentration profile. 187
Figure 4.9. Yield of butadiene as a function of residence time in an isothermal IMR with an oxygen partial pressure of 65 kPa. 188
Figure 4.10. Geometrical representation of selectivity of *n*-butane to butadiene at the point of maximum yield of butadiene in an isothermal IMR with an oxygen partial pressure of 65 kPa. 189
Figure 4.11. Selectivity of *n*-butane to butadiene as a function of butane concentration in an isothermal IMR with an oxygen partial pressure of 65 kPa. 190
Figure 4.12. Identification of point of maximum butane selectivity to butadiene in an isothermal IMR with an oxygen partial pressure of 65 kPa. 191
Figure 4.13. Identification of residence time necessary for maximum selectivity of butane to butadiene in an isothermal IMR with an oxygen partial pressure of 65 kPa. 192

Figure 5.1. Yield of species C as a function of species A. 199
Figure 5.2. Concentrations of C at various initial values of A. 200
Figure 5.3. Concentration locus for species C and A in a CSTR 201
Figure 5.4. Reaction scheme for the oxidative dehydrogenation of *1*-butene to butadiene. 205
Figure 5.5. IMR Configuration. 205
Figure 5.6. Butene-butadiene profile/locus for an IMR and a CSTR at an constant oxygen partial pressure of 65 kPa. 206
Figure 5.7. CSTR and IMR residence times versus butene concentration for a constant oxygen partial pressure of 65 kPa. 207
Figure 5.8. CSTR and IMR residence times versus mass fraction of butadiene for a constant oxygen partial pressure of 65 kPa. 208
Figure 5.9. Ratio of IMR and CSTR residence times versus butene concentration for a constant oxygen partial pressure of 65 kPa. 209
Figure 5.10. Ratio of IMR and CSTR residence times versus butadiene concentration for a constant oxygen partial pressure of 65 kPa. 210

Figure 6.1. Reaction scheme for the oxidative dehydrogenation (ODH) of *n*-butane and *1*-butene to butadiene including side reactions. 219
Figure 6.2. Conceptualised reactor structure for combination of reaction and mixing with fresh feed..... 230
Figure 6.3. Conceptualised reactor structure for combination of reaction and mixing with oxygen. 231
Figure 6.4. Projection of the set of extreme points derived from the RCC profile for the ODH of *n*-butane to butenes (sum of all three isomers) plotted in mass fraction space. 233
Figure 6.5. RCC profile of residence times and concentrations of butenes from the ODH of *n*-butane. 235

Figure 6.6. RCC operational oxygen control policy for the maximum yield of butenes from the ODH of *n*-butane.....236
Figure 6.7. RCC oxygen control policy as a function of residence time for the maximum yield of butenes from the ODH of *n*-butane. 237
Figure 6.8. Enlarged section of Figure 6.7 - RCC oxygen control policy as a function of residence time for the maximum yield of butenes from the ODH of *n*-butane 238
Figure 6.9. Set of extreme points derived from the RCC profile for the ODH of *n*-butane to butadiene in mass fraction space.....240
Figure 6.10. RCC profile of residence times and concentrations of butadiene from the ODH of *n*-butane 241
Figure 6.11. RCC operational control policy for the maximum yield of butadiene from the ODH of *n*-butane 243
Figure 6.12. RCC oxygen control policy as a function of residence time for the maximum yield of butadiene from the ODH of *n*-butane. 244
Figure 6.13. Enlarged section of Figure 6.12 - RCC oxygen control policy as a function of residence time for the maximum yield of butadiene from the ODH of *n*-butane 246
Figure 6.14. Set of extreme points derived from the RCC profile for the ODH of *1*-butene to butadiene. 248
Figure 6.15. RCC profile of residence times and concentrations of butadiene from the ODH of *1*-butene 249
Figure 6.16. RCC operational control policy for the maximum yield of butadiene from the ODH of *1*-butene 250
Figure 6.17. RCC oxygen control policy as a function of residence time for the maximum yield of butadiene from the ODH of *1*-butene. 251
Figure 6.18. Enlarged section of Figure 6.17 - RCC oxygen control policy as a function of residence time for the maximum yield of butadiene from the ODH of *1*-butene 252

Figure 6.19. Initial rate of reaction maxima for production of butenes and butadiene as a function of oxygen partial pressure at feed conditions. 254

Figure 7.1. Reaction mechanism for the oxidative dehydrogenation of *n*-butane to butene and butadiene. 263
Figure 7.2. Profiles of butane and butadiene at oxygen partial pressures of 15, 25, 45, 65, 70 and 85 kPa in an isothermal PFR with depleting oxygen. 265
Figure 7.3. Profiles of butane and butadiene at constant oxygen partial pressures from 85 kPa to 0.25 kPa in an isothermal IMR with constant oxygen partial pressure. 267
Figure 7.4. Butane:butadiene profile for a PFR operating at an initial and reducing oxygen partial pressure of 70 kPa. 269
Figure 7.5. A PFR and an IMR in series configuration incorporating by-pass and mixing. 269
Figure 7.6. A PFR and an IMR in series. Butane:butadiene concentration profiles for various values of mixing ratio, *q*. 271
Figure 7.7. A PFR and an IMR in series. Butane:butadiene concentration profiles. Oxygen partial pressure in feed to the IMR 1% of that in mixed output stream from the PFR. 276
Figure 7.8. A PFR and an IMR in series. Butane:butadiene concentration profile for a mixing ratio of 0.2 and mixing line AB from fresh butane feed point. 279
Figure 7.9. A PFR followed by two IMRs in series configuration incorporating by-pass and mixing. 279
Figure 7.10. A PFR followed by two IMRs in series configuration. Butane:butadiene concentration profiles. 281
Figure 7.11. Ratio of sum of rates of formation of carbon monoxide, carbon dioxide and water to the rate of formation of butadiene. An analysis of Figure 7.10 for a value of *q2* of 0.6. 284
Figure 7.12. Rate of formation of butadiene for a value of *q2* of 0.6. 285

Figure 7.13. Ratio of sum of rates of formation of carbon monoxide, carbon dioxide and water to the rate of formation of butadiene. An analysis of Figure 7.10 for a value of *q2* of 0.2. 286
Figure 7.14. Rate of formation of butadiene for a value of *q2* of 0.2..... 287
Figure 7.15. A PFR followed by two IMRs in series. Butane:butadiene concentration profiles. Oxygen partial pressure in feed to IMR2 1% of that in mixed stream from IMR1 and feed to the PFR..... 288
Figure 7.16. A PFR followed by two IMRs in series. Butane:butadiene concentration profiles. Values of *q1* and *q2* are 0.2 and 1.0 respectively. 290
Figure 7.17. Superimposition of Candidate Attainable Region (AR^C) upon Figure 7.15. 293

Figure 8.1. Mass concentration profiles for n-butane and butadiene from an IMR. Oxygen partial pressure range 0.25 kPa to 85 kPa. 301
Figure 8.2. Mass concentration profiles for *n*-butane and butadiene from a FBR. Oxygen partial pressures 85 kPa, 75 kPa and 40 kPa. 304
Figure 8.3. Mass concentration profiles for *n*-butane and butenes from an IMR. Oxygen partial pressure range 0.25 kPa to 85 kPa. 307
Figure 8.4. Mass concentration profiles for *n*-butane and butenes from a FBR. Oxygen partial pressure range 57 kPa to 85 kPa. 309
Figure 8.5. Mass concentration profiles for *1*-butene and butadiene from an IMR. Oxygen partial pressures 85 kPa and 0.25 kPa. 312
Figure 8.6. Mass concentration profile for *1*-butene and butadiene from a FBR. Oxygen partial pressure 80 kPa. 314
Figure 8.7. Mass concentration profile for *1*-butene and butadiene from a FBR. Oxygen partial pressure 50 kPa. 315
Figure 8.8. Mass concentration profile for *1*-butene and butadiene from a FBR. Oxygen partial pressure 30 kPa. 316
Figure 8.9. IMR:FBR configuration for the ODH of *n*-butane to butadiene. 320

Figure 8.10. Geometrical representation of the ODH of *n*-butane to butadiene in an IMR followed by a FBR. Feed to FBR is a mixture of output from the IMR to fresh feed to IMR in the ratio 0.4:0.6. 321
Figure 8.11. Profiles of maximum yields of butadiene and reactor configurations as functions of oxygen partial pressures from a series combination of an IMR followed by a FBR. 325
Figure 8.12. Residence times for the maximum yields of butadiene from an IMR:FBR series configuration. 327
Figure 8.13. Percentage improvement in butadiene production from an IMR:FBR series combination over that from a single IMR. 329
Figure 8.14. FBR:IMR configuration for the ODH of *n*-butane to butadiene. 335
Figure 8.15. Profiles of maximum yields of butadiene as functions of oxygen partial pressures from a series combination of a FBR followed by an IMR. 336
Figure 8.16. Residence times for the maximum yields of butadiene from a FBR:IMR series configuration. 338
Figure 8.17. Residence times for the maximum yields of butadiene from a FBR:IMR series configuration (linear:log scale). 339
Figure 8.18. IMR residence times and reciprocal of IMR oxygen partial pressures against oxygen partial pressure in feed to the initial FBR (linear:log scale). 341
Figure 8.19. Ratio of IMR residence time and reciprocal of oxygen partial pressure as a function of oxygen partial pressure. 343
Figure 8.20. Percentage improvement in butadiene production from an FBR:IMR series combination over that from a single FBR. 345
Figure 8.21. Percentage improvement in butadiene production from an FBR:IMR series combination over that from a single FBR (linear/log scale). 346

Figure 8.22. Profiles of maximum yields of butenes and reactor configurations as functions of oxygen partial pressures from a series combination of an IMR followed by a FBR. 353
Figure 8.23. Residence times for the maximum yields of butenes from an IMR:FBR series configuration. 354
Figure 8.24. Percentage improvement in butenes production from an IMR:FBR series combination over that from a single IMR. 355
Figure 8.25. Profiles of maximum yields of butenes and reactor configurations as functions of oxygen partial pressures from a series combination of a FBR followed by an IMR. 362
Figure 8.26. Residence times for the maximum yields of butenes from a FBR:IMR series configuration. 363
Figure 8.27 Residence times for the maximum yields of butenes from a FBR:IMR series configuration (linear:log scale). 364
Figure 8.28. Representation of the influence of oxygen partial pressure upon residence time for the maximum yields of butenes from a FBR:IMR series configuration (linear:log scale). 366
Figure 8.29. Ratio of IMR residence time and reciprocal of oxygen partial pressure as a function of oxygen partial pressure. 367
Figure 8.30. Percentage improvement in butenes production from a FBR:IMR series combination over that from a single FBR. 369
Figure 8.31. Percentage improvement in butenes production from a FBR:IMR series combination over that from a single FBR (linear:log scale). 370
Figure 8.32. Profiles of maximum yields of butadiene and reactor configurations as functions of oxygen partial pressures from a series combination of an IMR followed by a FBR. 376
Figure 8.33. Residence times for the maximum yields of butadiene from an IMR:FBR series configuration. 378
Figure 8.34. Percentage improvement in butadiene production from an IMR:FBR series combination over that from a single IMR. 379

Figure 8.35. Profiles of maximum yields of butadiene and reactor configurations as functions of oxygen partial pressures from a series combination of a FBR followed by an IMR. 385
Figure 8.36. Residence times for the maximum yields of butadiene from a FBR:IMR series configuration. 387
Figure 8.37. Residence times for the maximum yields of butadiene from a FBR:IMR series configuration (linear:log scale). 388
Figure 8.38. Residence times for the maximum yields of butadiene from a FBR. 389
Figure 8.39. Profiles of IMR residence times and reciprocal of oxygen partial pressures.for the maximum yields of butadiene. 390
Figure 8.40. Ratio of IMR residence time and reciprocal of oxygen partial pressure as a function of oxygen partial pressure. 391
Figure 8.41. Percentage improvement in butadiene production from a FBR:IMR series combination over that from a single FBR. 393
Figure 8.42. Percentage improvement in butadiene production from a FBR:IMR series combination over that from a single FBR (linear:log scale). 394

LIST OF TABLES

Table 1.1. Enthalpies and Gibbs energies of formation and isobaric heat capacities of gases from Reid (1987). 38
Table 1.2. Enthalpies and Gibbs energies of formation, equilibrium constants and extent of conversion at various temperatures for the ODH of *n*-butane. 39
Table 1.3. Enthalpies and Gibbs energies of formation, equilibrium constants and extent of conversion at various temperatures for the ODH of *1*-butene. 40
Table 1.4. Enthalpies and Gibbs energies of formation, equilibrium constants and extent of conversion at various temperatures for the ODH of butadiene. 41
Table 1.5. Variation of equilibrium composition with ΔG^0 and the equilibrium constant at 298K from Smith (2005). 41
Table 1.6. Explanation of acronyms used by Dixon to describe membrane reactors. 62
Table 1.7. Chemical reactions and rate expressions for the oxidative dehydrogenation of *n*-butane to butene and butadiene. 81
Table 1.8. Rate constants and activity coefficients from Téllez (1999a and 1999b) and Assabumrungrat (2002)..... 83

Table 3.1. Maximum butenes yields, selectivities and residence times from an IMR at various constant oxygen inlet partial pressures. 144
Table 3.2. Best butenes yields from the various reactor configurations ranked according to their closeness to the theoretical maximum yield of butenes. 148
Table 3.3. Comparison of maximum yields of butenes from an IMR and a FBR at different oxygen partial pressures..... 152

Table 3.4. Comparison of maximum yields of butadiene from an IMR and a FBR at different oxygen partial pressures..... 157
Table 3.5. Best butadiene yields from an IMR and a FBR ranked according to their closeness to the theoretical maximum yield of butadiene. 162

Table 6.1. Equations and stoichiometry for the oxidation of *n*-butane, *1*-butene and butadiene..... 220
Table 6.2. Residence times in DSR and corresponding optimal RCC oxygen partial pressures..... 245
Table 6.3. Critical oxygen partial pressures in feed stream to the DSR ... 253

Table 7.1. Maximum butadiene yields and residence times from a PFR with depleting oxygen at various oxygen inlet partial pressures. 266
Table 7.2. Maximum butadiene yields and residence times from an IMR at various constant oxygen inlet partial pressures..... 268
Table 7.3. Effect of mixing ratio, *q*, upon the maximum yield of butadiene and the associated residence time. 272
Table 7.4. Composition of feed stream to the second series reactor for different values of the mixing ratio, *q*. 274
Table 7.5. Maximum butadiene yields and residence times from an IMR at different constant oxygen inlet partial pressures. Feed stream of butane and oxygen only. 275
Table 7.6. Effect of mixing ratio, *q*, upon the maximum yield of butadiene and the associated residence time where the oxygen partial pressure in the feed is reduced by 99 %..... 277
Table 7.7. Effect of mixing ratio, *q2*, upon the maximum yield of butadiene and the associated residence time for a PFR followed by two IMRs in series. 282
Table 7.8. Individual reactor residence times for values of mixing ratio, *q2*. Value of mixing ratio, *q1*, 0.2. Oxygen partial pressure in feed to IMR1 is 1 % of that in off-take from PFR. 283

Table 7.9. Effect of mixing ratio, *q2*, upon the maximum yield of butadiene and the associated residence time for a PFR followed by two IMRs in series. 289
Table 7.10. Individual reactor residence times for values of mixing ratio, *q2*. Value of mixing ratio, *q1*, 0.2. Oxygen partial pressure in reactants to IMR2 is 1 % of that in the combined off-take from IMR1 and fresh feed. 292
Table 7.11. Best butadiene yields from the various reactor configurations ranked according to their closeness to the theoretical maximum yield of butadiene. 292

Table 8.1. Maximum yields of butadiene from an IMR and a FBR in series as functions of oxygen partial pressure. 332
Table 8.2. Maximum yields of butadiene from a FBR and an IMR in series as functions of oxygen partial pressures 349
Table 8.3. Maximum yields of butenes from an IMR and a FBR in series as functions of oxygen partial pressures 358
Table 8.4. Maximum yields of butenes from a FBR and an IMR in series as functions of oxygen partial pressures 373
Table 8.5. Maximum yields of butadiene from an IMR and a FBR in series as functions of oxygen partial pressures 382
Table 8.6. Maximum yields of butadiene from a FBR and an IMR in series as functions of oxygen partial pressures 397
Table 8.7. Lower limit of oxygen partial pressure range over which a FBR is superior to a FBR and an IMR. 400
Table 8.8. Lower limit of oxygen partial pressure range for superiority of a single FBR over a single IMR for maximum yields of hydrocarbon product. 401

LIST OF SYMBOLS

ΔH_0^0	Standard enthalpy of formation, kJ/mol, at 298K.
ΔH^0	Standard enthalpy of formation, kJ/mol, at temperature T.
ΔG_0^0	Standard Gibbs energy of formation, kJ/mol, at 298K
ΔG^0	Standard Gibbs energy of formation, kJ/mol, at temperature T
A, B, C, D	Constants in equation for heat capacity
A, B, C, D	Species A, B, C and D
$\boldsymbol{c}$	State vector of all variables describing the system
$\boldsymbol{c}^*$	Mixing state variable of the system
$\boldsymbol{c}^{\boldsymbol{0}}$	State variable of the system at the feed point
C_i	Concentration of species *i*, mol/s.
C_i^0	Initial concentration of species *i,* mols/s.
E_{ai}	Activation energy for species *i*, (kJ/mol)
K	Equilibrium constant, kJ/mol.K
k_i	Kinetic constant for reaction *i*, mol/kg s
p_i	Partial pressure of species *i*, atm.
R	Gas constant, 8.314 J/mol K
$\boldsymbol{r}$(c)	Reaction rate vector defined at $\boldsymbol{c}$
r_i	Rate of reaction of reaction *i*, mol/kg s
T	Feed temperature, K
T_0	Reference temperature, 773K
X	Conversion of hydrocarbon reactant at equilibrium

Greek Symbols

α	Control policy for combination of reaction and mixing
β	Control policy for addition of oxygen

θ_0	Selective oxidation catalyst site
λ_0	Non-selective oxidation catalyst site
$\boldsymbol{v}$	Mixing vector, $\boldsymbol{c}$ with $\boldsymbol{c}^*$
τ	Residence time
τ	The ratio $\frac{T}{298}$
τ_i	Residence time for species, *i*, seconds

NOMENCLATURE

AR	Attainable Region
AR^C	Candidate Attainable Region
CSTR	Continuously Stirred Tank Reactor
DSR	Differential Side-Stream Reactor
FBR	Fixed Bed Reactor
IMR	Inert Porous Membrane Reactor
ODH	Oxidative Dehydrogenation
PFR	Plug Flow Reactor
RCC	Recursive Convex Control Policy
RTR	Residence Time Ratio

CHAPTER 1

INTRODUCTION

1.1 Preamble

Over the last twenty years many papers have been published dealing with mapping the region, the Attainable Region (AR), within which all the reactants and products of a chemical reaction lay, assuming known feed conditions and process constraints. In particular, two chemical reaction systems have been studied intensively to determine the boundaries of the candidate Attainable Region (AR^C), namely the Trambouze and the Van de Vusse systems. These two examples, possessing but fictitious kinetics, nevertheless represented reactions of considerable academic and theoretical interest but suffered from the lack of relevance to problems of business significance.

Specifically, there is a general paucity of chemical reaction rates and kinetic data and in studying the Trambouze and Van de Vusse reactions assumptions had to be made which, although undeniably useful in mapping the boundaries of the AR, could not easily be applied to specific chemical reactions. The Trambouze and Van de Vusse reactions, however, do possess the advantage of mathematical simplicity coupled with the ability to model a wide range of reactor behaviour and resulting reactor configurations.

Recently Téllez (1999a) and Assabumrungrat, (2002) presented kinetic data for the oxidative dehydrogenation (ODH) of *n*-butane in a fixed-bed reactor and in an inert porous membrane reactor. The availability of kinetic equations and constants for this chemical reaction of commercial

importance consequently underpinned the research programme for this thesis.

1.2 Background to the Thesis

There are several aspects of this thesis that makes it unique in the sense that it brings together previously published works and applies them in an environment hitherto overlooked. Broadly, a comprehensive literature survey was done to assess recent (and in some cases, not so recent) developments in the fields of :

- Attainable regions
- Oxidative dehydrogenation
- Reactor designs and structures
- Reaction kinetics

The literature survey furthermore was constrained to seek published works in the above categories to the extent that they considered reactions of actual industrial relevance and, in particular, the synthesis of butenes and butadiene from *n*-butane.

The literature survey is presented in chronological sequence, i.e. from the earliest to the most recent.

I should mention from the outset that I have attempted to distil from these published works those aspects that I found to be both interesting in a broad sense and those that were relevant to my research work for this thesis. Whereas the reviews and analyses of the following published works

represent my work and my work alone, the published works are those of the cited authors. I have prepared synopses of these works and the conclusions of these cited authors and anywhere that I have used the precise terminology of these authors it was because of my inability to devise synonyms.

Before presenting my review and analysis of relevant publications, I introduce a summary of the process thermodynamics for the oxidative dehydrogenation of *n*-butane.

1.2.1 Process Thermodynamics

In the oxidative dehydrogenation (ODH) of *n*-butane and the subsequent ODH of the products, eleven chemical reactions are possible. In general terms these eleven reactions describe the ODH of *n*-butane to isomers of butene and to carbon monoxide and carbon dioxide, the ODH of *1*-butene to butadiene and to carbon monoxide and carbon dioxide and the ODH of butadiene to carbon monoxide and carbon dioxide. Water is an additional product in all these reactions.

For each of these eleven reactions, the equilibrium constant was calculated at four temperatures, 298K, 748K, 773K and 823K and the degree of conversion of the relevant hydrocarbon derived at each temperature. The temperatures of 748K, 773K and 823K were chosen because these were the temperatures for which the kinetic data developed by Assabumrungrat, (2002) and Téllez (1999a) were relevant.

Enthalpy of reaction and heat capacity are given by :

$\Delta H_T = \Delta H_{298} + \int_{298}^{T} \Delta C_p dT$ where $\Delta C_p = \Sigma \nu_i C_{pi}$

and

$C_{pi} = A + BT + CT^2 + DT^3$

The Gibbs energy of formation at temperature T, ΔG^0, was found to be

$$\Delta G^0 = \Delta H_0^0 + \left(\Delta G_0^0 - \Delta H_0^0\right)\tau - AT_0\left(\tau \ln \tau - \tau + 1\right) - \frac{BT_0^2}{2}\left(\tau^2 - 2\tau + 1\right) -$$

$$\frac{CT_0^3}{6}\left(\tau^3 - 3\tau + 2\right) - \frac{DT_0^4}{12}\left(\tau^4 - 4\tau + 3\right)$$

where $\tau = \frac{T}{T_0}$

The derivation of this expression is given in an Appendix to this chapter of my thesis.

Reid (1987) provided heats of formation and heat capacities of the gases associated with the oxidative dehydrogenation of *n*-butane and these are shown in Table 1.1.

Chemical Species	ΔH^{O}_{298}, kJ/mol	ΔG^{O}_{298}, kJ/mol	A	B	C	D
n-C_4H_{10}	-126.2	-16.10	9.487e+0	3.313e-1	-1.108e-4	-2.822e-9
O_2	0	0	2.811e+1	-3.680e-6	1.746e-5	-1.065e-8
1- C_4H_8	-0.126	71.34	-2.994e+0	3.532e-1	-1.990e-4	4.463e-8
Trans-*2*- C_4H_8	-11.18	63.01	1.832e+1	2.564e-1	-7.013e-5	-8.989e-9
Cis-*2*- C_4H_8	-6.99	65.9	4.396e-1	2.953e-1	-1.018e-4	-0.616e-9
C_4H_6	110.2	150.8	-1.687e+0	3.419e-1	-2.340e-4	6.335e-8
CO	-110.6	-137.4	3.087e+1	-1.285e-2	2.789e-5	-1.272e-8
CO_2	-393.8	-394.6	1.980e+1	7.344e-2	-5.602e-5	1.715e-8
H_2O	-242.0	-228.8	3.244e+1	1.924e-3	1.055e-5	-3.596e-9

Table 1.1. Enthalpies and Gibbs energies of formation and isobaric heat capacities of gases from Reid (1987).

Enthalpies and Gibbs energies of formation, equilibrium constants and extent of conversion at various temperatures for the ODH of butane, butenes and butadiene are shown in Tables 1.2, 1.3 and 1.4.

OXIDATION OF *N*-BUTANE					
Reaction : $C_4H_{10} + ½O_2 \rightarrow$ *1*-$C_4H_8 + H_2O$					
Temperature	ΔH^0	ΔG^0	K	X	Category
298K	-115.93	-141.36	6.00e+24	1.0	A
748K	-115.20	-180.72	4.17e+12	1.0	A
773K	-115.31	-182.91	2.29e+12	1.0	A
823K	-115.56	-187.28	7.69e+11	1.0	A
Reaction : $C_4H_{10} + ½O_2 \rightarrow$ Trans-*2*-$C_4H_8 + H_2O$					
298K	-126.98	-149.69	1.73e+26	1.0	A
748K	-126.69	-184.92	8.24e+12	1.0	A
773K	-126.83	-186.86	4.23e+12	1.0	A
823K	-127.14	-190.73	1.27e+12	1.0	A
Reaction : $C_4H_{10} + ½O_2 \rightarrow$ Cis-*2*-$C_4H_8 + H_2O$					
298K	-122.79	-146.80	5.39e+25	1.0	A
748K	-124.89	-182.41	5.47e+12	1.0	A
773K	-125.11	-184.33	2.85e+12	1.0	A
823K	-125.56	-188.16	8.73e+11	1.0	A
Reaction : $C_4H_{10} + O_2 \rightarrow C_4H_6 + 2H_2O$					
298K	-247.60	-290.70	9.00e+50	1.0	A
748K	-242.99	-359.42	1.26e+25	1.0	A
773K	-243.04	-363.31	3.55e+24	1.0	A
823K	-243.22	-371.08	3.56e+23	1.0	A
Reaction : $C_4H_{10} + {}^9/_2O_2 \rightarrow 4CO + 5H_2O$					
298K	-1 526.2	-1 677 5	1.085e+294	1.0	A
748K	-1 522.3	-1 912.4	3.522e+193	1.0	A
773K	-1 523.0	-1 925.4	1.282e+130	1.0	A
823K	-1 524.6	-1 951.4	7.116e+123	1.0	A
Reaction : $C_4H_{10} + {}^{13}/_2O_2 \rightarrow 4CO_2 + 5H_2O$					
298K	-2 659.0	-2 706.3	Inf	1.0	A
748K	-2 656.8	-2 781.4	1.688e+194	1.0	A
773K	-2 657.3	-2 785.5	1.685e+188	1.0	A
823K	-2 658.4	-2 793.8	2.068e+177	1.0	A

Table 1.2. Enthalpies and Gibbs energies of formation, equilibrium constants and extent of conversion at various temperatures for the ODH of *n*-butane.

OXIDATION OF *1*-BUTENE					
Reaction : $C_4H_8 + ½O_2 \rightarrow C_4H_6 + H_2O$					
Temperature	ΔH^0	ΔG^0	K	X	Category
298K	-131.67	-149.34	1.502e+26	1.0	A
748K	-127.79	-178.70	3.010e+12	1.0	A
773K	-127.74	-180.40	1.549e+12	1.0	A
823K	-127.66	-183.81	4.633e+11	1.0	A
Reaction : $C_4H_8 + 4O_2 \rightarrow 4CO + 4H_2O$					
298K	-1 410.3	-1 536.1	1.810e+269	1.0	A
748K	-1 407.1	-1 731.7	8.445e+120	1.0	A
773K	-1 407.7	-1 742.5	5.597e+117	1.0	A
823K	-1 409.1	-1 746.1	9.250e+111	1.0	A
Reaction : $C_4H_8 + 6O_2 \rightarrow 4CO_2 + 4H_2O$					
298K	-2 543.1	-2 564.9	Inf	1.0	A
748K	-2 541.6	-2 600.6	4.047e+181	1.0	A
773K	-2 542.0	-2 602.6	7.355e+175	1.0	A
823K	-2 542.8	-2 606.5	2.688e+165	1.0	A

Table 1.3. Enthalpies and Gibbs energies of formation, equilibrium constants and extent of conversion at various temperatures for the ODH of *1*-butene.

OXIDATION OF BUTADIENE					
Reaction : $C_4H_6 + {}^7/_2O_2 \rightarrow 4CO + 3H_2O$					
Temperature	ΔH^0	ΔG^0	K	X	Category
298K	-1 278.6	-1 386.8	1.205e+243	1.0	A
748K	-1 279.3	-1 553.0	2.805e+108	1.0	A
773K	-1 280.0	-1 562.1	3.613e+105	1.0	A
823K	-1 281.4	-1 580.3	1.997e+100	1.0	A
Reaction : $C_4H_6 + {}^{11}/_2O_2 \rightarrow 4CO_2 + 3H_2O$					
298K	-2 411.4	-2 415.6	Inf	1.0	A
748K	-2 413.8	-2 421.9	1.344e+169	1.0	A
773K	-2 414.2	-2 422.2	4.748e+163	1.0	A
823K	-2 415.1	-2 422.7	5.802e+153	1.0	A

Table 1.4. Enthalpies and Gibbs energies of formation, equilibrium constants and extent of conversion at various temperatures for the ODH of butadiene.

The hydrocarbon conversion at equilibrium, X, was calculated by solving the equation in which the stoichiometric ratio of products to reactants equals $\Delta G^0/RT$.

Category	**ΔG^0, kJ**	**K**	**Composition of Equilibrium Mixture**
A	-50	6e+8	Negligible Reactants
B	-10	57	Products Dominate
C	-5	7.5	
D	0	1.0	
E	+5	0.13	
F	+10	0.02	Reactants Dominate
G	+50	1.7e-9	Negligible Products

Table 1.5. Variation of equilibrium composition with ΔG^0 and the equilibrium constant at 298K from Smith (2005).

Scrutiny of the data in Tables 1.2, 1.3 and 1.4 indicates that when oxygen is present at or in excess of stoichiometric quantities, the oxidation of the hydrocarbon is both complete and rapid and at equilibrium no reactant is left.

Consequently, it behoves the addition of oxygen under controlled conditions and in less than the stoichiometric quantities to influence the yield and selectivity of the desired product. In the ODH of *n*-butane, a possible nine species including oxygen and water can be present and the presence of excess oxygen can result in the deep oxidation of all hydrocarbons to carbon monoxide, carbon dioxide and water, an undesirable situation.

1.2.2 Attainable Regions

The concept of an Attainable Region (AR) was first articulated four decades ago by Horn (1964) but, because of a probable inability to understand comprehensively its import, it languished in relative obscurity for another two decades until pioneering work at the University of the Witwatersrand in Johannesburg, South Africa became known. Glasser *et al*. (1987) investigated a problem of not inconsiderable interest namely, in an isothermal reactor, how could a geometrical area be identified that would contain all the reactants and products associated with a chemical reaction. Certain assumptions were made specifically that no change in volume occurred and that the only physical changes were those of mixing and reaction. It was concluded that not only could such a two-dimensional geometrical area, styled a Candidate Attainable Region (AR^C) be constructed but that it could be so developed through the use of conventional plug flow reactors (PFRs) and continuously stirred tank

reactors (CSTRs) in suitable configurations and with appropriate by-pass arrangements. The authors maintained that with the creation of an AR^C, it became possible to solve the problem of finding an optimum solution for an objective function which, for example, might be maximum yield, minimum residence time or maximum selectivity, provided these functions could be expressed in terms of the relevant species' concentrations. The authors also identified necessary conditions to which an AR had to comply, one of which that the profile of an AR always had to be convex. It must be noted, however, that the reactions considered by the authors were the Van de Vusse and the Trambouze, reactions of great academic curiosity but of limited application in commercial applications.

The geometry of the attainable region was examined again by Hildebrandt *et al*. (1990). In this paper several reaction systems, including the Trambouze, with assigned kinetics were studied to identify candidate attainable regions under isothermal and adiabatic conditions and with variable and constant density systems. The effects of direct (cold shot) and indirect (heat exchange) cooling upon the relevant AR^Cs were analysed. The reactors considered in this paper were PFRs and CSTRs with suitable by-pass arrangements. The usefulness and practicality of geometric ideas to solve reactor problems were confirmed. The authors conceded that, as yet, there were no means to conclude that the AR^C was the AR for the specified conditions or to use the words of the authors "as there is at present not a complete sufficiency condition, we have not proved that any optimum is a global one".

Hildebrandt and Glasser (1990) developed further the findings contained in their earlier papers. The Van de Vusse, Denbigh and Westerterp reactions were studied and a three-dimensional AR^C was identified for each reaction. The conclusions reached in this paper were the identification of some of the

properties of the surface of the AR and the realisation that the optimal reactor configuration almost always was a series-parallel configuration of PFRs, CSTRs with suitable by-pass arrangements. It was concluded that all the AR^Cs developed could be accomplished using only PFRs and CSTRs in series and with by-pass.

Nisoli *et al*. (1997) considered the applicability of the AR concept to identify the feasible compositions that can be obtained in processes combining simultaneous reaction, mixing and separation. Two non-ideal ternary reactive distillation processes of commercial interest were examined, the manufacture of dimethyl ether (DME) by dehydration of methanol and the synthesis of methyl tert-butyl ether (MTBE) from butene and methanol. A two-phase CSTR with a flash separator was studied and the PFR analysed consisted of a large number of two-phase CSTRs in series. In both of these reactors the vapour was separated from the liquid phase. The relevant AR^Cs were identified by the removal of vapour from the reaction sections and passing it to either to a condenser (DME) or to a distillation section (MTBE). Residue curves were used to get a better understanding of the fundamental process steps and to identify the AR^Cs. The authors concluded that the reactor-separator models studied have the same geometric properties in concentration space as the simple reactor models and, consequently, the procedures previously advocated by Glasser *et al.* (1987) are both applicable and valid.

Another study this time dealing with a reaction of industrial significance was the application of the attainable region concept to the free-radical polymerisation of poly(methyl methacrylate) (MMA) by Smith and Malone (1997). The authors extended the work of Glasser *et al*. (1987) to identify an AR for this reaction. From this AR the objective to find the limiting average molecular weights, polydispersities, monomer conversions, residual initiator

concentrations and reactor network residence times was reached. It was concluded that a CSTR, a CSTR with a by-pass stream and a CSTR followed by a PFR yielded the narrowest molecular weight distributions.

Feinberg and Hildebrandt (1997) for physical changes of reaction and mixing in an isothermal reactor studied the properties of the points that lay on the profile of an AR. The importance of these points, apart from fixing the boundaries of a reaction system, was that this is where optimum reactor configurations invariably could be found. The authors concluded that no matter how complex or how wide the spectrum of design conditions these boundary points always would be accessible via a combination of CSTRs, PFRs and Differential Sidestream Reactors (DSRs), a DSR being a PFR with the feed stream being supplied at the inlet and also along the length of the reactor.

Feinberg (1999) developed further the work of Feinberg and Hildebrandt (1997) to consider the attributes of DSR paths along the boundaries of an AR. Two possible scenarios for the rate of addition of feed along the length of a DSR were identified, one in which the rate of addition was a function of residence time the second where the rate was dependent upon the concentration profile inside the reactor. Feinberg posed the question as to whether there were mathematical equations to govern the side-stream addition rate for DSRs whose profiles lay on the AR boundary. In his paper Feinberg concluded that such equations did exist but of an increasing complexity as the number of dimensions to an AR increased.

Godorr *et al*. (1999) contrasted the case where the AR has been derived from given rate functions to where the rate function is dependent upon a process control condition such as temperature. For the latter scenario the

authors derived equations to describe the optimal control policies. The reactors considered were the CSTR, PFR and DSR. In this paper the authors made a perceptive statement to the effect that the AR concept clearly had applications in other fields of optimisation. Although this statement seems to have been couched in the relative narrow context of reaction engineering, the applicability of the AR concept has recently {Khumalo (2006)} been extended to the study of comminution problems. Godorr *et al.* concluded that the mathematical principles developed in their paper were of a sufficiently general nature for their application to non-chemical engineering problems such as the brachistochrone problem {brachistochrone – the curve along which a particle acted upon by a force such as gravity will pass in the shortest time from one given point to another, Chambers (1966), literally, shortest path. The brachistochrone problem was posed by Bernoulli in 1696} and that the AR concept when applied to optimisation would allow the optimal choice of a control variable that would influence how a single fundamental process operates at every point of the AR boundary.

McGregor *et al*. (1999) examined the relationship between the AR concept and Pontryagin's maximum principle. A simple non-mathematical definition of this principle is that it is used in optimal control theory to find the best possible control for taking a dynamic system from one state to another, especially in the presence of constraints for the state or input controls (Wikipedia free encyclopaedia). The relationship studied by McGregor *et al*. was for a limited class of problems and the conclusions were that the AR concept seemed to handle problems difficult to solve by the Pontryagin approach. The authors listed a set of postulates about the structure of the AR boundary for steady-state reactor synthesis. These postulates, it was claimed, would permit a more constructive identification of an AR boundary than the hitherto trial and error approach.

Feinberg (2000a) in an extension of his previous work examined the role of critical DSRs, that is those DSRs whose products are to be found on the boundary of an attainable region. Complex and intricate equations were derived to describe these critical reactors and the necessary conditions for the addition of feed along the length of the reactor, its composition and the reaction rates. Feinberg concluded by stating his apprehension over the effort required to solve these formidable equations for a critical DSR especially when they are derived for high dimensions. Because the critical DSR equations embodied the rate of formation function, $\mathbf{r}(\cdot)$, and because this function usually is derived from kinetic experiments and consequently likely to possess a degree of inaccuracy, Feinberg queried the dependence that could be placed upon the accuracy of the third or fourth derivatives of $\mathbf{r}(\cdot)$ present in his equations.

Feinberg (2000b) examined the circumstances under which the products from a continuous flow stirred tank reactor (CFSTR) would lie on the boundary of an attainable region. He developed equations to describe the necessary conditions and deduced that there were only very exceptional values of residence time and compositions necessary for these circumstances. He showed that the some of his conclusions in Feinberg (2000a) relating to critical DSRs were relevant also to critical CFSTRs.

Nicol *et al*. (2001) used the AR concept to find the optimum process design for an exothermic reversible reaction system with applied cooling and heating from a constant temperature source. Direct (cold shot) cooling was favoured at high temperatures and indirect cooling (heat exchange) was preferred at lower temperatures. In this paper, Nicol *et al*. used the symbol $\partial \mathrm{AR}^{\mathrm{C}}$ to describe the candidate AR boundary. The cost of heating, the manner in which heating and cooling was applied were found to be influencing factors upon the final reactor configuration.

Zhao *et al*. (2002) used the Van de Vusse reaction in conjunction with a CSTR, a PFR and a DSR to partition the attainable region into three regions, a CSTR region, a PFR region and a non-operational region. The point on the boundary of the AR demarcating the CSTR and the PFR regions coincided with the point of maximum selectivity of the reactant species relative to the feed species. The point on the boundary of the AR demarcating the PFR and the non-operational regions coincided with the point of maximum yield of the reactant species. The conclusions of the authors that a CSTR first be used and at a point where the maximum selectivity is attained the CSTR reactants and products are diverted to PFR. The reaction in the PFR is terminated when the maximum yield of the desired product species is achieved.

Kauchali *et al*. (2002) developed linear programming models for analysing ARs for rate vector fields in concentration space. A fully connected network of CSTRs was used to evolve one of these models. Two LP models were proposed, one using a systematic method to produce isothermal AR^Cs, the second to test whether the AR^Cs can be extended further. The LP models have the facility to cater for non-isothermal reaction problems. The authors claimed that the LP models resulted in more stringent necessary conditions for AR analysis than promulgated by earlier workers including Glasser *et al*. (1987), Hildebrandt and Glasser (1990) and Glasser *et al*. (1990).

Abraham and Feinberg (2004) introduced a novel concept for establishing the boundary of an AR. Hitherto, the practice had been to attempt to extend outwards further and further the boundary of an AR until no further extension proved possible, *ne plus ultra*. This practice might be called the expansion method. In this paper, Abraham and Feinberg approached the

problem of identifying the AR boundary from the opposite perspective by employing what might be called a contraction method. Abraham and Feinberg called this technique the method of bonding hyperplanes. This method was tested using the classic Van de Vusse reaction as an example. The initial starting point was the identification of a bounding polygon in concentration space within which would contain all attainable outcomes. As the number of hyperplanes was increased, so the polygon that emanated contracted in composition space and mirrored the profile of the AR boundary that the expansion method would have produced. Abraham and Feinberg showed that a one hundred and ten hyperplane bound resulted in an AR boundary to all extent indistinguishable from that derived from the expansion method. Because the contraction method did not assume any underlying reactor configuration it was concluded that the AR derived from the expansion method was in fact the full AR and consequently could be so styled instead of being referred to as a candidate AR.

Khumalo *et al.* (2006) departed from the traditional field of reaction engineering and applied the AR concept to solve problems in comminution. Industrial comminution requires significant capital outlay and has very high energy requirements and whereas there has always been common awareness that any effort to improve the efficiency of the comminution process could not fail to be beneficial, the categorisation and representation of the process variables had stayed relatively unchanged for many decades. Khumalo *et al.* defined an objective function, specific energy, and posed the question as to what size categories could be produced from the process commensurate with the efficient use of energy. Fundamentally, reaction and comminution were similar in as much as they both shared the same basic processes, mixing and reaction, the latter in the case of comminution being the breaking and cleaving of a large particle into smaller particles. Specific energy was used as the control variable to produce narrow product size distributions (PSDs) and Khumalo *et al*. developed ARs for the

comminution process and showed that the AR approach permitted not only the identification of all the PSDs possible from a feed material with a known PSD but also the various comminution steps to prepare a product with a required PSD and in addition how to do so with the most efficient use of energy. It was claimed by Khumalo *et al*. that the energy efficiencies of industrial comminution processes rarely exceed 8 %, a sobering reflection on the magnitude of the scope for improvement. The underlying assumption made in this paper was that the rate of comminution was dependent only upon the specific energy within the mill.

Seodigeng (2006) developed the Recursive Convex Control (RCC) policy as a numerical tool to identify the boundary of an attainable region, AR. The RCC method employs the mathematical features of basic processes, reaction and mixing, to identify the boundary of an AR that satisfies compliance criteria. These compliance criteria for an attainable region, AR, were specified by Glasser *et al*. (1987) and subsequently were clarified and refined by others including Hildebrandt and Glasser (1990), Nisoli *et al*. (1997) and Feinberg and Hildebrandt (1997). These criteria, simply expressed, are :

1. The AR includes all defined input and output states.
2. No rate vector on the boundary of the AR points outwards, i.e. all rate vectors must point inwards or be tangential or be zero.
3. The boundary of the AR is convex.
4. No basic process vectors on the AR boundary can intersect the AR boundary when extended backwards.
5. No plug flow trajectory exists within the complement of the AR such that a line linking two points of this trajectory can be extended to intersect the AR.

These criteria represent the guidelines for determining whether a geometrical space in a specified number of dimensions can be claimed to be an AR. In reality, the possibility that there might be additional criteria as yet unknown cannot be eliminated and, as a consequence, an AR that satisfies these known criteria, for the moment, can be but referred to as a candidate AR, an AR^C.

The RCC policy does not rely upon the starting assumption that a definite reactor configuration is to be used. Rather, the RCC concept contains a library of the individual mathematical characteristics of all processes and reactor types and uses these characteristics to develop an AR^C subject to the requirement for convexity. It is an iterative procedure and usually concludes when the difference in the value of a chosen function after the n^{th} iteration and the value of that function after the $(n\text{-}1)^{th}$ iteration is less than 0.1 % of the initial value. It was found that a maximum of ten iterations was sufficient to attain the required degree of convergence. Another feature of the RCC policy is that having determined the profile of an AR^C the reactor configuration(s) to attain any point on the boundary of or within the AR^C space can be found. Seodigeng confirmed the validity of his RCC concept by showing that its results tallied precisely to those earlier derived analytically for the Van de Vusse reaction. With this reassurance, Seodigeng applied his RCC technique to the water-gas shift reaction and to identify and analyse AR^Cs and optimal process flowsheets for the synthesis of ammonia and methanol. The RCC concept was used to analyse a four-dimensional stoichiometric Van de Vusse problem, a task that previously had been deemed too difficult to resolve. As part of his thesis, Seodigeng produced a software application that encapsulated the principles of his RCC policy and the successful use of this software requires no specialised awareness of AR theory. Computer run times for this software, it is claimed, are one tenth that of other comparable applications.

Khumalo *et al*. (2007) tested the assumption made in Khumalo *et al*. (2006) that the rate of comminution was dependent only upon the specific energy within the mill. Experiments were done on a small laboratory ball mill that involved the breakage of uniformly-sized particles into two distinct progeny size classes. The results were represented geometrically in two-dimensional space. The authors showed that the experimental results for a laboratory ball mill run at different ball loadings and different mill speeds could be correlated in terms of the specific energy within the mill.

Zhou and Manousiouthakis (2007) used the infinite dimensional state-space (IDEAS) method and an associated so-called shrink-wrap algorithm to develop ARs for variable density gas-phase fluids in a CSTR and in a PFR. Having first generated a boundary presumed to contain the true and full AR, the purpose of the shrink-wrap algorithm was to eliminate progressively extreme points within this boundary that failed to comply with necessary and sufficient conditions and in so doing to approximate the true AR, hence the term used by the authors, shrink-wrap. The outcome of this work was that objective functions like the maximisation of concentration, yield, selectivity and the minimising of reactor volume all could be evaluated within a linear programming model. Two classic chemical reactions, the Trambouze and the Van de Vusse, were used by Zhou and Manousiouthakis in demonstrating their linear programming model.

1.2.3 Oxidative Dehydrogenation (ODH)

One of the earliest papers dealing with the oxidative dehydrogenation of *n*-butane over a V/MgO catalyst was by Chaar *et al*. (1987). They found that the selectivity for dehydrogenation increased when the vanadium content of

the catalyst was increased with a maximum selectivity in the range of 24 to 54 wt% V_2O_5. At a temperature of 813K, the ODH selectivity increased with decreasing oxygen to butane ratio and with decreasing conversion. Selectivity for butenes was found to decrease with increasing temperature but increased for butadiene. With a decrease in the oxygen to butane ratio, selectivities for butenes and butadiene combined increased and values up to 60 % were recorded. Experiments were carried out at atmospheric pressure and the concentration of butane in the feed to a U-tube fixed bed reactor was 0.04 vol%. The oxygen feed concentration was varied over the range 0.04 to 0.08 vol%, the balance being helium. One interesting finding by the authors was the preferential formation of *1*-butene to that of trans-*2*-butene and cis-*2*-butene. The ratio of *1*-butene:trans-*2*-butene:cis-*2*-butene was almost always found to be 3:1:1. It was concluded that the presence of both vanadium oxide and magnesium oxide in the compound magnesium orthovanadate was responsible for the high selectivity of butane.

Téllez *et al*. (1997) studied the ODH of butane at temperatures between 723K and 823K in a fixed bed reactor (FBR) and in an inert catalytic membrane reactor (IMR). A V/MgO catalyst was used in their experiments. They claimed that the ODH of butane offered potential advantages over its thermal dehydrogenation because the former reaction is exothermic, needs no external heat input, avoids equilibrium limitations, runs at lower temperatures and produces lower yields of coke and cracking products. Téllez *et al*. stated that over V/MgO catalysts, the ODH reaction takes place using lattice oxygen present in the catalyst and provided there is sufficient oxygen present in the gas phase to replenish the lattice, the oxygen partial pressure seemed to have insignificant effect upon the activity of the catalyst. Téllez *et al*. confirmed the findings of Chaar *et al*. (1987) namely that whereas the total selectivity to dehydrogenated C_4 products increased with increasing temperature, the selectivity to butenes decreased and the selectivity to butadiene increased. It was concluded that an IMR presented a

safer operating vehicle than a FBR by virtue of the easier control of the temperature in the former than in the latter and the diminished likelihood of run-away conditions in an IMR. Another important finding was that best results were obtained when the butane and the diluent, helium, were co-fed at the tube inlet to the IMR and the oxygen was diffused through the membrane wall.

Cavini and Trifirò (1997) discussed aspects of the conversion of paraffin hydrocarbons to oxidised products and the parameters affecting the selectivity of the required products. Selectivity, according to the authors, was important in deciding the economics of a reaction process since it implied a superior utilisation of the feedstock, reduced operating costs and smaller material volumes. It was argued that the largest disincentive to the development of new oxidative products was the loss of valuable co-products as exemplified in oxidehydrogenation processes compared to dehydrogenation processes. An interesting comment by the authors was the identification of processes that no longer were of industrial interest, specifically the manufacture of butenes and butadiene from *n*-butane, there then being a surplus of these hydrocarbons. The desirable features of a catalyst for the oxidation of a paraffin were reported. Because of the high exothermic characteristics of oxidative reactions and because of the problems associated with the removal of this heat, Cavini and Trifirò claimed that a fluid-bed reactor in preference to a fixed-bed reactor was a better proposition for oxidative reactions so far as heat removal and the maintenance of isothermal conditions are concerned.

Kung and Kung (1997) examined the ODH of alkanes over vanadium magnesium oxides. The primary purpose of these ODH processes is the production of alkenes but there also is the unavoidable deep oxidation of

both reactants and products to carbon monoxide and carbon dioxide. The general reaction equations presented by Kung and Kung were :

$$C_nH_{2n+2} + ½O_2 \rightarrow C_nH_{2n} + H_2O$$

$$C_nH_{2n+2} + ½(3n + 1)O_2 \rightarrow nCO_2 + (n + 1)H_2O$$

Kung and Kung reported that the addition of vanadium to magnesium oxide significantly increased the activity and the dehydrogenation selectivity and in the case of the latter much more so than for V_2O_5. Without proffering an explanation, it was reported that catalytic behaviour also depends upon the alkane. The proposition was advanced that the oxygen that reacts with the alkane on the surface of the catalyst comes from the crystal lattice and that gas-phase oxygen is involved only after being adsorbed on other regions of the catalyst and then diffusing through the lattice to the active site. Kung and Kung concluded that a strong interaction between MgO and V_2O_5 to form magnesium vanadates was a desirable catalytic feature for the ODH of alkanes.

Soler *et al*. (1998) examined the ODH of *n*-butane using three types of reactor, an adiabatic fixed-bed reactor, a fluidised-bed reactor and an in-situ redox fluidised-bed reactor. To increase the selectivity to ODH products, Soler *et al.* argued that it was necessary to operate with as little as possible oxygen in the gaseous phase to minimise the formation of deep oxidation products, CO_x. At an operating temperature of 823K, the authors found that the selectivities to butenes and butadiene in a redox fluidised-bed reactor, a fluidised-bed reactor and a fixed-bed reactor were 52 %, 43 % and 32 % respectively while the selectivities to CO and CO_2 in the same reactors were 46 %, 52 % and 67 % respectively. Soler *et al*. concluded that an in-situ redox fluidised-bed reactor significantly increased the selectivity and yield of C_4 olefins at high butane conversions.

Lemonidou *et al*. (1998) investigated the ODH of *n*-butane over V/MgO catalysts with three objectives, to study the effect of the several phases of V/MgO catalysts on the ODH process, to investigate the influence of process variables on selectivities and to assess the rates of primary and secondary steps with the addition of intermediate products. The experiments were carried out at atmospheric pressure and at temperatures between 505^{o}C and 540^{o}C. The best performance was found to occur with a 30V/MgO catalyst containing 30 wt% V_2O_5, crystal phases $Mg_3(VO_4)_2$-MgO with a surface area of 54 m^2/g. Selectivities to butenes and butadiene were 55 % and to deep oxidation products 43 %. Butane conversion was 42 %. Another finding was that the overall selectivity to butenes and butadiene increased with temperature as a consequence of the higher activity energy of formation of alkenes compared to that of carbon oxides. However the selectivity to butenes decreased while that to butadiene increased. The reduction in butenes selectivity was attributed by Lemonidou *et al*. to further dehydrogenation and deep oxidation of the alkenes. On the basis of results from the 30V/MgO catalyst, it was found that the molar ratio of CO_2 to CO lay in the range 2.5-3. Lemonidou *et al.* concluded that the ODH of *n*-butane could be represented by a combined network of six reactions, three of which were primary parallel steps describing the production of butenes, carbon oxides and butadiene and three secondary parallel steps describing the oxidation of butenes to form butadiene and carbon oxides as well as the deep oxidation of butadiene to carbon oxides. The presence of steam in the feed stream was found to decrease the conversion of butane presumably due to the adsorption of water on selective active sites.

Soler *et al*. (1999) used a two-zone fluidised-bed reactor to investigate the ODH of *n*-butane between temperatures of 823K and 873K. Separate oxidation and reduction chambers in the same reactor vessel were created

and a V/MgO catalyst circulated between the two zones. Soler *et al*. considered the presence of gas-phase oxygen as being detrimental to selectivity and accordingly the two-zone reactor was designed to minimise the presence of oxygen in the reactor's atmosphere. Soler *et al*. postulated that the absence of gas-phase oxygen tended to favour the reaction of *n*-butane with catalyst lattice oxygen and resulted in the formation of butadiene in preference to carbon oxides. Soler *et al*. found that, when butane and oxygen were fed separately to the reactor instead of together, better butane conversions and overall butene butadiene selectivities were possible with lower overall deep oxidation selectivities. Again, under the co-feeding arrangement the equilibrium ratio of *1*-butene to cis-*2*-butene to trans-*2*-butene was 1:1:1.1 and 3:1:1 under the separate feeding arrangement. The latter ratio agrees with that reported by Chaar *et al*. (1987). Butadiene was found to be the preferential oxidative product in the two-zone reactor. Yields of butadiene from the two-zone reactor were 200 % better than from a conventional fluidised-bed reactor and the two-zone reactor exhibited improved safety features, specifically the prevention of the formation of explosive mixtures as a result of the isolation of the reduction and oxidative zones.

Téllez *et al.* (2000) studied the relationship between the state of the catalyst surface and the observed catalytic performance during the ODH of *n*-butane over a V/MgO catalyst. Téllez *et al.* quoted the findings of previous authors to the effect that the ODH reaction can take place in the absence of gas-phase oxygen using oxygen from the crystal lattice, the role of gas-phase oxygen, according to Téllez *et al.*, being to replenish spent lattice oxygen. Little influence of the oxygen partial pressure on the activity of the catalyst was seen. At a given *n*-butane conversion, a higher butadiene selectivity was observed with a decreasing oxygen:butane ratio. The selectivity of CO_x was advanced under high oxygen:butane ratios. Under oxygen-lean conditions the catalyst was found to be less active but more selective but was unstable

due to the formation of coke, a process that takes place faster on reduced catalysts.

Ge *et al*. (2001) used the ODH of *n*-butane to butenes and butadiene over a V/MgO catalyst to study the characteristics of an inert ceramic membrane reactor (IMR) and to compare them with those of a fixed-bed reactor (FBR). Oxygen supplied to a FBR in stoichiometric proportions with other reactants resulted in deep oxidation to carbon monoxide and carbon dioxide. Distribution of the oxygen along the length of an IMR was found to increase the selectivity to desired products. Oxygen partial pressure was found to be an important factor in the ODH of *n*-butane. Lattice oxygen was consumed during the dehydrogenation phase and was replenished by gas-phase oxygen. Ge *et al*. found that the FBR gave a lower selectivity and yield to butenes and butadiene than did an IMR. The importance of lowering the oxygen partial pressure in the reaction zone was confirmed as selectivities decreased with increasing oxygen partial pressures.

Alfonso *et al*. (2002) studied the ODH of *n*-butane on different V/MgO catalytic membranes. The driving force behind this work was the recognition that the deep oxidation of reactants and products to carbon monoxide and carbon dioxide still takes place resulting in a loss of selectivity and catalytic membranes were studied to determine their abilities to influence this undesirable deep oxidation process. It was found that the best feed configuration was to supply oxygen and an inert diluent to the outer (catalytically inactive) layer of the membrane and the butane to the inner (catalytically active) side of the membrane. For this feed configuration and a M29V/MgO membrane, Alfonso *et al*. reported butane and oxygen conversions of 24.5 % and 79 % respectively and an overall C4 (butenes and butadiene) selectivity of 54.3 %. The operating temperature was 550^{o}C. When the performances of the catalytic-membrane reactor and a fixed-bed

reactor were compared, it was found that for any given conversion the former reactor with the feed configuration described above provided a higher selectivity than the latter.

Ge *et al*. (2003) analysed the effect of incorporating carbon dioxide in the feed stock upon the ODH of *n*-butane over V/MgO catalysts in a fixed-bed reactor. Carbon dioxide is a mild oxidant and Ge *et al*. referred to publications where the ODH of ethane, propane, isobutene and ethylbenzene with CO_2 as an oxidant had been reported. Another claimed advantage for the addition of CO_2 to the feed in the catalytic oxidation of alkanes was the ensuing increase in selectivity and yield

Rubio *et al*. (2003) studied the kinetics of the ODH of *n*-butane on a V/MgO catalyst under anaerobic conditions. Under anaerobic conditions the oxygen for the ODH process comes from the catalyst lattice and as the supply of this oxygen declines during the reaction process so does the oxidation capability of the catalyst. The objective of Rubio *et al*. was to develop a kinetic model for the ODH of *n*-butane under these conditions. While the reactor functioned under anaerobic conditions there were, nevertheless, two types of oxygen present. The first was the lattice oxygen resulting in the presence of butenes, butadiene and carbon oxides, the second being weakly adsorbed oxygen on the surface of the catalyst resulting in the production of carbon oxides. The kinetic model developed by Rubio *et al*. took account of the presence of this second oxygen type. The experimental results of Rubio *et al*. indicated that the selectivity to olefins decreased when the catalyst is more reduced. The existence of both oxygen types, it was claimed by the authors, would help to explain why their results contradicted those of other researchers who found that under anaerobic conditions the more oxidising the conditions, the less selective was the catalyst.

Videl-Michel and Hohn (2004) looked at the effect of crystal size on the ODH of *n*-butane on V/MgO catalysts. The research attempted to answer the question whether metal oxide nanocrystals present in V/MgO catalysts have special catalytic properties for the ODH of *n*-butane, the primary purpose of these nanocrystals being to store and transport oxygen. Some nanocrystals reported by Videl-Michel and Hohn as being investigated by other workers were CeO_2 and TiO_2. The nanocrystals used by Videl-Michel and Hohn were a MgO nanocrystal-supported vanadium, labelled AP V/MgO, and this was compared to that of vanadium supported on conventionally-prepared MgO, labelled CP V/MgO. The reaction products from the experiments included oxygen, carbon monoxide, carbon dioxide, methane, ethane, ethylene, propane, propylene, *n*-butane, butene and pentane. What was surprising was the inability to find any trace of butadiene in the reaction products but it was surmised that small amounts of butadiene might have been hidden by the butene peak from the gas chromatograph. Videl-Michel and Hohn found that the AP and CP varieties showed markedly different characteristics. At similar butane conversions, for AP V/MgO selectivity to butene was higher than while CO, ethylene and propylene selectivities were all lower than for CP V/MgO.

1.2.4 Reactor Designs and Structures

Omtveit *et al*. (1994) described how it was possible to extend the attainable region concept as enunciated by Glasser *et al*. (1987) to cater for a reaction system where there were a large number of species present. The reaction system studied was the steam reforming system, characterised by three reactions and five components. The approach adopted by Omtveit *et al*. to handle the steam reforming reaction was to combine the concept of attainable regions with the theory of reaction invariance. The principle of

the conservation of atoms was an underlying feature of the approach adopted by Omtveit *et al*. The only processes studied by Omtveit *et al*. were mixing and reaction. Omtveit *et al*. found that for the steam reforming reaction and isothermal operation at 1050K their kinetic model predicted a CSTR reactor for maximum CO selectivity or a CSTR followed by a PFR for maximum CO yield. This paper by Omtveit *et al*. seems to have been one of the first, if not the first, to apply attainable region principles to a fairly complex reaction of industrial significance.

Rezac *et al*. (1994) and Rezac *et al*. (1995) are almost identical research papers but nevertheless containing some significant differences. The following synopsis, therefore, is an assessment of both. Rezac *et al*. (1994) and Rezac *et al*. (1995) both discussed the influence of membrane properties in ODH applications. The dehydrogenation of *n*-butane was used as a case study and the reactor configuration was two PFRs in series with an interstage unit incorporating a hydrogen-removal membrane. The concept of removing products selectively, in this instance hydrogen, from an equilibrium-constrained reaction mixture as a means to influence the achievable conversion is well established. The hydrogen-removal membranes used were polyimide-ceramic composite membranes. A noble metal supported on a porous inorganic substrate was used in the PFRs. The operating temperature was 755K. Rezac *et al*. found that at a temperature of 755K and with the addition of a hydrogen-removal membrane, the conversion of *n*-butane could be raised from 22 % (no hydrogen-removal membrane) to 33 % with insignificant hydrocarbon losses. At membrane temperatures below the critical temperature of *n*-butane, 425K, it was found that the membrane's ability to remove hydrogen from the hydrocarbon mixture was adversely affected because of plasticisation of the polymer matrix by the hydrocarbon vapours. Mixed-gas hydrogen/hydrocarbon selectivities were less than 20 but these selectivities improved to values above 75 when the membrane temperature was increased above 453K.

Almost total hydrogen removal was effected and this resulted in an improvement of 11 % for *n*-butane dehydrogenation in the second PFR.

In a comprehensive review Dixon (1999) summarised the status of catalytic inorganic membrane reactors. Because of the plethora of acronyms used to describe different reactor configurations, Dixon presented a table to explain these acronyms. The following Table 1.6 is taken from Dixon (1999), page 43. Alternative acronyms and explanations used by Dixon are shown in parentheses.

Acronym	Explanation
CMR	Catalytic Membrane Reactor
PBMR (IMR, IMRCF)	Packed Bed Membrane Reactor (Inert Membrane Reactor, Inert Membrane Reactor with Catalyst on Feed Side)
PBCMR	Packed Bed Catalytic Membrane Reactor
FBMR	Fluidised Bed Membrane Reactor
FBCMR	Fluidised Bed Catalytic Membrane Reactor
CNMR	Catalytic Non-Permselective Membrane Reactor
SLPCMRS	Supported Liquid-Phase Catalytic Membrane Reactor-Separator
PFR (PBR, FBR)	Plug Flow Reactor (Packed Bed Reactor, Fixed Bed Reactor)

Table 1.6. Explanation of acronyms used by Dixon to describe membrane reactors.

In his review Dixon (1999), *inter alia*, described three well-established areas of application of catalytic membrane reactors : (a) product removal, (b) reactant feed and (c) control of reactant contact in a non-permselective membrane.

A membrane reactor used for the preferential removal of a species basically has a shell-and-tube configuration. The tube is packed with a suitable catalyst through which the reactant feed passes. The shell side either contains an inert sweep gas or is at a lower pressure than that in the tube. The wall of the tube is the membrane. The removal of a product species from the reactants and products has the effect of shifting the reaction further to the product side of the chemical equation in accordance with Le Châtelier's principle and to increase the yield of products by conversion of reactants in excess of that dictated by normal equilibrium conditions. The reactor types for this area of application, referring to Dixon's table above, are PBMR, CMR and PBCMR.

A lower pressure on the shell side is required to obtain the driving force for the transport of the species through the membrane (tube) wall. This lower pressure is obtained either by a total pressure differential or by a difference in species' partial pressure across the tube wall. According to Dixon, neither option is attractive because they consume energy or because they result in a diluted gas stream that is wasteful of the permeating species. There is also for porous membranes the possibility of a flow of the inert gas from the shell side into the tube or the transport of reactants into the shell resulting in their loss for further conversion.

Dixon (1999) commented that product removal reactors have been investigated for decomposition reactions (HI, H_2S) and simple alkane dehydrogenations. Other uses of these reactors have been the cyclohexane dehydrogenation to benzene, the dehydrogenation of ethylbenzene to styrene, dehydrogenation of propane to propylene, methane steam reforming and the water-gas shift reaction. Other researchers have investigated the dehydrogenation of iso-butane and *n*-butane.

The second type of reactor is that where a reactant is added to the stream of reactants and products. Again a shell-and-tube configuration is used and the membrane constitutes a permeable (tube) wall. One reactant is distributed along the length of the reactor and permeates through the membrane wall from the shell-side into the tube of the reactor. This reactor type is used in systems where competing reactions take place, a case in point being the oxidation of a hydrocarbon. In this thesis the oxidative dehydrogenation of *n*-butane has been studied and the competing hydrocarbon products are butenes (all three isomers) and butadiene. In a specific application, the butenes may represent an undesirable side-product, the purpose being to produce the maximum yield of butadiene. The reactants are *n*-butane and oxygen and the planned distributive addition of oxygen along the length of the reactor can influence the yield of the desired produce be it either butene or butadiene.

Dixon pertinently comments that for this type of reactor the apparently-favourable kinetics quoted in the literature might well be unfavourable at the lower partial pressures of the added reactant that seem necessary for the maximisation of the desired product.

Using Dixon's classification, the reactor types used for the addition of a reactant are a PBMR, a CMR and a PBCMR. Another description of this reactor, not specifically identified by Dixon, is that it is a DSR, a Differential Sidestream Reactor.

The materials used to make dense solid oxide membranes require temperatures in excess of 700^{o}C to ensure good oxygen fluxes. V/MgO

membranes can function efficiently at lower temperatures between 500^{o}C and 600^{o}C.

These reactors have been used for the oxidative coupling of methane, the oxidative dehydrogenation of ethane to ethylene, propane to propylene and butane to butene.

The third classification of reactor is one used for the control of reactant contact. The two-sided geometry of a membrane permits the reactants to be contacted in different ways. The addition of two reactants, one from the shell-side of the reactor, the other from the tube side, results in their contact within the membrane. This reactor type has been used where the reactants are in a gaseous and a liquid phase and where it is necessary to keep the reactants apart until they reach the catalyst.

In a multi-phase membrane reactor, the principle is to improve contact between volatile and non-volatile reactants, for example, the hydrogenation of α-methylstyrene to cumene and the hydrogenation of nitrobenzene to aniline. These reactions usually are done in a slurry reactor where a volatile species has to diffuse through the liquid phase to reach the catalyst.

The multi-phase membrane reactor has the liquid on one side and the gas on the other side of a catalytically-impregnated porous ceramic tube. The ability of the gas to diffuse directly through the pores of the membrane to contact the liquid eliminates the need to diffuse through the liquid. Because of the high activity of catalysts used for the hydrogenation of olefins and in Fischer Tropsch reactions, this diffusion through a liquid phase very often constitutes a limiting step.

A reactor where the membrane simply provides a location for the creation of a reaction zone is termed a non-permselective CMR or a CNMR (Dixon's terminology, Table 1.6).

In the case of the reaction A + B → P, A would be fed on the tube side of the reactor and B on the shell side. The regulated partial pressures of A and B cause them to diffuse towards each other inside the membrane where they react. A reaction plane is created for an instantaneous reaction; for slower reactions there exists a reaction zone that by the right adjustment of reaction rate and permeability can be wholly contained within the membrane. This ensures that A does not get into the shell side and that B does not get into the tube side of the reactor. It also is possible to adjust the control parameters so that product P diffuses from the membrane to one side only, usually the tube side which makes the subsequent downstream separation significantly easier.

Dixon comments that this type of membrane reactor ensures that the reactants meet in a strict stoichiometric ratio since at steady-state conditions the diffusion rate of a reactant through the membrane is balanced by its consumption in the reaction. Changing the reactant flow rates tends to shift the zone to satisfy the stoichiometry.

The non-permselective membrane reactor has been used for the Claus reaction, in which gaseous sulphur dioxide is reacted with gaseous hydrogen sulphide to form liquid elemental sulphur and water,

$$SO_2\ (g) + 2H_2S\ (g) \rightarrow 3S\ (l) + 2H_2O\ (g)$$

and the selective catalytic reduction of NO_x with NH_3. Dixon comments that in both of these reactions it is essential to check the passage of one reactant (H_2S, NH_3) from one side of the membrane to the other.

Hou *et al*. (2001) developed a mathematical model to describe the ODH of propane in a DSR, a Differential Side-Stream Reactor. Propane was fed to the tube side of the DSR and the other reactant, oxygen, was distributed along the length of the reactor to the shell side. Oxygen diffused through the wall of the inert permeable membrane to contact the propane. The model developed by Hou *et al*. took account of the radial component of gas velocity from the shell side through the membrane (tube) wall. This work by Hou *et al.* built upon the research of Téllez *et al*. (1999b) for a mathematical model for the ODH of *n*-butane. Hou *et al*. heeded both isothermal and non-isothermal conditions in their model. It was concluded that the radial concentration profiles affect the selectivity and yield attainable in the reactor to an extent not previously foreseen. A propane to oxygen ratio of unity was found to result in the highest yield of propane.

1.2.5 Reaction Kinetics

Frey and Huppke (1933) dehydrogenated paraffins to the corresponding olefins and hydrogen over a catalyst prepared from air-dried chromic oxide gel. The catalyst was used to bring about equilibrium in mixtures of ethane, propane, *n*-butane and isobutene with their dissociation products and to derive the equilibrium constants for every possible reaction of the type $C_nH_{2n+2} \leftrightarrow C_nH_{2n} + H_2$. The experimental temperatures ranged between 623K and 973K. In considering the fractionation of *n*-butane into butenes, Frey and Huppke found that the vol. % of the butene isomers to be *1*-butene

26 %, trans-*2*-butene 43.5 % and cis-*2*-butene 30 %, the balance of 0.5 % being butadiene. At a temperature of 723K, the equilibrium constants for the dissociation of *n*-butane to *1*-butene, trans-*2*-butene and cis-*2*-butene were calculated as 0.042, 0.014 and 0.0087 atm. respectively. Equations for the free energies of dehydrogenation as functions of absolute temperature were derived by Frey and Huppke.

Kearby (1950) used a catalyst, catalyst 1707, originally developed by the Standard Oil Company of New Jersey to study the production of butadiene from butene. In this process it was necessary to keep the partial pressure of butene at a low value and initially this was accomplished by operating under a vacuum but this proved both expensive and unreliable. Accordingly, the partial pressure of butene was reduced by adding an inert diluent to the feed stream. Steam was chosen as the diluent for several reasons, chief among them being its ease of removal by condensation from the products and its capability to reduce carbon deposition. Catalyst 1707 emerged as a result of extensive research to find a catalyst capable of producing butadiene by the dehydrogenation of butene in the presence of steam and at the lowest temperature range, 850K to 950K, dictated by equilibrium considerations. At a temperature of 922K, atmospheric pressure, and a steam:feed volume ratio of 14:1, Kearby reported a total conversion of butene of 38 %, 28 % to butadiene. The selectivity to butadiene was 74 %. At a reduced temperature, 906K, and a steam:feed volume ratio of 7:1,the total butene conversion was 25 % of which 21 % represented butadiene. The selectivity to butadiene was 82 %.

Kearby found that the selectivity to butadiene decreased with an increase in the percentage of butene reacted over the 1707 catalyst. The statement is made that the production of carbon dioxide is ten times that of carbon monoxide but no experimental evidence is presented for this assertion. It

was claimed that the CO_x formed during the dehydrogenation process over the 1707 catalyst was the result of steam's reacting with carbon deposited on the catalyst.

When *n*-butane was dehydrogenated over the 1707 catalyst, the total conversion was 9.6 % of which 1.2 % was to butadiene. The selectivity to butadiene was 13 %.

Happel *et al*. (1966) used the catalytic dehydrogenation of butane and butenes to investigate the existence and magnitude of the stoichiometric step for a reversible reaction. According to the authors, the rate-determining step of a reversible reaction can be linked to the stoichiometric number of this step, a number that directly relates the overall kinetics to the chemical equilibrium constant. The catalyst used in the experiments was a chrome-alumina catalyst. The stoichiometric number, according to Happel *et al.*, is the number of times that any elementary step in a sequence occurs for each time the overall reaction, as represented by the overall chemical equation, occurs once. In the course of their experiments, Happel *et al*. found that the formation of coke was very much higher when the feed was butene and butadiene than it was for butane. This led to the assumption that in the catalytic dehydrogenation of butane, coke formation came about through the products of reaction and not from the reactant. Happel *et al.* produced kinetic equations for the dehydrogenation of butane and butene and for the hydrogenation of butadiene and concluded that a stoichiometric number of 2 was appropriate for the dehydrogenation of butane and butene.

Itoh and Govind (1989) presented simulation results for a palladium membrane reactor system with an exothermic oxidation reaction on the separation side and dehydrogenation of *1*-butene on the reaction side of the

membrane. Itoh and Govind listed the potential advantages of a membrane reactor over a conventional reactor as a) the integration of reaction and separation into a single process, b) the enhancement of thermodynamically limited or product-inhibited reactions, c) controlled reaction rates due to short contact time, d) reduced reaction temperatures, thereby minimising side reactions (catalyst fouling) and heating costs and e) the controlled surface concentration of reactants (the membrane functioning as the catalyst), thereby increasing the yield and selectivity. However, the development of membrane reactors is dependent upon 1) the availability of membranes that can withstand temperatures in excess of 500K, 2) the development of membranes that manifest good permeability and selectivity for the reaction products and 3) the development of membrane systems to permit effective heat transfer to or from the reaction zone.

In their simulation model for the dehydrogenation of *1*-butene, Itoh and Govind used the kinetic data presented by Happel *et al.* (1966). Itoh and Govind's reactor appears to have been a simple flat plate type containing a partition, a palladium membrane. Palladium can withstand high temperatures, is only permeable to hydrogen and exhibits catalytic properties for oxidation and dehydrogenation reactions. The reactor was divided into two sections by the membrane, a reaction section that was packed with a catalyst and in which the dehydrogenation of *1*-butene occurred and a separation section in which hydrogen from the dehydrogenation of *1*-butene in the reaction section reacted with a stream of air to form water vapour. As the hydrogen permeated through the palladium membrane wall and reacted with oxygen in the air, its partial pressure was reduced and so facilitated the flow of further hydrogen through the membrane wall.

Both isothermal and adiabatic conditions were considered by Itoh and Govind. The oxidation of hydrogen in the separation section is an exothermic process and the liberated heat flows from the separation section through the palladium membrane into the reaction section facilitating the dehydrogenation of *1*-butene which is an endothermic reaction. The juxtaposition of an exothermic reaction and an endothermic reaction was found by Itoh and Govind to be an extremely efficient heat management process and resulted in the complete conversion of *1*-butene in a short reactor length.

Oyama *et al*. (1990) studied the kinetics of the oxidation of ethane on a vanadium oxide, V_2O_5/SiO_2, catalyst. The authors commented that the main purpose for the selective oxidation of higher alkanes, propane, butane and pentanes, was to serve as substitutes for more expensive olefin feedstocks. In the case of lower alkanes, chiefly methane, research into selective oxidation has been driven by the discovery of large quantities of natural gas. The oxidation of ethane to produce ethylene had received scant attention because there existed a commercially practical route to this product via non-oxidative cracking. Ethane, however, is a plentiful constituent of natural gas and is the primary product from the conversion of methane by oxidative coupling resulting in Oyama *et al*.'s finding the necessary motivation for their research.

Ethylene was the most abundant product from the oxidation of ethane. Oyama *et al*. investigated the oxidation of ethylene to garner a better understanding of the ethane oxidation reaction. The following reaction network was envisaged by Oyama *et al*. for the oxidation of ethane.

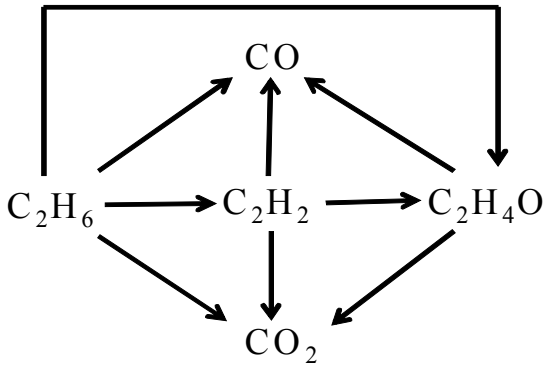


Figure 1.1. Reaction mechanism for the oxidation of ethane to ethylene and acetaldehyde from Oyama et al. (1990).

Apart from developing a series of kinetic equations for the oxidation of ethane, Oyama *et al*. concluded that the adjusting of the partial pressure of water vapour provided the best way to control the product selectivity.

Dejoz *et al*. (1997) investigated the ODH of *n*-butane in a fixed-bed reactor over a vanadium oxide catalyst supported on a heat-treated Al/Mg hydrotalcite to assess the effect of the reaction variables upon the selectivity to ODH products. The maximising of olefins selectivity is important to offset the deep oxidation of *n*-butane under the thermodynamically advantageous conditions that prevail. Experimental temperatures ranged from 773K to 823K. Yields and conversions of *1*-butene, 2-butenes (trans and *cis*), butadiene, carbon monoxide and carbon dioxide were plotted against butane conversion as well as reaction rates as a function both of butane and oxygen partial pressures. Kinetic expressions were derived for the circumstances where the partial pressures of oxygen and butane separately were held constant in the reactor. Dejoz *et al.* concluded that whereas butadiene can be produced directly from butane its production stems mainly from the ODH of butenes. It also was found that the selectivity to olefins was influenced by the reaction temperature.

Téllez *et al*. (1999a) derived kinetic rate equations for the ODH of *n*-butane on V/MgO catalysts to include the oxidation of all C_4 hydrocarbons present as a reactant or a product. The rate equations were established independently and then were validated by actual experiments in a tubular quartz fixed-bed reactor (FBR). The experimental temperatures ranged from 748K to 823K. The derived reaction rates were functions of the partial pressures of oxygen and the relevant hydrocarbon. Good correlation between the predicted rate equations and the experimental results was found for conversions up to 40 %. (Equations 27 and 28 of this reference were incorrectly represented. In equation 27 the expression $k_{12}PO_2$ in the numerator and denominator should be multiplied by 2 and in equation 28 the expression $k_{13}PO_2$ in the numerator and denominator also should be multiplied by 2).

Téllez *et al*. (1999b) used the ODH of *n*-butane over a V/MgO catalyst to simulate the performance of an inert membrane reactor (IMR). The reactor was a shell-and-tube one, the tube consisting of an inert ceramic walled membrane. Unlike a fixed-bed reactor in which the butane and oxygen would be co-fed to the reactor, in the IMR used by Téllez *et al*. the oxygen was distributed along through the shell along the length of the reactor and contacted the butane feed and products by diffusion through the membrane wall. Téllez *et al*. in this research paper simulated a FBR by the simple expedient of co-feeding oxygen with *n*-butane to the tube inlet only and by not supplying it to the shell side of the reactor. Good agreement existed between the predicted and actual characteristics of both a FBR and an IMR. An important aspect of this work was the determination of the extent of oxidation of the selective and non-selective catalyst sites. Kinetic rate equations and parameters were derived for the ODH of all five C_4 hydrocarbons, butane, the three isomers of butene and butadiene.

Soler *et al*. (2001) studied a fluidised-bed reactor with a V/MgO catalyst for the ODH of *n*-butane. In this reactor, two separate zones of activity were present, a region where catalyst oxidation occurred and a region where catalyst reduction took place. Butane was supplied to the top of the reactor and distributed down through the reactor by means of a movable inlet pipe. Oxygen was supplied at the bottom of the reactor through a distribution plate. The region above the movable butane inlet was the reduction zone and below the inlet was the oxidation zone. Catalyst in suspension is lifted upwards by the oxygen stream and is oxidised in the process. Depending upon the hydrodynamics and reactor geometry all this oxygen could be depleted in this oxidation zone in regenerating the catalyst lattices. After the catalyst has reached the inlet plate for butane the lattice oxygen begins to be reduced by interaction with the hydrocarbon. This reduction continues until, based upon the hydrodynamics of the system, it descends to the bottom of the reactor where the oxidation process begins again. An important aspect of the fluidised-bed reactor is the oxygen for the ODH of the *n*-butane is lattice oxygen and not gas-phase oxygen. Soler *et al*. found that a fluidised-bed reactor, under suitable operating conditions, can increase the selectivity and the yield to olefins, especially butadiene. The apparent advantages of this type of reactor include the temperature homogeneity through the bed, a significant advantage when considering highly-exothermic and temperature-sensitive reactions. However, the problems associated with scale-up from laboratory size to an industrial scale continue to limit the applicability of fluidised-bed reactors.

Pedernera *et al*. (2002) developed a kinetic model to simulate a catalytic-membrane reactor for the ODH of *n*-butane. The membrane incorporated a V/MgO catalyst. Segregated reactant feeds were applied to the shell-and-tube reactor configuration. The reactants each diffused through a two-zone

membrane in opposing directions and contacted each other at the catalytic interface. The membrane contained a diffusion layer and a V/MgO active layer. The reactor was such that the reactant feeds could be adjusted to accommodate either a co-feeding or a segregated feed system. The experimental results demonstrated that the partial pressure of oxygen in contact with the catalyst is the chief factor in influencing selectivities and that high oxygen partial pressures are deleterious to selectivity.

Assabumrungrat *et al*. (2002) compared the theoretical performances of a porous membrane reactor and a fixed-bed reactor for the ODH of *n*-butane using a V/MgO catalyst. In the porous membrane, oxygen was supplied to the shell-side of a reactor and introduced to the other reactant through an inert porous membrane. Assabumrungrat *et al*. found that a porous membrane reactor in which the oxygen feed distribution was controlled could result in a lower hot-spot temperature than that in a fixed-bed reactor. The rate expressions and kinetic parameters used by Assabumrungrat *et al*. were taken from Téllez *et al*. (1999a). Selectivity to C_4 hydrocarbons was found to increase with operating temperature. There were optimum feed ratios of air and *n*-butane for both the fixed-bed and the membrane reactors.

Rubio *et al*. (2002) studied the oxidation of *n*-butane to an unsaturated carbonyl compound, maleic anhydride $C_4H_2O_3$, in a two-zone fluidised bed reactor. The configuration and characteristics of the reactor were similar to that used by Soler *et al*. (2001). Rubio *et al*. discussed the importance of minimising the deep oxidation of a saturated hydrocarbon to enhance the selectivity and yield of the desired product. According to Rubio *et al*. the ODH of *n*-butane to olefins, despite its attraction to research workers, was not economically viable at the time; the only economically-viable process in which *n*-butane was oxidised catalytically on a large scale to more valuable products was to produce maleic anhydride. A perceived advantage of a two-

zone fluidised-bed reactor was the avoidance of having to constrain the concentration of *n*-butane when it is co-fed with air to prevent the formation of an explosive mixture. In a fixed-bed reactor this *n*-butane limitation is 1.8 vol. % and 4 vol. % in a single-zone fluidised-bed reactor. Rubio *et al*. concluded that, under similar conditions, the performance of the two-zone fluidised-bed reactor was superior to the fluidised-bed reactor with co-feeding of reactants.

Cortés *et al*. (2004) developed kinetic expressions for the ODH of *n*-butane over a doped V/MgO catalyst under anaerobic conditions. The experiments were performed in a fluidised-bed reactor in which catalyst lattice oxygen was consumed during the ODH process. Doping additives, Fe, Co and Mo, were added to the V/MgO catalyst and their effect upon yield and selectivity was assessed. Doping the V/MgO catalyst with 1 % Fe had the effect of increasing the *n*-butane oxidation constant to carbon monoxide and carbon dioxide and brought about a decrease in the formation of butadiene from *n*-butane as well as a reduction in the deep oxidation of butadiene, a decrease in butadiene yield and a larger yield of butene. The overall result of the addition of 1 % Fe to the V/MgO catalyst was an improvement in the selectivity to butenes and butadiene together.

1.3 Objective of the Thesis

The research work for this thesis had several objectives.

- To apply the principles of the Attainable Region (AR) concept to identify the theoretical maximum yields of hydrocarbon products achievable from the ODH process, to develop an understanding of those control parameters that affect these yields.

- Identify the reactor types and configurations necessary for maximising the yields of these hydrocarbon products.

- Develop a graphical technique for displaying the relationship between the feed to a reactor, the desired product yield and the relevant residence time in an IMR.

- Illustrate the principle that, under certain conditions and for certain chemical reactions, a series combination of a CSTR and a specific type of PFR, to wit an IMR (or in truth what conventionally is termed a differential side-stream reactor) may require a lesser overall residence time to achieve a specified yield of product than were a single IMR used.

- Apply the Recursive Convex Control (RCC) policy to confirm the findings of Chapter 2 and Chapter 3 of this thesis.

- Confirm the supposition that it was unlikely that a candidate Attainable Region for a chemical reaction could be extended further by a series combination of two or three reactors (Chapter 7).

- Study the effect of the geometric profile in mass concentration sub-space upon residence time for a hydrocarbon feed stock and the desired hydrocarbon product.

- Investigate the effect upon maximum yield of hydrocarbons of a series combination of FBR and an IMR and the reactor configurations required to attain these maxima (Chapter 8).

1.4 Outline of the Thesis

To avoid a possible misunderstanding, I wish to explain that an inert membrane reactor (IMR) in which one of the reactants is added along the length of the reactor also can be styled a differential side-stream reactor (DSR). The research papers that provided the kinetic data for the ODH of *n*-butane made reference to an inert porous membrane reactor for which I applied the acronym IMR. This term was used in my research papers published by *Industrial and Engineering Chemistry Research* (Chapter 2 and Chapter 3). Instead of this acronym I could equally have used that for the alternative description of a differential side-stream reactor, DSR. Consequently, in this thesis both acronyms are used to describe the same reactor, an inert porous membrane reactor.

With the reporting by Téllez (1999a and 1999b) of reaction rates and kinetic data for the oxidative dehydrogenation (ODH) of *n*-butanes to butene and butadiene in inert porous membrane reactors, it became possible to examine a specific chemical reaction of industrial interest. This particular reaction was picked for AR analysis for the following reasons. It is a reaction of considerable industrial and economic significance, secondly it was perceived to possess a degree of complexity with a potential of ten different product and reaction species and, apart from the work done by Omtveit *et al*. (1994) for the steam reforming system (three reactions and five components) no attainable region analyses had hitherto been attempted on a reaction network with the degree of complexity possessed by the ODH of *n*-butane. Another reason was the apparent high quality of the kinetic data for the ODH of *n*-butane but this not to belittle kinetic data for other reactions. The final factor was the personal challenge presented in tackling something new and highly complex but, I must add, the former is a feature of all academic research work.

Téllez (1999a and 1999b) developed equations for the rate expressions associated with the ODH of *n*-butane, the three isomers of butene (*1*-butene, trans-*2*-butene and cis-*2*-butene) and butadiene. Values of the respective rate constants also were provided. The experiments by Téllez (1999a and 1999b) were conducted in an inert porous membrane reactor operating at atmospheric pressure and within a feed temperature range of 748K to 823K.

In a more recent publication, Assabumrungrat (2002) compared the performance of a porous membrane reactor with that of a conventional fixed-bed reactor in the oxidative dehydrogenation of *n*-butane. The porous membrane reactor was used to add oxygen to the hydrocarbons in a controlled manner. By virtue of the pressure differential across the membrane, all reactants and products remained within the tubes of the reactor and could not diffuse into the reactor shell. Assabumrungrat (2002), in developing his mathematical models, used the kinetic and experimental data developed by Téllez (1999a and 1999b).

In the oxidative dehydrogenation of *n*-butane, Téllez (1999a and 1999b) postulated the following reaction mechanism.

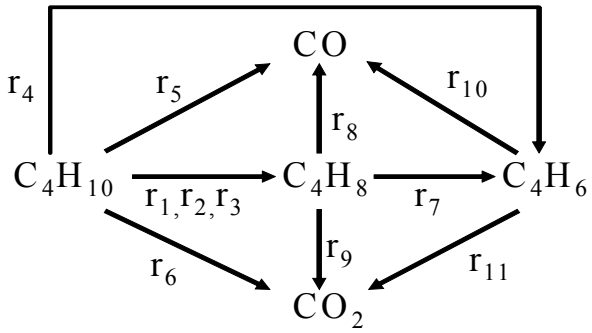


Figure 1.2. Reaction mechanism for the oxidative dehydrogenation of *n*-butane to butene and butadiene.

In Figure 1.2, the rates of reaction for the respective reactions are shown as r_1, r_2, r_3 etc. Including oxygen and water, there can be up to nine different substances present including the three isomers of butene, *1*-butene, trans-*2*-butene and cis-*2*-butene. Should sufficient oxygen be present and the reactions are permitted to proceed to equilibrium, all the hydrocarbons will be oxidised leaving but carbon monoxide, carbon dioxide, water and, in some instances, residual oxygen.

In Figure 1.2, the three isomers, *1*-butene, trans-*2*-butene and cis-*2*-butene have been lumped together as C_4H_8 (butene) in reactions 7, 8 and 9.

Using the kinetic data developed by Téllez (1999a and 1999b), the techniques used to identify a candidate Attainable Region for a particular chemical reaction were applied to the oxidative dehydrogenation of *n*-butane to butene and butadiene. One objective of this research was to establish the operating conditions necessary to maximise the yields of these products from a fixed feed of *n*-butane and *1*-butene and, in so doing, to identify a candidate AR for the systems butane:butadiene and butene:butadiene.

Téllez (1999a and 1999b) identified the independent balanced chemical reactions involved in the ODH of butane and their associated rate expressions as :

Reaction	Rate Expression
Oxidation of *n*-Butane	
(1). $C_4H_{10} + ½O_2 \rightarrow$ *1*-$C_4H_8 + H_2O$	$r_1 = k_1 * P_{C4H10} * \theta_0$
(2). $C_4H_{10} + ½O_2 \rightarrow$ Trans-*2*-$C_4H_8 + H_2O$	$r_2 = k_2 * P_{C4H10} * \theta_0$
(3). $C_4H_{10} + ½O_2 \rightarrow$ Cis-*2*-$C_4H_8 + H_2O$	$r_3 = k_3 * P_{C4H10} * \theta_0$
(4). $C_4H_{10} + O_2 \rightarrow C_4H_6 + 2H_2O$	$r_4 = k_4 * P_{C4H10} * \theta_0$
(5). $C_4H_{10} + {}^{9}/_{2}O_2 \rightarrow 4CO + 5H_2O$	$r_5 = k_5 * P_{C4H10} * \lambda_0$
(6). $C_4H_{10} + {}^{13}/_{2}O_2 \rightarrow 4CO_2 + 5H_2O$	$r_6 = k_6 * P_{C4H10} * \lambda_0$
Oxidation of *1*-Butene	
(7). *1*-$C_4H_8 + ½O_2 \rightarrow C_4H_6 + H_2O$	$r_7 = k_7 * P_{C4H8} * \theta_0$
(8). *1*-$C_4H_8 + 4O_2 \rightarrow 4CO + 4H_2O$	$r_8 = k_8 * P_{C4H8} * \lambda_0$
(9). *1*-$C_4H_8 + 6O_2 \rightarrow 4CO_2 + 4H_2O$	$r_9 = k_9 * P_{C4H8} * \lambda_0$
Oxidation of Butadiene	
(10). $C_4H_6 + {}^{7}/_{2}O_2 \rightarrow 4CO + 3H_2O$	$r_{10} = k_{10} * P_{C4H6} * \lambda_0$
(11). $C_4H_6 + {}^{11}/_{2}O_2 \rightarrow 4CO_2 + 3H_2O$	$r_{11} = k_{11} * P_{C4H6} * \lambda_0$
Oxidation and Reduction of Catalyst Sites	
(12). $O_2 + 2X \rightarrow 2X_0$	$r_{12} = k_{12} * P_{O2} * (1 - \theta_0)$
(13). $O_2 + 2Z \rightarrow 2Z_0$	$r_{13} = k_{13} * P_{O2} * (1 - \lambda_0)$

Table 1.7. Chemical reactions and rate expressions for the oxidative dehydrogenation of *n*-butane to butene and butadiene.

In Table 1.7, θ_0 and λ_0 refer to the oxidation of catalyst sites and are defined as :

Selective oxidation catalyst sites

$$\theta_0 = 2k_{12}*p_{oxygen} / (2k_{12}*p_{oxygen} + (k_1 + k_2 + k_3 + 2*k_4)*p_{butane} + k_7*p_{butenes})$$

Non-selective oxidation catalyst sites

$$\lambda_0 = 2k_{13}*p_{oxygen} / (2k_{13}*p_{oxygen} + (9k_5 + 3k_6)*p_{butane} + (8k_8 + 2k_9)*p_{butenes} + (7k_{10} + 11k_{11})*p_{butadiene})$$

X and Z refer to the reduced active sites of the catalyst.

X_0 and Z_0 refer to the oxidised active sites of the catalyst.

p_i is the partial pressure of the subscripted species, *i*, atm.

The rate expressions presented by Téllez (1999a and 1999b) indicate a dependency upon the partial pressures of butane, butene and butadiene and the selective (θ_0) and non-selective (λ_0) oxidation catalyst sites respectively. The latter two, in turn, are functions of the partial pressure of oxygen and of the partial pressures of butane, butene and butadiene.

The kinetic data for the system *n*-butane:butenes:butadiene used in this thesis were taken from Téllez (1999a and 1999b) and from Assabumrungrat (2002) and are shown in Table 1.8

Reaction	Rate Constant, k_{io}, mol/kg.sec	Activity Coefficient, E_{ai}, kJ/mol
$C_4H_{10} + ½O_2 \rightarrow$ *1*-$C_4H_8 + H_2O$	62.33 x 10^{-3}	144.9
$C_4H_{10} + ½O_2 \rightarrow$ Trans-*2*-$C_4H_8 + H_2O$	32.83 x 10^{-3}	142.7
$C_4H_{10} + ½O_2 \rightarrow$ Cis-*2*-$C_4H_8 + H_2O$	39.67 x 10^{-3}	139.1
$C_4H_{10} + O_2 \rightarrow C_4H_6 + 2H_2O$	30.83 x 10^{-3}	148.5
$C_4H_{10} + {}^9/_2O_2 \rightarrow 4CO + 5H_2O$	9.17 x 10^{-3}	175.5
$C_4H_{10} + {}^{13}/_2O_2 \rightarrow 4CO_2 + 5H_2O$	25.83 x 10^{-3}	138.4
$C_4H_8 + ½O_2 \rightarrow C_4H_6 + H_2O$	685.0 x 10^{-3}	164.7
$C_4H_8 + 4O_2 \rightarrow 4CO + 4H_2O$	32.33 x 10^{-3}	146.2

Reaction	Rate Constant, k_{io}, mol/kg.sec	Activity Coefficient, E_{ai}, kJ/mol
$C_4H_8 + 6O_2 \rightarrow 4CO_2 + 4H_2O$	115.67 x 10^{-3}	107.2
$C_4H_6 + {}^{7}/_{2}O_2 \rightarrow 4CO + 3H_2O$	118.17 x 10^{-3}	146.6
$C_4H_6 + {}^{11}/_{2}O_2 \rightarrow 4C\ O_2 + 3H_2O$	435 x 10^{-3}	102.0
$O_2 + 2X \rightarrow 2X_0$	2 995 x 10^{-3}	114.5
$O_2 + 2Z \rightarrow 2Z_0$	3 255 x 10^{-3}	5.5

Table 1.8. Rate constants and activity coefficients from Téllez (1999a and 1999b) and Assabumrungrat (2002).

The rate constant, $k_i = k_{io} \exp^{-(Eai/R)(1/T - 1/T0)}$

Where $T_0 = 773K$.

The equations for rates of formation, r_1 *to* r_9, of the several species are :

<u>*n*-Butane</u>

$r_1 = -((k_1 + k_2 + k_3 + k_4)*\theta_0 + (k_5 + k_6)*\lambda_0)*p_{butane}$

<u>Oxygen</u>

$a_1 = ((k_1 + k_2 + k_3 + k_4)*\theta_0 + (9k_5 + 13k_6)*\lambda_0)*0.5*p_{butane}$

$a_2 = (k_7*\theta_0 + 8k_8*\lambda_0)*0.5*p_{butenes} + 12*0.5*k_9*p_{butenes}*\lambda_0$

$a_3 = (7*k_{10} + 11*k_{11})*0.5*\lambda_0*p_{butadiene}$

$r_2 = -(a_1 + a_2 + a_3)$

<u>*1*-Butene</u>

$r_3 = (k_1*p_{butane} - k_7*p_{1\text{-}butene})*\theta_0 - (k_8 + k_9)*p_{1\text{-}butene}*\lambda_0$

Trans-*2*-Butene

$$r_4 = (k_2 * p_{butane} - k_7 * p_{trans\text{-}2\text{-}butene}) * \theta_0 - (k_8 + k_9) * p_{trans\text{-}2\text{-}butene} * \lambda_0$$

Cis-*2*-Butene

$$r_5 = (k_3 * p_{butane} - k_7 * p_{cis\text{-}2\text{-}butene}) * \theta_0 - (k_8 + k_9) * p_{cis\text{-}2\text{-}butene} * \lambda_0$$

Butadiene

$$r_6 = (k_4 * p_{butane} + k_7 * p_{butenes}) * \theta_0 - (k_{10} + k_{11}) * p_{butadiene} * \lambda_0$$

Carbon Monoxide

$$r_7 = 4(k_5 * p_{butane} * \lambda_0 + k_8 * p_{butenes} * \lambda_0 + k_{10} * p_{butadiene} * \lambda_0)$$

Carbon Dioxide

$$r_8 = 4(k_6 * p_{butane} * \lambda_0 + k_9 * p_{butenes} * \lambda_0 + k_{11} * p_{butadiene} * \lambda_0)$$

Water

$$r_9 = (k_1 + k_2 + k_3 + 2k_4) * p_{butane} * \theta_0 + 5(k_5 + k_6) * p_{butane} * \lambda_0 + (k_7 * p_{butenes} * \theta_0 + 4(k_8 + k_9) * p_{butenes} * \lambda_0 + 3(k_{10} + k_{11}) * p_{butadiene} * \lambda_0)$$

In these equations, p refers to the partial pressure of the subscripted hydrocarbon and the rate constants k_1 to k_{13} are those shown in Table 1.8. θ_0 and λ_0, the selective and non-selective oxidation catalysts sites, are as defined earlier.

N-butane (or *1*-butene) and oxygen are supplied together at the tube inlet of a PFR at atmospheric pressure and at a temperature of 773K. The PFR tubes are packed with the V/MgO catalyst. In a shell and tube IMR, the hydrocarbon and oxygen, at atmospheric pressure and at a temperature of 773K, are also fed to the tube inlet but a side stream of oxygen at a pressure of up to 6 bar inside the shell diffuses through an inert porous inorganic membrane along the length of the reactor to react with the hydrocarbons inside the tubes which are packed with catalyst. The porous membrane constitutes the permeable barrier between the oxygen and the hydrocarbon. Téllez (1999a and 1999b) used a SiO_2 – modified α - Al_2O_3 membrane to distribute oxygen to a PFR containing a V/MgO catalyst (24 wt % of V_2O_5) inside the tubes. The same catalyst was used in both the PFR and IMR reactors.

Because the partial pressure of oxygen influences the carbon mass fractions in the products, it was adopted as the primary independent control variable. In presenting the results of the mathematical analyses, the carbon mass fraction of carbon in the reactants and products was used since the atoms of carbon remain constant whereas the number of moles increases as the ODH reaction proceeds. In addition, mass fraction variables, unlike partial pressures, obey linear mixing rules. Linear mixing has the advantage of providing insight into the characteristics of the AR, one of which is that there cannot be a concavity at any point of the AR's profile. Were such a concave region to exist, it could be removed and transformed into a convex (i.e. a non-concave) region through a process of by-pass and mixing and, in so doing, extend the perimeter of the previous AR further and thus creating a new enlarged AR. Also by using carbon mass fractions, we can add oxygen without affecting the results and without having to consider the increase in the number of moles as the reaction proceeds.

In undertaking research into the ODH of butane and butene in the context of AR principles, the three chemical reactions shown in Figure 1.2 were identified. These are :

- The ODH of *n*-butane to form all three isomers of butene, *1*-butene, trans-*2*-butene and cis-*2*-butene. In their subsequent oxidation to butadiene, carbon monoxide, carbon dioxide and water, all three isomers were lumped together.
- The ODH of *n*-butane to form butadiene
- The ODH of *1*-butene to form butadiene

For each of these reactions, the following reactor scenarios were investigated :

- An isothermal PFR in which the reactor contents were kept at a constant temperature. For this scenario, the feed to the reactor consisted of either *n*-butane or *1*-butene together with oxygen. The concentration of oxygen was allowed to diminish through the normal ODH process. The isothermal temperature selected for these analyses was 773K.

- An isothermal IMR in which the reactants and products were kept at a constant temperature. The feed to the reactor consisted of either *n*-butane or *1*-butene together with oxygen. The partial pressure of oxygen in the stream was kept at a constant value equivalent to that in the feed by injecting fresh oxygen along the length of the reactor. The isothermal temperature selected was 773K.

Unless otherwise stated, all concentrations are expressed in carbon mass fractions.

In this thesis, the distinction is made between a fixed-bed reactor (FBR), a plug flow reactor (PFR) and an inert porous membrane reactor (IMR). All three reactors are shell-and-tube reactors with the V/MgO catalyst packed inside the tubes. The initial hydrocarbon feed and oxygen are supplied to the tube inlets of these reactors. Only in the case of the IMR is pressurised oxygen fed to the shell side and allowed to diffuse through the walls of the tubes. In the FBR and PFR configurations, the initial oxygen partial pressure is permitted to wane through the normal oxidative process whereas in the IMR, the additional oxygen injected along the length of the reactor maintains a constant partial pressure of oxygen equal to its initial feed value in the stream of reactants and products.

Two manuscripts, based upon the work in this thesis, have been published in *Industrial and Engineering Chemistry Research*. One of these manuscripts (see Chapter 2) was published in March 2004 and the second manuscript (see Chapter 3) in April 2006. In these manuscripts, the term Fixed Bed Reactor (FBR) has been used to describe a PFR.

A further two manuscripts have been published in *Chemical Engineering Progress*. The dates of publication of these manuscripts were March and April 2006. These two submissions are contained in Chapter 4 and Chapter 5 of this thesis.

In Chapter 6 of this thesis I present a paper that has been submitted for publication to *Industrial and Engineering Chemistry Research.* The date of publication has yet to be determined. The content of this paper relates to the application of the Recursive Convex Control (RCC) concept to the ODH of *n*-butane and *1*-butene, the purpose being to confirm the research findings

described in Chapter 2 and Chapter 3. In addition, the RCC concept was used to derive from first principles the idealised reactor configuration to attain the maximum yields of hydrocarbon products from the ODH process.

Consequently, the body of my thesis has been structured as a series of chapters, three of which contain the manuscripts published and submitted for publication in *Industrial and Engineering Chemistry Research* and two already published in *Chemical Engineering Progress*. These manuscripts are shown in my thesis as they have been published or submitted for publication. Each of these five chapters is wholly contained and can be read with but reference to the literature cited without having to refer to another chapter. There was additionally a considerably body of my research work over the last four years which has not been included in this thesis. From this total body of work, I have included in Chapter 7 what I regarded as one of the more interesting of my research findings, namely the practical implementation of reactors for the oxidative dehydrogenation of *n*-butane to butadiene.

In Chapter 8, I have studied the yields of hydrocarbon product from an IMR and a FBR when these two reactors are linked sequentially. Chapter 8 is an extension of the work reported in the previous chapter, Chapter 7. All three chemical reactions were studied under conditions when each reactor in turn was the leading unit. It was found that the geometric mass concentration profiles of the hydrocarbon reactant and product have a significant influence on the yields of product, the residence times for the maximum yields of this product and the reactor configurations required for these maxima.

1.5 Numerical and Integration Methods

The Matlab® ordinary differential equation solver, ode23t, was used to integrate the rate expressions. The Matlab® description of this solver is :

"ODE23t is a function handle that evaluates the right side of the differential equations. It is used to solve systems of equations in the form ***y' = f(t, y)*** *from time* T_0 *to* T_{Final} *with initial conditions* Y_0 *or to handle problems that involve a mass matrix,* ***M(t, y)y' = f(t, y)****. ODE23t can solve problems with a mass matrix that is singular, i.e., differential-algebraic equations (DAEs)".*

"Commonly used properties of the ode23t function handler include a scalar relative error tolerance, 1e-3 by default, and a vector of absolute error tolerances, 1e-6 by default".

All data reported in this thesis were derived through the application of Matlab® R2006a, Version 7.2.0.232 and its earlier Version 6, Release 13

1.6 Literature Cited

Abraham, T.K., Feinberg, M., (2004), Kinetic bounds on attainability in the reactor synthesis problem, *Industrial and Engineering Chemistry Research*, vol. 43, pp. 449-457.

Alfonso, M.J., Menéndez, M., Santamaría, J., (2002), *Chemical Engineering Journal*, vol. 90, pp. 131-138.

Assabumrungrat, S., Rienchalanusarn, T., Praserthdam, P., and Goto, S., (2002) Theoretical study of the application of porous membrane reactor to oxidative dehydrogenation of *n*-butane, *Chemical Engineering Journal*, vol. 85, pp. 69-79.

Cavini, F., Trifirò, F., (1997), Some aspects that affect the selective oxidation of paraffins, *Catalysis Today*, vol 36, pp. 431-439.

Chaar, M.A., Patel, D., Kung, M.C., Kung, H.H., (1987), Selective oxidative dehydrogenation of butane over V/MgO catalysts, *Journal of Catalysis*, vol. 105, pp. 483-498.

Chambers (1966), *Chambers's Twentieth Century Dictionary*, Edited by William Geddie, W. & R. Chambers, Edinburgh and London

Cortés, I., Rubio, O., Herguido, J., Menéndez, M., (2004), Kinetics under dynamic conditions of the oxidative dehydrogenation of butane with doped V/MgO, *Catalysis Today,* vol. 91-92, pp. 281-284.

Dejoz, A., LópezNieto, J.M., Melo, F., Vázquez, I., (1997), Kinetic study of the oxidation of *n*-butane on vanadium oxide supported on Al/Mg mixed oxide, *Industrial and Engineering Chemistry Research*, vol. 36, pp. 2558-2596.

Dixon, A.G., (1999), Innovations in Catalytic Inorganic Membrane Reactors, *Catalysis, vol. 14, The Royal Society of Chemistry,* pp. 40-92

Feinberg, M., and Hildebrandt, D., (1997), Optimal reactor design from a geometric viewpoint – I. Universal properties of the attainable region, *Chemical Engineering Science*, vol. 52, no. 10, pp. 1637-1665.

Feinberg, M., (1999), Recent results in optimal reactor synthesis via attainable region theory, *Chemical Engineering Science*, vol. 54, pp. 2535-2543.

Feinberg, M., (2000a), Optimal reactor design from a geometric viewpoint – Part II. Critical side stream reactors, *Chemical Engineering Science*, vol. 55, pp. 2455-2479.

Feinberg, M., (2000b), Optimal reactor design from a geometric viewpoint – Part III. Critical CFSTRs, *Chemical Engineering Science*, vol. 55, pp. 3553-3565.

Frey, F.E., Huppke, W.F., (1933), Equilibrium dehydrogenation of ethane, propane and the butanes, *Industrial and Engineering Chemistry*, vol. 25, no. 1, pp. 54-59.

Ge, S.H., Liu, C.H., Wang, L.J., (2001), Oxidative dehydrogenation of butane using inert membrane reactor with non-uniform permeation pattern, *Chemical Engineering Journal*, vol. 84, pp. 497-502.

Ge, S., Liu, C., Zhang, S., Li, Z., (2003), Effect of carbon dioxide on the reaction performance of oxidative dehydrogenation of *n*-butane over a V/MgO catalyst, *Chemical Engineering Journal*, vol. 94, pp. 121-126.

Glasser, D., Hildebrandt, D., Crowe, C., (1987), A geometric approach to steady flow reactors: the attainable region and optimisation in concentration space, *American Chemical Society*, pp. 1803-1810.

Godorr, S., Hildebrandt, D., Glasser, D., McGregor, C., (1999), Choosing optimal control policies using the attainable region approach, *Industrial and Engineering Chemistry Research*, vol. 38, no. 3, pp. 639-651.

Happel, J., Blanck, H., Hamill, T.D., (1966), Dehydrogenation of butane and butenes over chrome-alumina catalyst, *Industrial and Engineering Chemistry Fundamentals*, vol. 5, no. 3, pp. 289-294.

Hildebrandt, D., and Glasser, D., (1990), The attainable region and optimal reactor structures, *Chemical Engineering Science*, vol. 45, no. 8, pp. 2161-2168.

Hildebrandt, D., Glasser, D., and Crowe, C., (1990), Geometry of the attainable region generated by reaction and mixing: with and without constraints, *Industrial and Engineering Chemistry Research*, vol. 29, no. 49, pp. 49-58.

Horn, F.J.M., (1964), Attainable and non-attainable regions in chemical reaction technique, *Proceedings of the Third European Symposium on Chemical Reaction Engineering*, Amsterdam, The Netherlands, Pergamon Press, Oxford, UK, pp. 293-303.

Hou, K., Hughes, R., Ramos, R., Menéndez, M., Santamaría, J., (2001), Simulation of a membrane reactor for oxidative dehydrogenation of propane, incorporating radial concentration and temperature profiles, *Chemical Engineering Science*, vol. 56, pp. 57-67.

Itoh, N., Govind, R., (1989), Combined oxidation and dehydrogenation in a palladium membrane reactor, *Industrial and Engineering Chemistry Research*, vol. 28, pp. 1554-1557.

Kauchali, S., Rooney, W.C., Biegler, L.T., Glasser, D., Hildebrandt, D., (2002), Linear programming formulations for attainable region analysis, *Chemical Engineering Science*, vol. 57, pp. 2015-2028.

Kearby, K.K., (1950), Catalytic dehydrogenation of butenes, *Industrial and Engineering Chemistry*, vol. 42, no. 2, pp. 295-300.

Khumalo, N., Glasser, D., Hildebrandt, D., Hausberger, B., Kauchali, S., (2006), The application of the attainable region analysis to comminution, *Chemical Engineering Science*, vol. 61, pp. 5969-5980.

Khumalo, N., Glasser, D., Hildebrandt, D., Hausberger, B., (2007), An experimental validation of a specific energy-based approach for comminution, *Chemical Engineering Science*, vol. 62, pp. 2765-2776.

Kung, H.H., Kung, M.C., (1997), Oxidative dehydrogenation of alkanes over vanadium-magnesium oxides, *Applied Catalysis A:General*, vol. 157, pp. 105-116.

Lemonidou, A.A., Tjatjopoulos, G.J., Vasalos, I.A., (1998), Investigations on the oxidative dehydrogenation of *n*-butane over V/MgO-type catalysts, *Catalysis Today*, vol. 45, pp. 65-71.

McGregor, C., Glasser, D., Hildebrandt, D., (1999), The attainable region and Pontryagin's maximum principle, *Industrial and Engineering Chemistry Research*, vol. 38, no. 3, pp. 652-659.

Nicol, W., Hernier, M., Hildebrandt, D., Glasser, D., (2001), The attainable region and process synthesis: reaction systems with external cooling and heating. The effect of relative cost of reactor volume to heat exchange area on the optimum process layout, *Chemical Engineering Science*, vol. 56, pp. 173-191.

Nisoli, A., Malone, M.F., Doherty, M.F., (1997), Attainable regions for reaction with separation, *American Institute of Chemical Engineers Journal*, vol. 43, no. 2, pp. 374-387.

Omtveit, T., Tanskanen, J., Lien, K.M., (1994), Graphical targeting procedures for reactor systems, *Computers in Chemical Engineering*, vol. 18, Suppl., pp. S113-S118.

Oyama, S.T., Middlebrook, A.M., Somorjai, G.A., (1990), Kinetics of ethane oxidation on vanadium oxide, *Journal of Physical Chemistry*, vol. 94, no. 12, pp. 5029-5033.

Pedernera, M., Alfonso, M.J., Menéndez, M., Santamaría, J., (2002), Simulation of a catalytic membrane reactor for the oxidative dehydrogenation of butane, *Chemical Engineering Science*, vol. 57, pp. 2531-2544.

Reid, R., Prausnitz, J., Poling, B., (1987), The properties of gases and liquids, fourth edition, McGraw-Hill, New York.

Rezac, M.E., Koros, W.J., Miller, S.J., (1994), Membrane-assisted dehydrogenation of *n*-butane. Influence of membrane properties on system performance, *Journal of Membrane Science*, vol. 93, pp. 193-201

Rezac, M.E., Koros, W.J., Miller, S.J., (1995), Membrane-assisted dehydrogenation of *n*-butane, *Industrial and Engineering Chemistry Research*, vol. 34, pp. 862-868.

Rubio, O., Herguido, J., Menéndez, M., (2003), Oxidative dehydrogenation of *n*-butane on V/MgO catalysts – kinetic study in anaerobic conditions, *Chemical Engineering Science*, vol. 58, pp. 4619-4627.

Rubio, O., Mallada, R., Herguido, J., Menéndez, M., (2002), Experimental study on the oxidation of butane to maleic anhydride in a two-zone fluidised bed reactor, *Industrial and Engineering Chemistry Research*, vol. 41, pp. 5181-5186.

Seodigeng, T.G., (2006), Numerical Formulations for Attainable Region Analysis, Ph.D. thesis, University of the Witwatersrand, Johannesburg, South Africa.

Smith, R., (2005), Chemical Process Design and Integration, John Wiley and Sons Ltd., Table 3, p. 100.

Smith, R.L., Malone, M.F., (1997), Attainable regions for polymerisation reaction systems, *Industrial and Engineering Chemistry Research*, vol. 36, no. 4, pp. 1076-1084.

Soler, J., LópezNieto, J.M., Herguido, J., Menéndez, M., Santamaría, J., (1998), Oxidative dehydrogenation of *n*-butane on V/MgO catalysts. Influence of the type of contactor, *Catalysis Letters*, vol. 50, pp. 25-30

Soler, J., LópezNieto, J.M., Herguido, J., Menéndez, M., Santamaría, J., (1999), Oxidative dehydrogenation of *n*-butane in a two-zone fluidised-bed reactor, *Industrial and Engineering Chemistry Research*, vol. 38, pp. 90-97.

Soler, J., Téllez, C., Herguido, M., Menéndez, M., Santamaría, J., (2001), Modelling of a two-zone fluidised-bed reactor for the oxidative dehydrogenation of *n*-butane, *Powder Technology*, vol. 120, pp. 88-96.

Téllez, C., Menéndez, M., Santamaría, J., (1997), Oxidative dehydrogenation of butane using membrane reactors, *American Institute of Chemical Engineers Journal*, vol. 43, no. 3, pp. 777-784.

Téllez, C., Menéndez, M., Santamaría, J., (1999a), Kinetic study of the oxidative dehydrogenation of butane on V/MgO catalysts, *Journal of Catalysis*, vol. 183, pp. 210-221.

Téllez, C., Menéndez, M., Santamaría, J., (1999b), Simulation of an inert membrane reactor for the oxidative dehydrogenation of butane, *Chemical Engineering Science*, vol. 54, pp. 2917-2925.

Téllez, C., Abon, A., Dalmon, J.A., Mirodatos, C., Santamaría, J., (2000), Oxidative dehydrogenation of butane over V/MgO catalysts, *Journal of Catalysis*, vol. 195, pp. 113-124.

Videl-Michel, R., Hohn, K.L., (2004), Effect of crystal size on the oxidative dehydrogenation of butane on V/MgO catalysts, *Journal of Catalysis*, vol. 221, pp. 127-136.

Zhao, W., Zhao, C., Zhang, Z., Han, F., (2002), Strategy of an attainable region partition for reactor network synthesis, *Industrial and Engineering Chemistry Research*, vol. 41, pp. 190-195.

Zhou, W., Manousiouthakis, V.I., (2007), Variable density fluid reactor network synthesis – construction of the attainable region through the IDEAS approach, *Chemical Engineering Journal*, vol. 129, pp. 91-103.

Appendix to Chapter 1

Derivation of Equation for Gibbs Free Energy of Formation

$$\frac{\Delta G^0}{RT} = \frac{\Delta G_0^0}{RT_0} - \int_{T_0}^{T} \frac{\Delta H^0}{RT^2} dT \qquad (1)$$

Multiplying both sides by R gives

$$\frac{\Delta G^0}{T} = \frac{\Delta G_0^0}{T_0} - \int_{T_0}^{T} \frac{\Delta H^0}{T^2} dT \qquad (2)$$

$$\Delta H^0 = \Delta H_0^0 + \int_{T_0}^{T} \Delta C_p dT \qquad (3)$$

where $\Delta C_p = A + BT + CT^2 + DT^3$

and A = $\sum_i \nu_i A_i$, ….. , D = $\sum_i \nu_i D_i$ (4)

Consider the integral $\int_{T_0}^{T} \Delta C_p dT$

$$= A(T - T_0) + B(T^2 - T_0^2)/2 + C(T^3 - T_0^3)/3 + D(T^4 - T_0^4)/4 \qquad (5)$$

Consider the integral $\int_{T_0}^{T} \frac{\Delta H^0}{T^2} dT$

$$= \int_{T_0}^{T} \left\{ \frac{\Delta H_0^0 + A(T - T_0) + B(T^2 - T_0^2)/2 + C(T^3 - T_0^3)/3 + D(T^4 - T_0^4)/4}{T^2} \right\} dT \qquad (6)$$

$$= \int_{T_0}^{T} \left\{ \frac{\Delta H_0^0}{T^2} + \frac{A}{T} - \frac{AT_0}{T^2} + \frac{B}{2} - \frac{BT_0^2}{2T^2} + \frac{CT}{3} - \frac{CT_0^3}{3T^2} + \frac{DT^2}{4} - \frac{DT_0^4}{4T^2} \right\} dT \qquad (7)$$

=

$$\Delta H_0^0 \left(-\frac{1}{T} + \frac{1}{T_0} \right) + A \ln \frac{T}{T_0} - AT_0 \left(-\frac{1}{T} + \frac{1}{T_0} \right) + \frac{B}{2}(T - T_0) - \frac{BT_0^2}{2} \left(-\frac{1}{T} + \frac{1}{T_0} \right) +$$

$$\frac{C}{6}(T^2 - T_0^2) - \frac{CT_0^3}{3} \left(-\frac{1}{T} + \frac{1}{T_0} \right) + \frac{D}{12}(T^3 - T_0^3) - \frac{DT_0^4}{4} \left(-\frac{1}{T} + \frac{1}{T_0} \right) \qquad (8)$$

Let $\tau = \frac{T}{T_0}$

Equation (8) can be rewritten as

=

$$\Delta H_0^0\left(-\frac{1}{T_0\tau}+\frac{1}{T_0}\right)+A\ln\tau-AT_0\left(-\frac{1}{T_o\tau}+\frac{1}{T_0}\right)+\frac{B}{2}\left(T-T_0\right)-\frac{BT_0^2}{2}\left(-\frac{1}{T_0\tau}+\frac{1}{T_0}\right)+$$

$$\frac{C}{6}\left(T^2-T_0^2\right)-\frac{CT_0^3}{3}\left(-\frac{1}{T_0\tau}+\frac{1}{T_0}\right)+\frac{D}{12}\left(T^3-T_0^3\right)-\frac{DT_0^4}{4}\left(-\frac{1}{T_0\tau}+\frac{1}{T_0}\right) \qquad (9)$$

$$=\frac{\Delta H_0^0}{T_0}\left(\frac{\tau-1}{\tau}\right)+A\ln\tau-A\left(\frac{\tau-1}{\tau}\right)+\frac{BT_0}{2}\left(\tau-1\right)-\frac{BT_0}{2}\left(\frac{\tau-1}{\tau}\right)+$$

$$\frac{CT_0^2}{6}\left(\tau^2-1\right)-\frac{CT_0^2}{3}\left(\frac{\tau-1}{\tau}\right)+\frac{DT_0^3}{12}\left(\tau^3-1\right)-\frac{DT_0^3}{4}\left(\frac{\tau-1}{\tau}\right) \qquad (10)$$

$$=\frac{\Delta H_0^0}{T_0}\left(\frac{\tau-1}{\tau}\right)+A\left(\ln\tau-\frac{\tau-1}{\tau}\right)+\frac{BT_0}{2}\left(\tau-1-\frac{\tau-1}{\tau}\right)+$$

$$\frac{CT_0^2}{6}\left(\tau^2-1-\frac{2\tau-2}{\tau}\right)+\frac{DT_0^3}{12}\left(\tau^3-1-\frac{3\tau-3}{\tau}\right) \qquad (11)$$

$$=\frac{\Delta H_0^0}{T_0}\left(\frac{\tau-1}{\tau}\right)+A\left(\frac{\tau\ln\tau-\tau+1}{\tau}\right)+\frac{BT_0}{2}\left(\frac{\tau^2-2\tau+1}{\tau}\right)+$$

$$\frac{CT_0^2}{6}\left(\frac{\tau^3-3\tau+2}{\tau}\right)+\frac{DT_0^3}{12}\left(\frac{\tau^4-4\tau+3}{\tau}\right) \qquad (12)$$

Inserting equation (12) into equation (2) and multiplying by T we get

$$\Delta G^0 = \Delta G_0^0 \frac{T}{T_0} - \frac{\Delta H_0^0}{T_0}\left(\frac{\tau - 1}{\tau}\right)T - A\left(\frac{\tau \ln \tau - \tau + 1}{\tau}\right)T - \frac{BT_0}{2}\left(\frac{\tau^2 - 2\tau + 1}{\tau}\right)T -$$

$$\frac{CT_0^2}{6}\left(\frac{\tau^3 - 3\tau + 2}{\tau}\right)T - \frac{DT_0^3}{12}\left(\frac{\tau^4 - 4\tau + 3}{\tau}\right)T \qquad (13)$$

$$\Delta G^0 = \Delta G_0^0 \tau - \Delta H_0^0(\tau - 1) - AT_0(\tau \ln \tau - \tau + 1) - \frac{BT_0^2}{2}(\tau^2 - 2\tau + 1) -$$

$$\frac{CT_0^3}{6}(\tau^3 - 3\tau + 2) - \frac{DT_0^4}{12}(\tau^4 - 4\tau + 3) \qquad (14)$$

$$\Delta G^0 = \Delta H_0^0 + (\Delta G_0^0 - \Delta H_0^0)\tau - AT_0(\tau \ln \tau - \tau + 1) - \frac{BT_0^2}{2}(\tau^2 - 2\tau + 1) -$$

$$\frac{CT_0^3}{6}(\tau^3 - 3\tau + 2) - \frac{DT_0^4}{12}(\tau^4 - 4\tau + 3) \qquad (15)$$

CHAPTER 2

The Application of the Attainable Region Concept to the Oxidative Dehydrogenation of *1*-Butene to Butadiene in Inert Porous Membrane Reactors

---

The following paper was published in *Industrial and Engineering Chemistry Research*, **2004**, *43*, 1827-1831 with corrections subsequently published in *Industrial and Engineering Chemistry Research*, **2004**, *43*, 7208.

The numbering of the figures, as published in Industrial and Engineering Chemistry Research, has been prefixed with the reference (2) to this chapter of my thesis.

In this chapter of my thesis the referencing system required by the editors of *Industrial and Engineering Chemistry Research* has been changed to the Harvard system to comply with the requirements of the University of the Witwatersrand for the submission of theses.

2.1 Introduction

The Attainable Region (AR) concept uses a geometrical procedure to determine the boundaries of the region that include all possible reaction

products for a known feed condition. The procedure also allows the choice of reactor(s) and the sequencing of these reactors to maximise the selection of reactor products in terms of pre-defined objective functions. It is also possible to derive the process operating conditions commensurate with an optimum objective function.

The AR concept currently is being applied to industrial applications and in this paper the concept is used to study the manufacture of butadiene by the oxidative dehydrogenation (ODH) of *1*-butene (butene). Process operating conditions, specifically the partial pressure of oxygen, are reviewed. A candidate AR for the system butene-butadiene is proposed.

2.2 Background Literature

Over the last fifteen years several papers, including Glasser, Hildebrandt and Crowe (1987), have been published dealing with mapping the region (the Attainable Region) within which all the reactants and products of a chemical reaction lay, assuming known feed conditions. In particular, two chemical reaction systems have been studied to determine the boundaries of the candidate Attainable Region (AR), the Trambouze and the Van de Vusse. These two examples represented reactions of considerable academic and theoretical interest but suffered from the lack of direct applicability to problems of industrial significance. Specifically, there is a general paucity of chemical reaction rates and kinetic data and in studying the Trambouze and Van de Vusse reactions assumptions had to be made which, although undeniably useful in mapping the boundaries of the AR, could not easily be applied to specific chemical reactions. The Trambouze and Van de Vusse reactions, however, do possess the advantage of mathematical simplicity

coupled with the ability to model a wide range of reactor behaviour and resulting reactor configurations.

With the publication by Téllez, Menéndez and Santamaría (1997 and 1999b) of reaction rates and kinetic data for the oxidative dehydrogenation (ODH) of *n*-butanes to butene and butadiene in inert porous membrane reactors (IMRs), it became possible to examine a specific chemical reaction of industrial interest. Téllez, Menéndez and Santamaría (1999a) developed equations for the rate expressions associated with the ODH of *n*-butane, the three isomers of butene (*1*-butene, *cis*-*2*-butene and *trans*-*2*-butene) and butadiene. Values of the respective rate constants also were provided. The experiments by Téllez and his colleagues were conducted in an inert porous membrane reactor operating at atmospheric pressure and within a feed temperature range of 748K to 823K.

In a more recent publication, Assabumrungrat *et al*. (2002) compared the performance of a porous membrane reactor with that of a conventional fixed-bed reactor in the ODH of *n*-butane. The porous membrane reactor was used to add oxygen to the hydrocarbons in a controlled manner. Assabumrungrat *et al*., in developing their mathematical models, used the kinetic and experimental data developed by Téllez, Menéndez and Santamaría (1997, 1999a, 1999b).

The reaction network for the ODH of butene was postulated by Téllez, Menéndez and Santamaría (1999a, 1999b) as that in Figure 2.1.

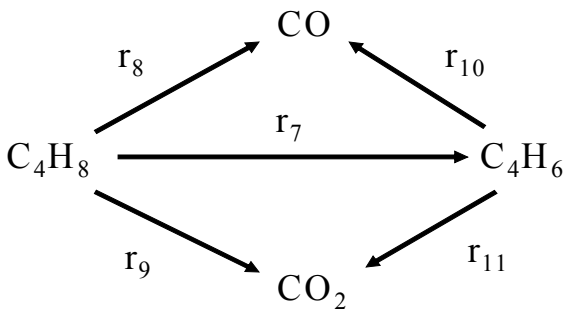


Figure 2.1. Reaction scheme for the ODH of butene to butadiene.

Using the kinetic data developed by Téllez, Menéndez and Santamaría, the techniques used to identify a candidate Attainable Region for a particular chemical reaction, Glasser, Hildebrandt and Crowe (1987), were applied to the oxidative dehydrogenation of butene to butadiene. The objective of this research was to establish the operating conditions necessary to maximise the yield of butadiene from a fixed feed of butene and, in so doing, to identify a candidate AR for the system butene-butadiene.

The chemical reactions involved in the ODH of butene are :

Oxidation of Butene

$C_4H_8 + ½O_2 = C_4H_6 + H_2O$ (r_7)

$r_7 = k_7 P_{C4H8} \theta_0$

$C_4H_8 + 4O_2 = 4CO + 4H_2O$ (r_8)

$r_8 = k_8 P_{C4H8} \lambda_0$

$C_4H_8 + 6O_2 = 4CO_2 + 4H_2O$ (r_9)

$r_9 = k_9 P_{C4H8} \lambda_0$

Oxidation of Butadiene

$C_4H_6 + {}^7/_2\, O_2 = 4CO + 3H_2O$ (r_{10})

$r_{10} = k_{10}P_{C4H6}\lambda_0$

$C_4H_6 + {}^{11}/_2\, O_2 = 4CO_2 + 3H_2O$ (r_{11})

$r_{11} = k_{11}P_{C4H6}\lambda_0$

Oxidation of Catalyst Sites

$\theta_0 = 2k_{12}P_{O2} / (2k_{12}P_{O2} + k_7P_{C4H8})$

$\lambda_0 = 2k_{13}P_{O2} / [2k_{13}P_{O2} + (8k_8+12k_9)P_{C4H8} + (7k_{10}+11k_{11})P_{C4H6}]$

Factors influencing the rate expressions presented by Téllez, Menéndez and Santamaría (1999a, 1999b) include the partial pressures of butene and butadiene and the selective (θ) and non-selective (λ) oxidation catalyst sites respectively. The latter two, in turn, are influenced by the partial pressure of oxygen and by the partial pressures of butene and butadiene.

2.3 Results

The mathematical model created to examine the ODH of butene assumed isothermal conditions and atmospheric pressure.

An initial feed of pure butene was used and the partial pressure of oxygen was varied over the range 0.25 to 85 kPa.

In presenting the results of the mathematical analyses, the mass fraction of carbon in the reactants and products was used since mass fraction variables obey the linear mixing rule. Linear mixing has the additional advantage of providing greater insight into the characteristics of the Attainable Region than is possible through using the partial pressures of the various components.

The mass fractions of carbon in the respective products and reactants are equal to their respective fractions on a carbon molar basis

It was recognised that the addition of oxygen served two purposes

- To provide heat by its exothermic reaction with the hydrogen released during the oxidation of butene and butadiene and in so doing to nullify the endothermic dehydrogenation of butene.

- To dehydrogenate butene to butadiene. (The dehydrogenation of both butene and butadiene to carbon monoxide and carbon dioxide is an unwanted side effect of the reaction process).

Initially two scenarios were considered. The first was feeding butene and oxygen, the latter at an initial specified partial pressure, to a stabilised (steady state) FBR and permitting the reaction to continue until either all the oxygen or all the butene was depleted. In the second scenario using an inert porous membrane reactor, the partial pressure of oxygen was maintained at

a constant specified level by the addition of fresh oxygen along the length of the IMR. The effect of reactor size upon yield of butadiene also was examined in both scenarios.

2.3.1 Scenario 1 – Depletion of Oxygen in a FBR.

The reactor configuration for this scenario is shown in Figure 2.2.

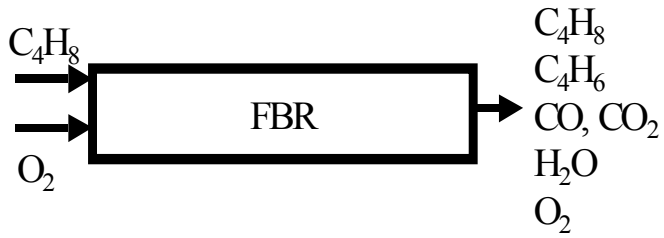


Figure 2.2. FBR Configuration.

Figure 2.3 below shows the 1-butene–butadiene profiles in two-dimensional concentration space for different oxygen partial pressures in the feed stream to a FBR.

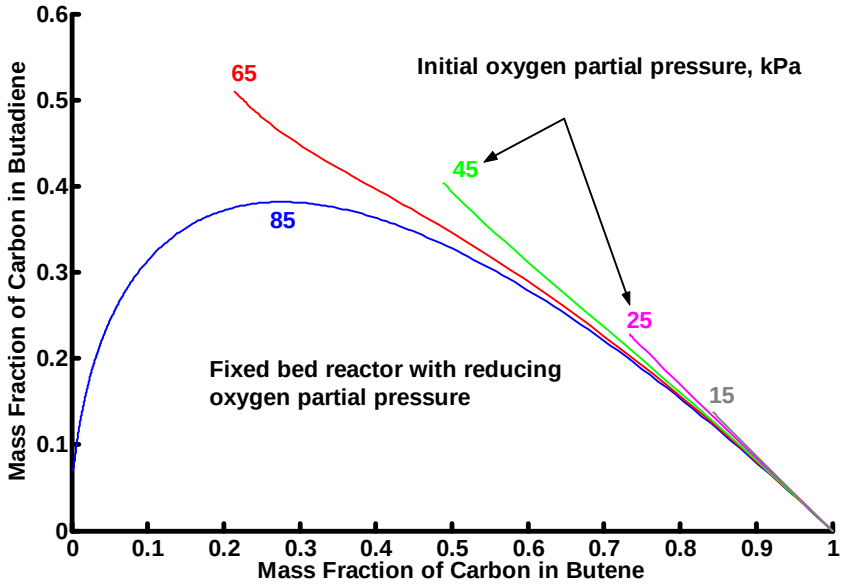


Figure 2.3. Profiles of butene and butadiene at oxygen partial pressures of 15, 25, 45, 65 and 85 kPa in a FBR.

At an initial oxygen partial pressure of 85 kPa, the reaction proceeds until all the oxygen has been depleted. When this occurs, the residual butene and butadiene concentrations are of 0.0009 and 0.07 respectively. The other components present on completion of the reaction, other than butene and butadiene, are carbon monoxide, carbon dioxide and water. All the oxygen has been utilised in the oxidation of butene and butadiene. The water gas shift reaction, i.e. the reaction of carbon monoxide and hydrogen was not considered by Téllez, Menéndez and Santamaría (1999a, 1999b).

If the initial partial pressure of oxygen is increased to 86 kPa, all the butene and butadiene is oxidised and there is residual oxygen present on completion of the reaction. At this initial partial pressure of oxygen, the supply of butene is the limiting factor.

At oxygen partial pressures less than 85 kPa, reaction ceases with oxygen depletion. At an initial oxygen partial pressure of 65 kPa, reaction cessation effectively occurs after a residence time of 20 seconds (at 45 kPa, cessation effectively occurs after a residence time of 9 seconds). When the reaction ceases, we are left with butene, butadiene, carbon monoxide, carbon dioxide and water. At this initial partial pressure of oxygen, the supply of oxygen is the limiting factor.

The maximum yield of butadiene, 0.51, occurs at an initial oxygen partial pressure of 65 kPa. The oxygen partial pressure at this stage has been reduced to slightly less than 0.0005 kPa. Residual butene has a concentration marginally in excess of 0.21.

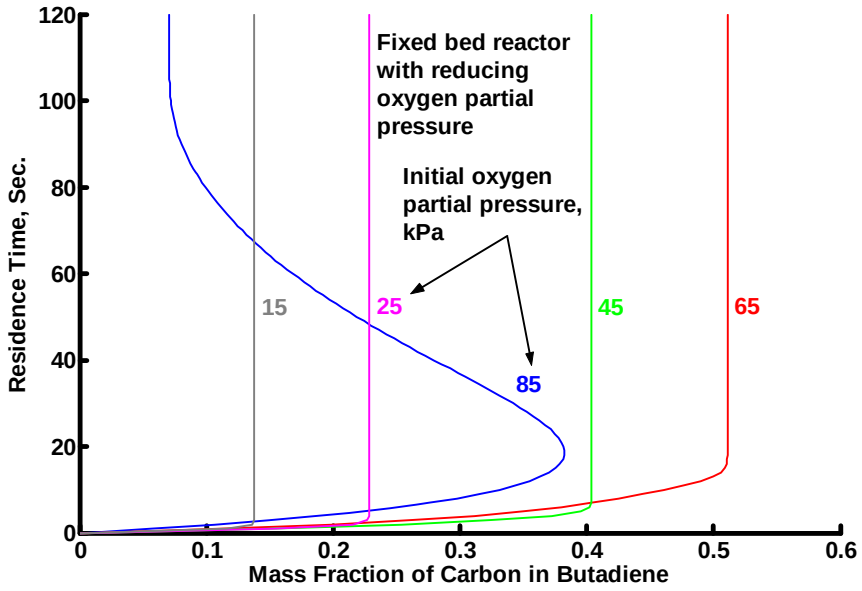


Figure 2.4. Residence times for butadiene at oxygen partial pressures of 15, 25, 45, 65 and 85 kPa in a FBR.

Figure 2.4 shows that the reaction times to attain the maximum yields of butadiene do not exceed 20 seconds for all oxygen partial pressures implying that the ODH reaction is a very fast one.

Figure 2.5 shows the residence times and the residual butene concentrations on reaction cessation at the respective oxygen partial pressures.

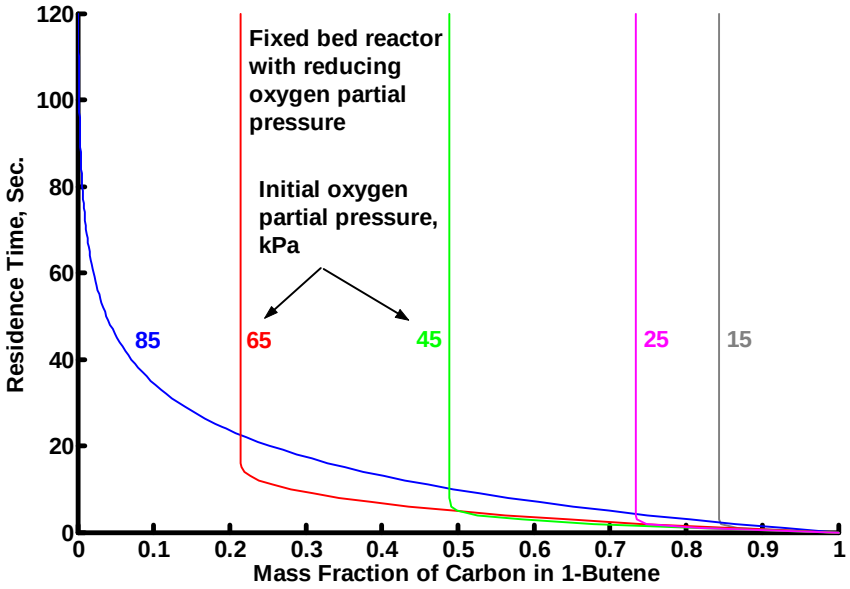


Figure 2.5. Residence times for butene at oxygen partial pressures of 15, 25, 45, 65 and 85 kPa in a FBR.

2.3.2 Scenario 2 – Replenishment of Oxygen in an IMR

The reactor configuration for this scenario is shown in Figure 2.6.

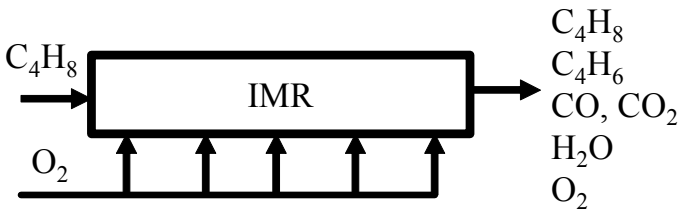


Figure 2.6. IMR Configuration.

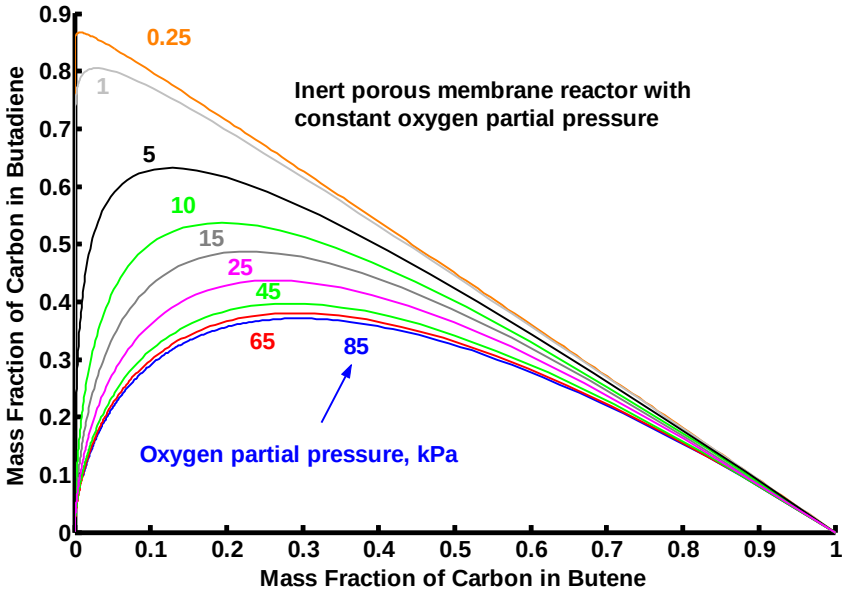


Figure 2.7. Profiles of butene and butadiene at constant oxygen partial pressures from 85 to 0.25 kPa in an IMR.

Figure 2.7 shows the effect of adding oxygen along the length of the reactor to maintain a constant oxygen partial pressure in the stream of reactants and products.

Figure 2.7 also shows that the convex shape of the butene-butadiene profiles decreases with reduced oxygen partial pressure. This trend particularly is noticeable at an oxygen (constant) partial pressure of 0.25 kPa when the butene-butadiene profile, in mass balance space, is almost a straight line, although still convex.

It is noticeable from Figure 2.7 that the maximum yield of butadiene increases and the residual butene decreases as the partial pressure of oxygen is reduced. At an oxygen partial pressure of 0.25 kPa, the maximum yield of butadiene is 0.87 with a commensurate low value of butene of 0.007. It is concluded that the lower the (constant) oxygen partial pressure in an inert porous membrane reactor, the greater is the yield of butadiene and the associated conversion (consumption) of butene.

The maximum yield of butadiene at an oxygen partial pressure of 0.25 kPa is 0.87 after a residence time of 147 seconds (see Figure 2.8).

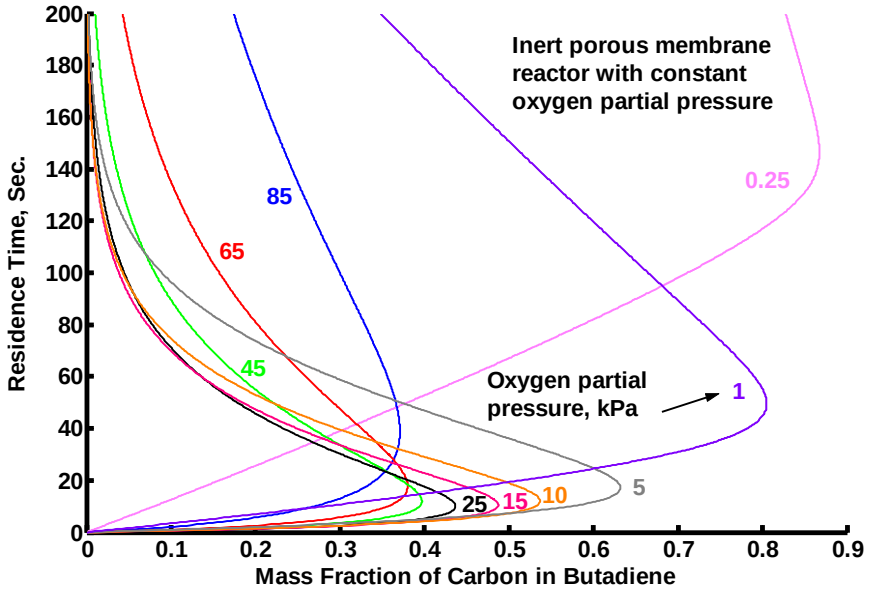


Figure 2.8. Residence times for butadiene at constant oxygen partial pressures from 85 to 0.25 kPa in an IMR.

A detailed analysis of Figure 2.8 shows that the residence time for maximum yield of butadiene initially decreases with reduced oxygen partial pressure over the range 85 kPa to 40 kPa.

Between the range 35 kPa to 15 kPa, the residence time for the maximum yield of butadiene is practically constant at 10 seconds. This represents the minimum residence time for butadiene yields between 0.4 and 0.5.

As the (constant) partial pressure of oxygen is reduced below 15 kPa, the residence times for the maximum yield of butadiene gradually increase. For partial pressures less than 1 kPa, the residence time for maximum yield of butadiene increases sharply.

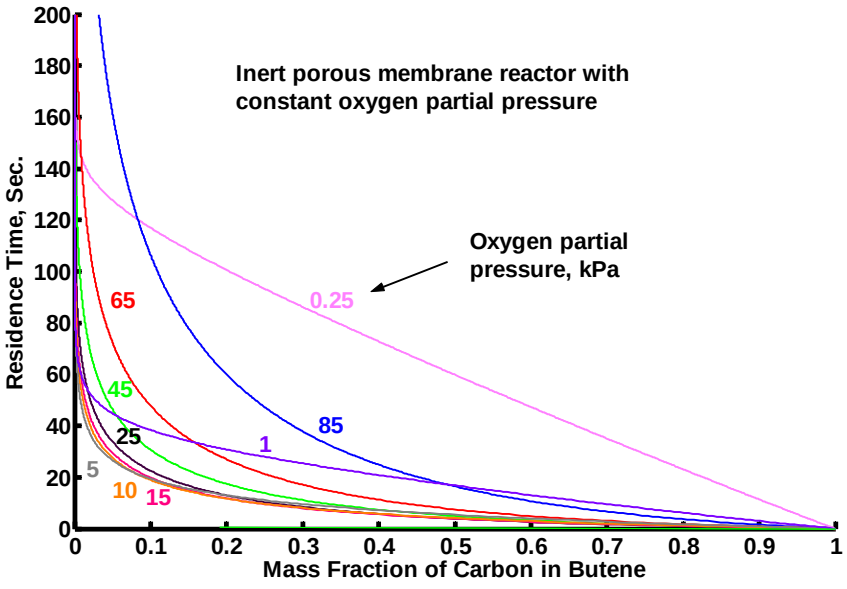


Figure 2.9. Residence times for the ODH of *1*-butene at constant oxygen partial pressures from 85 kPa to 0.25 kPa in an IMR.

Figure 2.9 shows the residence times for the ODH of *1*-butene at constant values of oxygen partial pressure over the residence time range of 0 to 200

seconds. Provided that the reactor is sized accordingly, i.e. the residence time is sufficiently large (approximately 190 seconds for 0.25 kPa) all the butene will be depleted.

Examination of Figure 2.7 supports the belief that the maximum yield of butadiene increases with decreasing oxygen partial pressure. Figure 2.8 shows that the reactor size (residence time) associated with the maximum yield of butadiene falls to a minimum and then increases.

This observation prompts the question as to what yield of butadiene could be attained at a very low oxygen partial pressure and a reactor of infinite size ?

This question was answered by defining a very low oxygen partial pressure as 0.000001 kPa and the results are shown in Figure 2.10 and Figure 2.11.

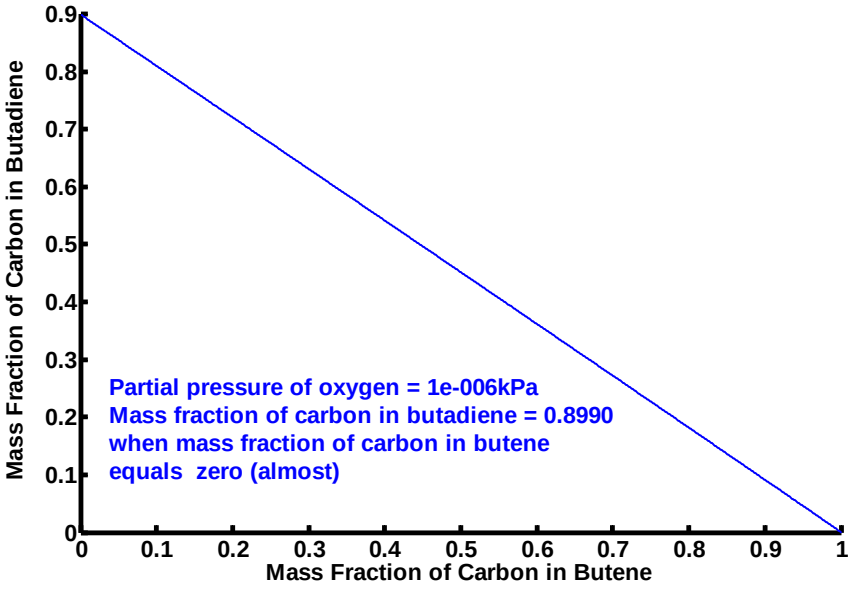


Figure 2.10. Profile of butene and butadiene at a very low constant oxygen partial pressure and in a very large IMR.

The maximum yield of butadiene at a very low oxygen partial pressure and as the concentration of butene tends to zero is 0.90.

The butene-butadiene profile in Figure 2.10 is convex over its entire length.

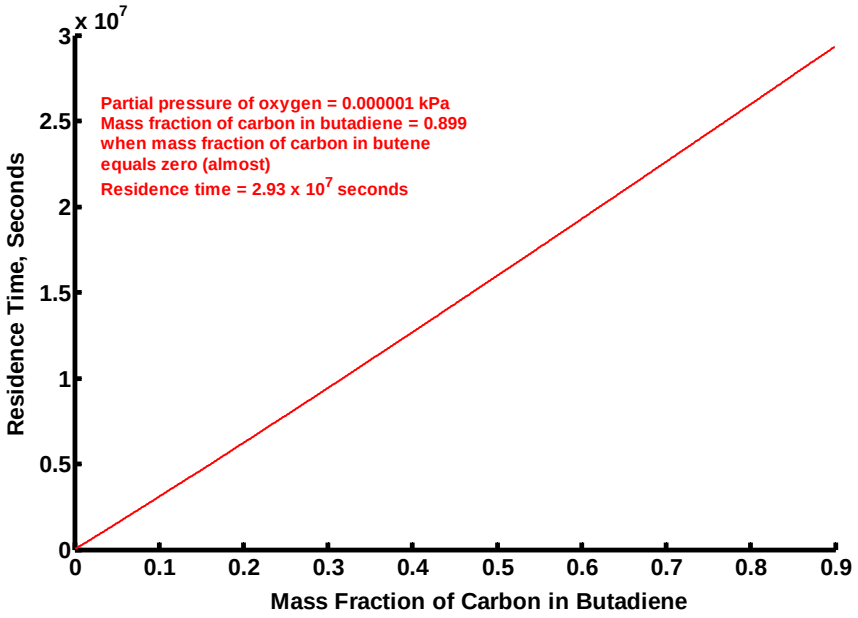


Figure 2.11. Butadiene residence times at a very low constant oxygen partial pressure and in a very large IMR.

Figure 2.11 shows that the residence time at a very low oxygen partial pressure for the total conversion of butene is 2.93 x 10^7 seconds. That such a large residence time is required for the total conversion of the butene can be inferred from Figure 2.8 which shows that the residence time for the maximum yield of butadiene increases almost asymptotically for (constant) oxygen partial pressures less than 1 kPa.

As has already been noted, for an IMR at a constant oxygen partial pressure of 0.25 kPa, the maximum yield of butadiene is 0.87 with a reactor size of 147 seconds. This represents an achievement of 96 % relative to the theoretical maximum butadiene yield of 0.90.

For a FBR with an initial oxygen partial pressure of 65 kPa and in which the oxygen is not replenished, the maximum yield of butadiene is 0.51 (see

Figure 2.3). This represents an achievement of 57 % relative to the theoretical maximum butadiene yield of 0.90.

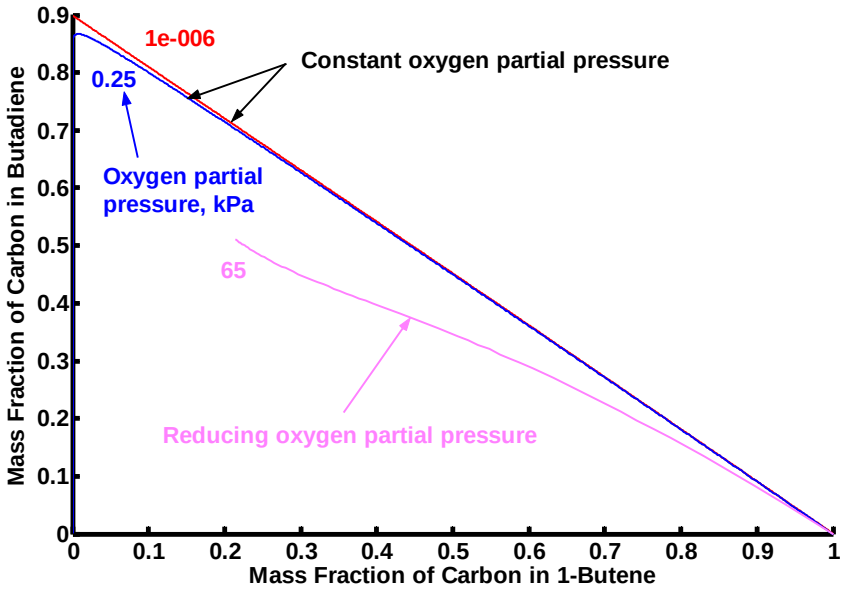


Figure 2.12. Profiles of butene and butadiene at different oxygen partial pressures for an IMR and for a FBR.

In Figure 2.12, for an FBR in which the initial oxygen is depleted through the normal oxidative process the maximum butadiene yield at 65 kPa is 0.51 at a residual butene value of 0.21.

Also shown in Figure 2.12 are the butene-butadiene profiles for an IMR in which the original oxygen partial pressures (0.25 and 0.000001 kPa) are maintained constant through the addition of fresh oxygen along the length of the reactor.

At an oxygen partial pressure of 0.25 kPa, the maximum butadiene yield is 0.87 at a residual butene value less than 0.01.

For a very low oxygen partial pressure (i.e. 0.000001 kPa), the maximum butadiene yield is 0.90 at a butene value infinitesimally close to zero.

It is noteworthy that the butene-butadiene profiles considered in Figure 2.12 (depleted oxygen at 65 kPa and constant oxygen at 0.25 kPa) all lie below the profile for a very low oxygen partial pressure.

From an analysis of Figure 2.3 to Figure 2.12 we conclude that the theoretical profile for maximum butadiene yield at a very low oxygen partial pressure represents the furthermost boundary within which all scenarios so far identified lie. Consequently, we believe that Figure 2.10 represents a candidate Attainable Region for the system butene-butadiene.

2.3.3 Effect of the Temperature

All the analyses conducted have been at the datum temperature of 773K, Assabumrungrat *et al.* (2002), and consequently our candidate Attainable Region shown in Figure 2.10 is applicable only at that temperature.

Figure 2.13 shows the effect of temperature upon the butene-butadiene profile.

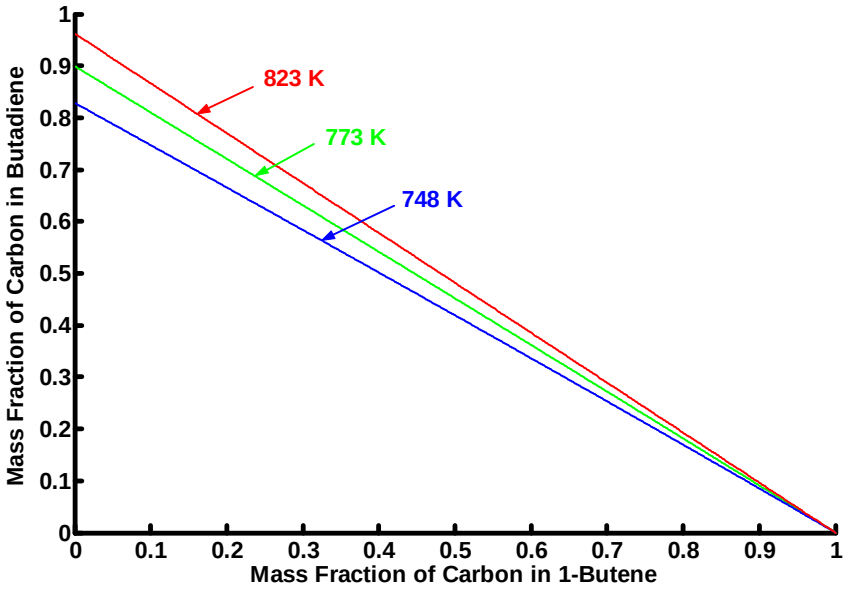


Figure 2.13. Effect of the temperature upon theoretical maximum yield of butadiene.

Examination of Figure 2.13 shows that an increase of the reactor temperature from 773K to 823K raises the maximum theoretical yield of butadiene from 0.90 to 0.96. Decreasing the operating temperature from 773K to 748K reduces the maximum theoretical yield of butadiene from 0.90 to 0.83.

From Figure 2.13 we conclude that the theoretical maximum yield of butadiene increases with temperature over the range 723K to 823K

Consequently, each of the three profiles shown in Figure 2.13 represents a candidate AR for the system butene- butadiene at the temperature indicated.

2.4 Conclusions

For initial oxygen partial pressures greater than 45 kPa in a FBR, a higher yield of butadiene can be attained without the addition of fresh oxygen than when the oxygen partial pressure is kept at a constant level in an IMR (Figure 2.3 and Figure 2.7). (At an oxygen partial pressure of 85 kPa, the butadiene yield from a FBR is 3 % greater than that from an IMR.)

For oxygen partial pressures less than 45 kPa, a higher yield of butadiene can be attained in an IMR when the oxygen partial pressure is kept at a constant level than when it is depleted through normal ODH process in a FBR (Figure 2.3 and Figure 2.7).

The best yield of butadiene identified in this study is 0.87 carbon mass fraction with a corresponding residence time of 147 seconds. This yield of butadiene represents 96 % of the theoretical quantity from an IMR of very large size with a very low oxygen partial pressure. The reactor configuration for this example was an IMR with a constant oxygen partial pressure of 0.25 kPa (Figure 2.7).

A candidate AR has been identified for the system butene-butadiene at a temperature of 773K. This candidate AR is shown in Figure 2.10. It represents an IMR with a (constant) very low oxygen partial pressure and of very large size. This candidate region contains all reactants and products so far identified.

2.5 Nomenclature

E_{ai} Activation energy for species *i*, (kJ/mol)

k_i Kinetic constant for reaction *i*, mol/kg s

P_i Partial pressure of species *i*, atm

r_i Rate of reaction of reaction *i*, mol/kg s

R Gas constant J/(mol.K), 8.314

T_0 Reference temperature, 773K

T Feed temperature, K

Greek Symbols

θ_0 Selective oxidation catalyst site

λ_0 Non-selective oxidation catalyst site

2.6 Literature Cited

Assabumrungrat, S. Rienchalanusarn, T. Praserthdam, P. and Goto, S. (2002) Theoretical study of the application of porous membrane reactor to oxidative dehydrogenation of *n*-butane, *Chemical Engineering Journal*, vol. 85, pp. 69-79.

Glasser, D., Hildebrandt, D. and Crowe, C. (1987) A geometric approach to steady flow reactors: the attainable region and optimisation in concentration space, *American Chemical Society*, pp. 1803-1810.

Téllez, C. Menéndez, M. Santamaría, J. (1999a) Kinetic study of the oxidative dehydrogenation of butane on V/MgO catalysts, *Journal of Catalysis*, vol. 183, pp. 210-221.

Téllez, C. Menéndez, M. Santamaría, J. (1999b) Simulation of an inert membrane reactor for the oxidative dehydrogenation of butane, *Chemical Engineering Science*, vol. 54, pp. 2917-2925.

Téllez, C. Menéndez, M. Santamaría, J. (1997) Oxidative dehydrogenation of butane using membrane reactors, *American Institute of Chemical Engineers Journal*, vol. 43, no.3, pp. 777-784

CHAPTER 3

The Oxidative Dehydrogenation of *n*-Butane in a Fixed Bed Reactor and in an Inert Porous Membrane Reactor - Maximising the Production of Butenes and Butadiene

---

The following paper was published in *Industrial and Engineering Chemistry Research,* **2006**, *45*, pp. 2661-2671

The numbering of the figures and tables as published in *Industrial and Engineering Chemistry Research* has been prefixed with the reference (3) to this chapter of my thesis.

In this chapter of my thesis the referencing system required by the editors of *Industrial and Engineering Chemistry Research* has been changed to the Harvard system to comply with the requirements of the University of the Witwatersrand for the submission of theses.

3.1 Abstract

The oxidative dehydrogenation (ODH) of *n*-butane (butane) produces three isomers of butene (*1*-butene, trans-*2*-butene and cis-*2*-butene) which in turn are oxidised to form butadiene. Butane also is oxidised directly to butadiene. In this simulation study, the authors have analysed the operating conditions required to produce the

maximum amount of butenes, i.e. all three isomers, and butadiene in a Fixed Bed Reactor (FBR) and in an Inert Porous Membrane Reactor (IMR).

The theoretical maximum yields of butenes and butadiene were found to be 0.119 and 0.800 carbon mass fractions respectively. The reactor configuration in both instances was a large IMR operating at a low constant partial pressure of oxygen in the stream of reactants and products.

It was found that 99.7 % and 83 % of the theoretical maximum yields of butenes and butadiene respectively can be achieved in an IMR with a constant oxygen partial pressure of 0.25 kPa. The corresponding residence times are 75 and 322 seconds.

Candidate Attainable Regions have been identified for the system sub-spaces butane-butenes and butane-butadiene.

3.2 Introduction

Olefins and dienes are precursors for a wide range of useful chemicals. A very attractive route to make them is via the oxidative dehydrogenation of hydrocarbons as these are readily available from crude oils and Fischer Tröpsch synthesis. The problem with this route is to try to minimise the oxidation of these hydrocarbons to other products such as carbon monoxide, carbon dioxide and water. However, such routes to olefins and dienes will only become practical when both the yield of product and the selectivity to the desired product are high.

1,3-butadiene is a high-volume and valuable intermediate organic chemical used in many industrial processes to produce rubber, resins and plastics. It is involved in several different reactions including addition, oxidation and substitution reactions but its main use is for polymerisation. Most *1,3*-butadiene is used in synthetic elastomer production and in adiponitrile production, the raw material for nylon 6,6 production. The overall demand for butadiene is expected to increase due to the growth of specialty uses for it, (USA Anon, INTERNET, http://www.inece.org/mmcourse/chapt1.pdf.)

Butadiene is usually produced by one of two processes (a) recovery from a mixed hydrocarbon stream and (b) by the oxidative dehydrogenation (ODH) of butenes.

In this paper, we examine the ODH of *n*-butane to butenes and butadiene. Butane is a readily available feedstock and is produced from crude oils and Fischer Tropsch synthesis and we believe that its conversion to butadiene offers potentially significant economic benefits. Another requirement is to achieve a high selectivity of butane to butadiene allied to high yields of butadiene.

Once the kinetics of the reactions are known it is important to optimise the reaction system to ensure that the economics of the process make it an attractive industrial option. In this paper we examine the possible maximum yields and selectivities and then the ways of achieving them in practice.

In an earlier paper, Milne *et al.* (2004), the authors studied the ODH of *1*-butene to butadiene in a FBR and in an IMR. It was found that in an IMR where the inlet oxygen partial pressure was maintained at a constant level along the length of the reactor, the maximum yield of butadiene increased as the oxygen partial pressure

was reduced. This earlier paper acknowledged the work done on the ODH of butane by Téllez *et al*. (1997, 1999a, 1999b) and Assabumrungrat *et al.* (2002).

The catalyst used in the FBR and IMR reactors was a V/MgO catalyst containing 24 % (by mass) of V_2O_5.

The reaction network for the ODH of butane was postulated by Téllez *et al.* (1997, 1999a and 1999b) as :

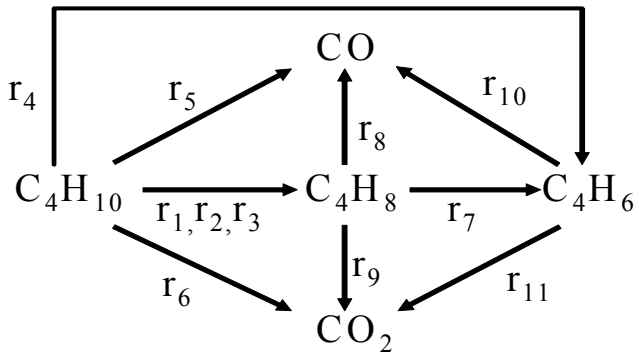


Figure 3.1. Reaction scheme for the oxidative dehydrogenation of butane to butenes and butadiene.

The three isomers, *1*-butene, *trans*-*2*-butene and *cis*-*2*-butene have been lumped together as C_4H_8 in reactions 7, 8 and 9.

The mathematical model created to describe and simulate the ODH of butane assumed isothermal conditions and atmospheric pressure. Maintaining atmospheric pressure in the reactor implied varying the size of the catalyst bed to attain the desired yields of butenes and butadiene.

Matlab®, Version 6, Release 13 was used for all the simulations. The kinetic rate expressions for the oxidation of butane, butenes and butadiene were taken from Téllez *et al.* (1999a). These expressions have, as variables, the partial pressures of oxygen and the hydrocarbons, butane, butenes and butadiene.

In principle, one would like to analyse the system using the Attainable Region (AR) method as this would give results for the optimum conditions and reactor structure to achieve a desired product. In this particular ODH study the size of the problem is too large to be currently analysed using this approach. However, when doing our analyses, some of the thinking behind this method is employed.

3.3 Results

An initial feed mixture of butane and oxygen was used and the partial pressure of oxygen was varied over the range 0.25 to 85 kPa. The feed temperature and the reactor isothermal temperature was 773K.

As in our earlier paper, Milne *et al.* (2004), all hydrocarbon concentrations are expressed in terms of mass fractions of carbon.

Three scenarios were considered. The first was feeding butane and oxygen, the latter at an initial specified partial pressure, to a stabilised (steady state) FBR and permitting the reaction to continue until either all the oxygen or all the butane was depleted. The effect of oxygen partial pressure in the feed stream upon the yields of butenes (Case 1) and butadiene (Case 2) was studied. In the second scenario, using a stabilised IMR, the partial pressure of oxygen was maintained at a constant specified

level by the addition of fresh oxygen along the length of the IMR. Again the effect of oxygen partial pressure in the feed stream upon the yields of butenes (Case 3), butadiene (Case 4) and butenes and butadiene combined (Case 5) was studied.

In a third scenario, the authors have explored the effect upon the candidate Attainable Region of deploying two very large IMRs in series and by incorporating a policy of by-pass and mixing.

The effect of residence time upon yields of butenes and butadiene was examined. In all instances, the reaction was permitted to attain equilibrium at which stage either the oxygen or the butane had been depleted. In effect, the stoichiometric ratio of oxygen in the feed was varied to simulate different reactant compositions.

Despite there being a spectrum of seven products other than butane and oxygen in the product stream, this study has concentrated only on butenes and butadiene. The yields of carbon monoxide, carbon dioxide and water were not considered.

3.3.1 Scenario 1, Case 1 : Depletion of Oxygen in a FBR – Production of Butenes

The reactor configuration for this scenario is shown in Figure 3.2.

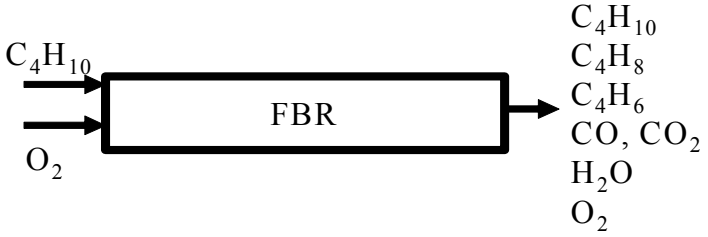


Figure 3.2. FBR Configuration.

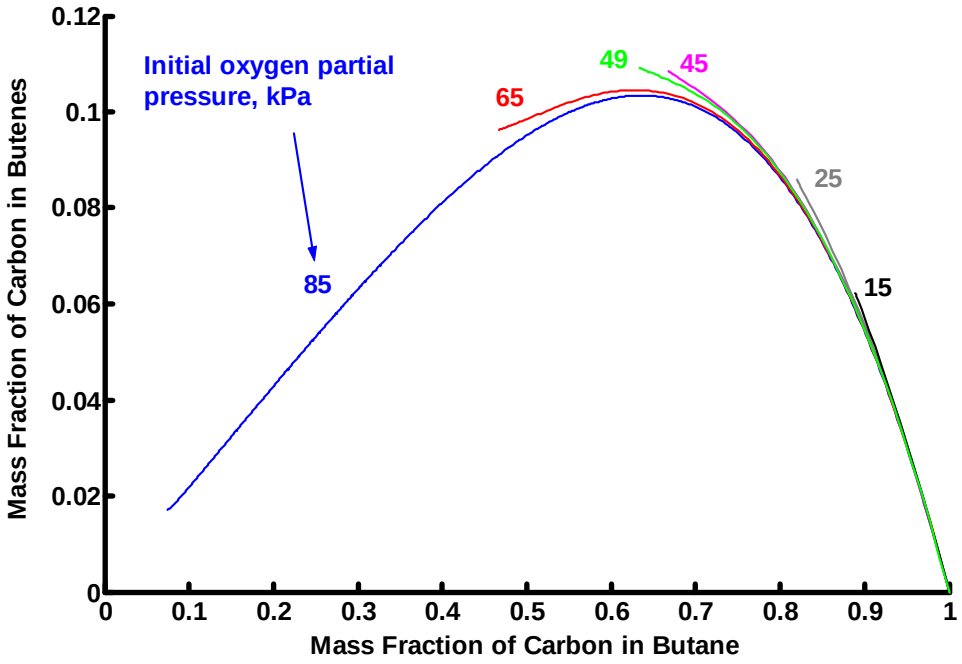


Figure 3.3. Profiles of butane and butenes at various oxygen partial pressures in a FBR.

Using the given rate equations and the initial conditions, that is of pure butane with the specified oxygen concentration (i.e. partial pressure), a total operating pressure of 1 atm. and an isothermal temperature of 773K, one can integrate the differential equations to obtain the results shown in Figure 3.3 where all butane and butenes concentrations are expressed in mass fractions of carbon.

In Figure 3.3, and in subsequent figures of concentration profiles, the various points on the profiles represent the concentrations of reactant and product were the reaction to be stopped at that point, i.e. after the concomitant residence time.

At initial oxygen partial pressures of 85 kPa and 86 kPa, the reaction proceeds until, at equilibrium, all the oxygen has been depleted. When this occurs, the residual

butane and butenes concentrations for an oxygen partial pressure of 85 kPa are 0.075 and 0.017 respectively. The other components present on completion of the reaction, other than butane, butenes and butadiene, are carbon monoxide, carbon dioxide and water. All the oxygen has been utilised in the oxidation of butane, butenes and butadiene.

If the initial partial pressure of oxygen is increased to 87 kPa, at equilibrium all the butane, butenes and butadiene are oxidised and there is residual oxygen present on completion of the reaction. At this initial partial pressure of oxygen, the supply of butane is the limiting factor.

At oxygen partial pressures less than 87 kPa, reaction ceases with oxygen depletion. At an initial oxygen partial pressure of 65 kPa, reaction cessation occurs after a residence time of 31 seconds (at 45 kPa, cessation occurs after a residence time of 14 seconds). Oxygen depletion was defined as when its partial pressure had fallen below 0.001 kPa and the commensurate reactor residence time at this milestone as noted.

The selectivity (S) of butane to butenes was defined as :

$$S_{Butane} = \frac{C_{Butenes}}{(C^{0}_{Butane} - C_{Butane})}$$

Usually, selectivity is calculated as the ratio of moles of product and moles of reactant consumed. In the case of the ODH of butane to butenes, carbon mass fractions can be used instead of moles because of the presence of four carbon atoms in each of the relevant hydrocarbon molecules, butane, butenes (and butadiene). This implies that the difference in the molar masses of butane and butenes which otherwise would render this definition invalid does not apply in this case.

A maximum yield of butenes, 0.109, occurs at an initial oxygen partial pressure of 49 kPa after a residence time of 16 seconds. Residual butane has a concentration of 0.634. If we examine Figure 3.3 in more detail, we see that the selectivity of butane to butenes (butenes formed divided by butane consumed) is given by the slope of a straight line from the feed point. Thus as the profiles shown in Figure 3.3 are bounded by convex curves with the greatest slope at the beginning (the feed point), the largest selectivity of butane to butenes occurs at small conversions. The partial pressure of oxygen present does not seem to affect this value significantly. At 85 kPa the initial slope is 0.65, at 15 kPa the initial slope is 0.60. Thus to get high selectivities commensurate with reasonable conversions, one would need a system with low conversions but embodying separation and recycle.

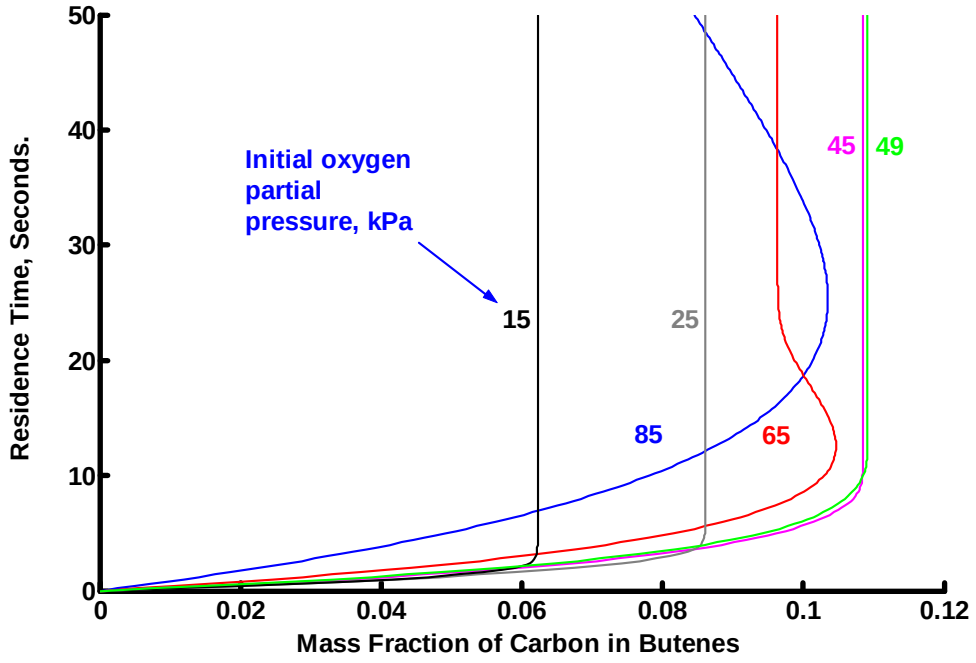


Figure 3.4. Residence times for butenes at various oxygen partial pressures in a FBR.

It is of interest to examine the residence times necessary to obtain the results shown in Figure 3.3. Figure 3.4 shows that the reaction times to attain the maximum yield of butenes do not exceed 25 seconds for all oxygen partial pressures, implying that the ODH reaction is a very fast one.

In Figure 3.4, the "kink" in the residence time profile for 65 kPa (and for 85 kPa at a residence time of 160 seconds) is attributed to the low concentration of oxygen resulting in no further net depletion of butenes. It was established that reaction was still occurring and butadiene was still being formed. This meant that the butenes was being oxidised to butadiene as fast as it were formed and/or that the butane was being oxidised to butadiene directly.

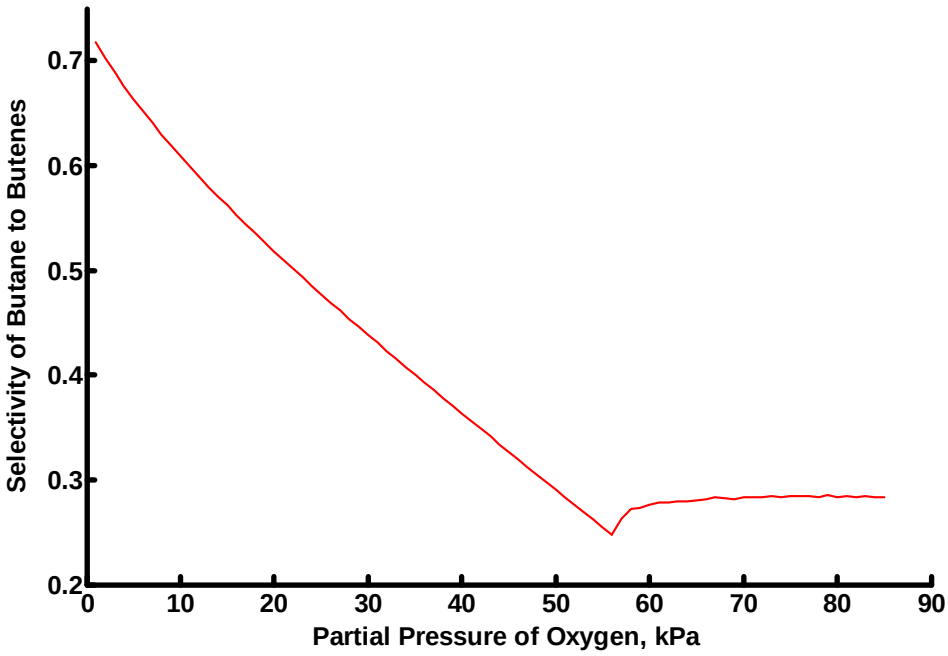


Figure 3.5. Selectivity of butane to butenes in a FBR as a function of initial oxygen partial pressure for conditions of maximum yield of butenes.

Figure 3.5 shows the selectivity profile for butane relative to butenes at maximum yield of butenes as a function of the initial oxygen partial pressure in a FBR.

The discontinuity in the selectivity at an oxygen partial pressure of 56 kPa is explained by reference to Figure 3.3. At oxygen partial pressures from 85 to 57 kPa, the final butenes concentration is less than the maximum butenes concentration. Below 57 kPa, the final and the maximum butenes concentrations are identical. As selectivity in Figure 3.5 is calculated for the maximum yield of butenes, a shift occurs at an oxygen partial pressure of 56 kPa. It is apparent from Figure 3.5 that for initial oxygen partial pressures in a FBR in excess of 56 kPa, the selectivity of butane to butenes is relatively unaffected by the oxygen partial pressure.

Figure 3.5 reveals indicates that butane selectivities for maximum butenes vary widely over the range of partial pressures. At 85 and 1 kPa butane selectivities are 0.28 and 0.72 respectively.

3.3.2 Scenario 1, Case 2 : Depletion of Oxygen in a FBR – Production of Butadiene

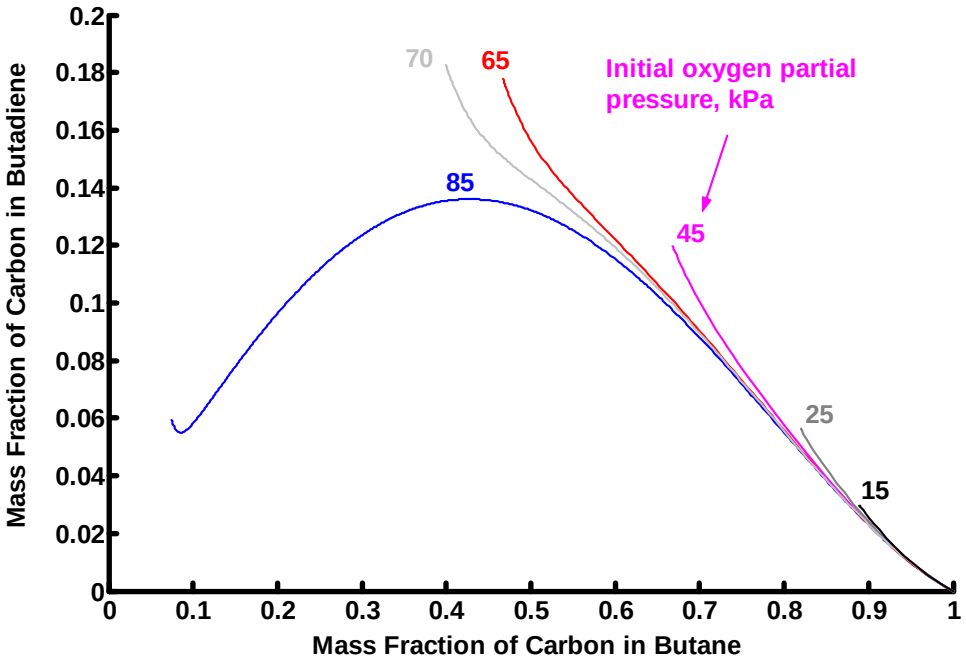


Figure 3.6. Profiles of butane and butadiene at various oxygen partial pressures in a FBR.

At an initial oxygen partial pressure of 85 kPa, the reaction proceeds until all the oxygen has been depleted. When this occurs, the residual butane and butadiene concentrations are 0.075 and 0.059 respectively.

In Figure 3.6, the "kink" at the end of the concentration profile for 85 kPa is attributed to the very low concentration of oxygen at that stage of the ODH process resulting in the preferential oxidation of butane to butadiene via reaction *r4* rather than to butene via reactions *r1*, *r2* and *r3*, as was shown diagrammatically in Figure 3.1.

If the initial partial pressure of oxygen is increased to 87 kPa, all the butane, butene and butadiene is oxidised and there is residual oxygen present on completion of the reaction. At this initial partial pressure of oxygen, the supply of butane is the limiting factor.

At oxygen partial pressures of 85 kPa and less, reaction ceases with oxygen depletion.

The maximum yield of butadiene from a FBR, 0.183, occurs at an initial oxygen partial pressure of 70 kPa. The residual butane has a concentration of 0.399. The residence time is 41 seconds.

A characteristic of all the butadiene:butane profiles shown in Figure 3.6 is the presence of a concave region between the feed point and the profile (at an oxygen partial pressure of 85 kPa, the concave region extends from the feed point to the tangential point at a butadiene concentration of about 0.09).

Figure 3.7 shows that the reaction times to attain the maximum yields of butadiene do not exceed 49 seconds for all oxygen partial pressures up to 85 kPa implying that the ODH reaction is a fast one.

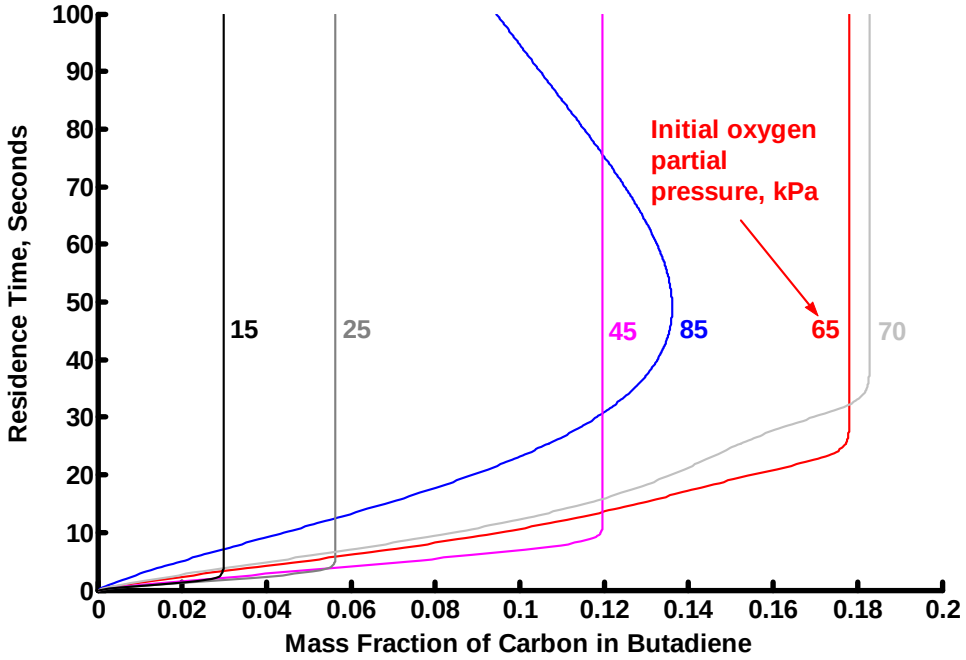


Figure 3.7. Residence times for butadiene at various oxygen partial pressures in a FBR.

The selectivity (S) of butane to butadiene was defined in the same manner as the selectivity of butane to butenes, namely :

$$S_{Butane} = \frac{C_{Butadiene}}{(C^{0}_{Butane} - C_{Butane})}$$

We may use Figure 3.6 to examine the selectivity of the butane to butadiene. The maximum selectivity is given by the line of maximum slope from the feed point (pure butane). Because of the concavity of the profiles in Figure 3.6, this will occur when the line is tangential to the curve or, where no tangent point exists, at the final point of the profile.

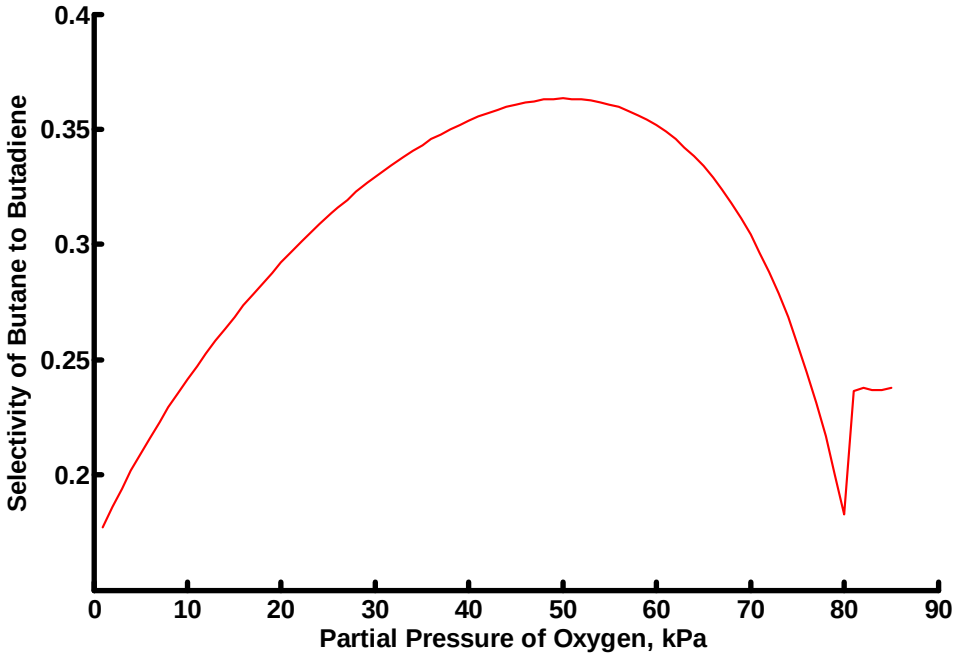


Figure 3.8. Selectivity of butane to butadiene in a FBR as a function of initial oxygen partial pressure for conditions of maximum yield of butadiene.

The discontinuity at an oxygen partial pressure of 80 kPa is explained by reference to Figure 3.6. At oxygen partial pressures from 85 to 81 kPa, the final butadiene concentration is less than the maximum butadiene concentration. Below 81 kPa, the final and the maximum butadiene concentrations are identical. As selectivity in Figure 3.8 is calculated for the maximum yield of butadiene, a shift occurs at an oxygen partial pressure of 80 kPa.

Figure 3.8 indicates that butane selectivities for maximum butadiene vary by 100 % over the range of partial pressures. At 85 and 1 kPa butane selectivities are 0.24 and 0.18 respectively with a maximum selectivity of 0.36 at an oxygen partial pressure of 50 kPa.

The consequence of this was that the supply of oxygen at an appropriate partial pressure was deemed to be an important factor for high yields of butenes and butadiene. To explore this hypothesis, the control of the oxygen supply to a different reactor configuration was examined. The reactor configuration was an IMR with oxygen injection along the length of the reactor to maintain a constant oxygen partial pressure in the gas mixture.

3.3.3 Scenario 2, Case 3 : Replenishment of Oxygen in an IMR – Production of Butenes.

The reactor configuration for this scenario is shown in Figure 3.9.

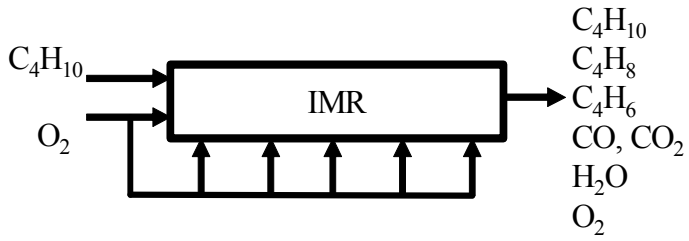


Figure 3.9. IMR Configuration

As before, we can integrate the system of differential equations describing this system. As previously, we will limit the total reactor tube-side pressure to 1 atm. and the isothermal temperature to 773K. Furthermore, we will assume that we supply the oxygen in such a way as to maintain its partial pressure in the reactor at a constant value equal to that in the feed stream and to replenish that consumed in the ODH process. Because of the way we analyse our results in terms of carbon mass fraction, this addition does not affect our analysis unduly.

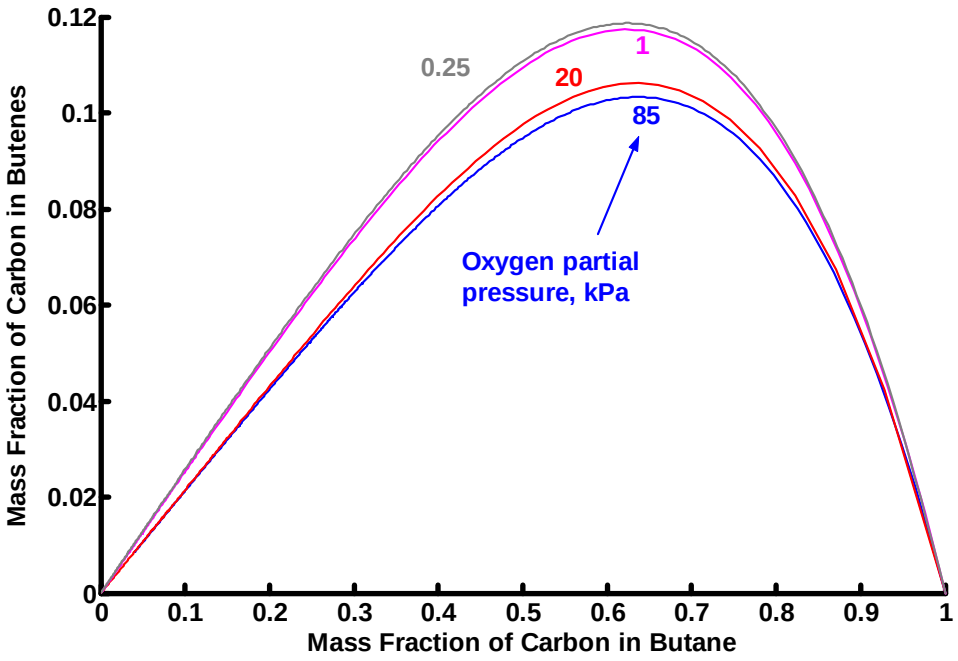


Figure 3.10. Profiles of butane and butenes at constant oxygen partial pressures from 85 kPa to 0.25 kPa in an IMR.

Figure 3.10 shows the effect of adding oxygen along the length of the IMR to maintain a constant oxygen partial pressure in the stream of reactants and products.

It is noticeable from Figure 3.10 that the maximum yield of butenes increases but marginally despite the significant reduction in oxygen partial pressure from 85 kPa to 0.25 kPa. At an oxygen partial pressure of 0.25 kPa, the maximum yield of butenes is slightly less than 0.119 with a commensurate residual butane value of 0.622. The associated residence time is 75 seconds (see Figure 3.11).

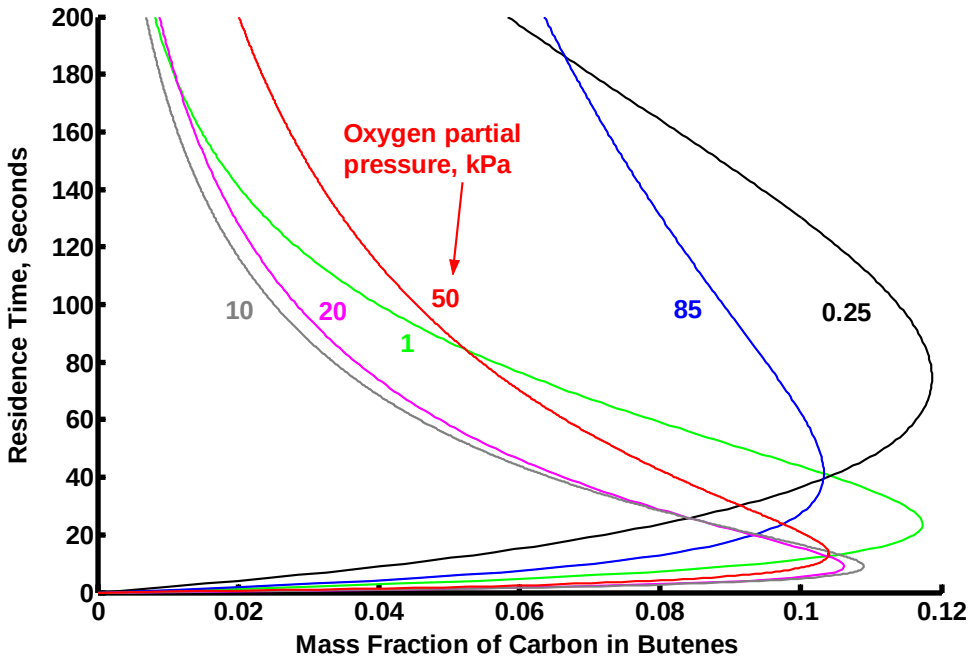


Figure 3.11. Residence times as a function of mass fraction of butenes at constant oxygen partial pressures from 85 kPa to 0.25 kPa in an IMR.

A detailed analysis of Figure 3.11 shows that the residence time for maximum yield of butenes decreases from a value of 41 seconds to 9 seconds with reduced oxygen partial pressure over the range 85 kPa to 10 kPa. One can further see that as the (constant) partial pressure of oxygen is reduced below 10 kPa, the residence times for the maximum yield of butenes gradually increase. For partial pressures less than 1 kPa, the residence time for the maximum yield of butenes increases sharply.

Figure 3.12 shows this interesting result more clearly, i.e. the residence times for the maximum yield of butenes at various oxygen partial pressures.

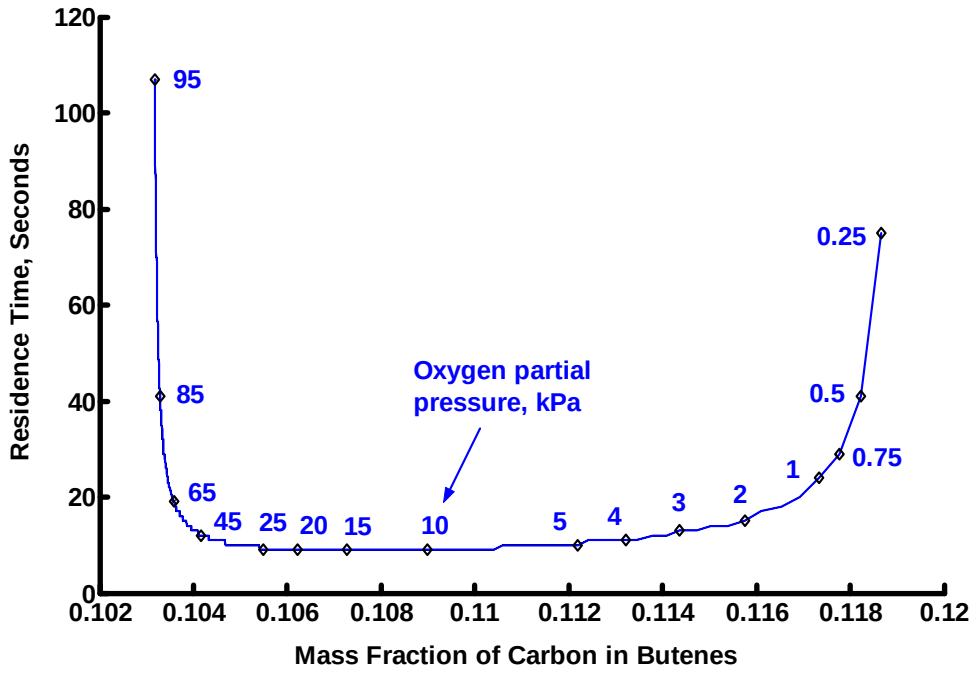


Figure 3.12. Residence times for maximum yield of butenes at constant oxygen partial pressures from 95 kPa to 0.25 kPa in an IMR.

A possible explanation for the shape of this curve is that high oxygen partial pressures require longer residence times due to the scarcity of other reactants. Once the oxygen partial pressure is reduced, so do the reaction rates. This implies a minimum in the curve as was found to be the case.

Maximum butenes yields, associated butane values, butenes selectivities and residence times from an IMR operating at a constant oxygen partial pressure are shown in Table 3.1.

Oxygen Partial Pressure, kPa	Maximum Butenes Yield	Associated Butane Value	Butane Selectivity	Residence Time, Seconds
85	0.103	0.638	0.286	41
65	0.104	0.634	0.283	19

Oxygen Partial Pressure, kPa	Maximum Butenes Yield	Associated Butane Value	Butane Selectivity	Residence Time, Seconds
49	0.104	0.639	0.288	13
45	0.104	0.641	0.290	12
25	0.106	0.645	0.297	9
15	0.107	0.632	0.291	9
10	0.109	0.633	0.297	9
5	0.112	0.637	0.309	10
1	0.117	0.621	0.309	24
0.49	0.118	0.626	0.316	41
0.25	0.119	0.622	0.314	75

Table 3.1. Maximum butenes yields, selectivities and residence times from an IMR at various constant oxygen inlet partial pressures.

From Figure 3.10 it is concluded that the maximum yield of butenes increases with decreasing oxygen partial pressure. Figure 3.11 and Figure 3.12 show that the residence times associated with the maximum yield of butenes falls to a minimum and then increases. The maximum selectivity of butane to butenes is attained at low oxygen partial pressures but the profile of these selectivities is fairly flat, the percentage difference between the observed minimum and maximum selectivities being but 10 %.

We conclude from Table 3.1 that the selectivity of butane for maximum yield of butenes in an IMR is but slightly influenced by the oxygen partial pressure.

This observation that increased butenes yield is associated with low oxygen partial pressure raises the question as to what yield of butenes could be attained at a very low oxygen partial pressure and in a very large reactor?

This question was answered by defining a very low oxygen partial pressure as 0.000001 kPa and the results are shown in Figure 3.13 and Figure 3.14.

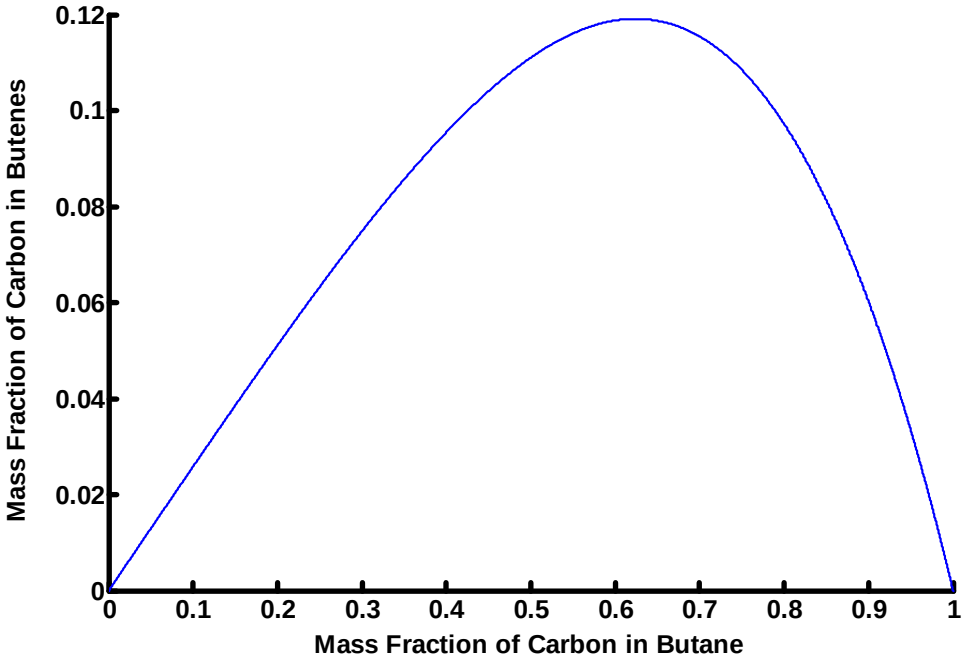


Figure 3.13. Profile of butenes and butane at a very low oxygen partial pressure and in a very large IMR.

The maximum yield of butenes at a very low oxygen partial pressure is 0.119 with a corresponding butane concentration of 0.623. The associated selectivity of butane to butenes is 0.316

As before, the butane-butenes profile in Figure 3.13 is convex over its entire length.

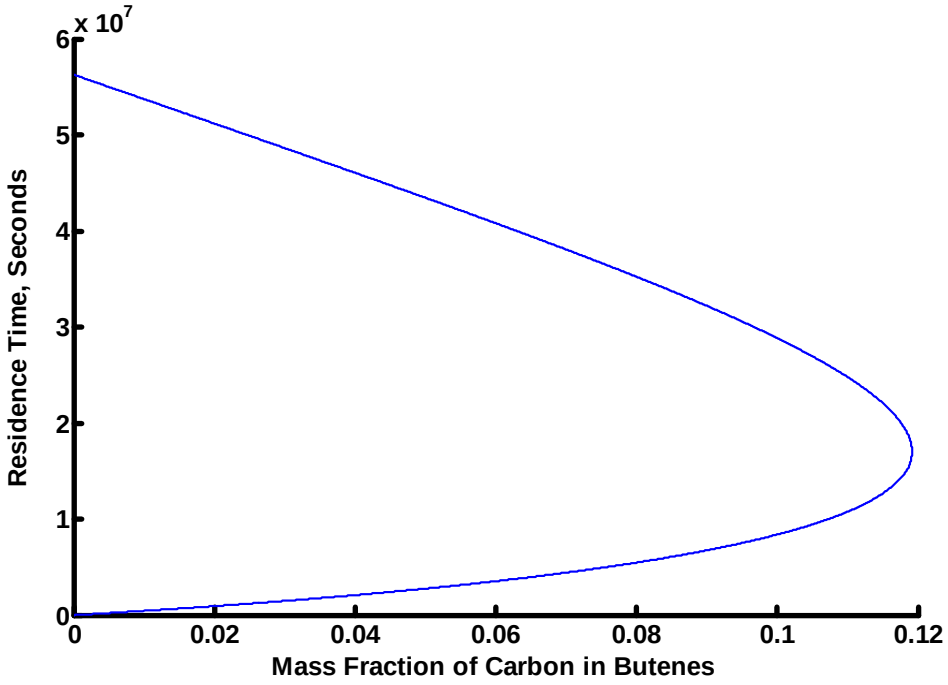


Figure 3.14. Residence time as a function of butenes concentrations at a very low oxygen partial pressure and in a very large IMR.

Figure 3.14 shows that the residence time at a very low oxygen partial pressure for the total conversion of butane is 5.63 x 10^7 seconds. The residence time for maximum yield of butenes is 1.7 x 10^7 seconds.

As has already been noted, for an IMR at a constant oxygen partial pressure of 0.25 kPa, the maximum yield of butenes is slightly less than 0.119 with a residence time of 75 seconds (residual butane 0.622). This, in a commensurately-sized reactor, represents an achievement of practically 100 % relative to the theoretical maximum butenes yield.

For a FBR with an initial oxygen partial pressure of 49 kPa and in which the oxygen is not replenished, the maximum yield of butenes is 0.109 with a residual butane concentration of 0.634 (see Figure 3.3). The residence time was 16 seconds. This

represents an achievement of 92 % relative to the theoretical maximum butenes yield of 0.119.

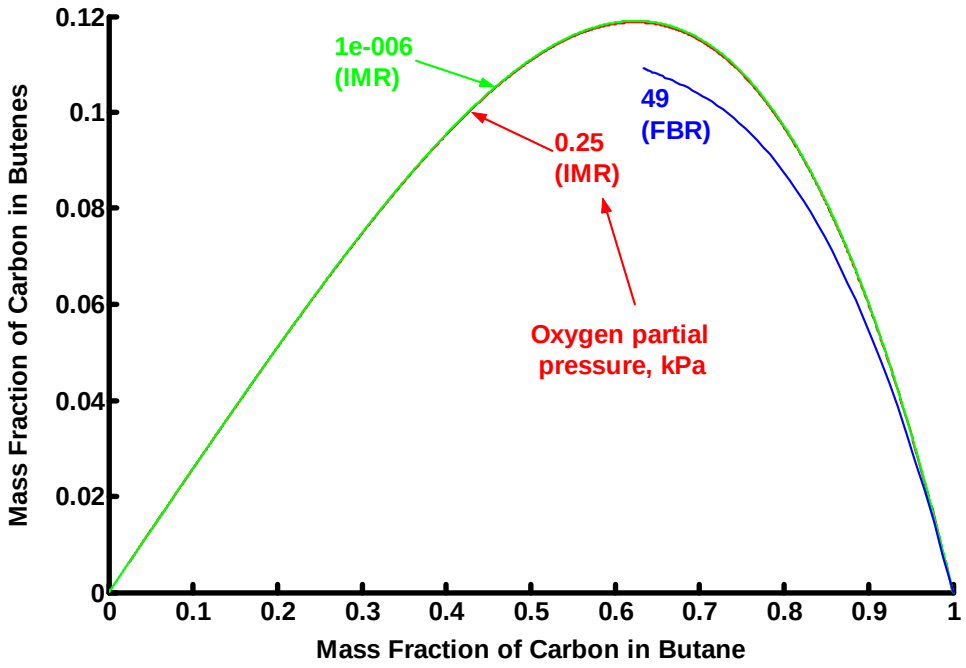


Figure 3.15. Profiles of butane and butenes at different oxygen partial pressures for an IMR and for a FBR.

In Figure 3.15, we show the FBR profile for an oxygen partial pressure of 49 kPa. Also shown are the butane-butenes profiles for an IMR in which the original oxygen partial pressures (0.25 and 0.000001 kPa) are maintained constant through the addition of fresh oxygen along the length of the reactor (the two profiles being practically identical).

It is noteworthy that the butane-butenes profiles considered in Figure 3.15 (depleted oxygen at 49 kPa and constant oxygen at 0.25 kPa) all lie below the profile for a very low oxygen partial pressure. The profile for an oxygen partial pressure of 0.25 kPa lies very close to but nevertheless below the profile for an oxygen partial pressure of 1 x 10^{-6} kPa.

From an analysis of Figure 3.15 we conclude that the theoretical profile for maximum butenes yield at a very low oxygen partial pressure represents the furthermost boundary within which all scenarios so far identified lie.

Consequently, we believe that Figure 3.13 represents a candidate AR for the system sub-space butane-butenes.

3.4 Butenes Yields

The best yields of butenes from the reactor configurations studied were compared with the theoretical best yield of butenes of 0.119 from an IMR of very large size. Ranked in order of their closeness to the theoretical best yield, the results from the reactor configurations are shown in Table 3.2.

Source	Maximum Butenes Yield	Associated Butane Yield	Residence Time, Seconds	Selectivity Butane to Butenes	% of Theoretical Butenes Yield	O_2 Partial Pressure, kPa	Reactor Configuration
Table 3.1	0.119	0.622	75	0.314	99.7 %	0.25	IMR
Table 3.1	0.118	0.626	41	0.316	99.2 %	0.49	IMR
Table 3.1	0.117	0.621	24	0.309	98.3 %	1	IMR
Table 3.1	0.112	0.637	10	0.309	94.1 %	5	IMR
Table 3.1	0.109	0.633	9	0.297	91.6 %	10	IMR
Figure 3.3	0.109	0.634	16	0.298	91.6 %	49	FBR
Table 3.1	0.107	0.632	9	0.291	90.0 %	15	IMR

Table 3.2. Best butenes yields from the various reactor configurations ranked according to their closeness to the theoretical maximum yield of butenes.

From Table 3.2 it is concluded that an IMR with a residence time of 75 seconds operating under a constant oxygen partial pressure of 0.25 kPa gives a maximum butenes yield of 0.1188 carbon mass fraction which is 99.7 % of the theoretical maximum yield of 0.1191.

The second highest yield also is from an IMR. The butenes yield of 0.1182 (99.2 % of the theoretical maximum yield) was achieved at a residence time of 41 seconds and at an oxygen partial pressure of 0.49 kPa.

In practical terms, all the reactor configurations shown in Table 3.2 produced maximum yields of butenes greater than or equal to 90 % of the theoretical maximum. If 90 % is accepted as the minimum criterion, the preferred reactor configuration is an IMR with a constant oxygen partial pressure of 5 kPa and a residence time of 10 seconds. The resulting maximum yield of butenes, 0.112, is 94.1 % of the theoretical maximum.

No concave sections were observed in any of the butane-butenes profiles investigated and consequently, no mixing strategies were applied.

3.4.1 Effect of the Temperature upon the Yield of Butenes

All the analyses conducted have been at the isothermal temperature of 773K, Téllez *et al.* (1999b) and Assabumrungrat *et al.* (2002), and consequently our candidate AR shown in Figure 3.13 is applicable only at that temperature.

Figure 3.16 shows the effect of temperature upon the butane-butenes profile in a very large IMR when the oxygen partial pressure is very low.

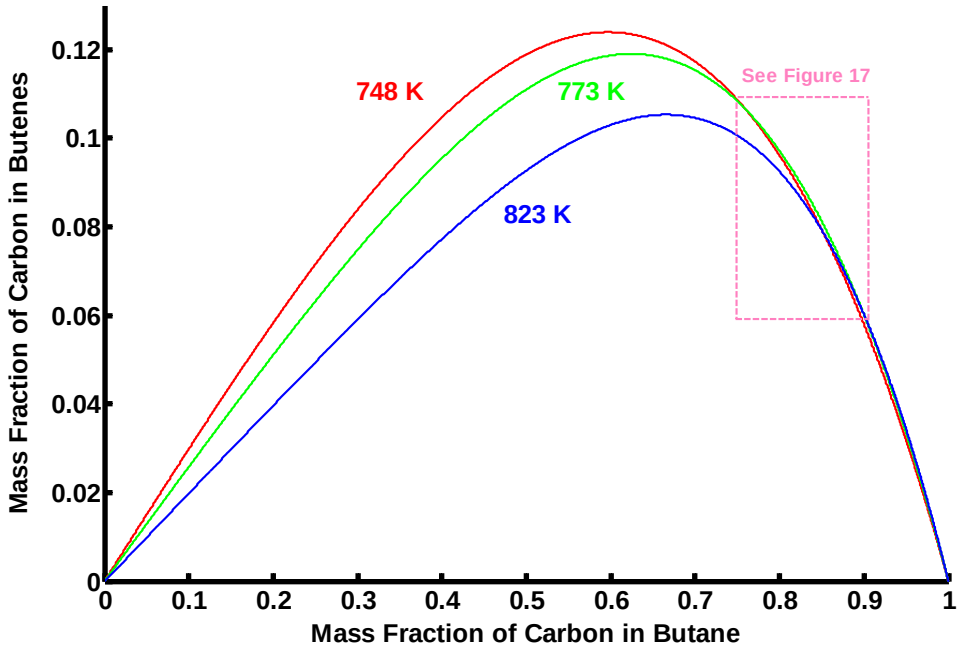


Figure 3.16. Effect of temperature upon theoretical maximum yield of butenes.

Examination of Figure 3.16 shows that increasing the reactor temperature from 773K to 823K reduces the maximum theoretical yield of butenes from 0.119 to 0.105 with an associated butane concentration of 0.665. The associated residence time was 5.39 x 10^6 seconds and the associated selectivity of butane at this temperature is 0.313. Decreasing the operating temperature from 773K to 748K marginally increases the maximum theoretical yield of butenes (from 0.119 to 0.124) with an associated butane concentration 0.596. The associated residence time was 3.15 x 10^7 seconds with a selectivity of butane at 748K of 0.307.

In the butane concentration range of 0.76 to 0.90 both an increase and a decrease in temperature results in slightly lower yields of butenes as the two profiles for 748K

and 823K lie under the profile for 773K. Refer to Figure 3.17 for a magnified view of this.

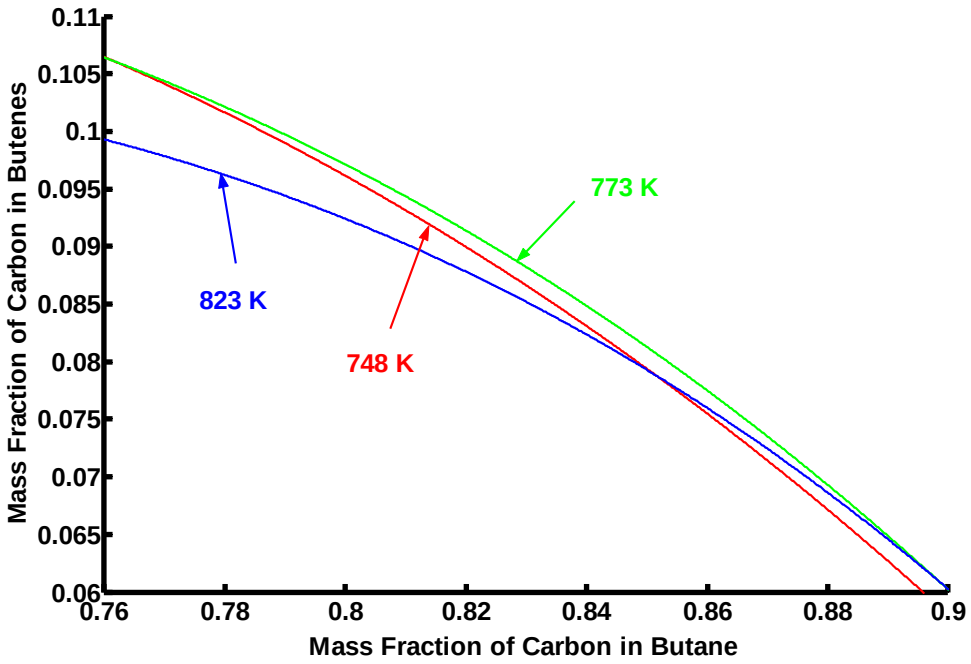


Figure 3.17. Magnified section of Figure 3.16.

Consequently, we maintain that each of the three profiles shown in Figure 3.16 represents a candidate AR for the system sub-space butane-butenes at the respective temperature.

To conclude our analysis, we investigated the circumstances at which the maximum yields of butenes from a FBR and an IMR are equivalent. A detailed analysis of Figure 3.3 and Figure 3.10 shows that at high oxygen partial pressures, a greater yield of butenes is obtained from a FBR than from an IMR and that at low oxygen partial pressures the converse is applicable. The critical value of oxygen partial pressure was found to be 39 kPa. At this pressure and greater, the maximum yield of butenes is greater from a FBR than from an IMR. Below 39 kPa, the maximum yields of butenes are greater from an IMR. The greatest percentage difference

between the maximum yields of butenes, 5 %, is at an oxygen partial pressure of 49 kPa.

Table 3.3 shows the respective values at oxygen partial pressures close to 39 kPa.

Oxygen Partial Pressure, kPa	**IMR**			**FBR**		
	Maximum Butenes	**Associated Butane**	**Residence Time, Seconds**	**Maximum Butenes**	**Associated Butane**	**Residence Time, Seconds**
36	0.105	0.631	11	0.102	0.740	10
37	0.105	0.634	11	0.103	0.732	10
38	0.105	0.637	11	0.104	0.724	10
39	0.104	0.640	11	0.105	0.717	11
40	0.104	0.642	11	0.106	0.709	11
41	0.104	0.628	12	0.107	0.701	11

Table 3.3. Comparison of maximum yields of butenes from an IMR and a FBR at different oxygen partial pressures.

3.4.2 Scenario 2, Case 4 : Replenishment of Oxygen in an IMR – Production of Butadiene.

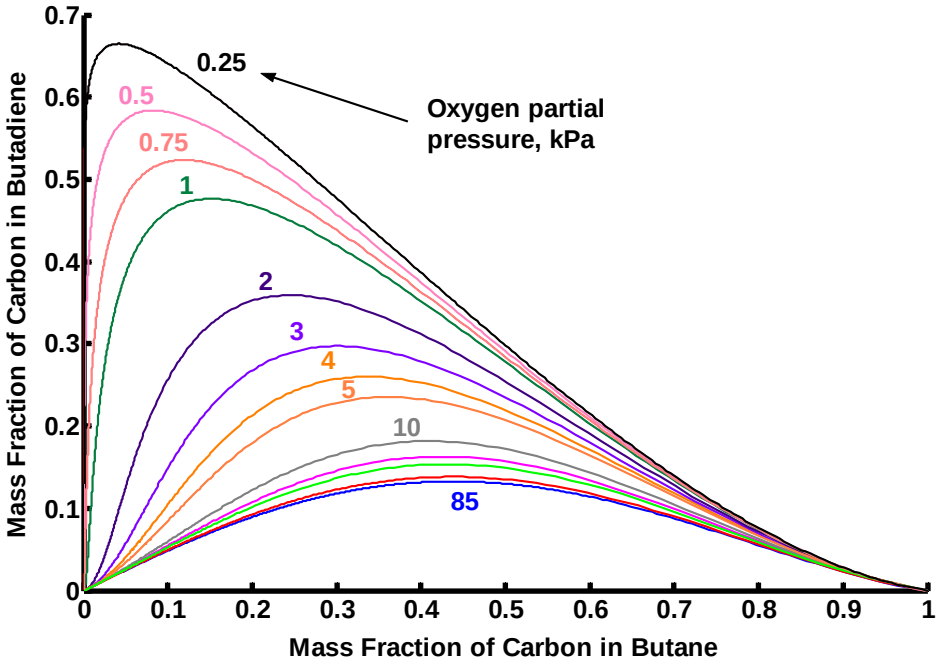


Figure 3.18. Profiles of butane and butadiene at constant oxygen partial pressures from 85 kPa to 0.25 kPa in an IMR.

Figure 3.18 shows the effect of adding oxygen along the length of the reactor to maintain a constant oxygen partial pressure in the stream of reactants and products.

It is noticeable from Figure 3.18 that the maximum yield of butadiene increases with the reduction in oxygen partial pressure from 85 kPa to 0.25 kPa. At an oxygen partial pressure of 0.25 kPa, the maximum yield of butadiene is 0.665 with a commensurate butane concentration of 0.042. The associated residence time is 322 seconds (see Figure 3.19).

Again, it should be noted that each of the profiles shown in Figure 3.18 exhibits a concave section. These concave regions can be removed through an appropriate mixing scenario (along a straight line from the feed point that is tangential to the profile) involving fresh reactant (butane) and reaction products. The maximum butane selectivity is found at the tangential point of the relevant profile.

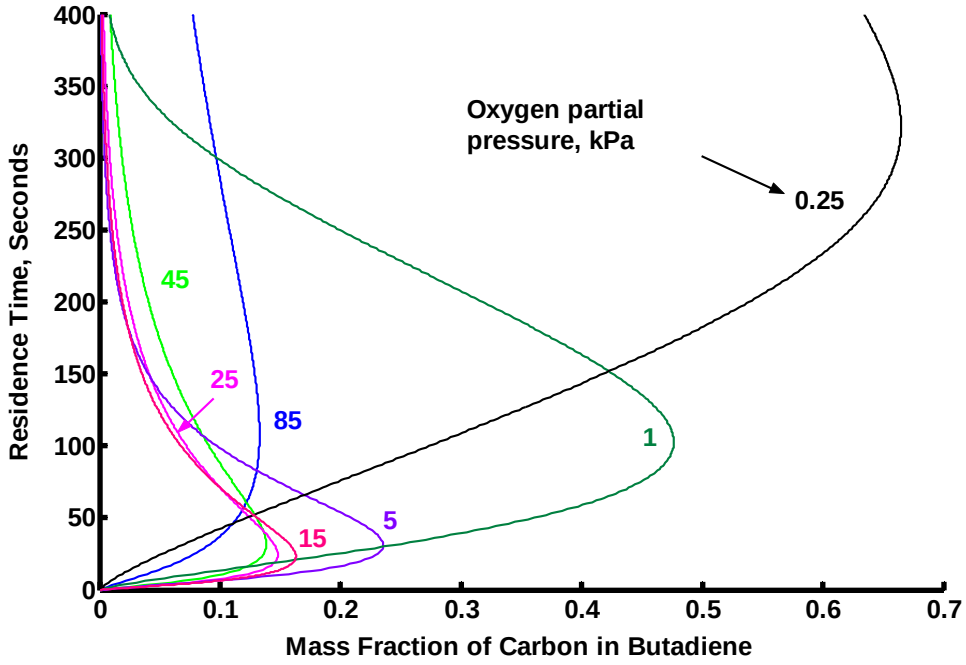


Figure 3.19. Residence times for butadiene at constant oxygen partial pressures from 85 kPa to 0.25 kPa in an IMR.

A detailed analysis of Figure 3.19 shows that the residence time for maximum yield of butadiene decreases from a value of 108 seconds to a minimum of 23 seconds over the oxygen partial pressure range of 85 kPa to 15 kPa.

As the partial pressure of oxygen is reduced below 15 kPa, the residence times for the maximum yield of butadiene gradually increase. For partial pressures less than

1 kPa, the residence time for maximum yield of butadiene increases sharply. These results are illustrated in Figure 3.20.

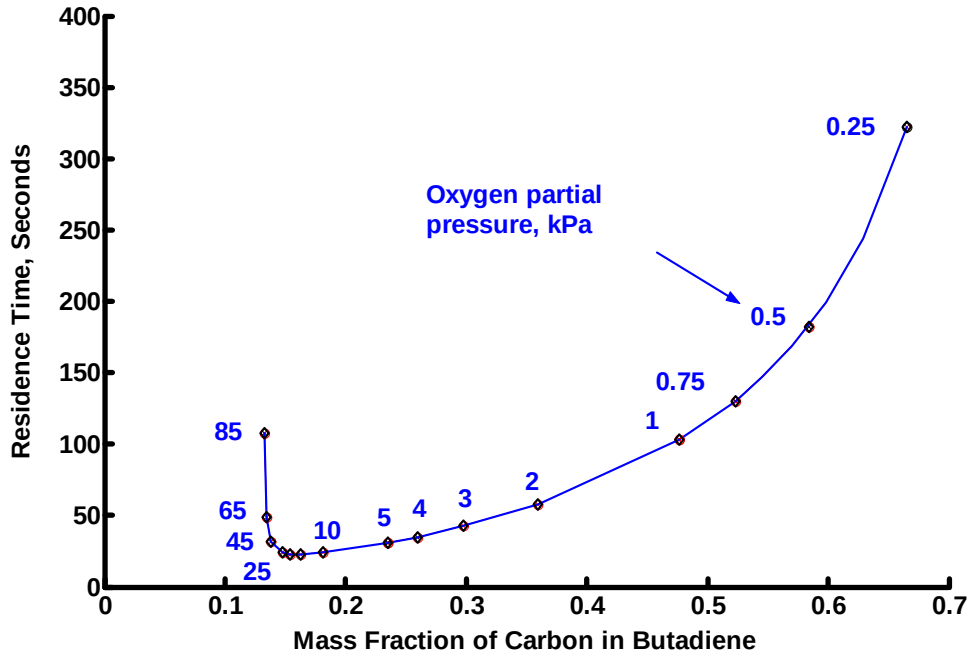


Figure 3.20. Residence times for maximum yield of butadiene at constant oxygen partial pressures from 85 kPa to 0.25 kPa in an IMR.

Figure 3.20 is a synthesis of Figure 3.19 and shows that the residence time associated with the maximum yield of butadiene falls to a minimum and then increases. As the oxygen partial pressure is decreased further below 0.25 kPa, the maximum yield of butadiene obtainable from an IMR tends asymptotically to a value of 0.8. However to attain this value, residence times have to be increased dramatically.

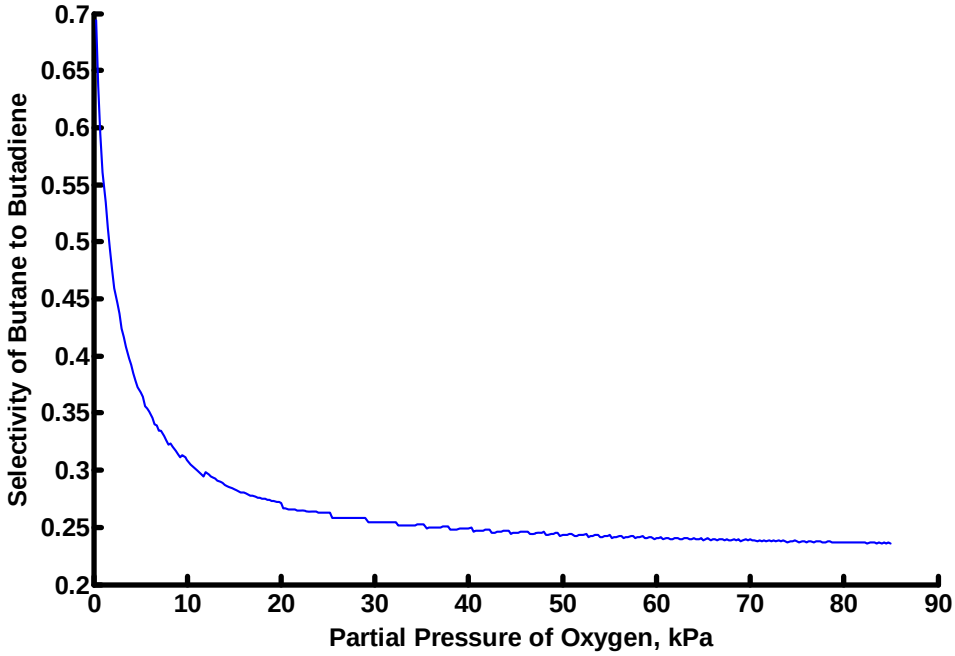


Figure 3.21. Selectivity of butane to butadiene in an IMR as a function of oxygen partial pressure for conditions of maximum yield of butadiene.

Figure 3.21 shows the effect of oxygen partial pressure on butane selectivity for maximum yield of butadiene. There is a wide variation of selectivities over the range of partial pressures from 0.24 at 85 kPa to 0.70 at 0.25 kPa.

To conclude our analysis of the production of butadiene, we investigated the circumstances at which the maximum yields from a FBR and an IMR are equivalent. An examination of Figure 3.6 and Figure 3.18 shows that at high oxygen partial pressures, a greater yield of butadiene is obtained from a FBR than from an IMR and that at low oxygen partial pressures the converse is applicable. The critical value of oxygen partial pressure was found to be 50 kPa. At this pressure and greater, the maximum yield of butadiene is greater from a FBR than from an IMR. Below 50 kPa, the maximum yields of butadiene are greater from an IMR. The greatest percentage difference between the maximum yields of butenes, 36 %, is at an oxygen partial pressure of 70 kPa.

Table 3.4 shows the respective values at oxygen partial pressures close to 50 kPa.

Oxygen Partial Pressure, kPa	IMR			FBR		
	Maximum Butadiene Value	Associated Butane Value	Residence Time, Seconds	Maximum Butadiene Value	Associated Butane Value	Residence Time, Seconds
48	0.138	0.440	33	0.130	0.643	14
49	0.137	0.438	34	0.133	0.634	15
50	0.137	0.436	35	0.136	0.625	16
51	0.137	0.440	35	0.140	0.616	16
52	0.137	0.438	36	0.143	0.606	18
53	0.137	0.436	37	0.146	0.597	18

Table 3.4. Comparison of maximum yields of butadiene from an IMR and a FBR at different oxygen partial pressures.

The question as to what yield of butadiene could be attained at a very low oxygen partial pressure and a reactor of very large size was answered by defining a very low oxygen partial pressure as 0.000001 kPa and the results are shown in Figure 3.22 and Figure 3.23.

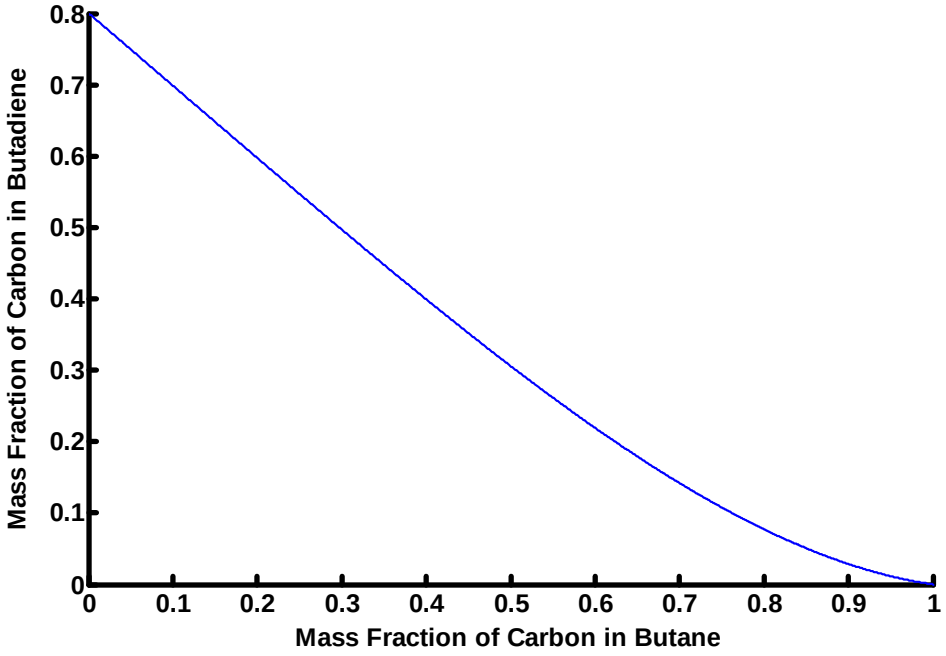


Figure 3.22. Profile of butane and butadiene at a very low oxygen partial pressure and in a very large IMR.

The maximum yield of butadiene at a very low oxygen partial pressure is 0.800. At this point, the initial butane feed has been totally depleted.

The butane-butadiene profile in Figure 3.22 is concave over its entire length and the maximum selectivity is given by the slope of the line from the feed point (1, 0) to its point of tangential contact with the profile (0.8, 0).

Figure 3.23 shows that the residence time at this very low oxygen partial pressure for the total oxidation of butane is 5.6×10^7 seconds.

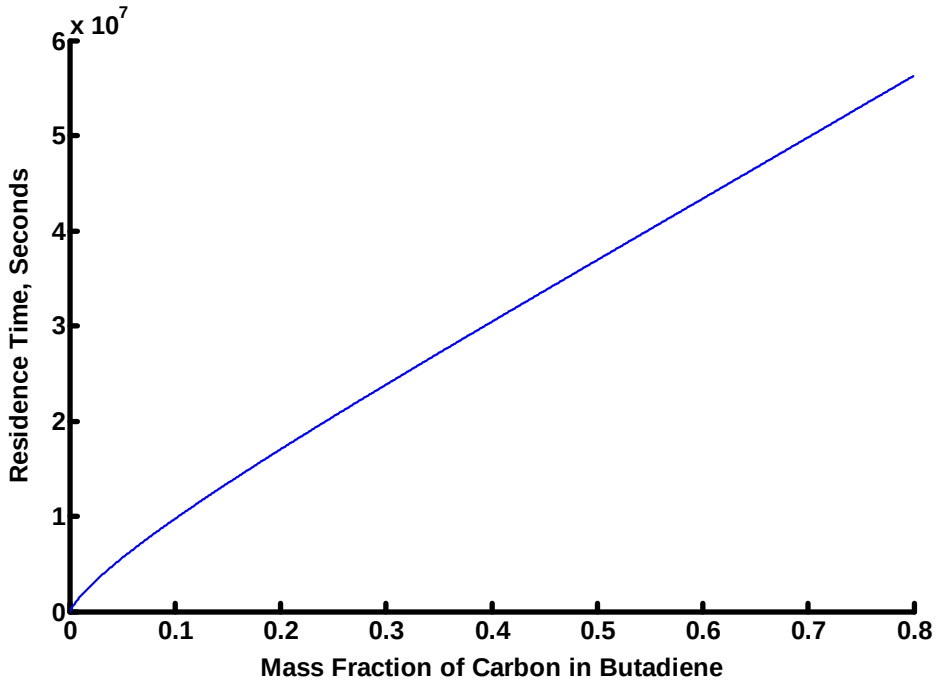


Figure 3.23. Residence times for butadiene production at a very low oxygen partial pressure and in a very large IMR.

As has already been noted, for an IMR at a constant oxygen partial pressure of 0.25 kPa, the maximum yield of butadiene is 0.665 with a residence time of 322 seconds (residual butane at this maximum yield of butadiene was 0.042). This represents an achievement of 83 % relative to the theoretical maximum butadiene yield of 0.800.

For a FBR with an initial oxygen partial pressure of 70 kPa and in which the oxygen is not replenished, the maximum yield of butadiene is 0.183 (see Figure 3.6). This represents an achievement of only 23 % relative to the theoretical maximum butadiene yield of 0.800. Residual butane concentration was 0.399.

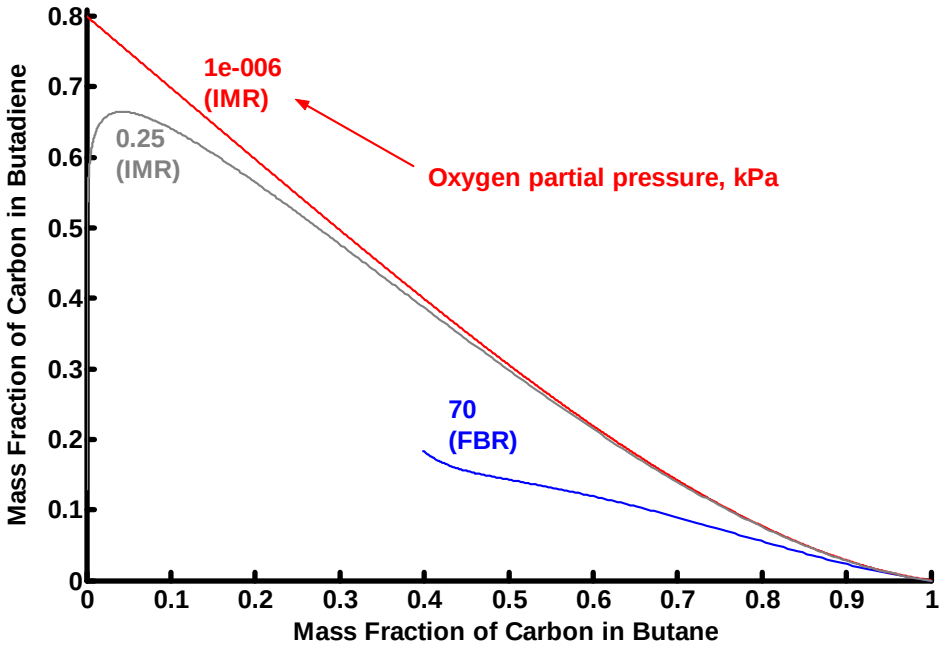


Figure 3.24. Profiles of butane and butadiene at different oxygen partial pressures for an IMR and for a FBR.

As well as the FBR profile for 70 kPa, Figure 3.24 also shows the butane-butadiene profiles for an IMR in which the original oxygen partial pressures (0.25 and 0.000001 kPa) are maintained constant along the length of the reactor.

It is significant that the butane-butadiene profiles considered in Figure 3.24 (depleted oxygen at 70 kPa and constant oxygen at 0.25 kPa) all lie below the profile for a very low oxygen partial pressure.

We have commented upon the concave shape of all the butane-butadiene profiles so far identified. The significance of a concavity is that in these instances it can be removed geometrically by a straight line from the feed point that is tangential to the profile. This is akin to taking fresh feed and mixing it with reactor products at the

tangent point. The tangent line, therefore, represents the locus of all possible mixing configurations.

Consequently, we can extend the area beneath the theoretical butane-butadiene profile by drawing the tangent from the feed point (point A) to the curve (point B).

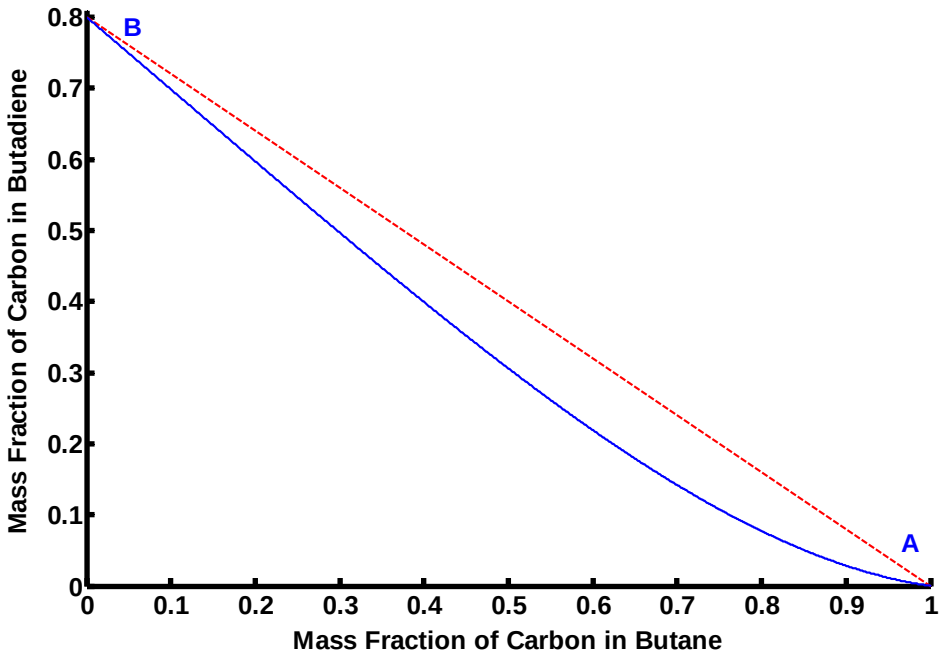


Figure 3.25. Profile of candidate AR for the system sub-space butane-butadiene.

We believe that the resulting expanded area represents a candidate AR for the system butane-butadiene in the sub-space shown. In terms of normal AR theory, it might be thought that the reactor configuration necessary to attain this candidate AR is a CSTR from point A to point B followed by an IMR from point B. This is not correct as Figure 3.25 is but a projection from the full space and only those reaction vectors in the sub-space are collinear with the mixing vectors in the sub-space.

3.4.3 Butadiene Yields

The best yields of butadiene from the reactor configurations studied were compared with the theoretical best yield of butadiene of 0.800 from an IMR of very large size. Ranked in order of their closeness to the theoretical best yield, the results from the reactor configurations are shown in Table 3.5.

Source	Maximum Butadiene Yield	Associated Butane Yield	Residence Time, Seconds	% of Maximum Theoretical Butadiene Yield	Oxygen Partial Pressure, kPa	Reactor Config-uration
Figure 3.18	0.665	0.042	322	83%	0.25	IMR
Figure 3.18	0.534	0.112	138	67 %	0.70	IMR
Figure 3.6	0.183	0.399	41	23 %	70.0	FBR

Table 3.5. Best butadiene yields from an IMR and a FBR ranked according to their closeness to the theoretical maximum yield of butadiene.

From Table 3.5 it is concluded that an IMR with a residence time of 322 seconds operating under a constant oxygen partial pressure of 0.25 kPa gives a maximum butadiene yield of 0.665 carbon mass fraction which is 83 % of the theoretical maximum yield of 0.800.

3.4.4 Effect of the Temperature upon the Yields of Butadiene

All the analyses conducted have been at the isothermal temperature of 773K and consequently our candidate AR shown in Figure 3.25 is applicable only at that temperature.

Figure 3.26 shows the effect of temperature upon the butane-butadiene profile in a very large IMR when the oxygen partial pressure is very low.

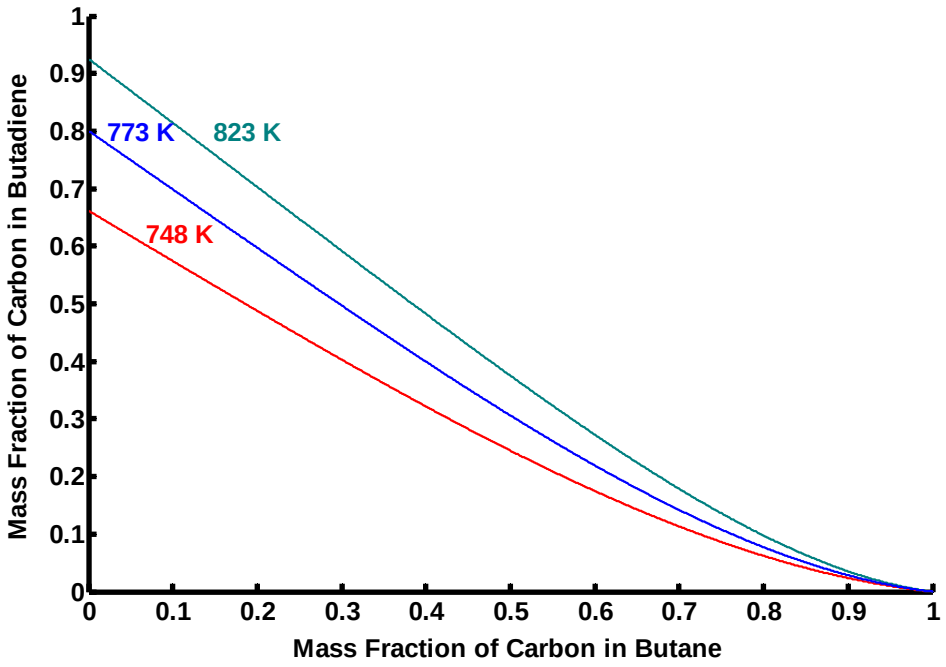


Figure 3.26. Effect of temperature upon theoretical maximum yield of butadiene

Examination of Figure 3.26 shows that an increasing the reactor temperature from 773K to 823K increases the maximum theoretical yield of butadiene from 0.800 to 0.925. The maximum selectivity of butane at 823K is 0.925. Decreasing the operating temperature from 773K to 748K decreases the maximum theoretical yield of butadiene from 0.800 to 0.661. The maximum selectivity at 748K is 0.661

From Figure 3.26 we conclude that the theoretical maximum yield of butadiene and the selectivity of butane increase with temperature over the range 773K to 823K. The maximum yield and selectivity decrease as the temperature is reduced from 773K to 748K.

3.4.5 Scenario 2, Case 5 : Replenishment of Oxygen in an IMR – Production of Butenes and Butadiene.

Finally, we answered the question as to what was the maximum combined yield of butenes and butadiene from an IMR operating at a constant oxygen partial pressure.

Figure 3.27 shows the profiles for butenes, butadiene and butenes plus butadiene as a function of butane concentration. The constant oxygen partial pressure was 85 kPa. Whereas the profile for butadiene shows a concave section and the profile for butenes does not, the profile for butenes and butadiene is convex over its entire length.

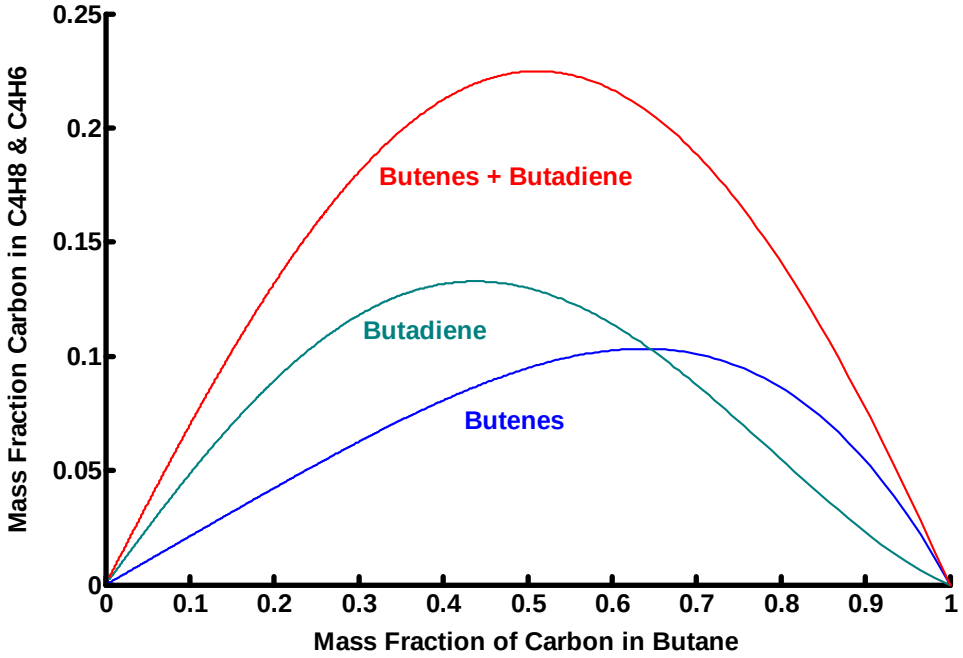


Figure 3.27. Profiles of butenes, butadiene and butenes plus butadiene against butane at a constant oxygen partial pressure of 85 kPa in an IMR.

Figure 3.28 shows the IMR residence time profiles for butenes, butadiene and butenes plus butadiene at an oxygen partial pressure of 85 kPa. The residence time for the maximum yield of butenes plus butadiene, 77 seconds, is greater than that for butenes (41 seconds, Table 3.1) and less than that for butadiene (108 seconds, Figure 3.19).

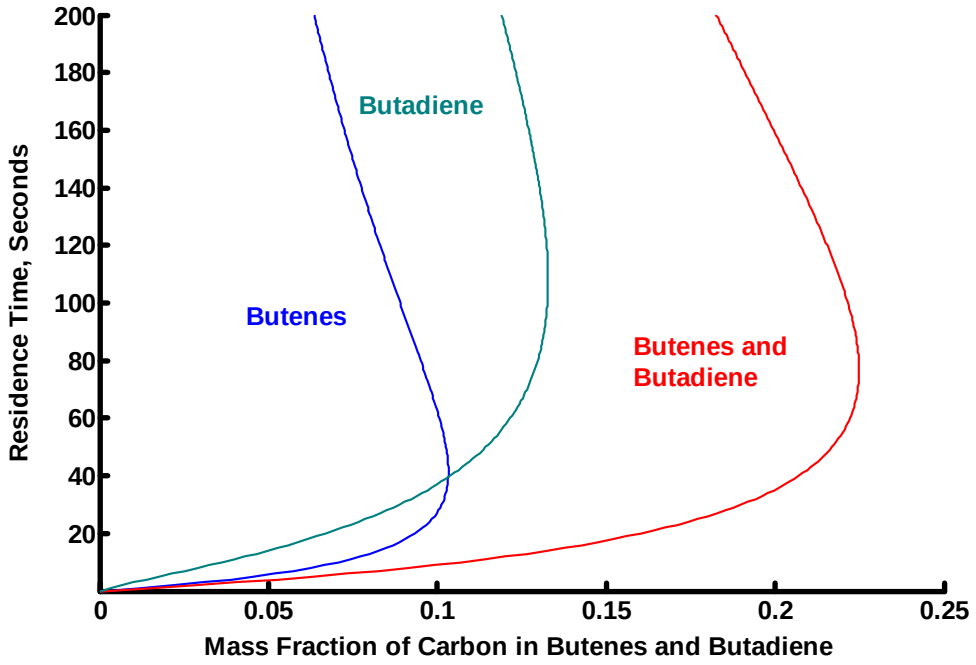


Figure 3.28. IMR residence times for butenes, butadiene and butenes plus butadiene at a constant oxygen partial pressure of 85 kPa.

Figure 3.29 shows the IMR concentration profiles for butenes plus butadiene as a function of butane concentration at constant oxygen partial pressures from 0.25 kPa to 85 kPa. At an oxygen partial pressure of 0.25 kPa, the maximum yield of butenes plus butadiene is 0.677 with a butane selectivity of 0.716 and a residence time of 307 seconds. The corresponding residence times at the same oxygen partial pressure are 75 seconds (butenes, Table 3.1) and 322 seconds (butadiene, Figure 3.19).

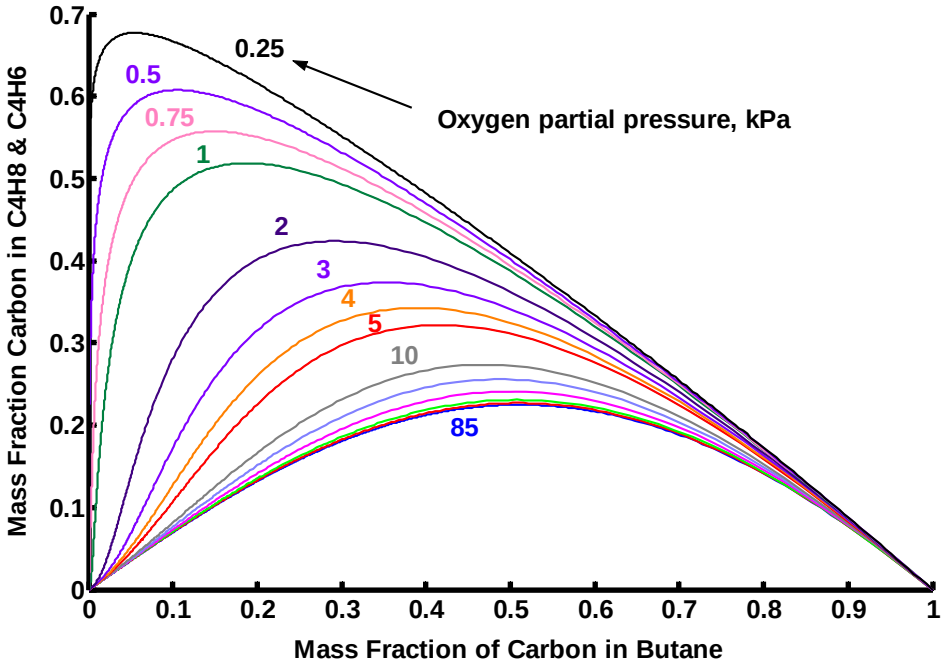


Figure 3.29. IMR profiles for butenes plus butadiene against butane at constant oxygen partial pressures.

At oxygen partial pressures of 15 kPa and less, a concave region exists in the profiles at low values of butane concentration. These regions could be extended by using a CSTR in series with the IMR.

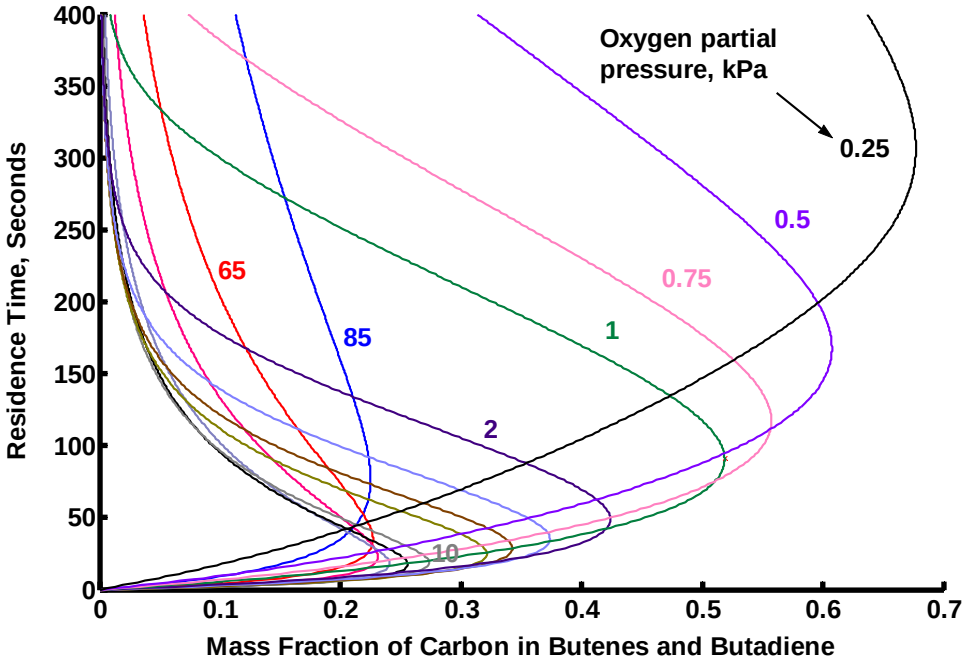


Figure 3.30. IMR residence times butenes plus butadiene at constant oxygen partial pressures.

Figure 3.30 exhibits the same pattern noticed in Figure 3.19, namely a drop in residence time for maximum yield of butenes plus butadiene from 77 seconds at 85 kPa to a minimum of 17 seconds at 15 kPa. At oxygen partial pressure less than 15 kPa, the residence times for the maximum yield of butenes plus butadiene increases to 307 seconds at 0.25 kPa. For reason of clarity, the 15 kPa profile has been omitted from Figure 3.30.

Over the range of oxygen partial pressures studied, the greatest selectivity of butane to butenes and butadiene combined was 0.72 at an oxygen partial pressure of 0.25 kPa and the least was 0.46 at an oxygen partial pressure of 85 kPa.

3.4.6 Scenario 3 : Extension of the Attainable Region – Two IMRs in Series.

Our previous studies of AR systems, Glasser *et al.* (1987), have led us to expect that filling in a concave region through a process of by-pass and mixing sometimes can result in a further extension of the AR by feeding this mixture to another IMR. Referring to Figure 3.25, were an IMR to be added to the process flow diagram with a feed taken from any point on the line AB, it might be possible to extend the AR beyond the line AB. However, in a two-dimensional sub-space, it is not always apparent that the region can be extended. To establish whether a region can be extended it would be necessary to consider higher dimensional profiles.

The reactor configuration for such an arrangement in the two-dimensional sub-space is shown in Figure 3.31.

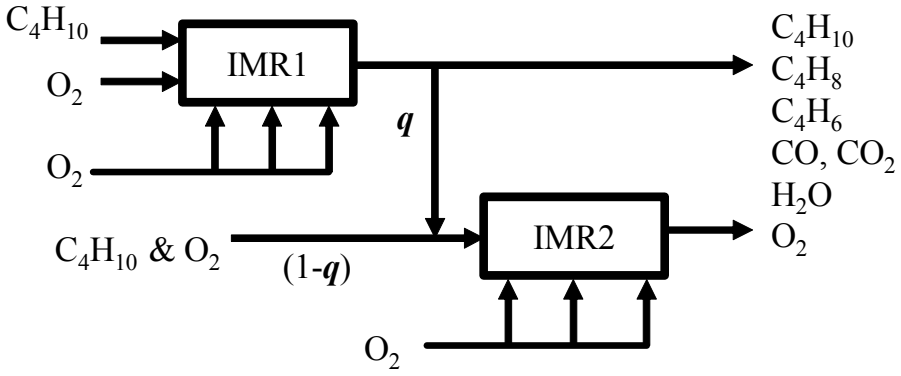


Figure 3.31. IMR Series Configuration.

The reactor configuration studied in Figure 3.31 was a very large IMR followed by a second equally large IMR. In this configuration, the output from IMR1 (i.e. point B in Figure 3.25) is mixed with butane (point A in Figure 3.25) in the volumetric ratio of q:(1-q). The constant oxygen partial pressure in each IMR was 0.000001 kPa.

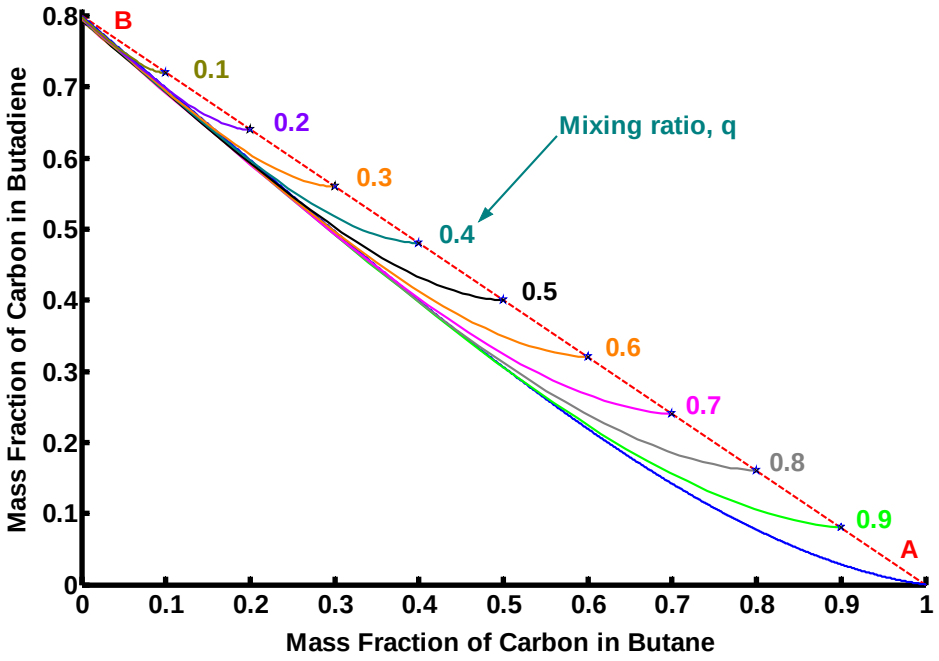


Figure 3.32. Butane-butadiene profiles from two IMRs in series.

In Figure 3.32 we show that such an arrangement has not resulted in any further extension of the AR beyond the tangent line AB. By taking a range of mixtures from the first IMR with varying mixing ratios, *q*, of final products and fresh reactants and supplying each feed to a second IMR, we have shown that each of the resulting butane-butadiene profiles lies wholly beneath the tangent line AB.

In Figure 3.25, the area enclosed by the straight line AB, the x-axis and the y-axis represents the boundaries of the region within which all scenarios so far identified lie.

Consequently, we believe that Figure 3.25 represents a candidate AR for the system sub-space butane-butadiene.

3.5 Conclusions

The best yield of butenes identified in this study from a reactor of finite size is slightly less than 0.119 with a corresponding residence time of 75 seconds. This yield of butenes represents almost 100 % of the theoretical maximum quantity from an IMR of very large size with a very low oxygen partial pressure. The reactor configuration for this example was an IMR with a constant oxygen partial pressure of 0.25 kPa.

A candidate AR has been identified for the system sub-space butane-butenes at an operating temperature of 773K. This candidate AR is shown in Figure 3.13.

In a realistically sized reactor, the best yield of butadiene identified in this study is 0.665 with a corresponding residence time of 322 seconds (Figure 3.18). This yield of butadiene represents 83 % of the theoretical quantity from an IMR of very large size with a very low oxygen partial pressure. The reactor configuration for this example was an IMR with a constant oxygen partial pressure of 0.25 kPa.

A candidate AR has been identified for the system sub-space butane-butadiene at a temperature of 773K. This candidate AR is shown in Figure 3.25.

In the ODH of *n*-butane, an increase in temperature reduces the maximum yield of butenes. A reduction in temperature increases the maximum yield of butenes.

In the ODH of *n*-butane, an increase in temperature increases the maximum yield of butadiene. A reduction in temperature reduces the maximum yield of butadiene.

The maximum yield of butenes plus butadiene found was 0.677 with a butane selectivity of 0.716. The reactor used was an IMR with a constant oxygen partial pressure of 0.25 kPa. The residence time was 307 seconds.

3.6 Nomenclature

C Carbon mass fraction of species *i*

C_i^0 Initial carbon mass fraction of species *i*

r_i Rate of reaction of reaction *i*, mol/kg s

S_i Conversion selectivity of species *i*

3.7 Literature Cited

Assabumrungrat, S., Rienchalanusarn, T., Praserthdam, P., Goto, S., (2002), Theoretical Study of the Application of Porous Membrane Reactor to Oxidative Dehydrogenation of *n*-Butane, *Chemical Engineering Journal*, vol. 85, pp. 69-79.

Glasser, D., Hildebrandt, D., Crowe, C., (1987), A Geometric Approach to Steady Flow Reactors: The Attainable Region and Optimisation in Concentration Space, *American Chemical Society*, pp. 1803-1810.

International Network for Environmental Compliance and Enforcement, Washington, DC, USA Anon, Industrial Processes. Web site www.inece.org/mmcourse/chapt1.pdf

Milne, D., Glasser, D., Hildebrandt, D., Hausberger, B., (2004), Application of the Attainable Region Concept to the Oxidative Dehydrogenation of *1*-Butene in Inert Porous Membrane Reactors, *Industrial and. Engineering Chemistry Research*, vol. 43, pp. 1827-1831.

Téllez, C., Menéndez, M., Santamaría, J., (1997), Oxidative Dehydrogenation of Butane using Membrane Reactors, *Journal of the American Institution of Chemical Engineers*, viol. 43, (No.3), pp. 777-784.

Téllez, C., Menéndez, M., Santamaría, J., (1999a), Kinetic Study of the Oxidative Dehydrogenation of Butane on V/MgO Catalysts, *Journal of Catalysis*, vol. 183, pp. 210-221.

Téllez, C., Menéndez , M., Santamaría, J., (1999b), Simulation of an IMR for the Oxidative Dehydrogenation of Butane, *Chemical Engineering Science*, vol. 54, pp. 2917-2925.

CHAPTER 4

Graphical Technique for Assessing a Reactor's Characteristics

---

The following paper was published by *Chemical Engineering Progress* in March 2006, Vol. 102, No. 3, pp. 46-51 under the title "Graphically Assess a Reactor's Characteristics" with corrections subsequently published in *Chemical Engineering Progress*, July 2006, Vol. 102, No. 7, p.6

The numbering of the figures and tables as submitted to *Chemical Engineering Progress* has been prefixed with the reference (4) to this chapter of my thesis.

In this chapter of my thesis the referencing system required by the editors of *Chemical Engineering Progress* has been changed to the Harvard system to comply with the requirements of the University of the Witwatersrand for the submission of theses.

4.1 Abstract

A graphical technique has been developed to illustrate the interplay between the feed concentration, the desired product yield and the residence time in a reactor.

The graphical technique can be used to analyse the characteristics of any reactor and of any reaction system for which dependable kinetic data are available.

Using the graphical technique described in this paper, the operating characteristics necessary for the maximum selectivity of a reactant can be found easily and quickly.

4.2 Introduction

It can be argued that the three most important characteristics of a reaction process are the feed concentration, the product concentration and the residence time. In effect, we have one dependent and two independent variables. Given any two, it is possible to determine the third. In this paper the authors present a graphical method for assessing the residence time, product yields and required feed concentrations for any reactor and for any reaction mechanism. The principles expounded in this paper have been applied to the Oxidative Dehydrogenation (ODH) of *n*-butane to butadiene in an Inert Porous Membrane Reactor (IMR) with a V/MgO catalyst.

4.3 Results

Consider the following reactions in a reactor:

$$A + B \rightarrow C + D$$
$$C + B \rightarrow E + F$$

Species A reacts with species B to form C and D in the presence of a suitable catalyst. As species C is formed, it reacts with species B to form E and F. Let us assume that the reactions has been studied in sufficient detail to derive the effective rate constant, k_i, and the reaction rate, r_i, for each species. The reaction is such that at equilibrium all of species A has been consumed as has species C. The reaction variables are the absolute and relative feed concentrations of A and B. The order of the reaction is immaterial as is the nature of the reaction itself. Also, it matters not whether the reaction is isothermal or adiabatic or whether it takes place in a Plug Flow Reactor (PFR) or in a Continuously Stirred Tank reactor (CSTR).

What we wish to develop is a simple graphical technique to allow us, at a glance, to evaluate the interdependence of feed concentration, product yield and residence time.

Let us assume further that, in examining this reaction, we wish to study the yield of species C with respect to species A. The basis of calculation is an initial molar concentration of A of unity (the units chosen are irrelevant so long as consistency is observed).

So, how do we go about developing this graphical representation ? There are three key steps.

4.3.1 Step 1. Evaluate the Yield of C as a function of A

Using the known kinetic mechanism for the reaction, evaluate the yield of C as a function of time. In practice this is accomplished by solving the equations for the yield of species *C* with respect to residence time, τ, for the relevant reactor configuration.

$dC_c/d\tau = r_c$ (for a PFR)
$C_c - C_c^0 = \tau\ (r_c)$ (for a CSTR)

Plot the yield of C as a function of A. Let us assume that the resulting profile is as shown in Figure 4.1 below. The scale of the y-axis is arbitrary as is the shape of the profile.

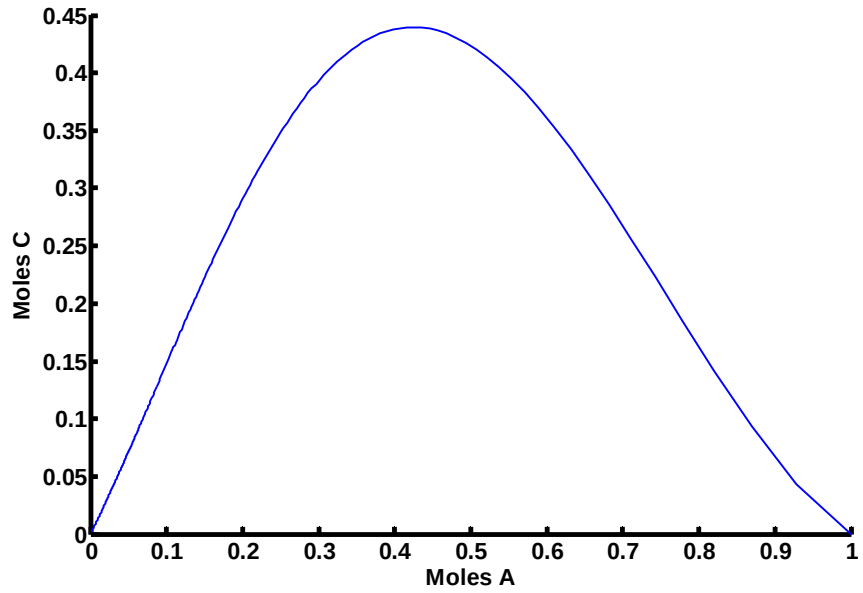


Figure 4.1. Yield of species C as a function of species A.

4.3.2 Step 2. Step off the Various Residence Times

Superimpose on the profile shown in Figure 4.1 the various residence times. Again, these points are easily derived from the integration results. We can select any appropriate incremental residence time step.

We then get Figure 4.2 below.

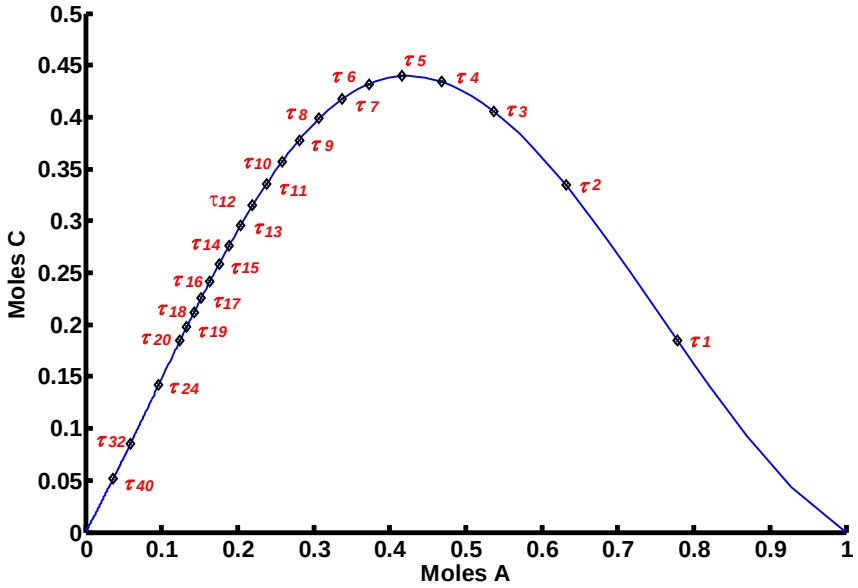


Figure 4.2. Concentrations of A and C at various values of residence time, τ.

4.3.3 Step 3. Repeat Step 1 and Step 2

Repeat steps 1 and 2 for different initial molar values of A.

Figure 4.3 below shows the results of the third step but for clarity we have identified only the first five values of residence time, τ.

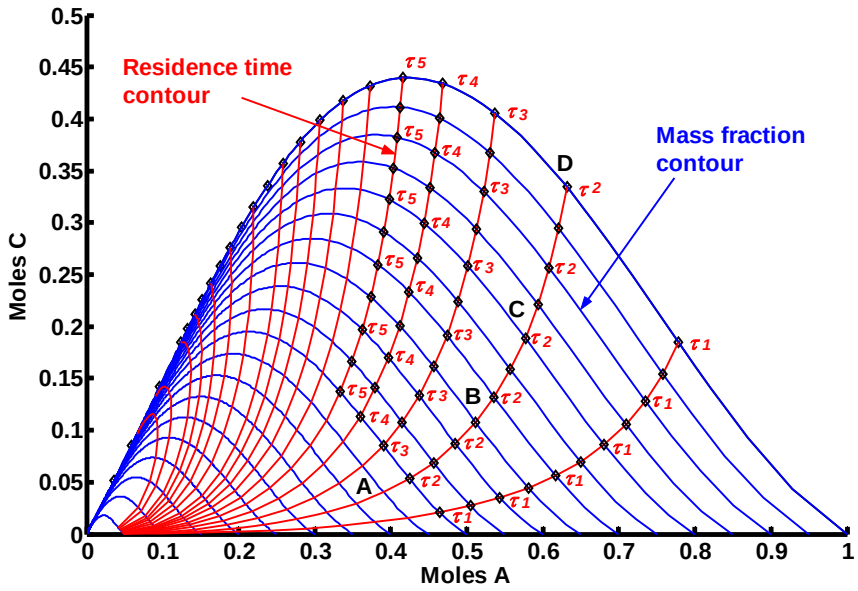


Figure 4.3. Concentrations of A and C at various initial molar values of A.

In Figure 4.3 above, for each profile of A and C, we have identified the respective molar concentrations corresponding to the residence times, *τ1, τ2, τ3* etc. A line then is drawn through those points sharing a common residence time. Referring to Figure 4.3, the line A-B-C-D represents the locus for residence time *τ2* on all the profiles which it intersects.

That concludes the preparation of the topography.

How then is it used and what can be derived from such a topography ?

In other papers, Milne *et al.* (2004 and 2006), the authors studied the oxidative dehydrogenation (ODH) of *n*-butane, butene and butadiene in an IMR and found that the yield of the desired hydrocarbon was enhanced by maintaining the partial pressure of oxygen at a low constant value. The oxygen partial pressure was judged to be an important operating parameter. The graphical technique described in this paper consequently was developed to determine the IMR feed conditions for any desired product yield and *vice versa* as well as the associated residence time, these parameters being a function of the oxygen partial pressure.

The reaction network for the ODH of *n*-butane was postulated by Téllez *et al.* (1999a and 1999b) as:

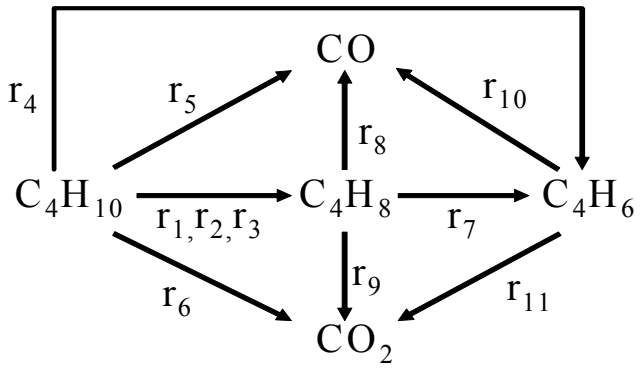


Figure 4.4. Reaction scheme for the ODH of *n*-butane to butene and butadiene.

The reactor configuration chosen for this scheme is shown in Figure 4.5.

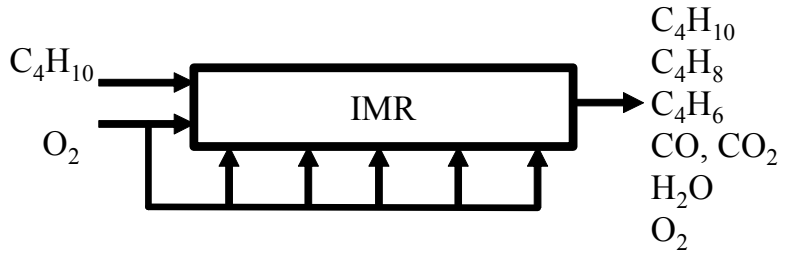


Figure 4.5. IMR Configuration.

The kinetic data used by the authors were taken from Téllez *et al.* (1997) and Assabumrungrat *et al.* (2002). A V/MgO catalyst was deployed. The several topographical views were derived by applying the three steps described in this paper.

In effect, each topography shows, for a particular key operating parameter (in this case, oxygen partial pressure), the interplay between three variables, feed concentration, product concentration and residence time.

In presenting our results, the mass fraction of carbon in the reactants and products was used since mass fraction variables, unlike partial pressures, obey linear mixing rules.

4.4 Interpretation of Graphs

To demonstrate the usefulness of the graphical technique, the example of the ODH of *n*-butane to butadiene is taken. The behaviour of this system was studied by Milne *et al.* (2004 and 2006), at many values of constant

IMR oxygen partial pressure from which the results at one value, 65 kPa, are shown in this paper.

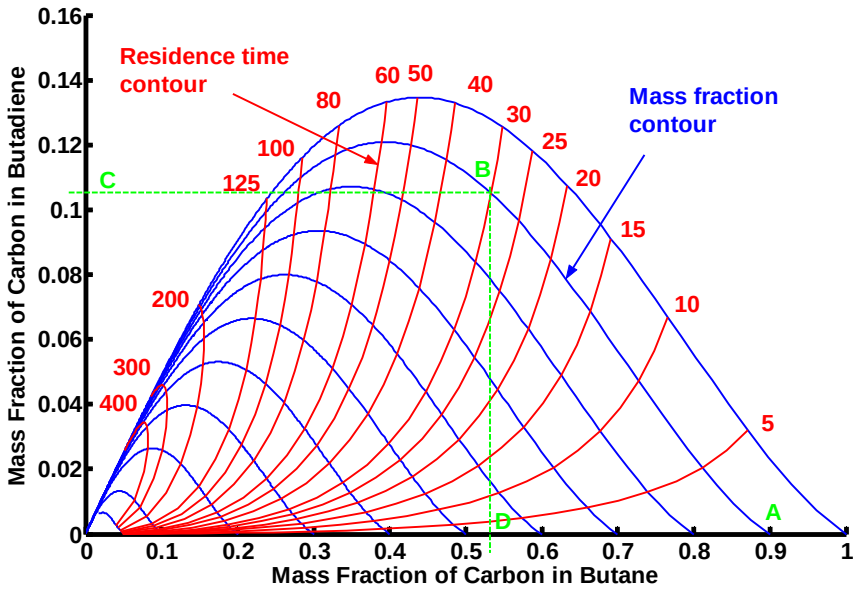


Figure 4.6. Topography of *n*-butane to butadiene at an oxygen partial pressure of 65 kPa (simplified diagram).

Figure 4.6, a simplified version of Figure 4.7, shows part of the topography for the system *n*-butane:butadiene at an oxygen partial pressure of 65 kPa.

The residence time contours in Figure 4.6 are lines within the region of constant residence time (expressed in seconds). Residence time values are shown along the outer periphery. The mass fraction contour lines are the ODH profiles for butane:butadiene for a specific feedstock concentration of *n*-butane, expressed as carbon mass fraction.

The diagram shown in Figure 4.4 is a complex reaction system and there can be a total of nine species depending upon the hydrocarbon feedstock.

Consequently, Figure 4.6 represents a two-dimensional snap-shot of part of this detailed multi-component system and shows those hydrocarbons of greatest value and interest, in this instance butane and butadiene. Similar two-dimensional pictures can be developed easily for other components as functions of the relevant feedstock and reactor operating parameter.

The product composition from a known feedstock, *n*-butane, (0.90 butane, point A in Figure 4.6, expressed as mass fraction of carbon) for a specific oxygen partial pressure (65 kPa) and for a specific residence time (30 seconds, point B) can be found by tracing the relevant mass fraction contour from the x-axis, point A, to its intersection with the residence time contour line (line AB). The composition of the other hydrocarbon, butadiene, then can be read from the y-axis, 0.105 carbon mass fraction (point C) and the residual feedstock composition can be read from the x-axis, 0.54 carbon mass fraction (point D).

The following questions are easily answered by reference to a topographical diagram.

- Given a reactor with a known residence time and a desired yield of a specific product, what feed composition is required?

- What is the maximum possible yield of a specific product from a reactor at a given operating parameter value (oxygen partial pressure)?

- What influence does residence time have upon yields for a given feed composition?

- What residence time is required to obtain the maximum yield of specific product from a given feed composition?

Figure 4.7 below is presented as an example of the *n*-butane:butadiene topographies at one value of PFR oxygen partial pressure. Similar topographies would be features of other reaction systems and other reactors.

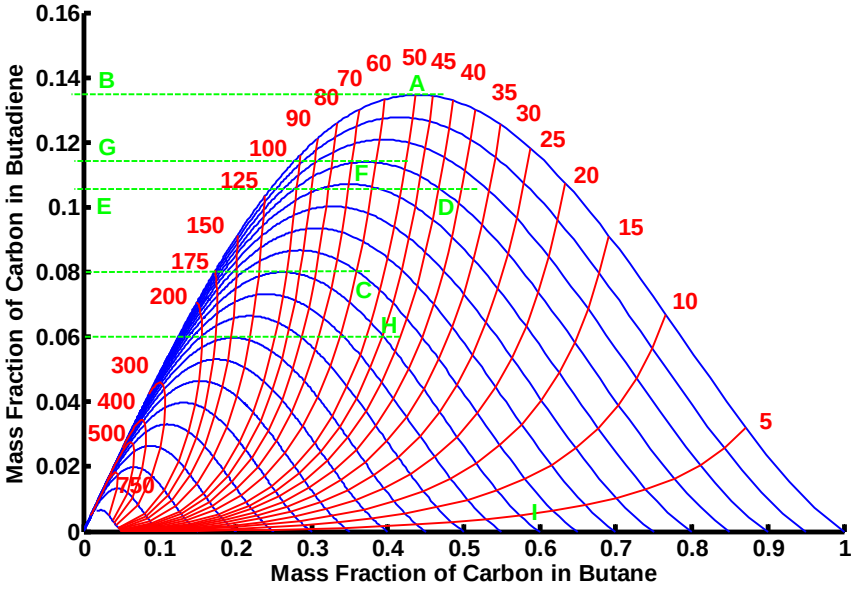


Figure 4.7. Topography of ODH of *n*-butane to butadiene at an oxygen partial pressure of 65 kPa.

Let us use Figure 4.7 to answer some specific questions.

- Question. What is the best yield of butadiene from a PFR operating at a constant oxygen partial pressure of 65 kPa?

- Answer. The best yield of butadiene is found by locating the maximum butadiene concentration within the region shown in

Figure 4.7. This maximum value occurs at point A and corresponds to a butadiene concentration of 0.135, point B, at a residence time of 49 seconds and for an initial butane feed concentration of unity.

- Question. Given a feed concentration of 0.65 butane and a desired butadiene yield of 0.08, what residence time is required?

- Answer. Find the butane concentration of 0.65 on the x-axis and trace the mass fraction contour from that value to where it intersects the horizontal line emanating from a value of 0.08 on the y-axis. The point of intersection, C, lies on the residence time contour of 60 seconds which is the required answer.

- Question. We have a residence time of 40 seconds. Our butane feed concentration is 0.85 carbon mass fraction. Can we obtain a butadiene yield of 0.12?

- Answer. Trace the butane mass fraction contour from the 0.85 value on the x-axis to its point of intersection, D, with the residence time contour of 40 seconds. This corresponds to a butadiene concentration of 0.106, point E. This represents the best butadiene yield available and consequently a yield of 0.12 is unattainable. By following the 0.85 butane mass fraction contour to its apogee at point F, we see for this butane feed concentration that the maximum butadiene yield is 0.114, point G, at a residence time of 63 seconds. Increasing the residence time beyond 63 seconds results in a *decrease* in butadiene yield as the butadiene is oxidised to carbon monoxide, carbon dioxide and water.

- Question. We have a reactor with a residence time of 45 seconds and we wish to have a butadiene yield of 0.06. What butane feed concentration is required?

- Answer. Find the point of intersection, H, of the 45 second residence time contour and the horizontal line from the y-axis value of 0.06 butadiene. From point H, trace the mass fraction contour, line HI, back to the x-axis to find the required butane feed concentration of 0.60.

The Figure 4.7 topography also shows clearly the relationship between residence time and butane feed composition for a fixed yield of butadiene. If we reduce the residence time, the required butane feed composition increases (and *vice versa*).

4.5 Maximum Selectivity of a Reactant

Let us re-examine Figure 4.6 again, but this time we draw the tangent AB from the feed point to the concentration profile. What can an analysis of this geometry tell us ?

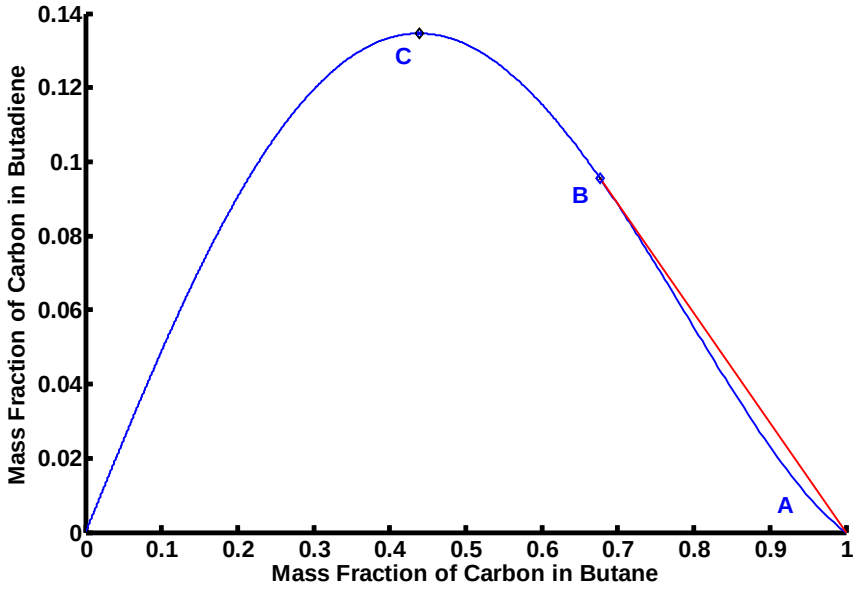


Figure 4.8. Topography of *n*-butane to butadiene at an oxygen partial pressure of 65 kPa Tangent AB drawn from the feed point to the concentration profile.

In the concentration profile shown in Figure 4.8, the concentration of butadiene, initially zero, rises to a maximum value, 0.13, and then wanes to zero as it becomes progressively oxidised to form carbon monoxide, carbon dioxide and water. The concentration of butane corresponding to the maximum yield of butadiene is 0.44. Normally, it would be an objective to maximise the yield of butadiene in which case the reaction would be stopped after 49 seconds.

The relationship between yield of butadiene and residence time is shown in Figure 4.9.

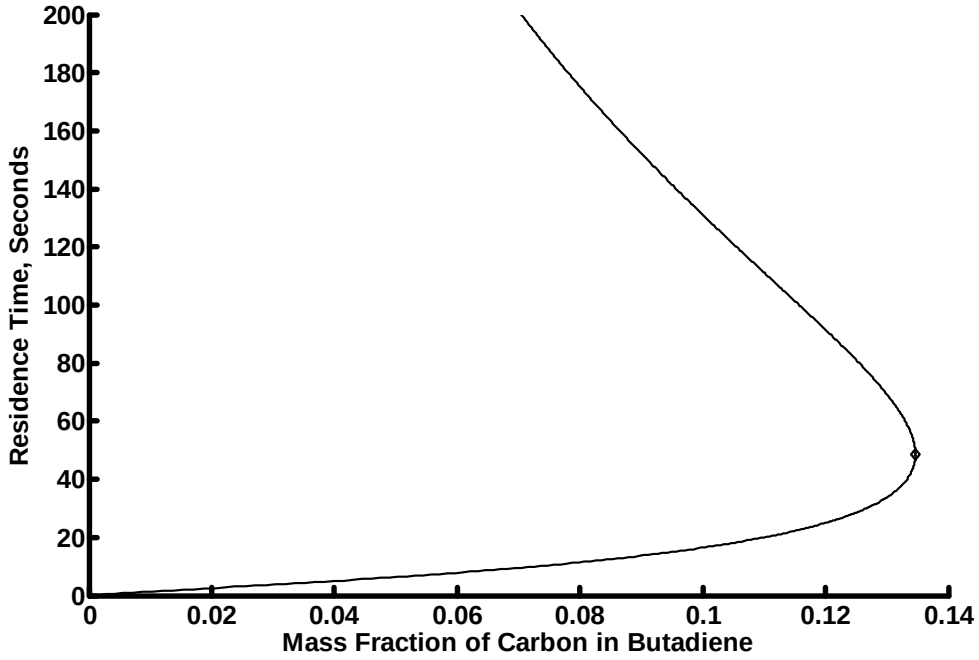


Figure 4.9. Yield of butadiene as a function of residence time in an isothermal IMR with an oxygen partial pressure of 65 kPa.

At this maximum butadiene yield point of 0.13, the selectivity of butane to butadiene is 0.24. This means that 0.24 units of butadiene were produced from one unit of butane. This leads to the question as to whether it is possible to produce a greater amount of butadiene from one unit of butane and, if so, where would the relevant operating point be located on the profile shown in Figure 4.8?

The answer to this question lies in finding the point on the profile where the selectivity of butane to butadiene is a maximum.

Algebraically, selectivity of butane to butadiene at any point x is defined as

(Concentration of butadiene at point x – initial concentration of butadiene) ÷ (concentration of butane at point x – initial concentration of butane)

The selectivity as calculated from this equation always is negative.

Geometrically, the selectivity of butane to butadiene at the point of maximum butadiene yield is shown in Figure 4.10 as ratio of the two sides of the right-angled triangle ADC, namely CD divided by AD.

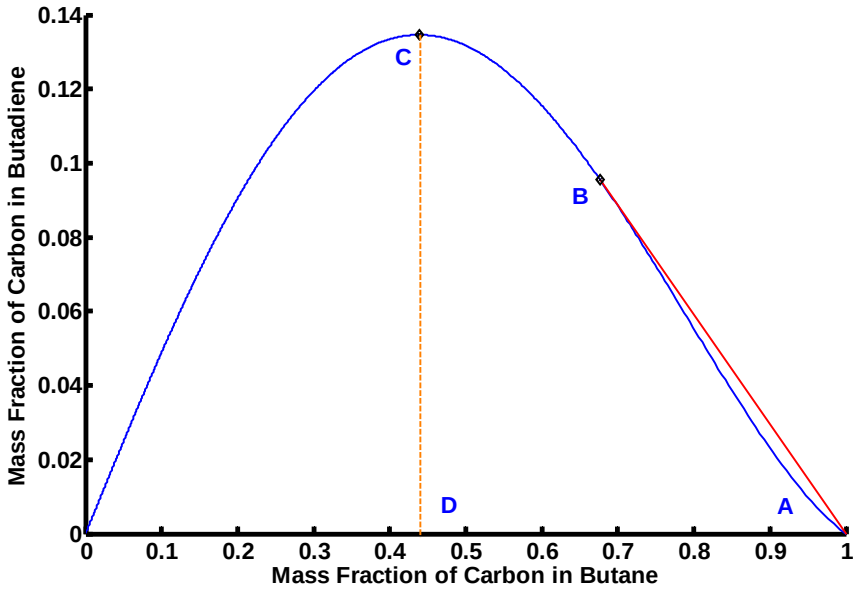


Figure 4.10. Geometrical representation of selectivity of *n*-butane to butadiene at the point of maximum yield of butadiene in an isothermal IMR with an oxygen partial pressure of 65 kPa.

Another way to interpret this selectivity is that it is the tangent of the angle DÂC.

Figure 4.11 shows the selectivity of butane to butadiene as a function of butane concentration. (The selectivity in Figure 4.11 is shown as a positive quantity).

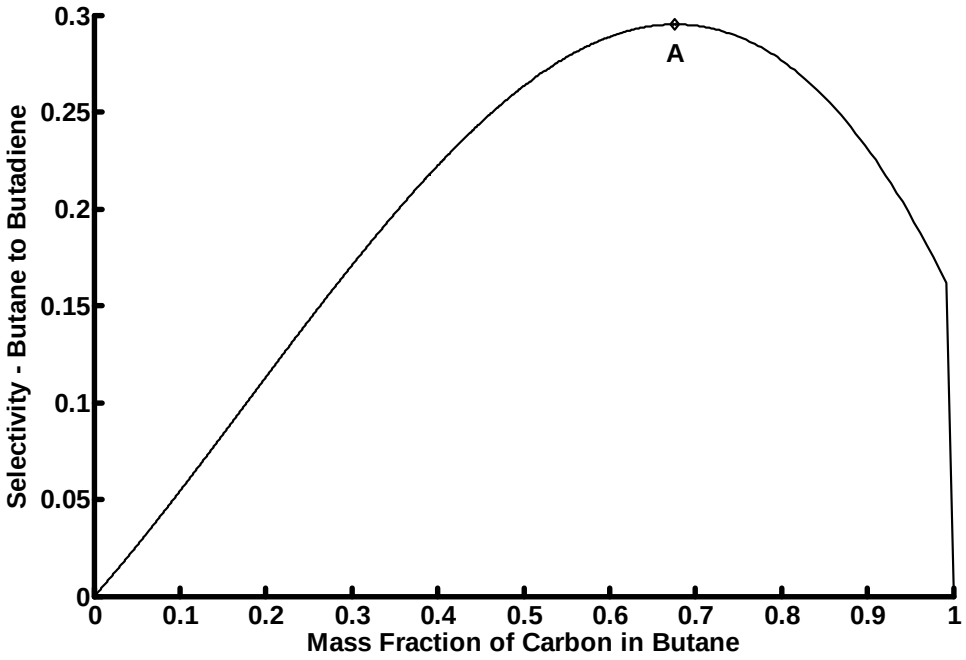


Figure 4.11. Selectivity of *n*-butane to butadiene as a function of butane concentration in an isothermal IMR with an oxygen partial pressure of 65 kPa.

Maximum selectivity of *n*-butane to butadiene is shown as point A in Figure 4.11 and is equal to 0.295. Point A corresponds to a butane concentration of 0.676.

If we transpose this value of 0.676 to the butane:butadiene profile of Figure 4.8, we identify the point where we can produce the maximum yield of butadiene per unit consumption of butane. This is shown as point B in Figure 4.12 and it corresponds to the point of intersection of the tangent

from the feed point to the concentration profile. The concentration of butadiene at point B is 0.096.

Point B in Figure 4.12 represents not only the point of maximum selectivity but also the point on the concentration profile from which a line to the feed point (unit concentration of butane, zero concentration of butadiene) subtends the maximum angle to the x-axis. This means that the line from the feed point to the profile at point B is tangential to the profile. This tangent line is shown as AB in Figure 4.12.

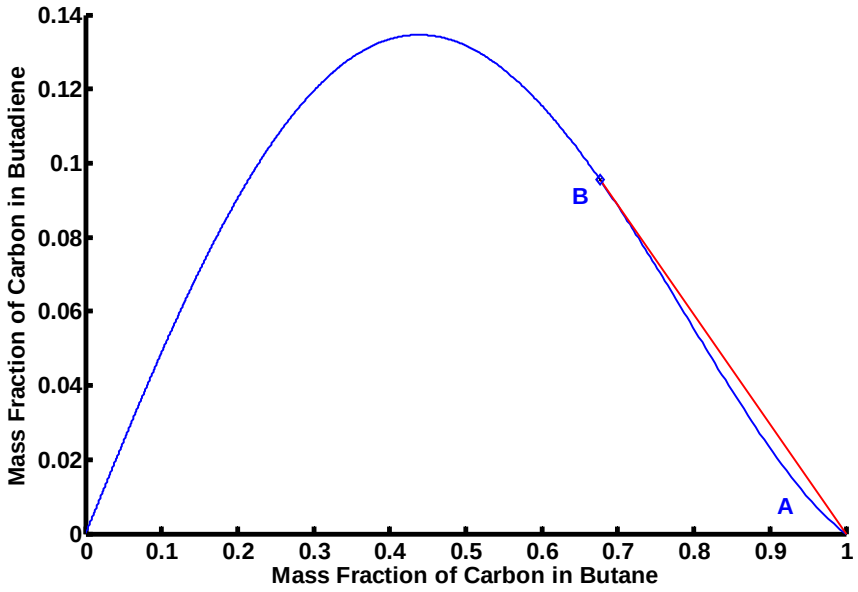


Figure 4.12. Identification of point of maximum butane selectivity to butadiene in an isothermal IMR with an oxygen partial pressure of 65 kPa.

Transposing this concentration of 0.676 to the residence time profile of butane gives the residence time necessary for the maximum selectivity. This is shown in Figure 4.13.

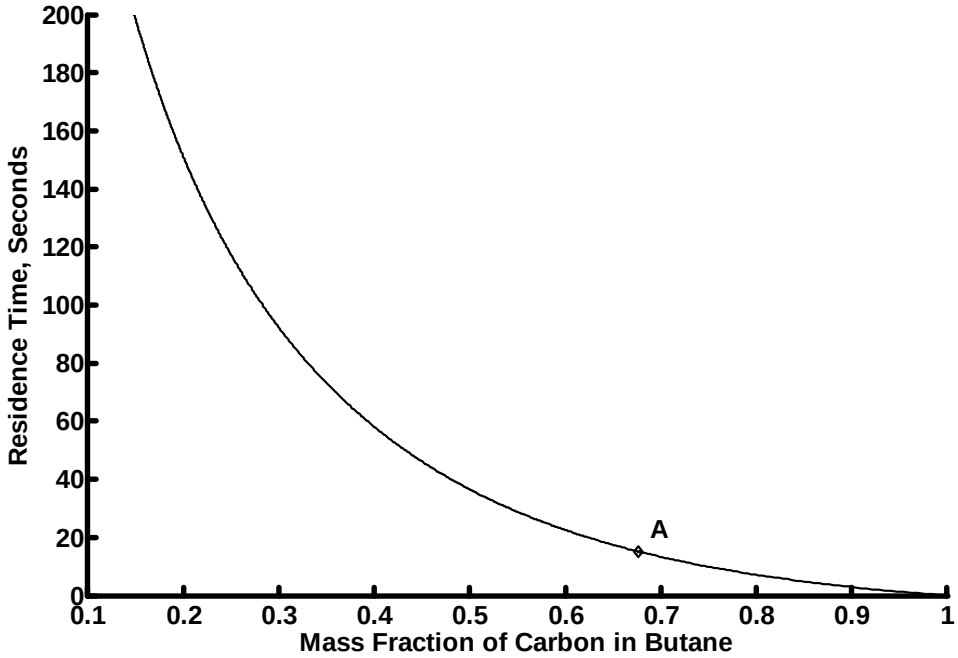


Figure 4.13. Identification of residence time necessary for maximum selectivity of butane to butadiene in an isothermal IMR with an oxygen partial pressure of 65 kPa.

From Figure 4.13, the residence time for the maximum selectivity of butane to butadiene is seen to be 15 seconds.

The significance of this geometrical arrangement is that it provides an easy means to ascertain the point on the profile where the highest yield of product (butadiene) can be obtained relative to the least usage (consumption) of a reactant (butane). Simply, from the feed point, draw a tangent to the profile. The point where the tangent meets the profile is the point of maximum selectivity. The associated residence time can be ascertained from the reactant residence time profile.

It should be noted that this geometrical principle is applicable only if there is a concavity in the profile between the feed point and the maximum point on the profile. If there is no concavity and instead the shape of the profile is convex, then the point of maximum selectivity occurs at the feed point, an impractical operating point in so far as the yield of product is concerned.

The other characteristic of the tangent to a concentration profile namely that through a process of by-pass and mixing and, in effect by filling in the concavity, it extends the region within which products and reactants can be found, has been noted by Glasser *et al.* (1987 and 1997). Accordingly, the region bounded by the line AB and the concentration profile from point B to the co-ordinates [0, 0] is a candidate Attainable Region (AR) for the system butane:butadiene in the concentration sub-space shown.

4.6 Conclusions

We believe that the topography of any reaction system and for any reactor can be developed easily, given reliable kinetic data, using the graphical technique advocated in this paper.

The topography thus developed provides a useful design tool for engineers and permits an improved understanding of a reactor's behaviour and characteristics.

The geometrical techniques described in this paper can be used to find the reactor conditions for maximum selectivity of reactant to product.

4.7 Nomenclature

A, B, C, D Species A, B, C and D

C_i Concentration of species *i*, mol/s.

C_i^0 Initial concentration of species *i,* mols/s.

r_i Rate of reaction of species *i*, mol/kg s

k_i Kinetic rate constant for species *i*, mol/kg s

Greek Symbols

τ_i Residence time for species, *i*, seconds

4.8 Literature Cited.

Assabumrungrat, S., Rienchalanusarn, T., Praserthdam, P., Goto, S., (2002), Theoretical study of the application of porous membrane reactor to oxidative dehydrogenation of *n*-butane, *Chemical Engineering Journal*, vol. 85, pp. 69-79.

Glasser, D., Hildebrandt, D., Crowe, C., (1987), A geometric approach to steady flow reactors: the attainable region and optimisation in concentration space, *American Chemical Society*, pp. 1803-1810.

Glasser, D., Hildebrandt, D., (1997), Reactor and Process Synthesis, *Computers and Chemical Engineering*, vol 21, Suppl., S775-S783.

Milne, D., Glasser, D., Hildebrandt, D., Hausberger, B., (2004), Application of the Attainable Region Concept to the Oxidative Dehydrogenation of *1*-Butene in Inert Porous Membrane Reactors, *Industrial and. Engineering Chemistry Research*, vol. 43, pp. 1827-1831.

Milne, D., Glasser, D., Hildebrandt, D., Hausberger, B., (2006), The Oxidative Dehydrogenation of *n*-Butane in a Fixed Bed Reactor and in an Inert Porous Membrane Reactor - Maximising the Production of Butenes and Butadiene, *Industrial and Engineering Chemistry Research*, vol. 45 pp. 2661-2671.

Téllez, C., Menéndez, M., Santamaría, J., (1999a), Kinetic study of the oxidative dehydrogenation of butane on V/MgO catalysts, *Journal of Catalysis*, vol. 183, pp. 210-221.

Téllez, C., Menéndez, M., Santamaría, J., (1999b), Simulation of an inert membrane reactor for the oxidative dehydrogenation of butane, *Chemical Engineering Science*, vol. 54, pp. 2917-2925.

Téllez, C., Menéndez, M., Santamaría, J., (1997), Oxidative Dehydrogenation of Butane using Membrane Reactors, *Journal of the American Institution of Chemical Engineers*, vol. 43, (No.3), pp. 777-784.

CHAPTER 5

Graphical Technique for deciding when to switch from a Plug Flow Reactor to a Continuously Stirred Tank Reactor (and v*ice versa*) to reduce Residence Time.

The following paper has been published by *Chemical Engineering Progress* in April 2006, Vol. 102, No. 4, pp. 34-37 under the title "Reactor Selection : Plug Flow or Continuously Stirred Tank?"

The numbering of the figures and tables as submitted to *Chemical Engineering Progress* has been prefixed with the reference (5) to this chapter of my thesis.

In this chapter of my thesis the referencing system required by the editors of *Chemical Engineering Progress* has been changed to the Harvard system to comply with the requirements of the University of the Witwatersrand for the submission of theses.

5.1 Abstract

In an earlier paper, Milne *et al.* (2006a), the authors proposed a graphical technique for assessing the performance characteristics of a plug flow reactor (PFR).

An extension of this graphical technique can be used (a) to derive the performance of a continuously stirred tank reactor (CSTR) for the same feed and the same operating conditions and (b) to determine which of the two reactor types represents the best choice, in terms of residence time, for a particular reaction.

The concept of a Residence Time Ratio (RTR) was advocated, namely the ratio between the comparable residence times for a PFR and a CSTR.

The graphical technique proposed in this paper has been applied to the Oxidative Dehydrogenation (ODH) of *1*-butene (butene) to butadiene in an Inert Porous Membrane Reactor (IMR) with a V/MgO catalyst.

5.2 Introduction

It is the opinion of the authors that the use today of a gas-phase CSTR for a chemical reaction is mainly confined to a laboratory and that the predominant rector type in industrial usage is a PFR or a modification of a PFR, for example, an IMR. The authors believe that, under certain circumstances, the use of a CSTR in industry in preference to or in conjunction with a PFR can be justified, specifically in terms of the required residence time. In some instances a PFR and a CSTR in series can be shown to require a smaller total residence time than a single PFR.

5.3 Results

There are seven steps to obtain the information for choosing between a CSTR and a PFR.

5.3.1 Step 1. Evaluate the Yield of C as a function of A

In our earlier paper, Milne *et al.* (2006a), we showed how the yield of species *C* can be plotted as a function of species *A* for the following reactions in a PFR:

$$A + B \rightarrow C + D$$
$$C + B \rightarrow E + F$$

Let us assume that the reactions have been studied in sufficient detail to derive the effective rate constant, k_i, and the reaction rate, r_i, for each species under the reactor mass and heat transfer conditions. The reaction is such that at equilibrium all of species A has been consumed as has species C.

Using the known kinetic mechanism for the reaction, evaluate the yield of C as a function of time. In practice this is accomplished by solving the equations for the yield of species *C* with respect to residence time, τ, for the relevant reactor configuration.

$$dC_c/d\tau = r_c \text{ (for a PFR)}$$

$$C_c - C_c^{\,0} = \tau\,(r_c) \text{ (for a CSTR)}$$

Plot the yield of C as a function of A. Let us assume that the resulting profile is as shown in Figure 5.1 below. The scale of the y-axis in this figure is arbitrary as is the shape of the profile for the general case.

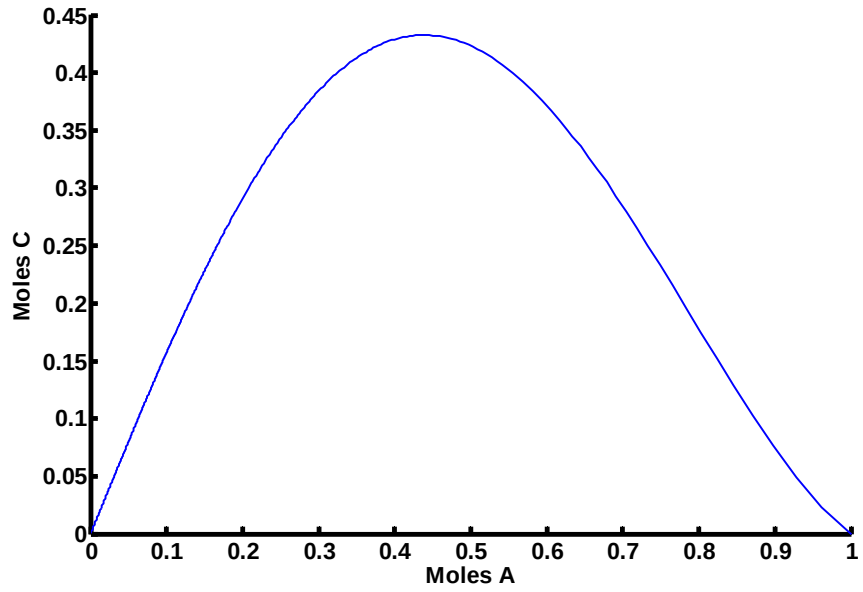


Figure 5.1. Yield of species C as a function of species A.

5.3.2 Step 2. Add the Yields of C for Other Molar Values of A

We now repeat Step 1 for different initial molar values of *A*.

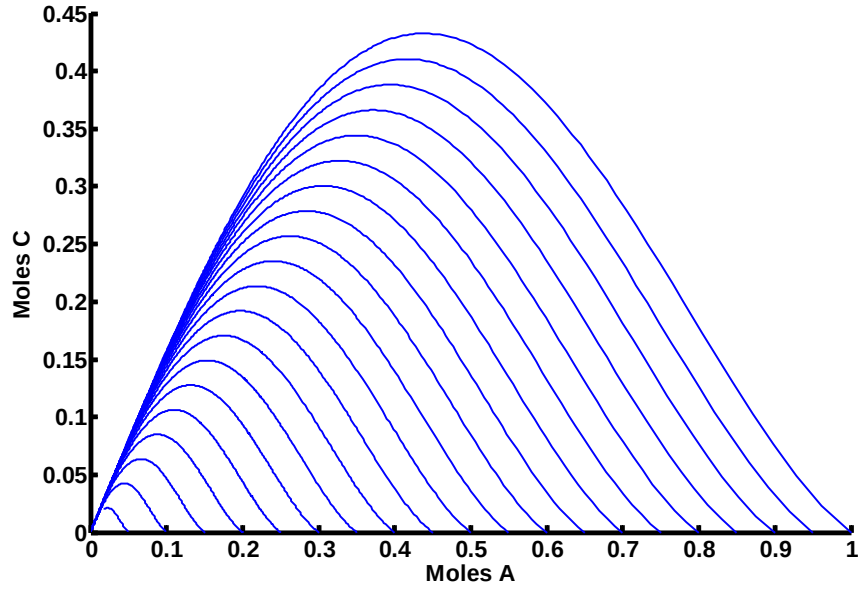


Figure 5.2. Concentrations of C at various initial values of A.

5.3.3 Step 3. Draw Tangents to the Profiles

Using Figure 5.2, from the feed concentration of *A* corresponding to unity molar concentration, [1,0], draw tangents to each of the other profiles. The points of intersection of the tangents with the profiles define the concentration locus for a CSTR with a molar feed concentration of unity for species *A* and operating under the same conditions as in the PFR, namely flow rate, temperature and pressure.

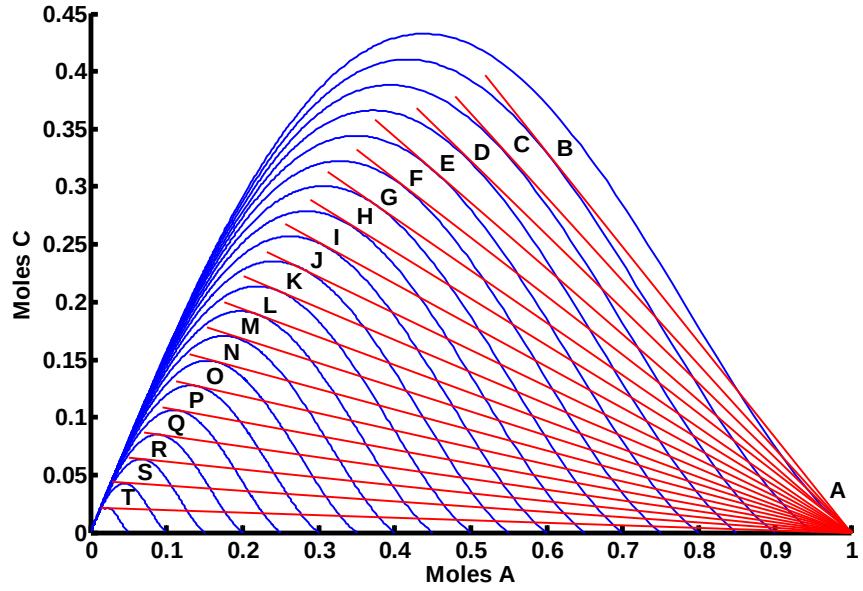


Figure 5.3. Concentration locus for species C and A in a CSTR

The concentration locus for the family of CSTRs is A-B-C-D-E-F-G-H-I-J-K-L-M-N-O-P-Q-R-S-T.

How do we know that the points A to T in Figure 5.3 above represent the concentration locus for a CSTR ? Because the geometrical derivation of this locus is based upon the fact that it lies upon those boundary regions of an PFR profile where the rate vector is collinear with the tangent from the feed point to each PFR profile in the two-dimensional space, A and C , Glasser *et al.* (1987 and 1997).

5.3.4 Step 4. Calculate the CSTR Residence Times

Reading the coordinates for each point on the CSTR locus, calculate the relevant residence time, τ, from the equation

$\tau_i = \Delta(c_i - c_i^0) / r_i$

The residence times for the CSTR are obtained by dividing the change in concentration by the corresponding rate expression. For a CSTR, this rate expression is the rate at the point of operation and thus is called the Instantaneous Rate.

This gives us the residence time, expressed in seconds, required to achieve each point on the CSTR locus.

5.3.5 Step 5. Calculate the PFR Residence Times

Reading the coordinates for each point on the PFR profile from [1,0], calculate the relevant residence time, τ, from the equation

$$\tau_i = \int_{\tau_1}^{\tau_2} (c_i / r_i)\, d\tau$$

The residence times for the PFR are obtained by integrating the concentration divided by the corresponding rate expression with respect to time. For a PFR, this is equivalent to dividing the conversion by the reaction path averaged reaction rate, aptly named the Average Rate.

5.3.6 Step 6. Plot the Residence Times as Functions of Species A and C.

Plot the CSTR and the PFR residence times as functions of species *A* and of species *C*

Examples of these two curves for a specific reaction are shown below in Figure 5.7 and Figure 5.8

5.3.7 Step 7. Plot the Ratio of PFR to CSTR Residence Times as Functions of Species A and C.

For a specific concentration of species *A*, plot the ratio of the corresponding PFR residence time to that of the corresponding CSTR residence time. We call this ratio the Residence Time Ratio (RTR).

An example of this curve for a specific reaction is shown below in Figure 5.9.

Repeat for values of species *C*.

An example of this curve for a specific reaction is shown below in Figure 5.10.

Where the RTR is greater than unity, the CSTR residence time for a specific concentration of species *i* is less than that for the equivalent PFR. Where the RTR is less than unity, the PFR residence time for a specific concentration of species *i* is less than that for the equivalent CSTR.

This concludes the procedure required to derive the CSTR locus and to assess the catalyst requirements of a PFR and a CSTR.

What is the practical application of this technique ?

In earlier papers, Milne *et al.* (2004 and 2006b), the authors studied the oxidative dehydrogenation (ODH) of *n*-butane, butene and butadiene in an IMR and found that the yield of the desired hydrocarbon was enhanced by maintaining the partial pressure of oxygen at a low constant value. The oxygen partial pressure was judged to be an important operating parameter. Using this data, the graphical technique described in this paper was applied to determine the CSTR concentration locus for the ODH of butene to butadiene, the respective reactor residence times and to derive and analyse the resulting RTR profiles.

The reaction network for the ODH of butene was postulated by Téllez *et al.* (1999a and 1999b) as:

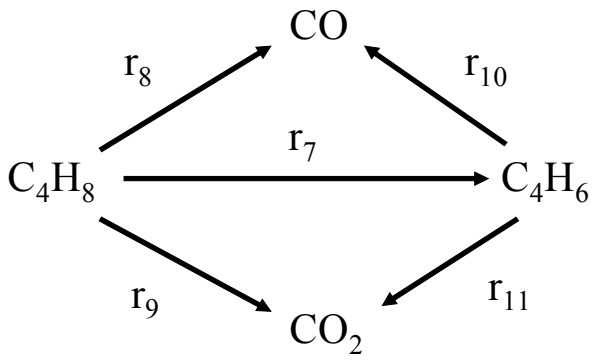


Figure 5.4. Reaction scheme for the oxidative dehydrogenation of *1*-butene to butadiene.

The reactor configuration for this scheme is shown in Figure 5.5.

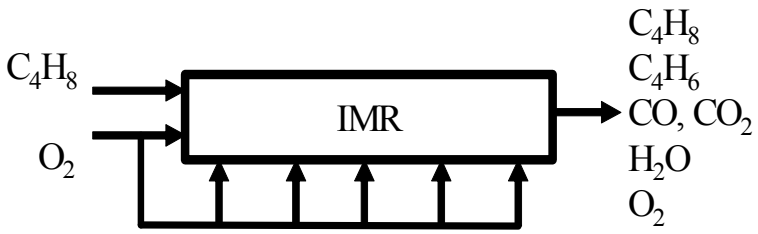


Figure 5.5. IMR Configuration.

The CSTR locus for the ODH of butene to butadiene for an initial (and constant) oxygen partial pressure of 65 kPa is shown in Figure 5.6.

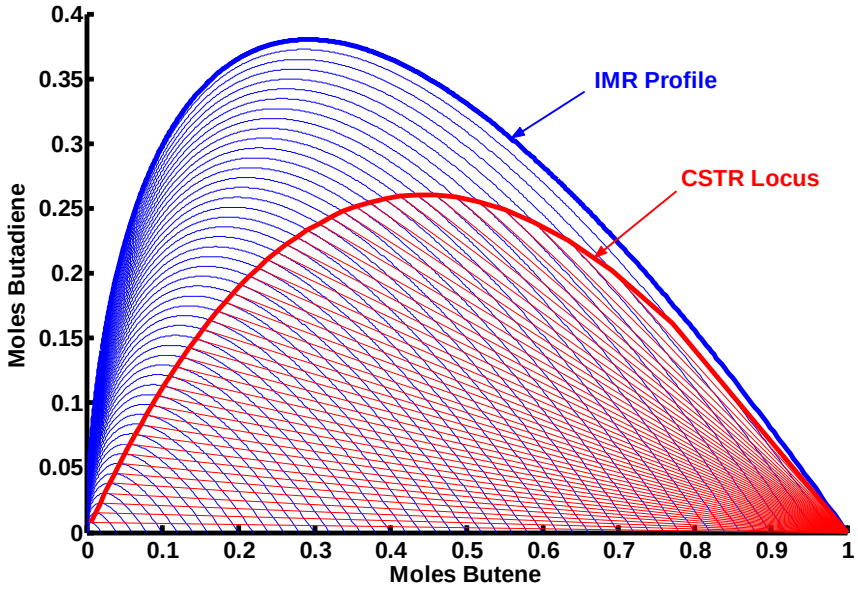


Figure 5.6. Butene-butadiene profile/locus for an IMR and a CSTR at an constant oxygen partial pressure of 65 kPa.

Figure 5.6 shows that the maximum butadiene yield in a CSTR at a constant oxygen partial pressure of 65 kPa is approximately 0.26 moles and that at this maximum value the corresponding moles of butene is 0.44. For the IMR, the maximum butadiene yield is 0.38 at a butene concentration of 0.29.

Analysis of Figure 5.6 allows a comparison to be made between residence times for CSTR and IMR reactors for a constant oxygen partial pressure in both systems.

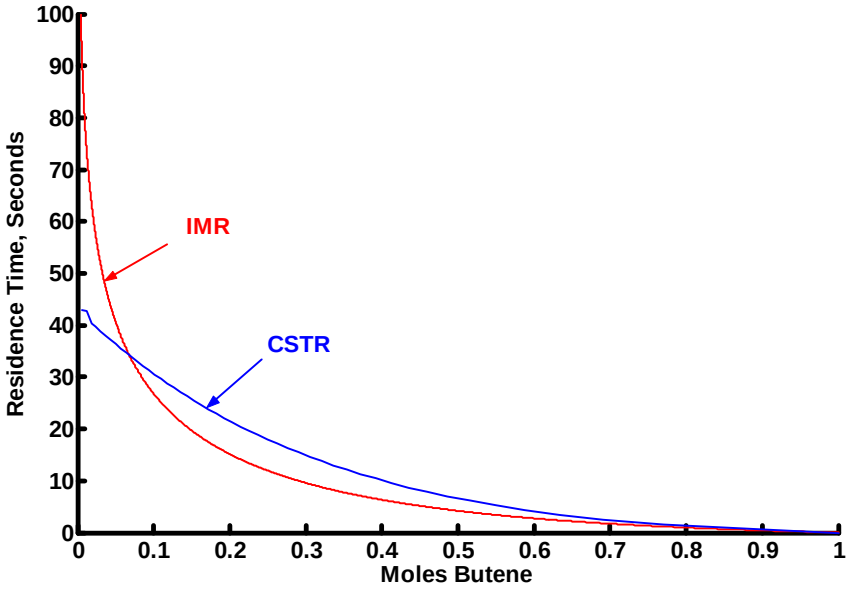


Figure 5.7. CSTR and IMR residence times versus butene concentration for a constant oxygen partial pressure of 65 kPa.

Figure 5.7 shows the respective residence times for butene. It indicates that at a constant oxygen partial pressure of 65 kPa and for butene concentrations greater than 0.07 IMR residence times are less than those for a CSTR.

At a butene concentration of 0.07, the two curves cross and below this value the residence times for an IMR are greater than those for a CSTR. The significance of the point of intersection is that it defines the operational parameters (in terms of butene) where it becomes advantageous to switch from a CSTR to an IMR (and *vice versa*) from the perspective of residence time.

Figure 5.8 shows the respective residence times for a CSTR and an IMR in terms of moles of butadiene.

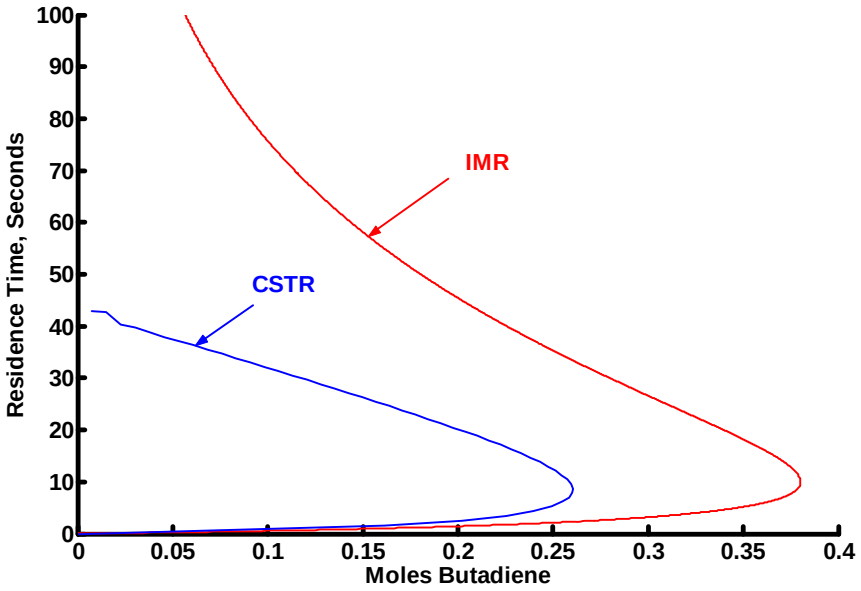


Figure 5.8. CSTR and IMR residence times versus mass fraction of butadiene for a constant oxygen partial pressure of 65 kPa.

Figure 5.8 shows that for all butadiene concentrations, IMR residence times are less than those for a CSTR. It always will be more advantageous to deploy an IMR with a residence time less than 9 seconds for any desired yield of butadiene from a CSTR.

Butadiene yields greater than 0.26 cannot be obtained from a CSTR operating at a constant oxygen partial pressure of 65 kPa.

Figure 5.9 shows the ratio of IMR and CSTR residence times as a function of butene concentration. Values of the ratio were derived from an analysis of Figure 5.7.

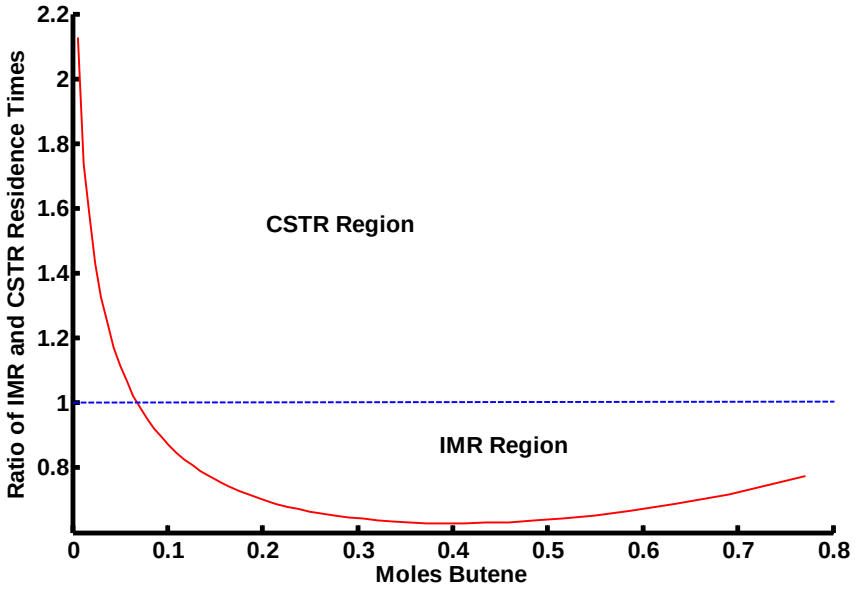


Figure 5.9. Ratio of IMR and CSTR residence times versus butene concentration for a constant oxygen partial pressure of 65 kPa.

In Figure 5.9 the horizontal broken line demarcates the boundary above which the CSTR region exists and below which is the IMR region. The CSTR region is that region within which a CSTR requires a smaller residence time than does an IMR for the same selectivity. Similarly, the IMR region is that region within which an IMR requires a smaller residence time than does a CSTR for the same selectivity. Figure 5.9 indicates that for butene concentrations greater than 0.07, an IMR reactor has a smaller residence time than does a CSTR. Once the butene concentration falls below 0.07, a CSTR requires a smaller residence time than an IMR.

Figure 5.10 shows the ratio of IMR and CSTR residence times as a function of butadiene concentration.

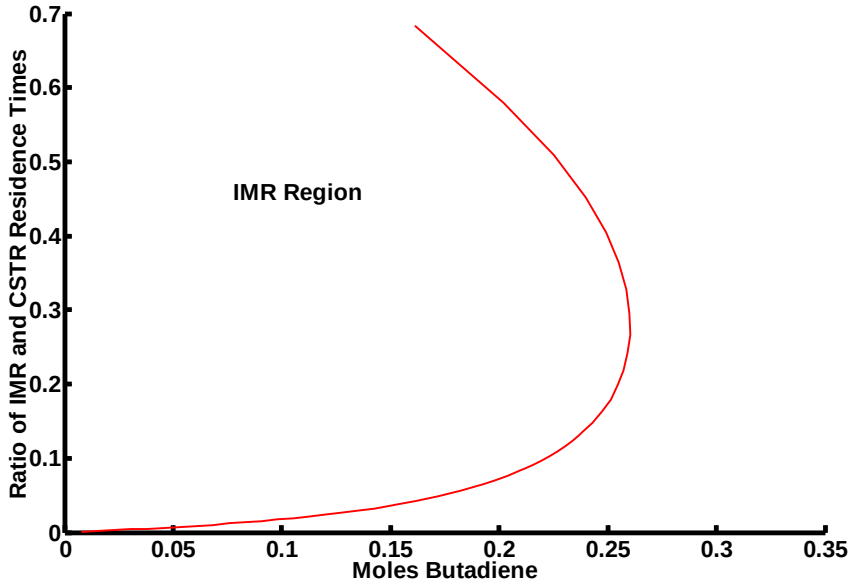


Figure 5.10. Ratio of IMR and CSTR residence times versus butadiene concentration for a constant oxygen partial pressure of 65 kPa.

Figure 5.10 indicates that all values of the RTR are less than unity and, as a result, an IMR has a smaller residence time than a CSTR as the butadiene concentration increases from an initial zero to its maximum of 0.26. This condition continues to hold as the butadiene concentration wanes (though its oxidation to carbon monoxide, carbon dioxide and water).

However, this need not always be the case and there may well be instances for different reactants over another catalyst where the RTR for one of the products transverses a value of unity and, in so doing, demarcates CSTR and IMR (PFR) regions.

5.4 Conclusions

The derivation of the Residence Time Ratio allows an assessment to be made of the relative residence times in a PFR and a CSTR.

It has been established that the series combination of an IMR and a CSTR for the ODH of butene to butadiene requires less residence time than does a single IMR when the depletion of butene is of importance. Where residence time is an important factor in the overall economic choice between a PFR and a CSTR, this graphical technique provides a simple and a powerful tool to assist in choosing the right reactor configuration.

5.5 Nomenclature

c_i Concentration of species *i*, moles/second

c_i^0 Initial concentration of species *i*, moles/second

r_i Rate of reaction of species *i*, mol/kg s

Greek Symbols

τ_i Residence time for species, *i*, seconds

5.6 Footnote

Subsequent to the publication of this paper in *Chemical Engineering Progress*, the Residence Time Concept advocated in this chapter was compared with another process tool used to identify the interface between a PFR and a CSTR. This other tool, the Levenspiel (1972) concept, plots, for a reactant species, the inverse of its rate of reaction against the conversion of that species. By virtue of the units, mols/kg.s and mols/kg, the area beneath the graph plotted has the units of time, i.e. residence time. A Levenspiel plot shows, for a specified conversion, the residence time for a PFR and for a CSTR. The total area under the curve gives the PFR residence time, the area of the rectangle which touches the inverse rate curve gives the residence time for a CSTR.

A Levenspiel plot is based upon the assumption that the stoichiometric ratio between the reactants remains constant along the length of the PFR or, in the case of a CSTR, that the stoichiometric ratio between the residual reactants (if any) at the exit from the reactor is the same as that in the feed. Another assumption is the rate of reaction is a function of the concentration of the reactant. One drawback is that the Levenspiel model does not address the case where the stoichiometric ratio is neither a constant nor the instance where multiple parallel and complex reactions occur. Furthermore, the Levenspiel plot, in identifying separate reactor times for a PFR and a CSTR, does not address the issue of minimising the total residence time by a different reactor configuration, i.e. a possible series combination of a PFR and a CSTR.

The reactions studied in this thesis, the ODH of butane to butenes and butadiene (and, in this chapter, the ODH of *1*-butene to butadiene) in essence are all first order reactions, the reaction rates being a function of

respective partial pressures. These reactions, however, are more complicated than the reaction model proposed by Levenspiel, there being a potential ten species of reactant and product present. In the ODH of butane, butene and butadiene, the stoichiometric ratio between the hydrocarbon reactant and oxygen is not constant and the subsequent reactions are many, parallel and complex.

It is my belief that the RTR concept addresses the inherent limitations of the Levenspiel concept in as much as the latter does not consider the overall process flow diagram. The Levenspiel plot for a single process unit, a PFR or a CSTR, identifies the residence time for each of these units for a required conversion. On the contrary, the RTR concept looks at the overall process requirements and answers the question as what combination of reactor units is necessary for ensuring the minimum overall residence time for a specified conversion. Furthermore, the RTR hypothesis permits the analysis of those reactions of such complexity for which the Levenspiel approach fails to provide a satisfactory analysis.

Notwithstanding the comments in the previous paragraphs, a caveat is necessary. The diagrams used in Chapter 5 to advance the argument regarding limitations in the Levenspiel method are two-dimensional projections from multi-dimensional surfaces. This implies that the true profile for the RTR not necessarily is a straight line but more likely to be a curved surface. What appears to be apparent in a two-dimensional plane, firstly, is a big simplification of the true state of the many species and, secondly, any conclusions from an analysis of the simplified diagram in themselves have to be simplified conclusions that, in the knowledge that the RTR is not really a straight line, do not really apply necessarily to a complex multi-dimensional reaction environment.

Consequently, the assertion regarding the Levenspiel method made in this Footnote remain a personal and an as-yet unsubstantiated belief. A more thorough investigation into the merits of the RTR and Levenspiel methods by another researcher perhaps could be warranted.

5.7 Literature Cited

Glasser, D., Hildebrandt, D., Crowe, C. (1987), A geometric approach to steady flow reactors: the attainable region and optimisation in concentration space, *American Chemical Society*, pp. 1803-1810.

Glasser, D., Hildebrandt, D., (1997), Reactor and Process Synthesis, *Computers and Chemical Engineering*, vol 21*,* Suppl., S775-S783.

Levenspiel, O., (1972), *Chemical Reaction Engineering Second Edition*, Wiley International, Singapore, Chapters 6-7.

Milne, D., Glasser, D., Hildebrandt, D., Hausberger, B., (2004), Application of the Attainable Region Concept to the Oxidative Dehydrogenation of *1*-Butene in Inert Porous Membrane Reactors, *Industrial and. Engineering Chemistry Research*, vol. 43, pp. 1827-1831.

Milne, D., Glasser, D., Hildebrandt, D., Hausberger, B., (2006a), Graphically Assess a Reactor's Characteristics, *Chemical Engineering Progress,* vol. 102, no. 3, pp. 46-51.

Milne, D., Glasser, D., Hildebrandt, D., Hausberger, B., (2006b), The Oxidative Dehydrogenation of *n*-Butane in a Fixed Bed Reactor and in an Inert Porous Membrane Reactor - Maximising the Production of Butenes and Butadiene, *Industrial and Engineering Chemistry Research,* vol. 45, pp. 2661-2671.

Téllez, C., Menéndez, M., Santamaría, J., (1999a), Kinetic study of the oxidative dehydrogenation of butane on V/MgO catalysts, *Journal of Catalysis*, vol. 183, pp. 210-221.

Téllez, C., Menéndez, M., Santamaría, J., (1999b), Simulation of an inert membrane reactor for the oxidative dehydrogenation of butane, *Chemical Engineering Science*, vol. 54, pp. 2917-2925.

CHAPTER 6

The Application of the Recursive Convex Control (RCC) policy to the Oxidative Dehydrogenation of n-Butane and 1-Butene

---

The following paper has been submitted for publication in *Industrial and Engineering Chemistry Research.*

In this research paper, I have been assisted by Dr. Tumisang Seodigeng, whose development of the RCC concept and its associated software constituted his Ph.D. thesis (Seodigeng, 2006). Dr. Seodigeng's contribution to this paper, apart from many valuable discussions in interpreting the results from the RCC policy, was to prepare the several graphical representations presented in this paper. The decision as to which graphical outputs were required was mine alone.

This chapter of my thesis presents this research paper as it has been submitted for publication to *Industrial and Engineering Chemistry Research.*

The numbering of the figures and tables as submitted to *Industrial and Engineering Chemistry Research* has been prefixed with the reference (6) to this chapter of my thesis.

In this chapter of my thesis the referencing system required by the editors of *Industrial and Engineering Chemistry Research* has been changed to the

Harvard system to comply with the requirements of the University of the Witwatersrand for the submission of theses.

6.1 Abstract

Attainable Region (AR) ideas have previously been used to identify candidate attainable regions (AR^Cs) for the oxidative dehydrogenation (ODH) of *n*-butane to butenes and butadiene and in so doing to identify the maximum possible yields of different hydrocarbon product. Because of the large dimensionality of the problem it was not possible then to do a complete AR analysis.

Among the configurations considered it was found that the reactor configuration for the respective AR^Cs in all instances was an inert membrane reactor (IMR) functioning as a differential side-stream reactor in which one of the reactants, oxygen, was introduced along the length of the reactor so as to maintain a very low and constant value of its partial pressure. Nevertheless despite producing high yields of product extremely large and impractical residence times ensued.

In this paper a new tool, the Recursive Convex Control (RCC) policy, is used to identify the AR^Cs in the full dimensional space. These AR^Cs showed excellent agreement with those previously published and the optimal reactor structures presented in those publications have been confirmed albeit with different oxygen control parameters. The maximum yields are now achieved with very much lower residence times.

These results also confirm the benefit from using the AR approach on problems where a full AR analysis is not possible.

6.2 Introduction.

The Attainable Region method is a way of finding the optimum reactor structure for reaction systems with known kinetics. This is done by first finding the region of all possible outputs for all the species for the fundamental physical processes occurring in the system. For simple homogeneous reactors this is chemical reaction and mixing, (Glasser, 1987). The problem with using AR analysis has been both the numerical difficulty in finding a candidate attainable region (AR^C) that satisfies all the specified conditions and the difficulty resulting from the absence of a known sufficiency condition, (Feinberg and Hildebrandt, 1997, Seodigeng, 2006).

Three dimensional problems have been solved graphically in a somewhat unstructured manner. Algorithms have been devised but have not been too successful in solving higher dimensional problems (Abraham and Feinberg, 2004, Zhou and Manousiouthakis, 2008). Recently the Recursive Convex Control (RCC) method has been developed and used successfully on higher dimensional problems. It is the purpose of this paper to apply the RCC method to a complex problem previously studied using the AR approach in a lower dimension than that of the actual reaction. It is also important to understand how successful this latter approach was when compared to the use of the RCC algorithm across the full dimensionality of the chemical reaction (Seodigeng, 2006, Seodigeng *et al*., 2007).

Consequently, the purpose of this paper is three-fold. Firstly to use the RCC method to confirm the earlier results (Milne *et al*, 2004, Milne *et al*, 2006), secondly to confirm the applicability of the RCC method to derive candidate attainable regions and finally to apply the method to solving multi-dimensional problems in reaction kinetics for chemical reactions of industrial significance.

The system previously studied (Milne *et al*, 2004, Milne *et al*, 2006), was the oxidative dehydrogenation (ODH) of *n*-butane and *1*-butene to butadiene and it is examined again in this paper. The kinetic rate expressions for the ODH of *n*-butane (Téllez, *et al*, 1999a and 1999b) were used to describe the several reactions and the catalyst in question was a V/MgO catalyst containing 24 wt % of V_2O_5. The hydrocarbon feed was either *n*-butane or *1*-butene. The other reactant was oxygen. In using the RCC algorithm no assumptions were made or needed to be made as to the choice and sequencing of reactor(s) needed to identify the AR^C.

The reaction network shown in Figure 6.1 for the ODH of *n*-butane and *1*-butene was postulated (Téllez, *et al*, 1999a and 1999b) as :

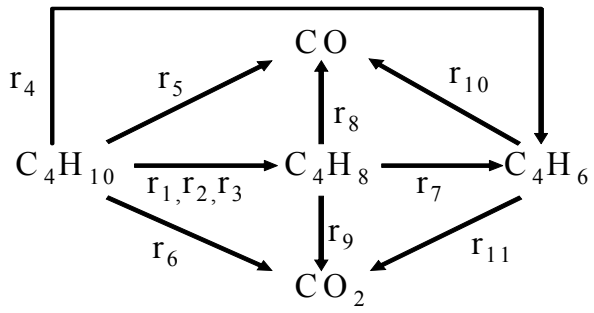


Figure 6.1. Reaction scheme for the oxidative dehydrogenation (ODH) of *n*-butane and *1*-butene to butadiene including side reactions.

In Figure 6.1 the main products are identified but do they do not represent balanced reactions.

The relevant oxidation equations and the stoichiometry are shown in Table 6.1

Oxidation of *n*-Butane
(1). $C_4H_{10} + ½O_2 \rightarrow$ *1*-$C_4H_8 + H_2O$
(2). $C_4H_{10} + ½O_2 \rightarrow$ Trans-*2*-$C_4H_8 + H_2O$
(3). $C_4H_{10} + ½O_2 \rightarrow$ Cis-*2*-$C_4H_8 + H_2O$
(4). $C_4H_{10} + O_2 \rightarrow C_4H_6 + 2H_2O$
(5). $C_4H_{10} + {}^{9}/_{2}O_2 \rightarrow 4CO + 5H_2O$
(6). $C_4H_{10} + {}^{13}/_{2}O_2 \rightarrow 4CO_2 + 5H_2O$
Oxidation of *1*-Butene
(7). *1*-$C_4H_8 + ½O_2 \rightarrow C_4H_6 + H_2O$
(8). *1*-$C_4H_8 + 4O_2 \rightarrow 4CO + 4H_2O$
(9). *1*-$C_4H_8 + 6O_2 \rightarrow 4CO_2 + 4H_2O$
Oxidation of Butadiene
(10). $C_4H_6 + {}^{7}/_{2}O_2 \rightarrow 4CO + 3H_2O$
(11). $C_4H_6 + {}^{11}/_{2}O_2 \rightarrow 4CO_2 + 3H_2O$

Table 6.1. Equations and stoichiometry for the oxidation of *n*-butane, *1*-butene and butadiene.

Previous papers (Milne *et al*, 2004, Milne *et al*, 2006) showed that the maximum possible theoretical yields of butenes and butadiene from the ODH of *n*-butane were from a very large inert membrane reactor (IMR) operating under conditions of a very low and constant oxygen partial pressure. It was shown in these previous papers that these theoretical maximum yields all emanated from an IMR in which one of the reactants,

oxygen, was added along the length of the reactor according to a pre-defined regimen, namely so as to keep its partial pressure constant at its initial value. An alternative description for such an IMR which is consistent with AR theory is a differential side-stream reactor (DSR) and in this paper the latter acronym DSR is used.

In practice, the results entailed the use of a reactor of such a size as to make its practical implementation well-nigh impossible. However, what these earlier papers showed were the limitations on the amounts of butenes and butadiene that could be derived from the ODH of *n*-butane and *1*-butene and, consequently, provided a guideline for assessing the efficiencies of other reactor configurations. It must be noted that in these previous papers the reactors that were studied were chosen in advance and did not arise as an outcome of the attainable region analysis. That the optimal reactor configuration emerges from the analysis of the results is one of the strengths of the AR method and hence the use of the RCC algorithm.

With the reaction scheme in Figure 6.1 there is a very large increase in the number of moles as the reaction proceeds. To use the AR method with linear mixing laws, as in the earlier papers (Milne *et al*, 2004, Milne *et al*, 2006), all hydrocarbon concentrations are expressed in terms of mass fractions of carbon, the number of carbon atoms remaining constant from the beginning to the end of the reaction.

The procedure used to identify an Attainable Region (AR) for a chemical process almost without exception, commencing with the feed to the reactor, has been to develop an initial boundary profile and iteratively extend it further by an expansive process until certain criteria (Glasser *et al*, 1987, Feinberg and Hildebrandt, 1997, Abraham and Feinberg, 2004) have been

satisfied. The adverb *almost* is used deliberately because recently there have been efforts to specify the boundary of an AR by a contraction process as proposed by Abraham and Feinberg (2004) (bounding hyper-planes) and Manousiouthakis (2004) (the "shrink-wrap" process). Here again, in the absence of certainty, no guarantee exists that the limit recognised either by the bounding hyper-planes or the "shrink-wrap" methods truly represented the extreme boundary of an AR. All that can be said is that the true boundary lies somewhere between the limits from the expansion and contraction processes.

In the ODH of *n*-butane the reaction system comprises nine chemical species including oxygen and water. When residence time is considered, the ODH of *n*-butane requires a ten-dimensional space for a complete description. In our earlier papers the kinetic equations were applied to the nine species within the ten dimensions from which two-dimensional projections were abstracted. Where extensions of these two-dimensional concentration spaces were possible, i.e. through the elimination of any concave areas, they were done solely within the two-dimensional spaces and not by intrusion into higher dimensional hyperspaces.

What is proposed in this paper is to deploy an alternative tool, the RCC algorithm, firstly to confirm the previously found theoretical maximum yields of butenes and butadiene, secondly to check whether the earlier postulated reactors were the optimal and finally to examine the possibility of attaining these theoretical maxima in a reactor of a smaller and more practical size than was indicated previously (Milne *et al*, 2004, Milne *et al*, 2006). As part of this process, we shall identify AR^Cs and maximum yields for the different reaction scenarios.

Whereas the RCC method in other applications has been used primarily to find the boundary of a candidate Attainable Region (AR^C), it can equally be applied to derive necessary configurations and parameters to attain this boundary. Within this context, we shall use the RCC concept to answer the following questions :

- What reactor configuration(s) are needed to obtain the maximum yields of butenes and butadiene from the ODH of *n*-butane and *1*-butene?
- What operating parameters are required for these maximum yields?
- What residence times are necessary for these maximum yields within the identified reactor configurations?
- What are the respective candidate attainable regions for these reactions?

6.3 Recursive Convex Control Policy Tool

In this section we give a brief background and description of the Recursive Convex Control (RCC) policy method as presented by Seodigeng (2006, 2007). The Recursive Convex Control (RCC) policy is an automated software application requiring no specialised knowledge of attainable region theory as the necessary aspects of this theory are incorporated in the application. The RCC technique develops iteratively an AR^C from the interior (the expansive method). This iterative process incorporates the work of Feinberg and Hildebrandt (1997) in which work the universal properties of the attainable region were recognised. One of the properties recognised

by Feinberg and Hildebrandt was that the extreme points on the boundary of an AR^C always can be accessed by basic reactor types in simple combinations. These basic reactor types are a continuous-flow stirred-tank reactor (CSTR), a plug-flow reactor (PFR) and a differential side-stream reactor (DSR). The RCC software employs the mathematical characteristics of these reactors and, without necessarily starting from an assumed reactor premise, juggles their permutations and combinations to push the boundary continually outwards until the necessary criteria described above have been satisfied, thus attaining a *ne plus ultra* condition. The RCC algorithm requires, as input, the kinetic data for the various reactants and expected products of the chemical process being studied.

Consider now a steady flow system in which fundamental processes of reaction and mixing are permitted to occur. The state of the system components can be represented by the vector $\boldsymbol{c}$ providing information about concentrations, mass fractions or partial pressures of reactants, intermediates, and products. The instantaneous change in the system state, $d\boldsymbol{c}$, due to the reaction process occurring as a result of residence time progression, $d\tau$, is represented by,

$$d\boldsymbol{c} = \boldsymbol{r(c)}d\tau \qquad (1)$$

The reaction rate vector, $\boldsymbol{r(c)}$, provides the information about the system's reaction kinetics. If we mix state $\boldsymbol{c}$ with another achievable state $\boldsymbol{c}^*$ in a linear mixing space, the resultant state will lie along the mixing vector defined by,

$$\boldsymbol{v} = (\boldsymbol{c}^* - \boldsymbol{c}) \qquad (2)$$

Consider a system where the processes of reaction and mixing are permitted simultaneously to bring about a change on state ***c***. The overall change in the system's state then is given by,

$$d\boldsymbol{c} = [\boldsymbol{r(c)} + \alpha(\boldsymbol{c}^* - \boldsymbol{c})]d\tau \qquad (3)$$

The process combination control policy describing the proportion to which mixing occurs relative to reaction is denoted by the scalar α.

Feinberg and Hildebrandt (1997) and Feinberg (2000a, 2000b) developed a theory to describe the geometric properties of the structure of the attainable region boundary. For steady-state flow systems with the occurrence of reaction and mixing, the AR boundary was shown to be shaped by surfaces of manifolds of either of reaction or of mixing. These surfaces were shown to emanate from trajectory highways at which the two processes of reaction and mixing combined in an optimally-controlled fashion. Feinberg (2000a) derived analytical formulations for these trajectory highways to which the control policy α, had to conform according to a strictly regulated optimal function of the system state, ***c.*** The unit operation in which the combination of reaction and mixing occurs in this optimally controlled manner is called a critical differential side-stream reactor, DSR, {Feinberg (2000a)}. This type of reactor can be conceptualised as a plug flow reactor with the addition of material of some state $\boldsymbol{c}^*$ along the length of the reactor. The rate of change of the state of the material with residence time along the reactor is described by an expression similar to equation (3),

$$d\boldsymbol{c} = [\boldsymbol{r(c)} + \alpha_{opt}(\boldsymbol{c}, \boldsymbol{c}^*)\boldsymbol{v}(\boldsymbol{c}^*, \boldsymbol{c})]d\tau \qquad (4)$$

In equation (4), τ is the residence time, providing some information about the space or length dimensionality of the reactor and $\alpha_{opt}(\boldsymbol{c}, \boldsymbol{c}^*)$ is the optimal control policy for the two processes of reaction and mixing. The analytical

formulations for $\alpha_{opt}(\boldsymbol{c}, \boldsymbol{c}^*)$, as demonstrated by Feinberg (2000a), involve complex mathematical derivations, even for systems with few reactants and idealised simple theoretical kinetics. However, it should be emphasised that once these optimal combinations have been identified the completion of the AR boundary is clear-cut and straightforward using only the processes of reaction or mixing.

Consequently, it is against this background that the theory of the recursive constant control methodology for identifying candidate AR boundaries was formulated (Seodigeng, 2006, 2007). For systems considering only reaction and mixing, it was proposed that once the optimal trajectory highways representing the combinations of the two fundamental processes demarcating the structure of the boundary have been identified, the rest of the boundary can be completed with surfaces of manifolds that represent states attained by the processes of either reaction or mixing alone.

The Recursive Convex Control (RCC) policy algorithm (Seodigeng, 2006, 2007) iteratively applies all combinations of all permitted fundamental processes to approximate the trajectory highways that shape the outline of the AR boundary from which distinct process manifold surfaces originate, giving rise to the final shape of the boundary. This technique iteratively uses constant values for the control policy α, to delineate approximately the $\alpha_{opt}(\boldsymbol{c}, \boldsymbol{c}^*)$ function along the DSR trajectory, for systems where only the processes of reaction and mixing are allowed.

The RCC algorithm can be summarised to embody four main stages in its execution (Seodigeng, 2006, 2007).

1. The initialisation stage during which the starting state points are identified. Single process operation trajectories are generated from all system feed states and *convexified* to locate all extreme state points that form the convex hull and to eliminate all interior state points.

2. The growth stage in which a grid of process operation control policy values are engendered.

3. The iteration stage in which each extreme point that is an output state from combinations of fundamental processes is produced. Where the control policy is α_i, the first process combination profile should have a control policy value of $(\alpha_{i-1} + \alpha_i)/2$ and the second profile should have a control policy with a value of $(\alpha_{i+1} + \alpha_i)/2$. This step uses mid-point interpolation and populates the control policy grid with more values. The data set is then *convexified* to locate all extreme points that enclose the convex hull and eliminate all interior state points. This stage is repeated until the termination criteria are satisfied.

4. From all extreme points that are output states to combinations of fundamental processes distinct process trajectories are generated to complete the AR^C.

A point x is an extreme point if it is a vertex of the convex hull. An extreme point does not lie in the interior of any line segment bounding the facets of the polytope. In particular, $\boldsymbol{x} \in C$ is extreme if there exist no points $x_1, x_2 \in C$, such that $\lambda x_1 + (1-\lambda)x_2 = x$, with $0 < \lambda < 1$.

It should be clear from the above description that the final output from the RCC algorithm is a set of discrete points, all of them being extreme points

for the boundary of the AR^C. Thus what we obtain in the end is a discretised numerical approximation to the boundary. Obviously we can get closer approximations by a finer discretisation, and as usual we have to balance the accuracy of the final approximation with the computing time and power needed to obtain it. In this paper good results were obtained on standard PCs without an inordinate amount of computer time.

The RCC concept has been used (Seodigeng, 2006, 2007) to identify candidate attainable regions for the synthesis of ammonia and methanol and to study the water-gas shift reaction. In addition to using it to identify and analyse AR^Cs it was also used to identify optimal process flowsheets for these reactions of industrial interest. Furthermore, the RCC concept has been deployed by Seodigeng (2006) to analyse a four-dimensional stoichiometric Van de Vusse problem, a task that previously had been deemed too difficult to solve using the available methods.

6.4 Results

The RCC technique has been employed to identify AR^Cs for the following reactions.

- Case 1: ODH of *n*-butane to form butenes (all three isomers)
- Case 2: ODH of *n* -butane to form butadiene
- Case 3: ODH of *1*-butene to form butadiene

The partial pressure of oxygen in the feed was varied between 85 kPa and a very low value and should a DSR be selected by the RCC algorithm as one of the three possible reactors additional oxygen would be supplied *optimally*

along the length of the DSR so as to attain the profile of the AR^C. This reactor configuration is styled a *critical* DSR (Feinberg and Hildebrandt, 1997, Abraham and Feinberg, 2004). The isothermal temperature for all reactions was 773K.

The results of these calculations are values of concentrations in terms of mass fractions of the boundary values of a convex region in a higher dimensional space. In order to present these results in a way that is understandable to the reader we will present graphical results of two dimensional projections in terms of the variables of interest.

To apply the RCC algorithm to the ODH of *n*-butane and *1*-butene several modifications and definitions have been added. Two formulations for combinations of processes for all three case studies of interest have been considered. The first formulation is the combination of the processes of reaction and mixing with the fresh feed material as given by equation (3) above, described by

$$\frac{d\boldsymbol{c}}{d\tau} = \boldsymbol{r}(\boldsymbol{c}) + \alpha(\boldsymbol{c}^* - \boldsymbol{c}) \qquad 0 <= \alpha <= 1 \qquad (5)$$

The RCC process, at each section of the reactor where the mixed feed is added, selects the optimal value of α required for the further extension of the attainable region space.

Equation (5) says that the rate of change in the state vector of all the variables, $\boldsymbol{c}$, with respect to residence time, τ, is equal to the reaction rate vector defined at $\boldsymbol{c}$, $\boldsymbol{r(c)}$, plus the product of α and the difference between the mixing state variable of the system, $\boldsymbol{c}^*$, and $\boldsymbol{c}$, the state vector of all variables describing the system.

The combinations of the processes as described can be conceptualised as a type of DSR depicted in Figure 6.2. The addition of butane and oxygen as reactants is controlled by the control policies, α_1, α_2, α_3 …… α_n.

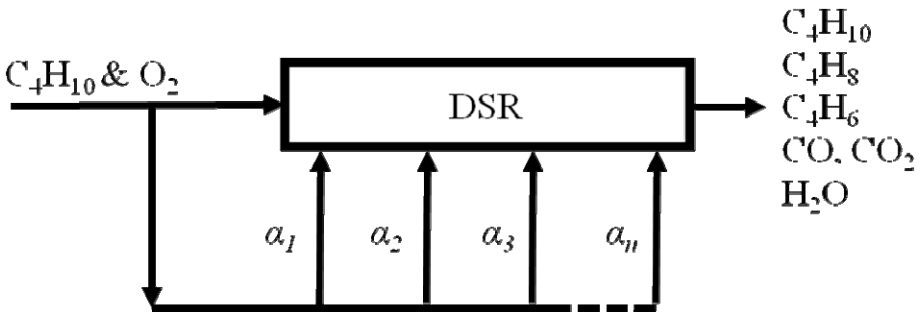


Figure 6.2. Conceptualised reactor structure for combination of reaction and mixing with fresh feed

The second combination is the representation of the combination of reaction and mixing with only one feed component, oxygen.

$$\frac{d\boldsymbol{c}}{d\tau} = \boldsymbol{r}(\boldsymbol{c}) + \beta(\boldsymbol{c}_{O2}^{0} - \boldsymbol{c}_{O2}) \qquad 0 <= \beta <= 1 \qquad (6)$$

The RCC process, at each section of the reactor where the mixed feed is added, selects the optimal value of β required for the further extension of the attainable region space.

Equation (6) says that the rate of change in the state vector of all the variables, $\boldsymbol{c}$, with respect to residence time, τ, is equal to the reaction rate vector defined at $\boldsymbol{c}$, $\boldsymbol{r(c)}$, plus the product of β and the difference between the

mixing state variable of oxygen at the feed point, c_{O2}^{0},and c_{O2}, the state vector of oxygen.

The control policy for oxygen addition, β, can be chosen to induce either a constant or a variable oxygen partial pressure along the length of the reactor as the reaction occurs. The unit operation for this type of combination is illustrated in Figure 6.3.

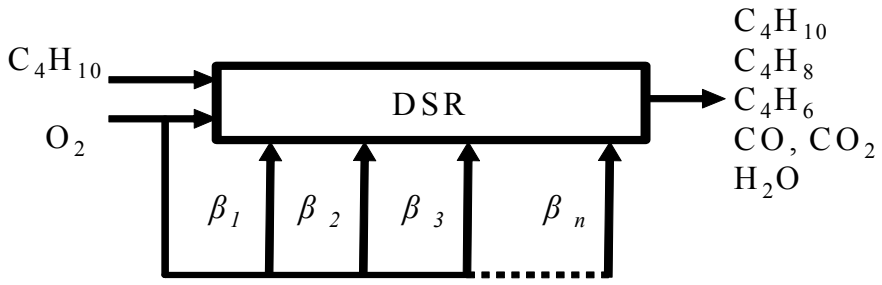


Figure 6.3. Conceptualised reactor structure for combination of reaction and mixing with oxygen.

The bounds of the mixing control policy α in equation (5) were chosen to be [0, 10 000] with 5 000 constant values spaced at exponentially increasing increments. The same number of points and the exponential distribution was chosen for β in equation (6). The value of the control policy was varied to maintain the partial pressure of oxygen from a very low value to 85 kPa. The automatic population and refinement strategy of the RCC algorithm was applied to populate the control policy values and refine the grid spacing as necessary throughout the calculation procedure as described by Stage 4 of the algorithm. The termination criterion adopted for this multi-dimensional problem is the growth rate of the attainable region hyper-volume. The algorithm was set to terminate the continuation of iterations when the hyper-growth rate per iteration falls below 1 % or the number of iteration exceeded

100. These calculation specifications became the standard for all three case studies.

For the process combination represented by equation (5) and illustrated in Figure 6.2 and Figure 6.3, the feed partial pressure of oxygen was varied from 0.0001 kPa to 85 kPa and the control policies for mixing, α and β, were varied for each partial pressure.

The RCC algorithm functions by finding a set of extreme points of a convex region. To complete the boundary of the AR^C these points would be linked by hyper planes. In this paper we have just kept the points and when we draw the projections we merely project the extreme points. We are then able to see the extreme points in this subspace as the furthermost envelope of these points. This point should become clearer when viewing the results in the subsequent figures.

6.4.1 Case 1 – ODH of *n*-butane to form butenes.

In the ODH of *n*-butane to butenes, we have nine possible chemical substances. These include oxygen and water as well as the oxidation both of butane and butenes to butadiene, the latter in this case being considered as an undesirable by-product. To these nine substances, a tenth variable, residence time, can be added.

Figure 6.4 is the two dimensional projection of the AR^C identified by the RCC method for the ODH of *n*-butane to butenes.

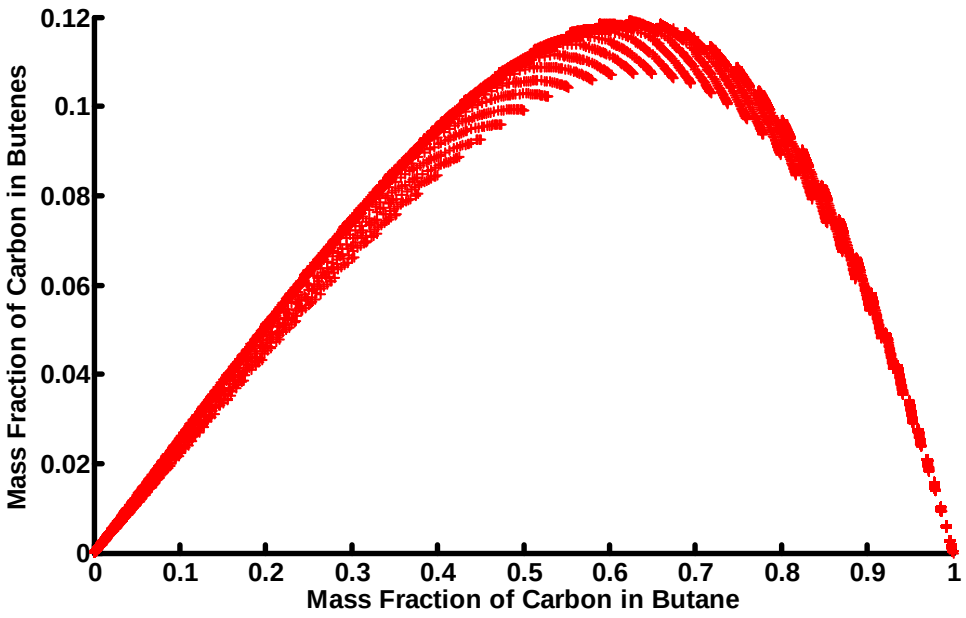


Figure 6.4. Projection of the set of extreme points derived from the RCC profile for the ODH of *n*-butane to butenes (sum of all three isomers) plotted in mass fraction space.

Figure 6.4 shows the extreme points of the profiles in mass fraction space for the yield of butenes (sum all three isomers) from the ODH of *n*-butane as derived from the application of the RCC method. Figure 6.4 is a two-dimensional projection from a ten-dimensional hypersurface. Note that the boundary in this space is represented by the envelope of all the boundary points. The graph is presented in this form because the identification of the AR^C results from the envelope of these discrete points in the boundary. By sufficient repetition of the calculations for the discrete points the AR^C profile emerges.

In developing these profiles the RCC method considered all possible permutations and combinations of a CSTR, a PFR and a DSR to extend the profile to its furthest extreme. In addition, the control variable, the partial pressure of oxygen in the feed, was varied over the entire spectrum from 85 kPa to a very low value to produce these profiles.

The boundary of AR^C identified for this reaction in our earlier paper (Milne *et al*, 2006) is indistinguishable from the boundary in Figure 6.4. This figure shows that the maximum yield of butenes (the sum of all three isomers, *1*-butene, trans-*2*-butene and cis-*2*-butene) from the ODH of *n*-butane as a function of *n*-butane concentration is 0.119 and occurs at an *n*-butane concentration of 0.623.

Detailed analysis of the results from this RCC application (not shown in this paper) confirmed that the outermost limit was commensurate with a DSR to which the supply of oxygen was controlled according to a specific regimen.

Apart from commencing without presuming a particular reactor configuration, another fundamental difference between the RCC algorithm and the comparatively simplistic approach adopted in our earlier papers is that any extension of a concave area by transformation into a convex area is accomplished across all the hypersurfaces and not within a two-dimensional projection from these hypersurfaces. The fact that the two different approaches provided similar outcomes will be discussed later in this paper.

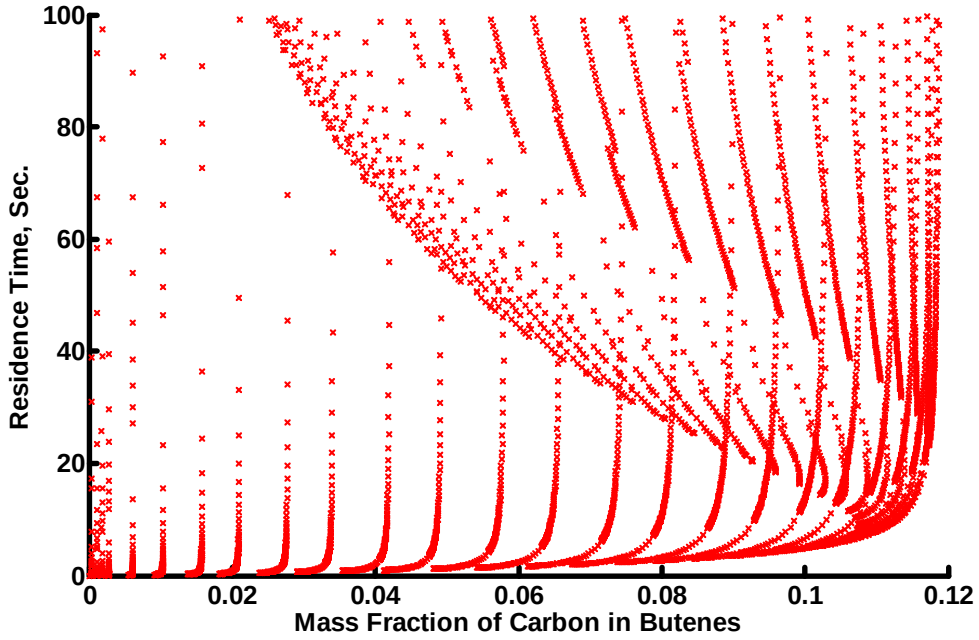


Figure 6.5. RCC profile of residence times and concentrations of butenes from the ODH of *n*-butane.

Figure 6.5 is a two dimensional projection in concentration of butenes: residence time space from all the hypersurfaces. It shows that the maximum yield of butenes, 0.119 is achieved at a residence time close to 100 seconds. This can be compared with the 1.7 x 10^7 seconds derived earlier (Milne *et al*, 2006). Note that one can achieve virtually the maximum yield after about only 20 seconds.

Figure 6.5 indicates that the residence time increases asymptotically as the concentration of butenes increases above 0.118. In our previous paper (Milne *et al*, 2006), this characteristic also had been observed as well as the fact that butane-butenes concentration profiles for oxygen partial pressures of 0.25 kPa and 0.000001 kPa were indistinguishable so close were they to each other.

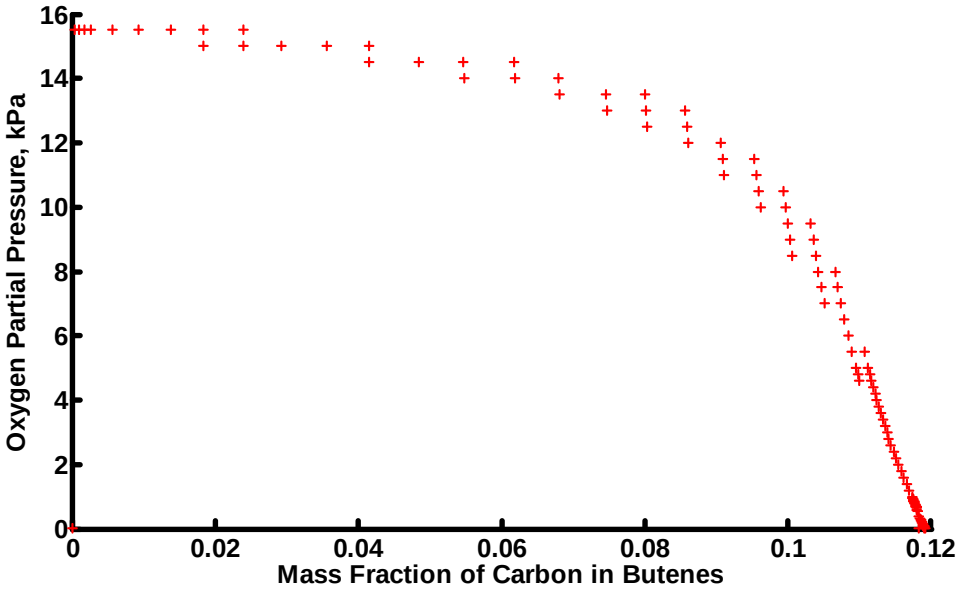


Figure 6.6. RCC operational oxygen control policy for the maximum yield of butenes from the ODH of *n*-butane

In Figure 6.6 we show the calculated optimal control policy for the partial pressure of oxygen as a function of the yield of butenes. Figure 6.6, in effect, says that the initial partial pressure to the reactor configuration should be 15.5 kPa and should be held constant at this level by the addition of fresh oxygen until the yield of butenes has reached 0.025 carbon mass fraction. This implies that initially the reactor should be a DSR with a policy of constant oxygen partial pressure.

Once the yield of butenes has attained 0.025 carbon mass fraction, there is a change in the oxygen partial pressure. It now starts to wane from a value of 15.5 kPa to zero. According to the RCC results, if the partial pressure along the remaining length of the DSR is controlled in this manner and allowed to be completely exhausted, the maximum yield of butenes can be secured.

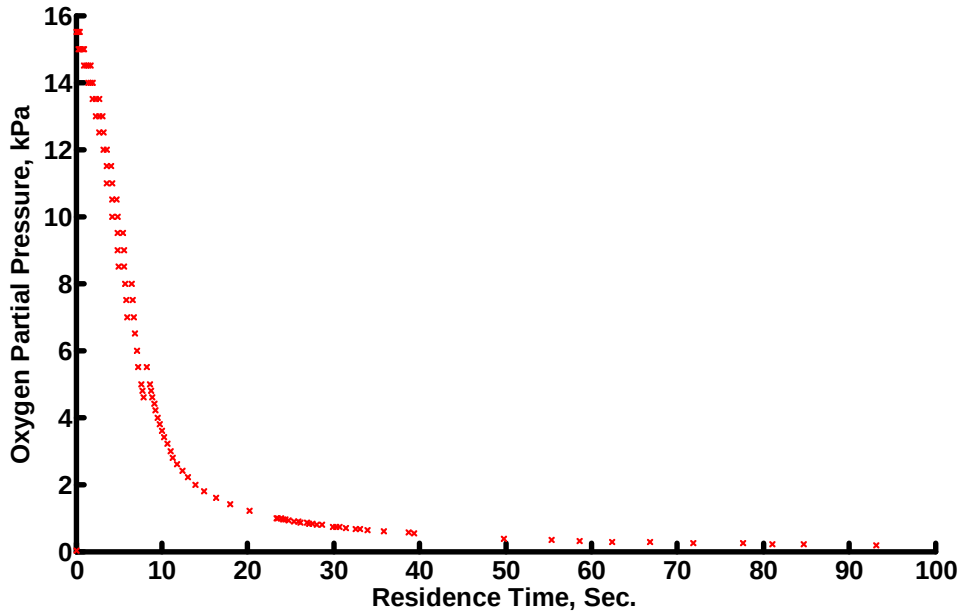


Figure 6.7. RCC oxygen control policy as a function of residence time for the maximum yield of butenes from the ODH of *n*-butane.

In Figure 6.7 we show the calculated optimal control policy for the partial pressure of oxygen as a function of residence time.

Figure 6.7 shows that the partial pressure of oxygen is held constant at 15.5 kPa for approximately 0.5 seconds after which the oxygen is allowed to be totally depleted at the rate specified in Figure 6.7. The total residence time for this critical DSR is approximately 100 seconds.

Figure 6.8 shows an expanded view of Figure 6.7 at low values of residence time.

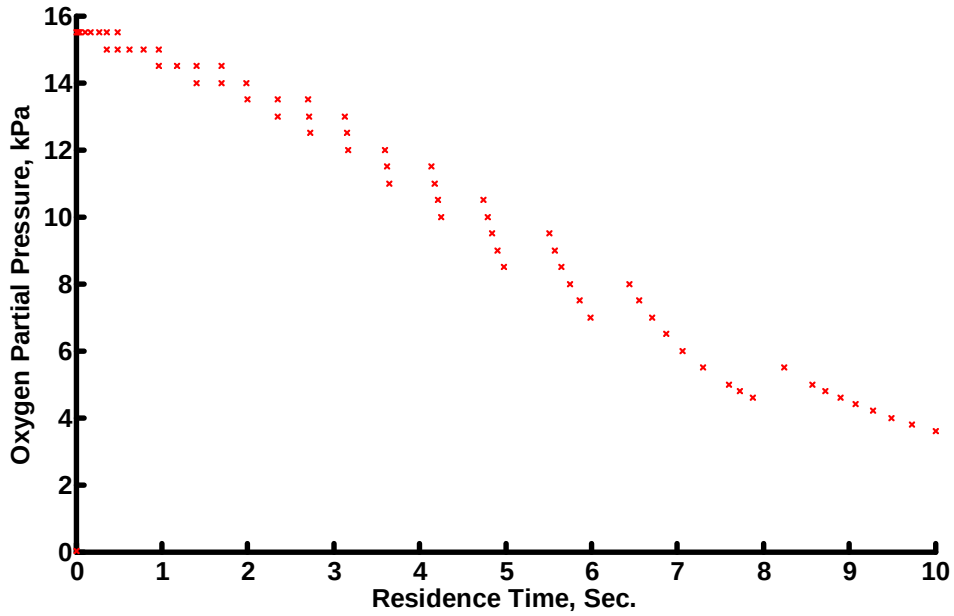


Figure 6.8. Enlarged section of Figure 6.7 - RCC oxygen control policy as a function of residence time for the maximum yield of butenes from the ODH of *n*-butane

It is concluded that a DSR, the feed to which is a stream of *n*-butane and oxygen, the partial pressure of the latter being 15.5 kPa, is capable of providing the maximum possible yield of butenes after a total residence time of 100 seconds provided the flow of oxygen along the length of the DSR follows a defined pattern. Previously it had required a total residence time of 1.7×10^7 seconds to achieve this yield of butenes for which the oxygen partial pressure was held at an extremely low constant value.

However, it must be stated that our previous paper (Milne *et al*, 2006) showed that with a residence time of 75 seconds, it was possible to achieve a yield of butenes of 99.7 % of the theoretical maximum possible. The

reactor configuration for this was a DSR with a constant oxygen partial pressure of 0.25 kPa.

We conclude that the controlled addition of oxygen as shown in Figure 6.7 to a DSR effectively yields the theoretical maximum amount of butenes from the ODH of *n*-butane and can do so within a residence time of 100 seconds. Consequently, the RCC concept has confirmed our previous finding that for a residence time between 75 and 100 seconds and a carefully configured oxygen addition control policy it is possible to produce yields of butenes close to the theoretical maximum quantity.

6.4.2 Case 2 – ODH of *n*-butane to form butadiene.

In our earlier paper (Milne *et al*, 2006) the theoretical maximum yield of butadiene from the ODH of *n*-butane was found to be 0.800 carbon mass fraction. All the initial feed of *n*-butane was effectively oxidised to produce this quantity of butadiene.

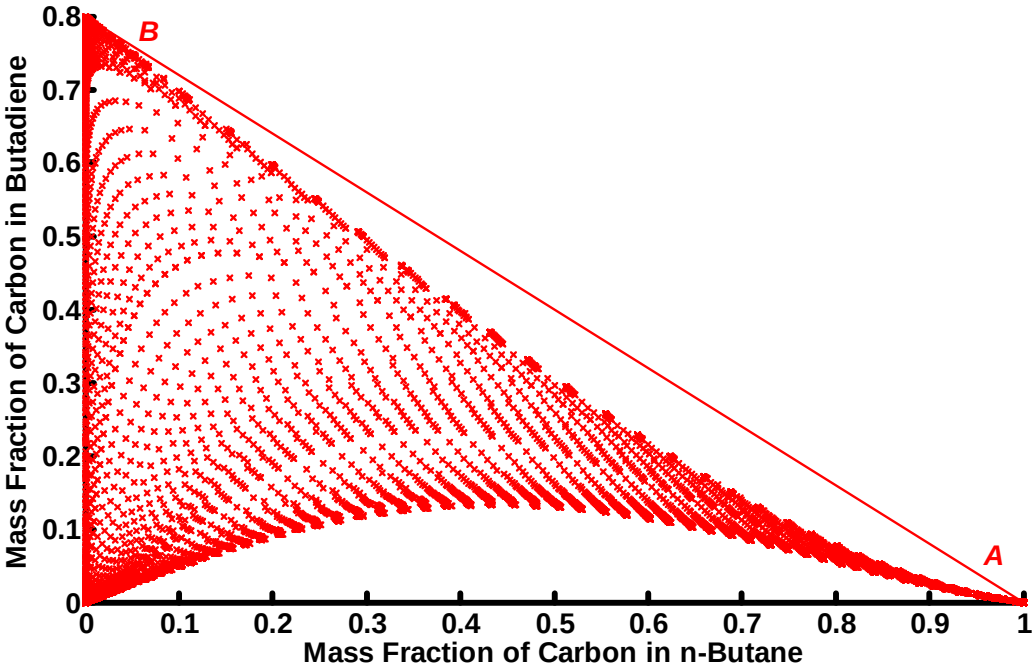


Figure 6.9. Set of extreme points derived from the RCC profile for the ODH of *n*-butane to butadiene in mass fraction space.

Figure 6.9 shows the profiles in mass fraction space for the yield of butadiene from the ODH of *n*-butane as derived from the application of the RCC method. It is a two-dimensional projection from a ten-dimensional hypersurface. As in Case 1 above for the production of butenes from *n*-butane, in developing these profiles the RCC method considered all possible permutations and combinations of a CSTR, a PFR and a DSR to extend the profile to its furthest extreme. In addition, the control variable, the partial

pressure of oxygen in the feed, was permitted to vary over the entire spectrum from 85 kPa to a very low value to produce these profiles.

The RCC maximum yield of butadiene, 0.799 carbon mass fraction, was obtained when the initial *n*-butane had been reduced to 6 x 10^{-5} carbon mass fraction. These concentrations agree with those shown earlier (Milne *et al*, 2006).

As discussed above the AR^C is the convex hull of the extreme points. Thus the marked concavity apparent in Figure 6.9 indicates a hyper plane covering a large region of space. It was removed by mixing fresh feed, Point A, with product from Point B in various ratios, the locus for all the resulting outputs lying along the line AB. The putative AR^C for the system *n*-butane and butadiene was bounded by the two axes and the line AB. This region matched that identified in our earlier paper (Milne *et al*, 2006).

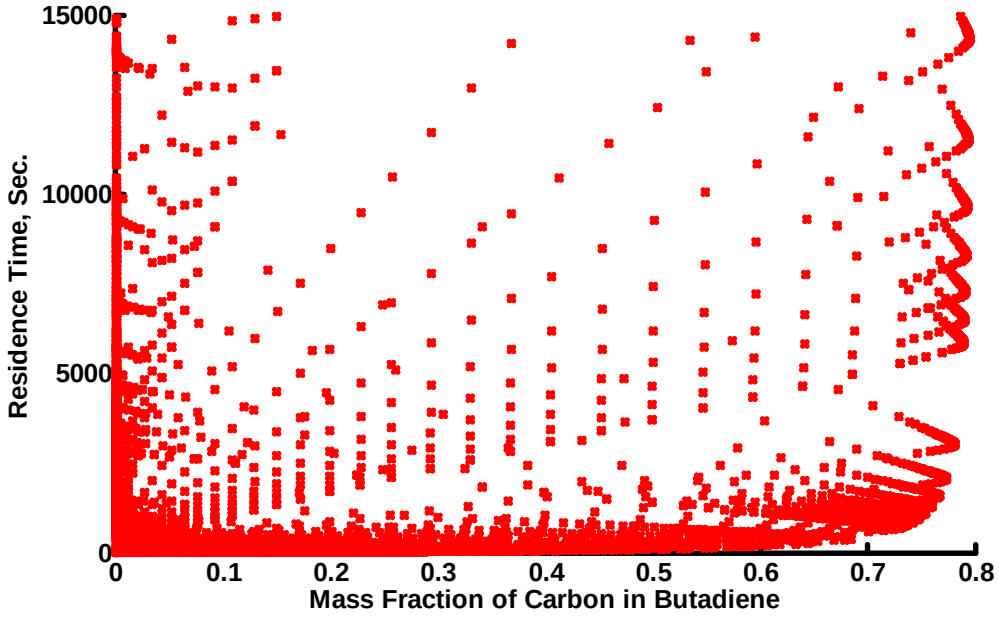


Figure 6.10. RCC profile of residence times and concentrations of butadiene from the ODH of *n*-butane

In Figure 6.10 we show the RCC residence times for the maximum yield of butadiene from the ODH of *n*-butane. A total residence time of approximately 15 000 seconds is required to yield a butadiene concentration of 0.8 carbon mass fraction. This residence time can be compared with the 5.6×10^7 seconds derived for the DSR reactor in the earlier paper (Milne *et al*, 2006).

In our previous paper (Milne *et al*, 2006) we showed that a butadiene yield of 0.665 carbon mass fraction or 83 % of the theoretical maximum could be obtained from a DSR with a constant oxygen partial pressure of 0.25 kPa and with a residence time of 322 seconds.

An enlargement (not shown) of Figure 6.10 shows that the equivalent yield of butadiene, 0.665 carbon mass fraction, is possible after a residence time of 332 seconds. The difference between the 322 and the 332 seconds most likely is within the accuracy of the calculations

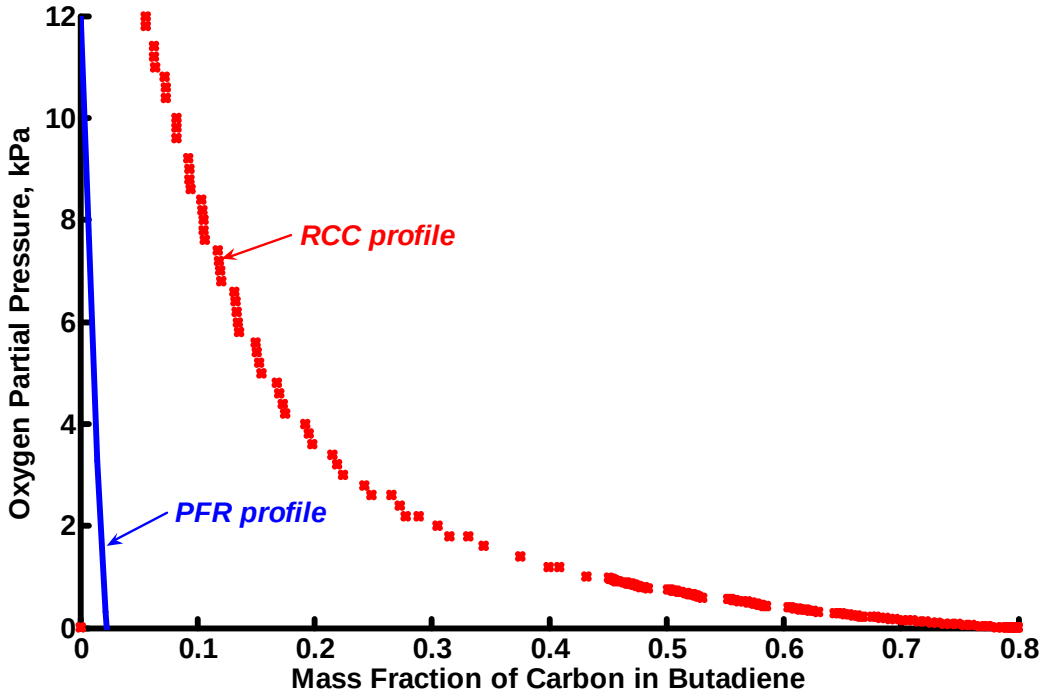


Figure 6.11. RCC operational control policy for the maximum yield of butadiene from the ODH of *n*-butane

In Figure 6.11 we show the control policy for the partial pressure of oxygen as a function of the yield of butadiene. Figure 6.11, in effect, says that the initial partial pressure to the reactor configuration should be 12 kPa and should be permitted to drop rapidly until the yield of butadiene has reached 0.154 carbon mass fraction. This would seem to imply that initially the reactor should be a plug flow reactor (PFR) one in which the initial oxygen concentration is allowed to wane through the normal ODH reaction process and one in which no supplementary oxygen is made available to compensate for that used. In this particular instance this is not so. In a PFR where the oxygen partial pressure of 12 kPa is depleted through the normal ODH process, the oxygen partial pressure profile (Milne *et al*, 2006) has been superimposed on Figure 6.11. It is clear that the RCC result stipulates a more controlled and less precipitous decline in the initial oxygen partial pressure. The interpretation to be drawn from Figure 6.11 is that oxygen is

added from the beginning to compensate for that lost through the ODH process. The reactor configuration for this is a DSR. Thus the reactor configuration, accordingly, for this scenario is the same as that shown in Figure 6.2.

Close scrutiny of Figure 6.11 for a butadiene concentration of 0.665 carbon mass fraction shows that the associated oxygen partial pressure is 0.23 kPa thus providing good agreement with the conclusion from our previous paper (Milne *et al*, 2006).

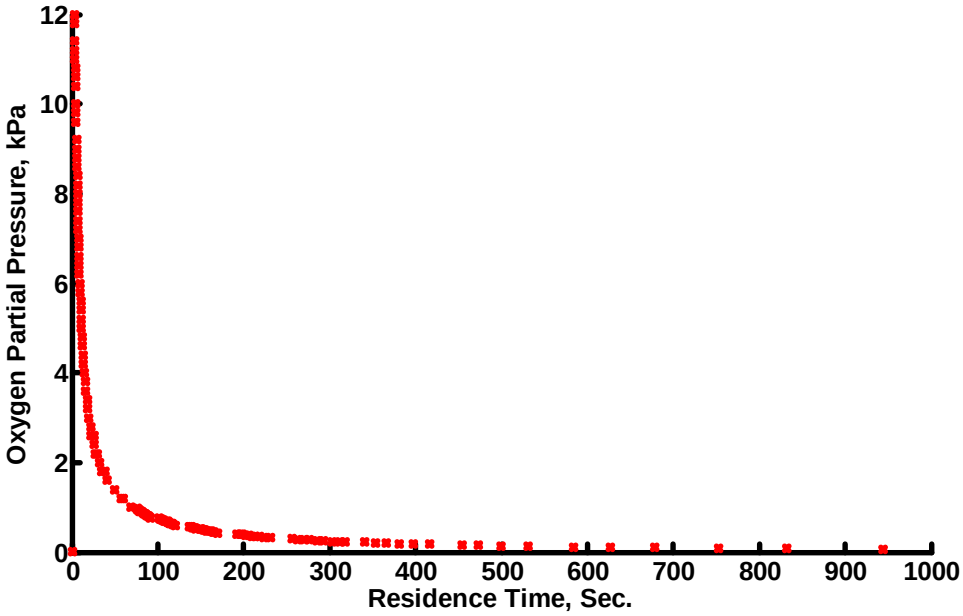


Figure 6.12. RCC oxygen control policy as a function of residence time for the maximum yield of butadiene from the ODH of *n*-butane.

Figure 6.12 shows that the RCC residence time for this critical DSR is approximately 1 000 seconds. After this time the oxygen partial pressure has been reduced to 0.07 kPa. That the profile for this curve for residence times in excess of 1 000 seconds is very flat may be seen from the following table.

Table 6.2 shows the corresponding optimum oxygen partial pressures at residence times from 1 000 to 20 000 seconds.

Residence Time, Sec.	**Oxygen Partial Pressure, kPa**
1 000	0.07
5 000	0.01
10 000	0.006
15 000	0.004
20 000	0.003

Table 6.2. Residence times in DSR and corresponding optimal RCC oxygen partial pressures.

It is apparent from Table 6.2, contrary to Case 1 above, that there is no clean termination of residence time at a very low oxygen partial pressure value. It is believed that this results from an inherent lack of discrimination within the RCC algorithm when multi-dimensional surfaces are very flat, a topic to which we shall return later in this particular case study.

Figure 6.13 shows an expanded view of Figure 6.12 at low values of residence time.

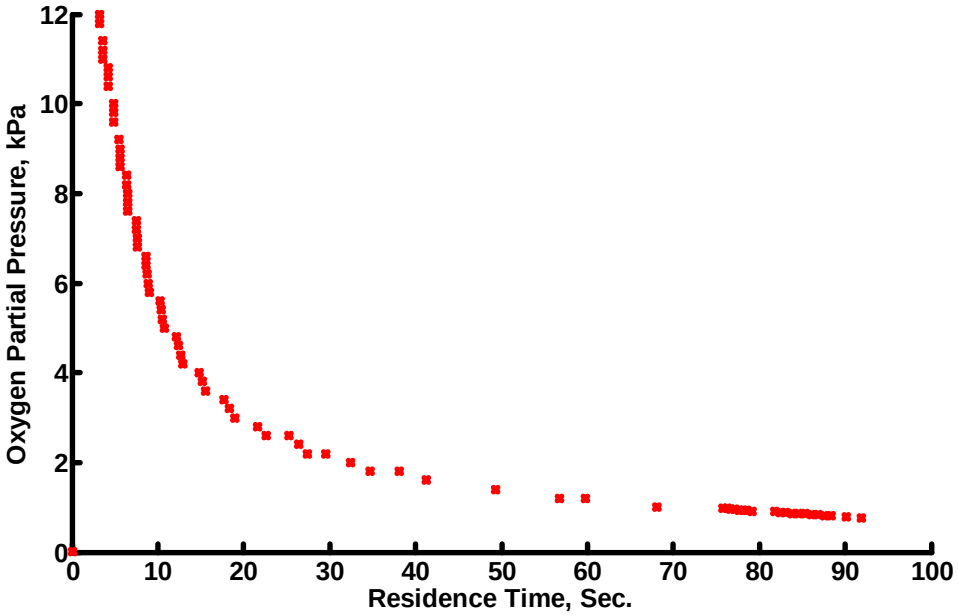


Figure 6.13. Enlarged section of Figure 6.12 - RCC oxygen control policy as a function of residence time for the maximum yield of butadiene from the ODH of *n*-butane

In a PFR where the inlet oxygen partial pressure is 12 kPa, all the oxygen was shown to be depleted after a residence time of 3 seconds (Milne *et al*, 2006).

Scrutiny of the RCC profiles for maximising the yield of butadiene from the ODH of *n*-butane reveals an enigma. The inlet oxygen partial pressure of 12 kPa is coincident with a butadiene yield of 0.06 and after a residence time of approximately 3 seconds. The RCC method yielded no data for the range of butadiene values from zero to 0.06 and for residence times less than 3 seconds. Why?

It seems as if in multi-dimensional space, the hypersurface(s) of the RCC region is (are) extremely flat for the initial yields of butadiene from *n*-

butane and for the initial (and final) residence times. The RCC concept, as explained earlier in this paper, strives iteratively to extend an attainable region by creating a convex surface until the conditions of constraint call a halt to this process. If the initial surface of the region is planar, it is surmised, the establishment of a convex hull within the current accuracy of the RCC concept becomes very difficult. The incipient identification of a potential convex surface becomes apparent only after approximately three seconds.

It is concluded that a maximum butadiene yield of 0.8 carbon mass fraction can be obtained from a DSR where the addition of oxygen is rigorously controlled. The total residence time for this yield is 15 000 seconds, significantly less than the 5.6×10^7 seconds previously recorded (Milne *et al*, 2006). However, at a residence time of 1 000 seconds, the yield of butadiene is 0.745 carbon mass fraction, 93 % of the theoretical maximum. With a residence time of 332 seconds, the butadiene yield is 0.665 carbon mass fraction, 83 % of the theoretical maximum.

6.4.3 Case 3 – ODH of *1*-butene to form butadiene.

In our earlier paper (Milne *et al*, 2004), the maximum yield of butadiene resulting from the ODH of *1*-butene was found to be 0.899 carbon mass fraction. All the initial feed of *1*-butene was effectively oxidised to produce this quantity of butadiene.

The residence time necessary for this yield of 0.899 carbon mass fraction in butadiene was 2.93 x 10^7 seconds.

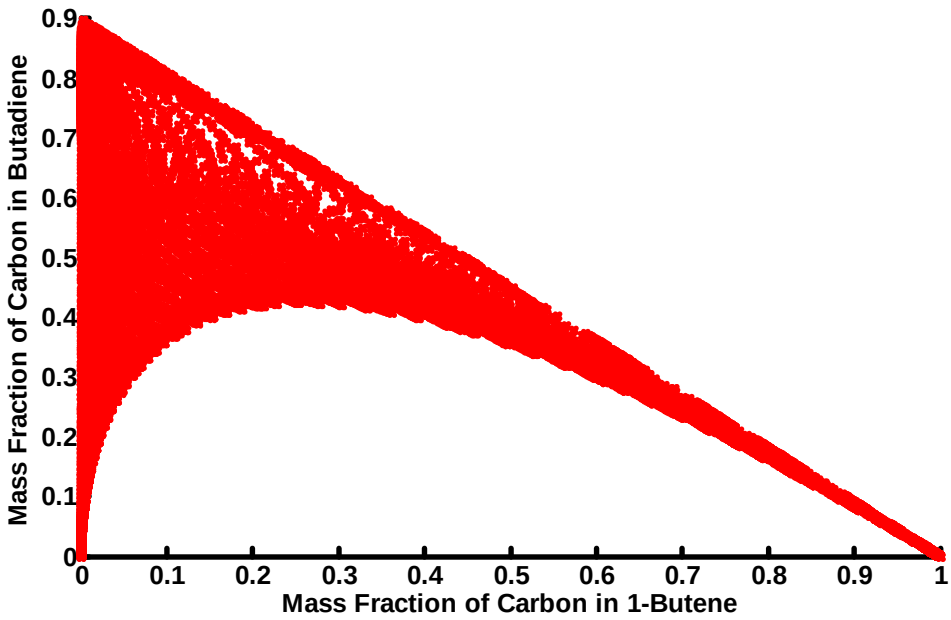


Figure 6.14. Set of extreme points derived from the RCC profile for the ODH of *1*-butene to butadiene.

Figure 6.14 is the AR^C in mass fraction space identified by the RCC concept for the ODH of *1*-butene to butadiene. It agrees with the candidate region identified in our previous paper (Milne *et al*, 2004).

In the ODH of *1*-butene to butadiene, there are six chemical species present including water and oxygen. With the addition of residence time a seventh variable is present. Accordingly, Figure 6.14 is a two-dimensional projection from a seven-dimensional hypersurface.

The maximum yield of butadiene from the RCC algorithm, 0.896 carbon mass fraction, was obtained after the initial concentration of *1*-butene had been reduced to 0.003. These concentrations agree closely with those of 0.899 and zero shown earlier (Milne *et al*, 2004).

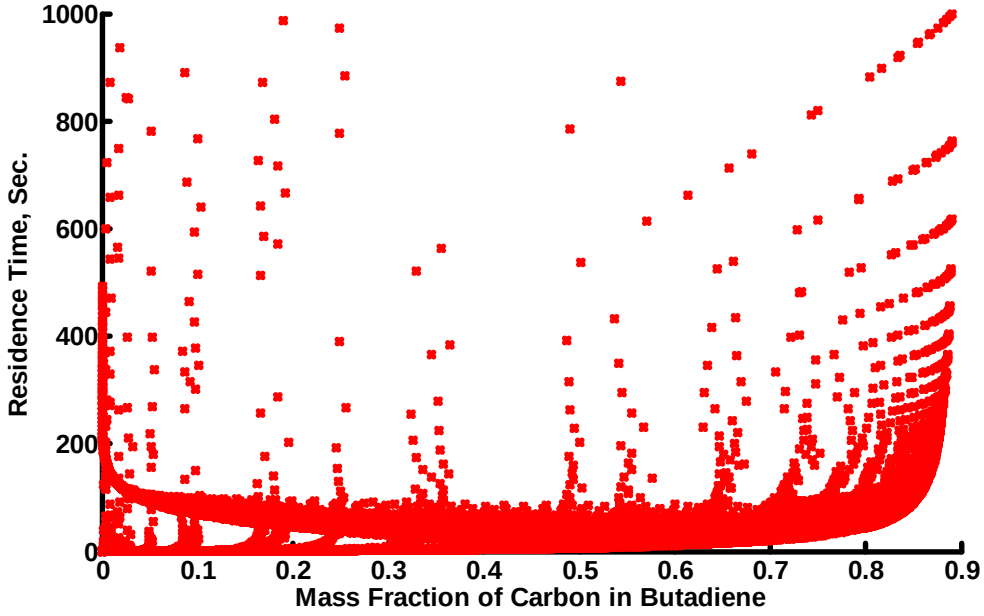


Figure 6.15. RCC profile of residence times and concentrations of butadiene from the ODH of *1*-butene

Figure 6.15 shows that the maximum yield of butenes, 0.896 is achieved after a residence time close to 1 000 seconds. This can be compared with the 2.93×10^7 seconds derived earlier (Milne *et al*, 2004).

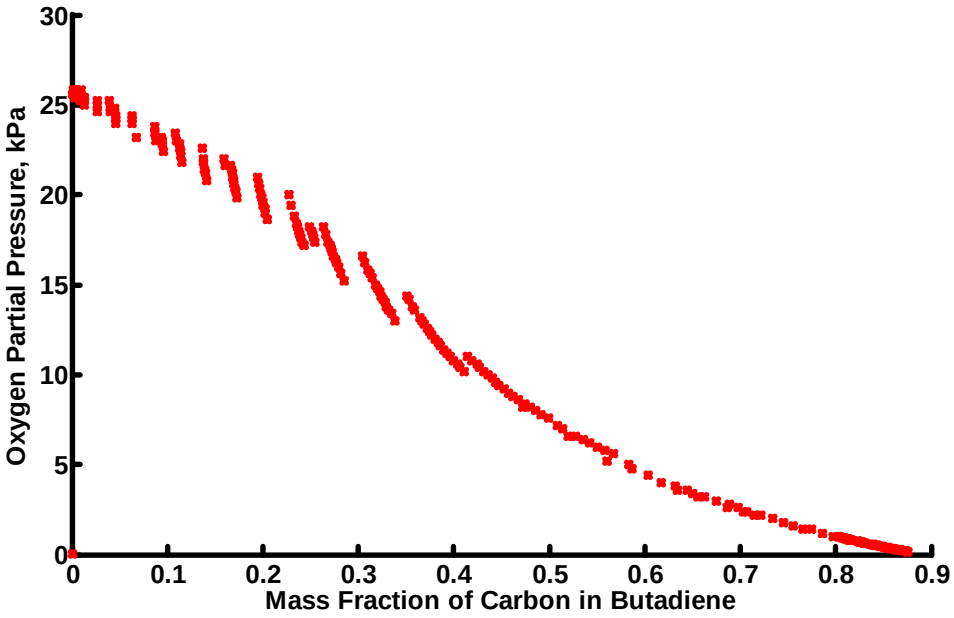


Figure 6.16. RCC operational control policy for the maximum yield of butadiene from the ODH of *1*-butene

In Figure 6.16 we show the control policy for the partial pressure of oxygen as a function of the yield of butadiene. Figure 6.16, in effect, says that the initial partial pressure to the reactor configuration should be 25.5 kPa and briefly should be held constant at this level until the yield of butadiene has reached 0.0133 carbon mass fraction.

Once the yield of butadiene has attained 0.0133 carbon mass fraction, there is a change in the oxygen partial pressure. It now starts to decrease from a value of 25.5 kPa to zero. According to the RCC results, if the partial pressure along the length of this DSR is controlled in this manner and allowed to be completely exhausted, the maximum yield of butadiene can be secured.

The reactor configuration, accordingly, for this scenario is the same as that shown in Figure 6.2.

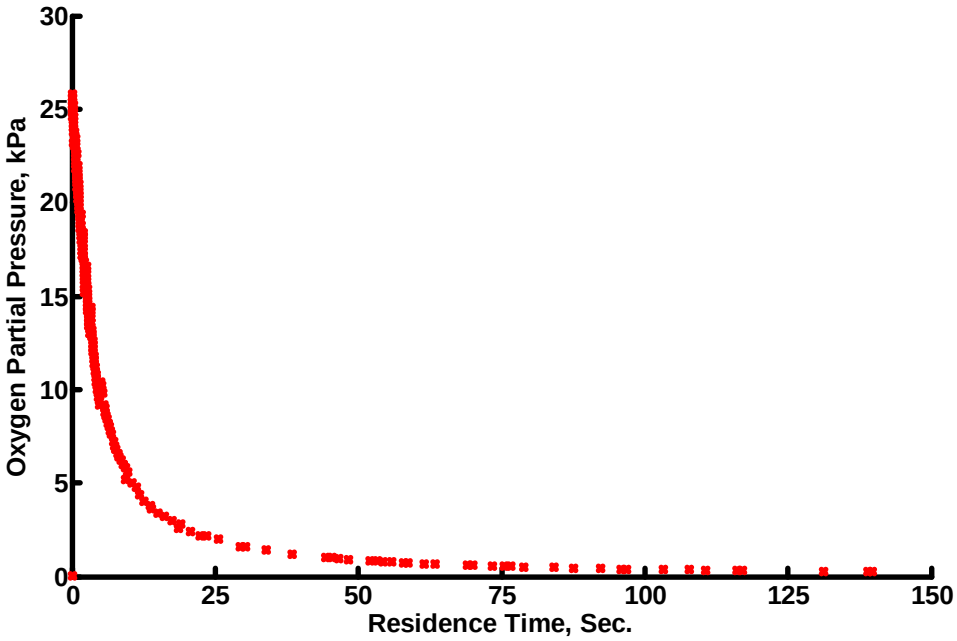


Figure 6.17. RCC oxygen control policy as a function of residence time for the maximum yield of butadiene from the ODH of *1*-butene.

Figure 6.17 shows that the initial residence time for the DSR is approximately 0.5 seconds (see Figure 6.18) after which the oxygen is allowed to fall as specified in Figure 6.16 and Figure 6.17. The total residence time for the DSR is approximately 150 seconds.

Figure 6.18 shows an expanded view of Figure 6.17 at low values of residence time.

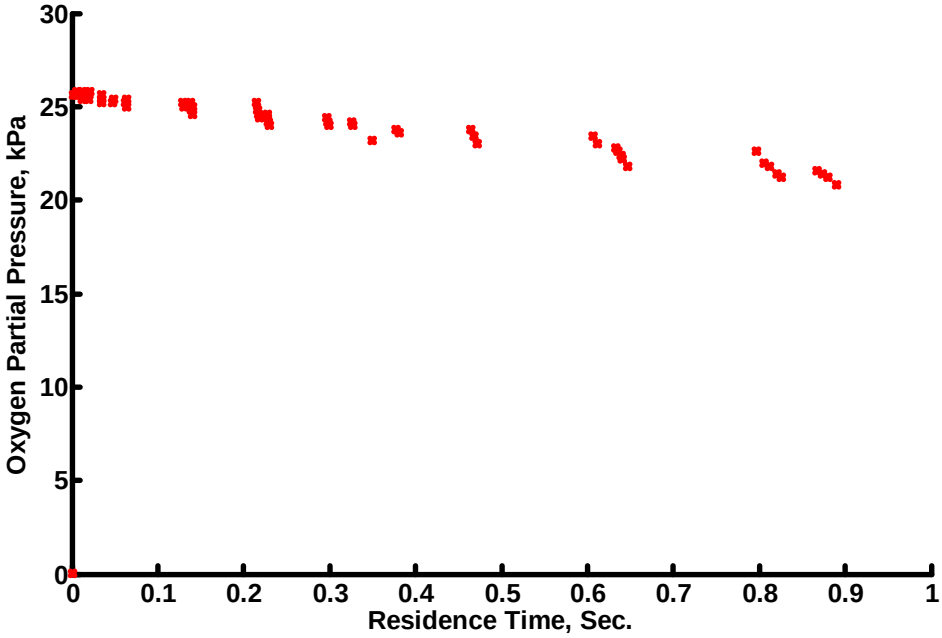


Figure 6.18. Enlarged section of Figure 6.17 - RCC oxygen control policy as a function of residence time for the maximum yield of butadiene from the ODH of *1*-butene

It is concluded that a DSR with a feed of *1*-butene and oxygen, the latter with an initial partial pressure of 25.5 kPa and which is supplemented along the length of the reactor in a prescribed manner can yield the maximum possible amount of butadiene, 0.9 carbon mass fraction, at a total residence time of 150 seconds. This residence time is significantly better that the 2.93 x 10^7 seconds previously noted (Milne *et al*, 2004).

We previously noted (Milne *et al*, 2004) that when the oxygen partial pressure is kept constant at 0.25 kPa in a DSR, the maximum yield of butadiene from the ODH of *1*-butene is 0.87 carbon mass fraction or 96 % of the theoretical maximum. This yield was associated with a residence time of 147 seconds. This result, we believe, has been confirmed by our RCC analysis.

6.5 Discussion of Results

The RCC method identified for each of the three cases reviewed in this paper a critical value for the oxygen partial pressure in the feed to the reactor. These critical partial pressures are shown in the following table.

Reaction	Partial Pressure of Oxygen in Feed to First Reactor
n-Butane - Butadiene	12 kPa
n-Butane - Butenes	15.5 kPa
1-Butene - Butadiene	25.5 kPa

Table 6.3. Critical oxygen partial pressures in feed stream to the DSR

An analysis of the results from the RCC method leads to the conclusion that the optimal feed oxygen partial pressures for the stipulated reactions with the objective of maximising the yield of product within the confines of the smallest possible reactor(s) are as shown in Table 6.3 above. We should like to confirm the justification for these critical oxygen partial pressures.

Harking back to our description of the RCC method earlier in this paper, we stated that one of its cardinal features is to scan the entire spectrum of values of the mixing variable α and the oxygen partial pressure for a specific thermodynamic state and to choose the maximum value necessary to extend the boundary of the region to its permissible limit. In the case of the initial value for the oxygen partial pressure, the RCC algorithm had to select the

conditions necessary to achieve the maximum instantaneous yield of product, either butenes or butadiene. This is equivalent to determining the oxygen partial pressures at which the initial rates of reaction for butenes and butadiene were maximised.

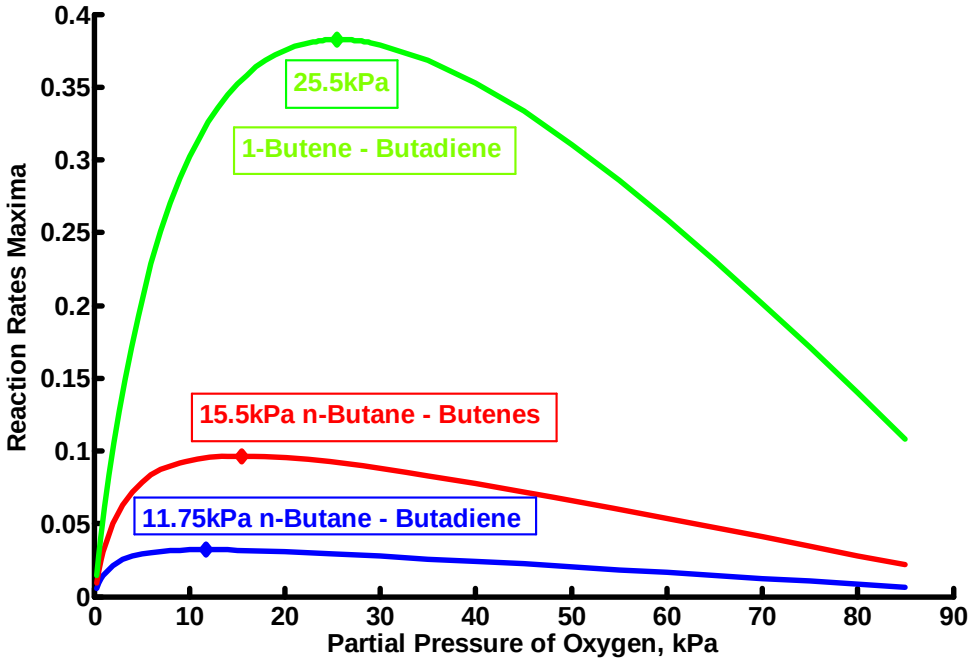


Figure 6.19. Initial rate of reaction maxima for production of butenes and butadiene as a function of oxygen partial pressure at feed conditions.

Figure 6.19 shows the maximum values for the initial rates of reaction for the production of butenes and butadiene as functions of oxygen partial pressure at the respective feed conditions. It can be seen that as the oxygen partial pressure in the feed is reduced from 85 kPa, the maximum values of the relevant reaction rates first increase. The oxygen partial pressures at which the relevant rates attain a maximum are indicated on the graph. These values confirm those derived from the RCC analysis in Table 6.3 with the modest exception of those for the ODH of *n*-butane to butadiene. This is encouraging evidence that the RCC algorithm is working as it was intended. In the case of the ODH of *n*-butane to butadiene the difference between the

two values of 11.75 kPa and 12 kPa is slight and in all probability a manifestation of the RCC method's lack of mathematical finesse in the presence of an essentially planar topography.

6.6 Conclusions

The Attainable Region analysis of the ODH of *n*-butane and *1*-butene has been undertaken using two tools, the simplistic method as reported in our earlier papers (Milne *et al*, 2004, Milne *et al*, 2006) and the more complex Recursive Convex Control (RCC) policy as developed by Seodigeng (Seodigeng, 2006, 2007). Whereas the simplistic approach depends upon a starting premise of a specific reactor configuration, the RCC policy does not and the optimal reactor configuration for attainment of the AR^C emerges from the latter as an output. The simplistic approach, as might be expected, has been found to be both easier to apply and to understand.

Convexification, i.e. the elimination of any concave surfaces, with the simplistic tool can be accomplished only in a two-dimensional projection of the multi-dimensional hypersurfaces. On the contrary, this convexification by the RCC policy occurs across all the multi-dimensional hypersurfaces. Candidate attainable regions (AR^Cs) developed by the RCC method agree with those previously identified (Milne *et al*, 2004, Milne *et al*, 2006).

The RCC method shows that for the ODH of *n*-butane to butenes and butadiene and for the ODH of *1*-butene to butadiene, a DSR possessing predefined control patterns for the addition of oxygen can yield the maximum amounts of hydrocarbon product at residence times of several

orders of magnitude lower than previously was reported (Milne *et al*, 2004, Milne *et al*, 2006).

The RCC method confirmed the maximum yields of hydrocarbon products previously reported (Milne *et al*, 2004, Milne *et al*, 2006). The RCC method confirmed the findings of these previous publications that with one exception very high percentages, in excess of 95 %, of the theoretical maximum yields of hydrocarbon products can be attained with residence times less than 150 seconds. The one exception is the ODH of *n*-butane to butadiene where 93 % of the theoretical maximum yield of butadiene can be achieved at a residence time of 1 000 seconds. For a residence time of 332 seconds, a yield of 83 % of the theoretical maximum is predicted. Because of the apparent planar surfaces generated for the ODH of *n*-butane to butadiene, the RCC method has difficulty in generating suitable convex surfaces.

The RCC concept has been shown in this paper to be a powerful tool for AR analyses and for determining the associated reactor configurations. Over and above this it has also been shown that the simplified methods used in the earlier papers (Milne *et al*, 2004, Milne *et al*, 2006) can also produce useful results particularly with respect to the maximum concentrations that can be achieved.

6.7 List of Symbols

6.7.1 Abbreviations

AR	Attainable Region
AR^C	Candidate Attainable Region
CSTR	Continuously Stirred Tank Reactor
DSR	Differential Side-Stream Reactor
IMR	Inert Membrane Reactor
ODH	Oxidative Dehydrogenation
PFR	Plug Flow Reactor
RCC	Recursive Convex Control Policy

6.7.2 Symbols

α	Control policy for combination of reaction and mixing
β	Control policy for addition of oxygen
$\boldsymbol{c}^0$	State variable of the system at the feed point
$\boldsymbol{c}^*$	Mixing state variable of the system
$\boldsymbol{c}$	State vector of all variables describing the system
$\boldsymbol{r}(c)$	Reaction rate vector defined at $\boldsymbol{c}$
τ	Residence time
$\boldsymbol{v}$	Mixing vector, $\boldsymbol{c}$ with $\boldsymbol{c}^*$

6.8 Literature Cited

Abraham, T.K., Feinberg, M., (2004), Kinetic bounds on attainability in the reactor synthesis problem, *Industrial and Engineering Chemistry Research*, vol. 43, pp. 449-457.

Burri, J.F., Wilson, S.D., Manousiouthakis, V. I., (2000), Infinite Dimensional State-space approach to reactor network synthesis: application to attainable region construction, *Computers and Chemical Engineering*, **26**, no. 6, pp. 849 – 862.

Feinberg, M. and Hildebrandt, D., (1997), Optimal reactor design from a geometric viewpoint – I. Universal properties of the attainable region, *Chemical Engineering Science*, vol. 52, no. 10, pp. 1637-1665.

Feinberg, M., (2000a), Optimal reactor design from a geometric viewpoint II: Critical side-stream reactors, *Chemical Engineering Science*, **55**, pp. 2455 – 2479.

Feinberg, M., (2000b), Optimal reactor design from a geometric viewpoint III: Critical CFSTRs, *Chemical Engineering Science*, **55**, pp. 3553 – 3565.

Glasser, D., Hildebrandt, D. and Crowe, C., (1987), A., Geometric Approach to Steady Flow Reactors: The Attainable Region and Optimisation in Concentration Space, *American Chemical Society*, pp. 1803-1810.

Kauchali, S., Rooney, W.C., Biegler, L.T., Glasser, D., Hildebrandt, D., (2002), Linear programming formulations for attainable region analysis, *Chemical Engineering Science*, **57** (11), pp. 2015-2228.

Manousiouthakis, V. I., Justanieah, A. M., Taylor, L. A., (2004), The Shrink-Wrap algorithm for the construction of the attainable region: an application of the IDEAS framework, *Computers and Chemical Engineering*, **28**, pp. 1563 – 1575.

Milne, D., Glasser, D., Hildebrandt, D., Hausberger, B., (2004), Application of the Attainable Region Concept to the Oxidative Dehydrogenation of *1*-Butene in Inert Porous Membrane Reactors, *Industrial and. Engineering Chemistry Research*, vol. 43, pp. 1827-1831 with corrections subsequently published in *Industrial and Engineering Chemistry Research*, vol. 43, p. 7208.

Milne, D., Glasser, D., Hildebrandt, D., Hausberger, B., (2006), The Oxidative Dehydrogenation of *n*-Butane in a Fixed Bed Reactor and in an Inert Porous Membrane Reactor - Maximising the Production of Butenes and Butadiene, *Industrial and Engineering Chemistry Research*, vol. 45, pp. 2661-2671.

Rooney, W.C., Hausberger, B.P., Biegler, L.T., Glasser, D., (2000), Convex attainable region projections for reactor network synthesis, *Computers and Chemical Engineering*, **24**, no. 2-7, pp. 225 – 229.

Seodigeng, T., Hausberger, B., Hildebrandt, D., Glasser, D., (2007), Recursive constant control policy algorithm for attainable region analysis, *Computers and Chemical Engineering,* (submitted for publication).

Seodigeng, T.G., Numerical formulations for attainable region analysis, (2006), Ph.D. thesis, University of the Witwatersrand, Johannesburg, South Africa.

Téllez, C., Menéndez, M., Santamaría, J., (1999a), Kinetic study of the oxidative dehydrogenation of butane on V/MgO Catalysts, *Journal of Catalysis*, vol. 183, pp. 210-221.

Téllez, C., Menéndez, M., Santamaría, J., (1999b), Simulation of an inert membrane reactor for the oxidative dehydrogenation of butane, *Chemical Engineering Science*, vol. 54, pp. 2917-2925.

Zhou Wen, Manousiouthakis, Vasilios I., (2006), Non-ideal reactor network synthesis through IDEAS: Attainable region construction, *Chemical Engineering Science*, **61**, pp. 6936-6945.

Zhou Wen, Manousiouthakis, Vasilios I., (2008), On dimensionality of Attainable Region Construction for Isothermal Reactor Networks, *Computers and Chemical Engineering,* vol. 32, 3, pp. 439-450.

Zhou, W., Manousiouthakis, V.I., (2007), Variable density fluid reactor network synthesis – construction of the attainable region through the IDEAS approach, *Chemical Engineering Journal*, vol. 129, pp. 91-103.

CHAPTER 7

Practical Implementation of Reactors for the Oxidative Dehydrogenation of *n*-Butane to Butadiene

---

7.1 Introduction

In Chapter 3, I investigated the oxidative dehydrogenation of *n*-butane (butane) to butadiene and identified a candidate Attainable Region (AR^C) for the system in the two-dimensional sub-space butane:butadiene. This candidate Attainable Region (AR^C) was bounded by the *x*-axis, the concentration of butane, the *y*-axis, the concentration of butadiene and a trajectory representing the butane:butadiene profile corresponding to an inert porous membrane reactor (IMR) of very high residence time and operating at a very low constant oxygen partial pressure. This paper did not consider whether additional and judicious combinations of IMRs with and without the addition of extra oxygen might result in comparable yields of butadiene at more preferable residence times. A kinetic model based on a V/MgO catalyst was used to simulate the performances of both reactors.

In this chapter I have considered the effect upon yields and residence times of operating a PFR with depleting oxygen in series with one or more IMRs with constant oxygen partial pressure. Several reactant by-pass and mixing strategies also were studied. The best yields of butadiene and the associated residence times from each reactor configuration are reported together with their ranking in terms of the theoretical maximum butadiene yield.

The reaction network for the ODH of butane was shown in Figure 1.2 and is repeated in Figure 7.1 below.

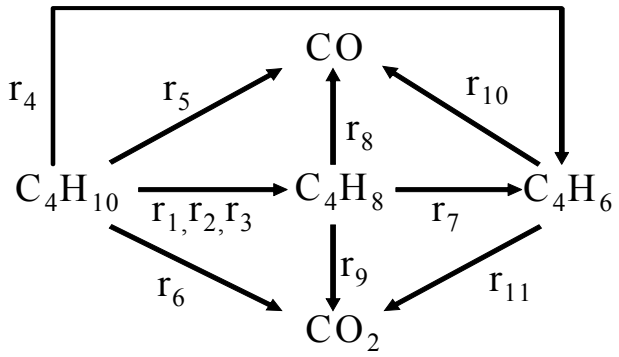


Figure 7.1. Reaction mechanism for the oxidative dehydrogenation of *n*-butane to butene and butadiene.

Kinetic data for the system butane:butadiene were derived from Téllez *et al.* (1999a, 1999b) and from Assabumrungrat *et al*. (2002).

As was explained in Chapter 1, all concentrations and yields are expressed in terms of mass fractions of carbon.

In this thesis I have used the two acronyms FBR (fixed bed reactor) and PFR (plug flow reactor) to describe a reactor in which the initial oxygen partial pressure is permitted to wane in accordance with the ODH process. In this chapter, the acronym PFR is used.

7.2 Two Reactors in Series

In Chapter 3, I examined two reactor configurations with different operating characteristics, a PFR in which the initial feed of oxygen is depleted and the second, an IMR, where fresh oxygen is added along the length of the reactor to maintain the oxygen partial pressure in the catalyst bed at a constant value. The highest theoretical yield of butadiene, 0.800 carbon mass fraction, was possible using an IMR of very large residence time and operating under a very low constant oxygen partial pressure. This configuration represented an impractical scenario. However, a constant oxygen partial pressure of 0.25 kPa in an IMR with a residence time of 322 seconds produced a butadiene yield of 0.665 carbon mass fraction which was 83 % of the theoretical maximum.

The butane:butadiene concentration profiles for a PFR were shown in Figure 3.6 and are repeated in Figure 7.2.

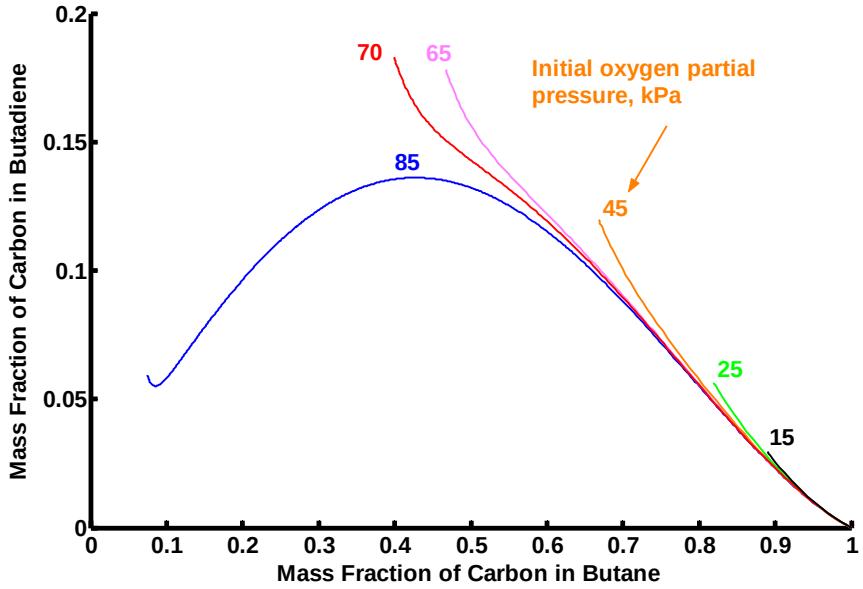


Figure 7.2. Profiles of butane and butadiene at oxygen partial pressures of 15, 25, 45, 65, 70 and 85 kPa in an isothermal PFR with depleting oxygen.

The theoretical maximum yield of butadiene of 0.800 carbon mass fraction provides a target for evaluating alternative reactor configurations with the purpose of assessing the practicality of such configurations combined with economic considerations, specifically residence time.

I now intend to study the yields of butadiene and associated residence times from a combination of a PFR without the injection of additional oxygen in series with an IMR with the injection of additional oxygen under different operating conditions. Specifically, I shall study reactor systems incorporating the by-pass and mixing of reactants and products.

The maximum butadiene yields and associated data from a PFR without the injection of additional oxygen are shown in Table 7.1. This data was compiled from an analysis of Figure 7.2.

Oxygen Partial Pressure	Maximum Butadiene Yield	Associated Butane Value	Butane Selectivity	Residence Time, Seconds
87 kPa	0.135	0.430	0.237	55
85 kPa	0.136	0.428	0.238	49
70 kPa	0.183	0.399	0.304	41
65 kPa	0.178	0.467	0.334	31
50 kPa	0.136	0.625	0.363	17
45 kPa	0.120	0.668	0.361	14
25 kPa	0.056	0.820	0.312	8
15 kPa	0.030	0.889	0.269	6

Table 7.1. Maximum butadiene yields and residence times from a PFR with depleting oxygen at various oxygen inlet partial pressures.

At an initial oxygen partial pressure of 87 kPa in a PFR in which the initial oxygen concentration was permitted to wane through the normal ODH process, there was no residual butane at equilibrium. Below this partial pressure there was no residual oxygen, i.e. not all the butane was oxidised.

A characteristic of all the butane:butadiene profiles shown in Figure 7.2 is the presence of a concave region between the feed point and the maximum point of the profile. The significance of such a concave region is that it can be removed and transformed into a non-concave region through a process of by-pass and mixing and, in so doing, extend the previous profile further thus creating a new enlarged area beneath the profile.

The maximum yield of butadiene from this PFR was associated with an initial oxygen partial pressure of 70 kPa.

Butadiene yields from an IMR (Figure 3.18) operating at a constant oxygen partial pressure are shown in Figure 7.3 and Table 7.2.

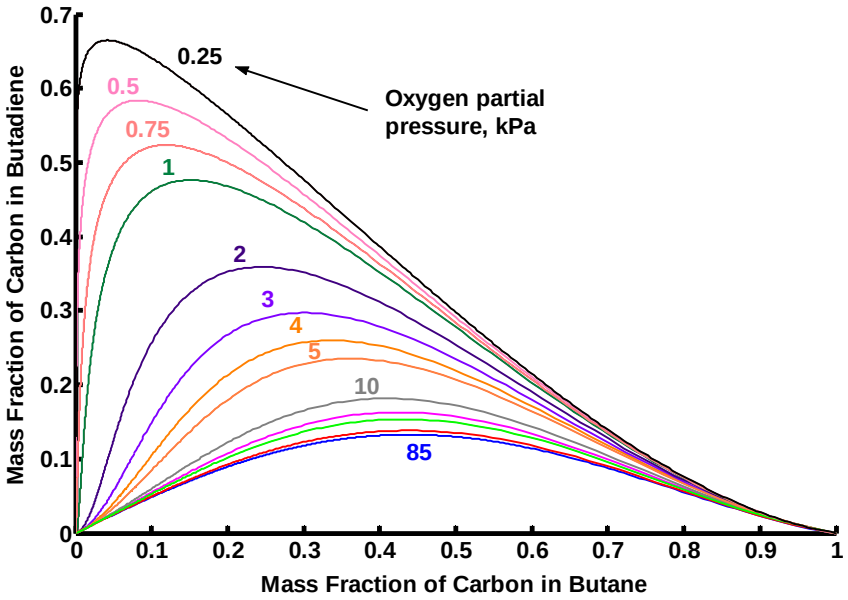


Figure 7.3. Profiles of butane and butadiene at constant oxygen partial pressures from 85 kPa to 0.25 kPa in an isothermal IMR with constant oxygen partial pressure.

Oxygen Partial Pressure	Maximum Butadiene Yield	Associated Butane Value	Butane Selectivity	Residence Time, Seconds
85 kPa	0.133	0.438	0.236	108
70 kPa	0.134	0.439	0.239	56
65 kPa	0.135	0.437	0.239	49
45 kPa	0.138	0.436	0.245	32
25 kPa	0.148	0.437	0.263	24
15 kPa	0.163	0.426	0.284	23
10 kPa	0.182	0.411	0.308	24
5 kPa	0.235	0.360	0.368	31
1 kPa	0.476	0.150	0.561	103

Oxygen Partial Pressure	Maximum Butadiene Yield	Associated Butane Value	Butane Selectivity	Residence Time, Seconds
0.70 kPa	0.534	0.112	0.602	138
0.25 kPa	0.665	0.042	0.694	322

Table 7.2. Maximum butadiene yields and residence times from an IMR at various constant oxygen inlet partial pressures.

A characteristic of all the butane:butadiene profiles shown in Figure 7.3 is the presence of a concave region between the feed point and the maximum point of the profile.

It is worth while to examine the butane:butadiene profile from a PFR operating at an initial oxygen partial pressure of 70 kPa and in which the oxygen supply is depleted through the normal ODH process, as is shown in Figure 7.4.

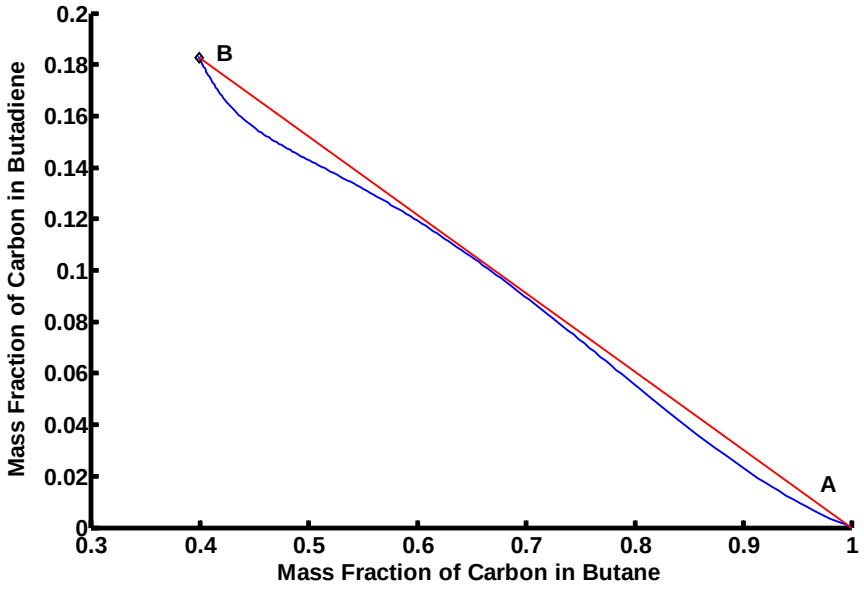


Figure 7.4. Butane:butadiene profile for a PFR operating at an initial and reducing oxygen partial pressure of 70 kPa.

It will be noted that there are two pronounced concave sections in the profile shown in Figure 7.4 and that the entire butane:butadiene profile lies under the line AB. Milne *et al.* (2004) have shown that over this section of the profile higher yields of butadiene can be achieved through a policy of by-pass and mixing and that the locus of all butadiene yields under such a policy is represented by the line from feed point, Point A, to the PFR profile at Point B. An example of the PFR configuration to implement this operating policy is shown in Figure 7.5.

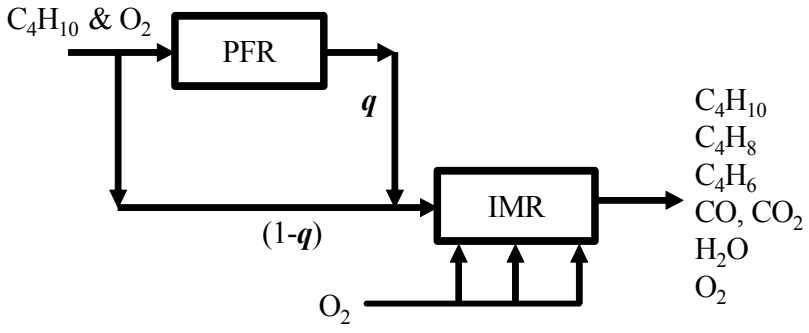


Figure 7.5. A PFR and an IMR in series configuration incorporating by-pass and mixing.

Consequently, this reactor configuration was used as the basis for examining the relationship between butadiene yields and residence time.

Point B in Figure 7.4 represented the best yield of butadiene commensurate with the (effective) total depletion of the oxygen. This yield was 0.183 carbon mass fraction of butadiene at a residual butane amount of 0.399 carbon mass fraction. This yield of butadiene was achieved after a residence time of 41 seconds (Table 7.1). Point B represents the yields of butadiene and butane after a residence time of 41 seconds and Point A represents feed of butane to the reactor, i.e. at a residence time of 0 seconds.

Consider a PFR and an IMR in series as shown in Figure 7.5. In the first reactor, the initial oxygen partial pressure shall be reduced through the normal ODH reactions. Upon completion of the ODH process, the remaining reactants and products are removed, mixed with a fresh feed of butane (and oxygen) in a fixed ratio, q, and this combined stream passed as feed to the second reactor in which the oxygen partial pressure shall be kept constant at its initial value i.e. its value in the mixed streams entering the IMR.

In Chapter 3 it was seen that a higher yield of butadiene is possible when the IMR operates under conditions of a constant low partial pressure of oxygen than when the normal depletion of oxygen takes place.

Referring to Figure 7.5, the initial oxygen partial pressure in the feed stream to the PFR was 70 kPa. Maximum yield of butadiene was obtained after a

residence time of 41 seconds with the total depletion of the oxygen. Consequently, the PFR was sized so that its exit stream (and part feed to the IMR) contains a butadiene concentration of 0.183 carbon mass fraction. The partial pressure of oxygen in the exit stream from the PFR is to all intents and purposes zero. In addition, a fresh feed of butane (carbon mass fraction 1.0) containing oxygen at a partial pressure of 70 kPa was mixed with this stream in various proportions to "fill in" the concave region shown in Figure 7.4.

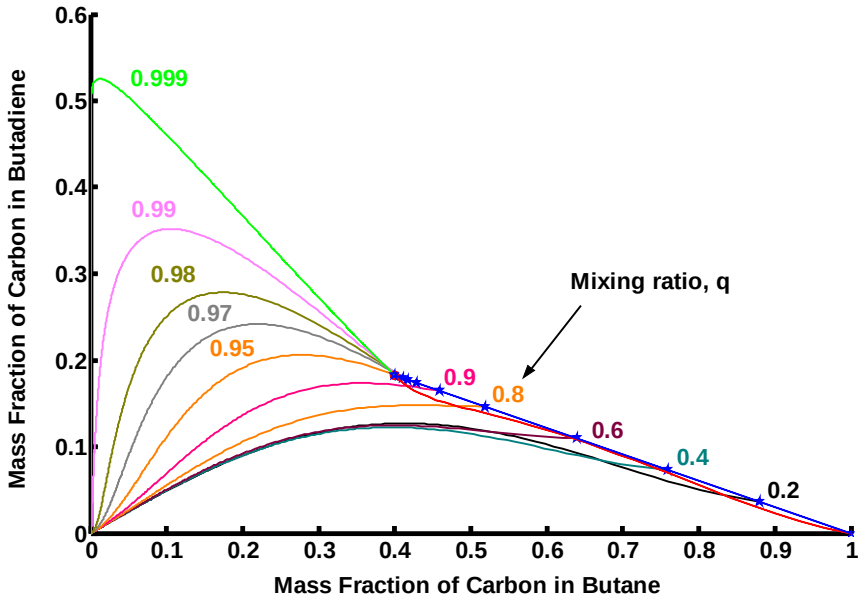


Figure 7.6. A PFR and an IMR in series. Butane:butadiene concentration profiles for various values of mixing ratio, *q*.

Figure 7.6 shows the several butane:butadiene profiles from an IMR operating at a constant oxygen partial pressure, a function of the mixing ratio *q*, and where the feed is a mixed feed made up from the product from the PFR mixed with a fresh-stream of butane and oxygen, the latter at a partial pressure of 70 kPa and mixed in various proportions, *q*. A *q* value of unity corresponds to no mixing, i.e. no fresh feed, with the output from the

PFR being supplied to the IMR. A *q* value of zero corresponds to bypassing the PFR completely and feeding butane and oxygen to the IMR.

The salient information from Figure 7.6 is presented in Table 7.3.

Mixing Ratio, *q*	**Maximum Butadiene Yield**	**Associated Butane Value**	**Residence Time, Seconds**	**Oxygen Partial Pressure, kPa**
1.00	0.254	0.321	10 000	4.8×10^{-4}
0.999	0.526	0.012	676	0.06
0.99	0.352	0.105	144	0.55
0.98	0.278	0.173	96	1.11
0.97	0.242	0.219	78	1.66
0.95	0.206	0.279	63	2.78
0.90	0.173	0.359	52	5.63
0.80	0.148	0.436	48	11.51
0.60	0.125	0.403	61	24.09
0.40	0.122	0.396	72	37.90
0.20	0.127	0.411	82	53.12
0	0.134	0.439	56	70.00

Table 7.3. Effect of mixing ratio, *q*, upon the maximum yield of butadiene and the associated residence time.

In Table 7.3, the values shown for butane are those corresponding to the maximum yields of butadiene from the IMR. The residence times are the combined residence times of the PFR and the IMR necessary to attain the maximum yield of butadiene. The oxygen partial pressure for each value of *q* is the partial pressure of oxygen in the combined feed to the IMR.

At a mixing ratio of 1.0, the maximum yield of butadiene, 0.254, was achieved after a residence time of 10 000 seconds. The oxygen partial pressure in the feed to the IMR was extremely low (4.8×10^{-4} kPa) and it was not considered practical to investigate larger residence times in an attempt to determine a greater butadiene yield. In Figure 7.6, the profile for a q value of zero has been omitted as it corresponds to feeding a mixture of butane and oxygen, the latter at a partial pressure of 70 kPa directly to an IMR, the yields being those shown in Table 7.2

It is noteworthy that higher yields of butadiene are associated with higher values of the mixing ratio, q, because higher values of q result in lower oxygen partial pressures. In addition, if a tangent is drawn from the fresh butane feed point (mass fraction 1.0) to the profiles for q values greater than 0.95 a pronounced concavity is evident. This mixing line could be used through an appropriate by-pass and mixing strategy to establish new feed streams for a third reactor. Equally, for q values less than 0.8, a tangent drawn from the mixing feed point to the profile encloses a concave region which through a process of by-pass and mixing could be employed to establish new feed streams apart from obtaining higher butadiene yields.

The apparent strangeness of Figure 7.6 above in as much as it portrays an extraordinary improvement in selectivity from the second series reactor, an IMR, is not as unexpected as might otherwise appear. I refer to the case where only a smidgen of the original feed is supplied to the second reactor, i.e. a value for the mixing ratio, q, of 0.999. As a consequence of this mixing, the effective oxygen partial pressure in the feed to the IMR is 0.06 kPa (Table 7.3).

The adjective extraordinary is a relative one in as much as the profile for a q value of 0.999 is perceived to be at odds with a similar profile for another value of q. It also suggests an element of surprise or unexpectedness. To explain this paradox, I shall take as my datum profile that which corresponds to a q value of 0.9 and shed some light on why there is such a pronounced difference between the two butane-butadiene profiles.

For q values of 0.9 and 0.999, the composition of the feeds (carbon mass fraction) and the oxygen partial pressures (kPa) to the IMR are

q	C_4H_{10}	C_4H_8	C_4H_6	CO	CO_2	pO_2
0.9	0.4592	0.0772	0.1645	0.0681	0.2310	5.63 kPa
0.999	0.3997	0.0857	0.1826	0.0756	0.2564	0.06 kPa

Table 7.4. Composition of feed stream to the second series reactor for different values of the mixing ratio, q.

In Table 7.4, all three isomers of butene have been included in the totals for C_4H_6. Oxygen partial pressures were taken from Table 7.3.

When q is 0.9, the maximum yield of butadiene from the IMR is 0.1734 carbon mass fraction (Table 7.3). For a q value of 0.999, the maximum yield of butadiene from the IMR is 0.526 carbon mass fraction. This represents a three-fold increase in the maximum yield of butadiene. The question is whether such an increase is ordinary or extraordinary ?

To resolve this issue in the simplest manner, let us consider the partial pressure of oxygen in the feed streams to the IMR for the two values of q, 0.06 kPa and 5.63 kPa respectively (Table 7.3).

We have shown (Table 7.2) that in an IMR where the oxygen partial pressure is kept at a low constant value, high yields of butadiene are possible from the ODH of butane. In Table 7.5 below, we show the same information as in Table 7.2 but for the oxygen partial pressures associated with mixing ratios of 0.9 and 0.999.

q	**Oxygen Partial Pressure**	**Maximum Butadiene Yield**	**Associated Butane Value**	**Butane Selectivity**	**Residence Time, Seconds**
0.9	5.62 kPa	0.224	0.373	0.357	29
0.999	0.056 kPa	0.757	0.009	0.764	1 172

Table 7.5. Maximum butadiene yields and residence times from an IMR at different constant oxygen inlet partial pressures. Feed stream of butane and oxygen only.

From Table 7.5, the ratio of the maximum yield of butadiene at a *q* value of 0.999 to that at a value of 0.9 is 3.4. With some reservations, we conclude that the different profiles of Figure 7.6 do not represent an extraordinary or an unexpected situation but that a three-fold increase in yields of butadiene can be expected when the oxygen partial pressure is reduced from 5.63 kPa to 0.06 kPa and that this increase follows from the mathematical attributes of the kinetic data.

The reservations referred to in the previous paragraph are that the data in Table 7.5 relate to an IMR where the feed is only butane and oxygen, the latter at the listed partial pressures. In Figure 7.6, the feeds to the second series reactor, despite the same oxygen partial pressures as in Table 7.5, contain, as well as butane, butenes, butadiene, carbon monoxide, carbon

dioxide and water, the presence of these compounds resulting in lower partial pressures of butane than those associated with Table 7.5.

7.2.1 Reduction of Oxygen Partial Pressure in Feed to Second Reactor

Consider now the effect of reducing the oxygen partial pressure in the (mixed) feed to the IMR. We shall reduce the oxygen partial pressure by 99 % to 1 % of its value in the mixed feed and explore the effects of various mixing ratios upon the yield of butadiene and required reactor residence time. A reduction of 99 % was adopted in recognition of our earlier findings that maximum yields from an IMR were achievable when the oxygen partial pressure was very small.

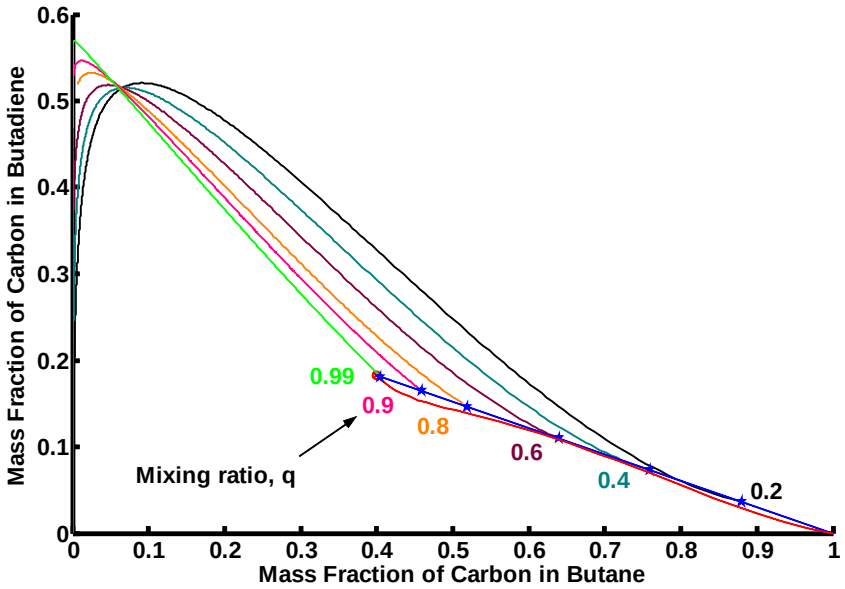


Figure 7.7. A PFR and an IMR in series. Butane:butadiene concentration profiles. Oxygen partial pressure in feed to the IMR 1% of that in mixed output stream from the PFR.

The salient information from Figure 7.7 is presented in Table 7.6.

Mixing Ratio, *q*	**Maximum Butadiene Yield**	**Associated Butane Value**	**Residence Time, Seconds**	**Oxygen Partial Pressure, kPa**
1.00	0.184	0.398	10 000	4.8×10^{-6}
0.999	0.266	0.309	10 000	5.5×10^{-4}
0.99	0.570	0.001	5 021	5.5×10^{-3}
0.98	0.566	0.002	2 670	1.1×10^{-2}
0.97	0.563	0.004	1 876	1.7×10^{-2}
0.95	0.557	0.006	1 230	2.8×10^{-2}
0.90	0.547	0.012	728	5.6×10^{-2}
0.80	0.533	0.023	459	0.12
0.60	0.519	0.047	305	0.24
0.40	0.515	0.070	243	0.38
0.20	0.521	0.091	206	0.53
0	0.534	0.112	138	0.70

Table 7.6. Effect of mixing ratio, *q*, upon the maximum yield of butadiene and the associated residence time where the oxygen partial pressure in the feed is reduced by 99 %.

The oxygen partial pressures in Table 7.6 are those partial pressures in the mixed stream to the IMR. At a mixing ratio of 1.0, the maximum yield of butane, 0.184, was achieved after the ODH reaction was interrupted after a residence time of 10 000 seconds. The oxygen partial pressure in the feed to the IMR was extremely low, 4.8×10^{-6} kPa, and it was not considered practical to investigate a larger residence time in an attempt to determine a greater butadiene yield. A similar argument applies to the mixing value of 0.999 where the oxygen partial pressure in the IMR was 5.5×10^{-4} kPa.

Examination of Figure 7.7 shows that all the profiles exhibit concavities relative to their respective mixing feed points and, most noticeably, with respect to the fresh butane feed point to the PFR (butane mass fraction of unity). The most pronounced concavity resulting from the series configuration of the PFR and the IMR is associated with a q value of 0.2. The significance of this most pronounced concavity is that, through a policy of by-pass and mixing, it would be possible to extend the whole region the furthermost and thus the boundary of a candidate Attainable Region (AR^C). Because we wish to investigate the effect of a PFR and an IMR in series in establishing a candidate Attainable Region (AR^C), we shall draw the tangent, i.e. a by-pass mixing line, from the feed point to the butane:butadiene profile corresponding to a q value of 0.2. This line will be used through an appropriate by-pass and mixing strategy to establish new feed streams for a third reactor.

7.3 Three Reactors in Series

Figure 7.8 shows the mixing line, AB, from the fresh feed point (butane mass fraction 1.0) to the profile corresponding to a mixing ratio, q, of 0.2. Point B corresponds to a residence time of 119 seconds from the start of the reaction in the IMR.

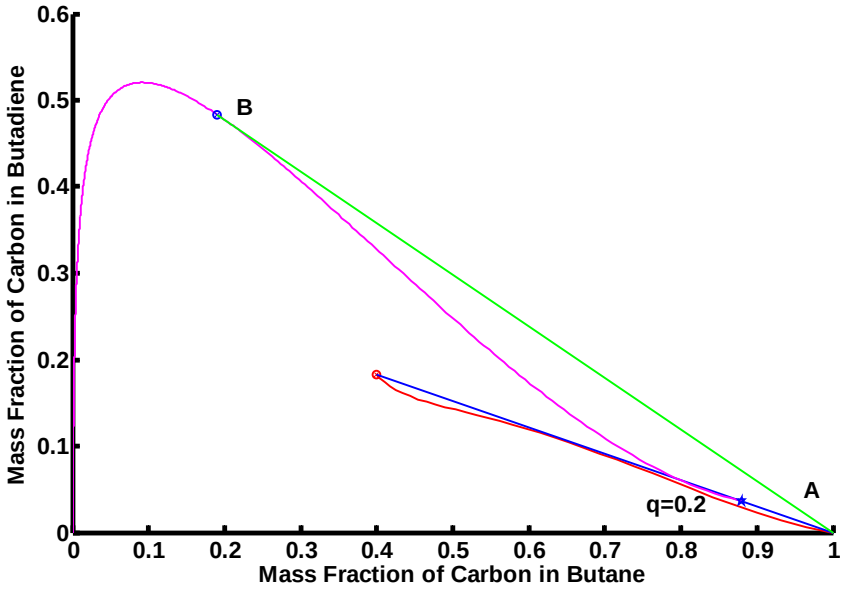


Figure 7.8. A PFR and an IMR in series. Butane:butadiene concentration profile for a mixing ratio of 0.2 and mixing line AB from fresh butane feed point.

The reactor configuration incorporating a second IMR is shown in Figure 7.9.

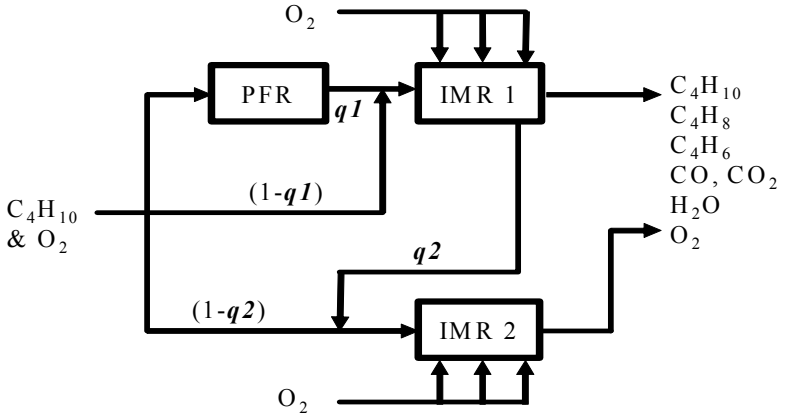


Figure 7.9. A PFR followed by two IMRs in series configuration incorporating by-pass and mixing.

In Figure 7.9, the mixing ratio, *q1*, of PFR products and fresh feed to IMR1 has the value 0.2.

The operating strategy is to feed butane and oxygen to the PFR and stop the reaction after 41 seconds. The remaining reactants and products are mixed with fresh butane and oxygen in a 20:80 ratio (*q1* = 0.2) and fed to IMR1. The reaction in IMR1 will be interrupted after 119 seconds, mixed with fresh butane and oxygen (partial pressure of the latter 70 kPa) in various ratios and supplied to the second IMR. The maximum butadiene yields from this second IMR shall be studied.

If we take the side stream at Point A (butane and oxygen, the latter at a partial pressure of 70 kPa) and feed it alone (i.e. *q2*=0) to IMR2, the maximum butadiene yield and residual butane are 0.134 and 0.439 respectively after a total residence time of 56 seconds (Table 7.2). This is tantamount to eliminating the PFR and IMR1 completely.

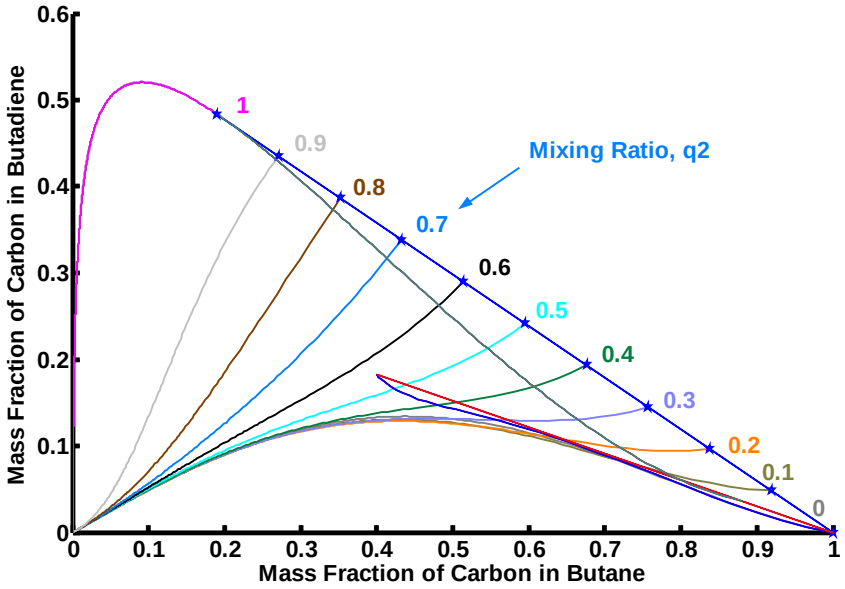


Figure 7.10. A PFR followed by two IMRs in series configuration. Butane:butadiene concentration profiles.

Figure 7.10 shows the various butane:butadiene concentration profiles when the oxygen partial pressure in the feed to IMR2 is kept constant at its value in the mixed stream from the PFR and to IMR1.

Table 7.7 shows the salient information of Figure 7.10.

Mixing Ratio, *q2*	**Maximum Butadiene Yield**	**Associated Butane Value**	**Residence Time, Seconds**	**Oxygen Partial Pressure, kPa**
1.00	0.521	0.091	207	0.53
0.90	0.435	0.271	148	5.93
0.80	0.387	0.352	136	11.61
0.70	0.339	0.433	124	17.58
0.60	0.290	0.514	112	23.87
0.50	0.242	0.595	101	30.50

Mixing Ratio, *q2*	**Maximum Butadiene Yield**	**Associated Butane Value**	**Residence Time, Seconds**	**Oxygen Partial Pressure, kPa**
0.40	0.193	0.676	89	37.51
0.30	0.145	0.757	77	44.93
0.20	0.129	0.432	100	52.79
0.10	0.131	0.430	98	61.13
0	0.134	0.439	56	70.00

Table 7.7. Effect of mixing ratio, *q2*, upon the maximum yield of butadiene and the associated residence time for a PFR followed by two IMRs in series.

In Table 7.7 the value for butane is that corresponding to the maximum yield of butadiene from IMR2. The residence time is the combined residence times of the PFR, IMR1 and IMR2 necessary to attain the maximum yield of butadiene. The oxygen partial pressure is the partial pressure of oxygen in the combined feed to IMR2.

A *q2* value of 0 is the same as feeding a mixture of butane and oxygen, the latter at a partial pressure of 70 kPa directly into IMR2 by-passing PFR and IMR1. The maximum butadiene yield and residence time consequently are as was shown in Table 7.2.

A *q2* value of 1.0 is the same as interrupting the reaction in IMR1 after 119 seconds and feeding the mixture of reactants and products into another IMR, in effect permitting the reaction to continue. The resulting concentration profile is the same as is shown in Figure 7.8 for a PFR and an IMR in series and the maximum yield of butadiene and the residence time for this maximum yield are as shown in Table 7.6 for a *q1* value of 0.2.

A breakdown of the individual reactor residence times is given in Table 7.8. The residence times for the second IMR, IMR2, are those necessary to attain the maximum yield of butadiene.

Mixing Ratio, *q2*	**Residence Time, Seconds**			
	PFR	**IMR1**	**IMR2**	**Total**
1.00	41	119	47	207
0.90	41	107	0	148
0.80	41	95	0	136
0.70	41	83	0	124
0.60	41	71	0	112
0.50	41	60	0	101
0.40	41	48	0	89
0.30	41	36	0	77
0.20	41	24	35	100
0.10	41	12	45	98
0	0	0	56	56

Table 7.8. Individual reactor residence times for values of mixing ratio, *q2*. Value of mixing ratio, *q1*, 0.2. Oxygen partial pressure in feed to IMR1 is 1 % of that in off-take from PFR.

Examination of Figure 7.10 shows that for mixing values of *q2* of 0.3 and greater there is no increase in butadiene yield above the initial feed concentration. This is because for these values of *q2* the ratio of the sum of rates of formation of carbon monoxide, carbon dioxide and water to the rate of formation of butadiene is both less than unity and negative over the full spectrum of butane concentrations. The negativity stems from the fact that the rate of formation of butadiene never attains a positive value indicating a continuous and sustained depletion of this hydrocarbon.

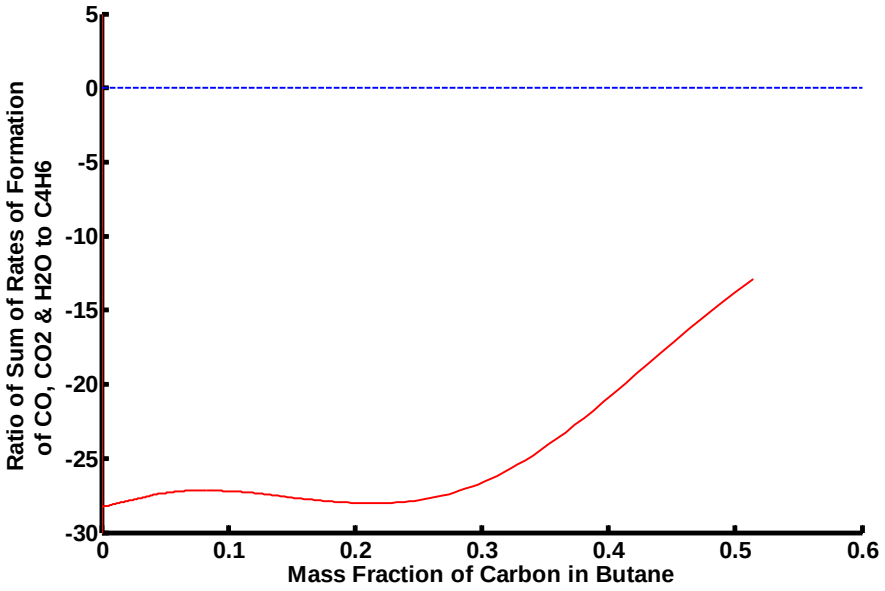


Figure 7.11. Ratio of sum of rates of formation of carbon monoxide, carbon dioxide and water to the rate of formation of butadiene. An analysis of Figure 7.10 for a value of *q2* of 0.6.

Figure 7.11 shows this ratio for a *q2* value of 0.6. The horizontal broken line in Figure 7.11 corresponds to a value of nought on the vertical ordinate. Above this line, the combined rates of formation of carbon monoxide, carbon dioxide and water are both positive and greater than that for butadiene. Below this line, the converse is true. However, Figure 7.11 shows that the ratio is negative over the full spectrum of butane concentrations. As the rates of formation of carbon monoxide, carbon dioxide and water individually are both monotonic and rising, the interpretation of this negative ratio is that the rate of formation of butadiene must be negative meaning that the butadiene is continually depleted. This manifestation is shown in Figure 7.12 below.

Figure 7.11 clearly shows the preferential conversion of butane to carbon monoxide, carbon dioxide and water for a *q2* value of 0.6. In Figure 7.12

below the actual rate of formation of butadiene is seen to be negative over the entire range of butane values. The horizontal broken line corresponds to a value of nought on the vertical ordinate.

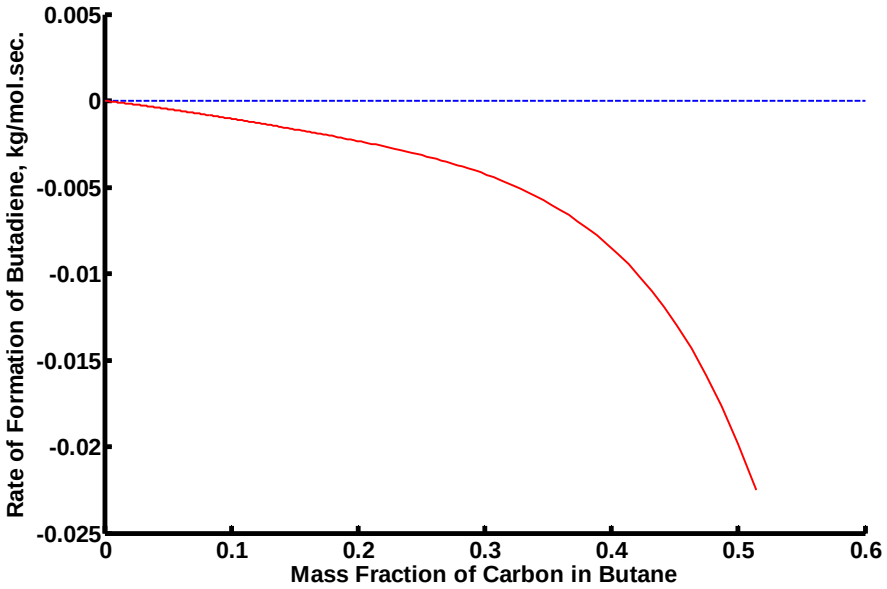


Figure 7.12. Rate of formation of butadiene for a value of *q2* of 0.6.

As a comparison, Figure 7.13 shows the ratio of the rates of formation of carbon monoxide, carbon dioxide and water to butadiene for a *q2* value of 0.2.

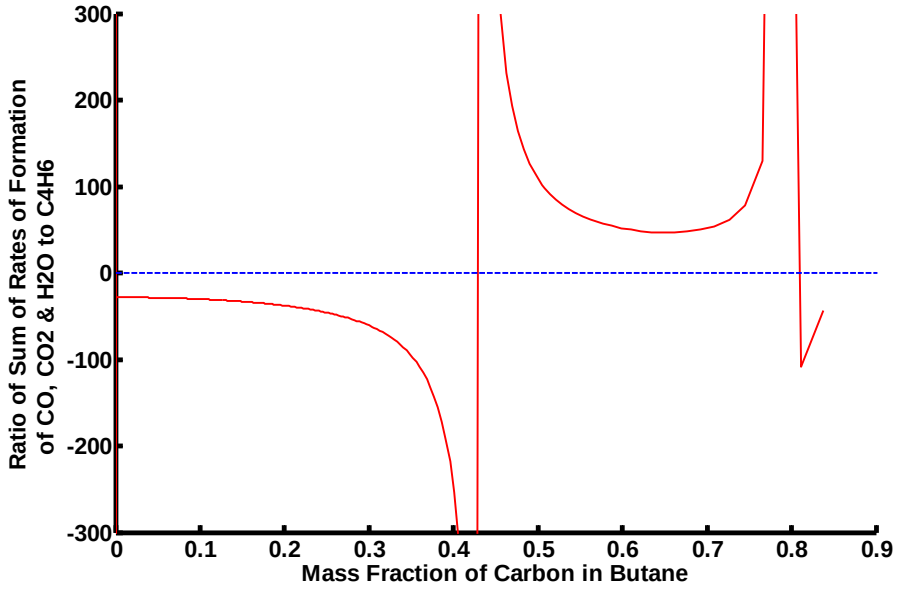


Figure 7.13. Ratio of sum of rates of formation of carbon monoxide, carbon dioxide and water to the rate of formation of butadiene. An analysis of Figure 7.10 for a value of *q2* of 0.2.

The horizontal broken line in Figure 7.13 corresponds to a value of nought on the vertical ordinate, the boundary below which is the region where the ratio of the combined rates of reaction for carbon monoxide, carbon dioxide and water to the reaction rate of butadiene is negative and above which it is positive. As was stated previously, because the individual rates of reaction of carbon monoxide, carbon dioxide and water are both monotonic and rising, the interpretation of Figure 7.13 is that initially, butadiene is being depleted until the butane concentration has been reduced to 0.79. At this asymptotic point the ratio becomes positive and the butadiene concentration begins to increase. The maximum butadiene concentration occurs at a butane value of 0.43 (see Figure 7.10), the second asymptote. Thereafter, the butadiene concentration wanes and ultimately is completely oxidised to carbon monoxide, carbon dioxide and water.

In Figure 7.14 below, the rate of formation of butadiene for a *q2* value of 0.2 is plotted as a function of butane concentration. Initially it is negative. Between butane values of 0.79 and 0.43, the rate of formation is positive and below values of 0.43, it again becomes negative.

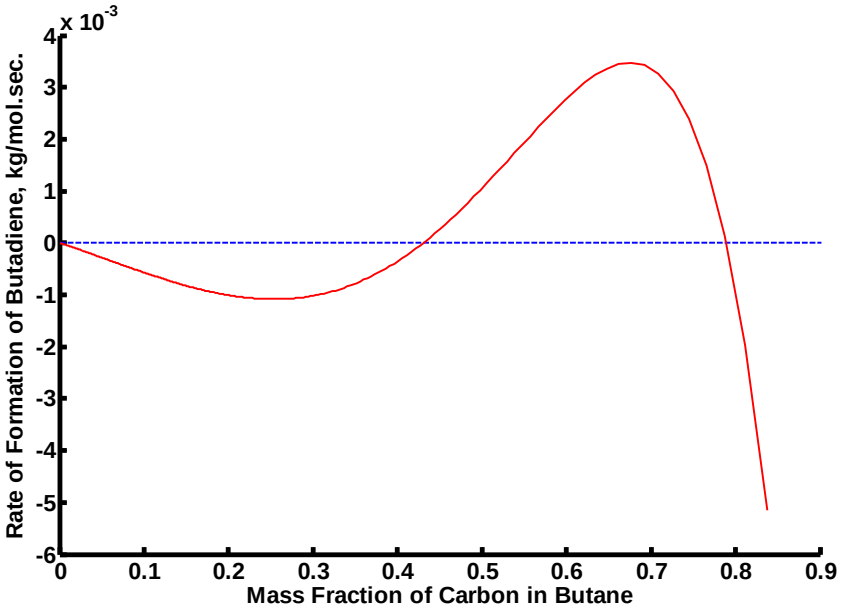


Figure 7.14. Rate of formation of butadiene for a value of *q2* of 0.2.

Figure 7.15 shows the effect on butadiene yields and residence times when the oxygen partial pressure in the feed to IMR2 is reduced to 1 % of its value in the combined stream from IMR1 and the feed to the PFR.

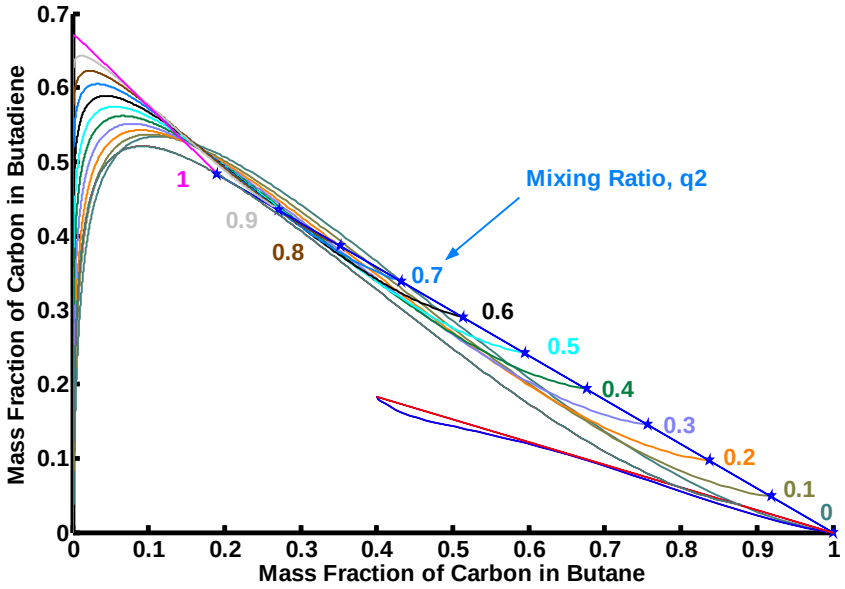


Figure 7.15. A PFR followed by two IMRs in series. Butane:butadiene concentration profiles. Oxygen partial pressure in feed to IMR2 1% of that in mixed stream from IMR1 and feed to the PFR.

Table 7.9 shows the salient information of Figure 7.15.

Mixing Ratio, *q2*	**Maximum Butadiene Yield**	**Associated Butane Value**	**Residence Time, Seconds**	**Oxygen Partial Pressure, kPa**
1.00	0.670	0.001	2 760	5.3×10^{-3}
0.90	0.643	0.011	577	5.9×10^{-2}
0.80	0.623	0.022	440	0.12
0.70	0.605	0.032	377	0.18
0.60	0.589	0.043	335	0.24
0.50	0.575	0.055	303	0.31
0.40	0.562	0.067	274	0.38
0.30	0.551	0.077	249	0.45
0.20	0.543	0.089	225	0.53
0.10	0.537	0.100	202	0.61

Mixing Ratio, *q2*	**Maximum Butadiene Yield**	**Associated Butane Value**	**Residence Time, Seconds**	**Oxygen Partial Pressure, kPa**
0	0.534	0.112	138	0.70

Table 7.9. Effect of mixing ratio, *q2*, upon the maximum yield of butadiene and the associated residence time for a PFR followed by two IMRs in series.

In Table 7.9 the oxygen partial pressure shown in the fifth column is that in the feed to IMR2 and is 1% of that in mixed stream from IMR1 and fresh feed to the PFR.

The *q2* value of 0 shown in Table 7.9 is the same as feeding a mixture of butane and oxygen, the latter at a partial pressure of 0.7 kPa directly into IMR2 by-passing PFR and IMR1. The maximum butadiene yield and residence time consequently are as was shown in Table 7.2.

The *q2* value of 1.0 shown in Table 7.9 is the same as interrupting the reaction in IMR1 after 119 seconds and feeding the mixture of reactants and products into another IMR but with the partial pressure of oxygen in the stream reduced by 99 %. The maximum yield of butadiene of 0.670 has been achieved from an initial feed of butane with a carbon mass fraction of unity to a PFR with an oxygen partial pressure of 70 kPa. Refer to Figure 7.16 for a geometrical delineation of this reactor configuration.

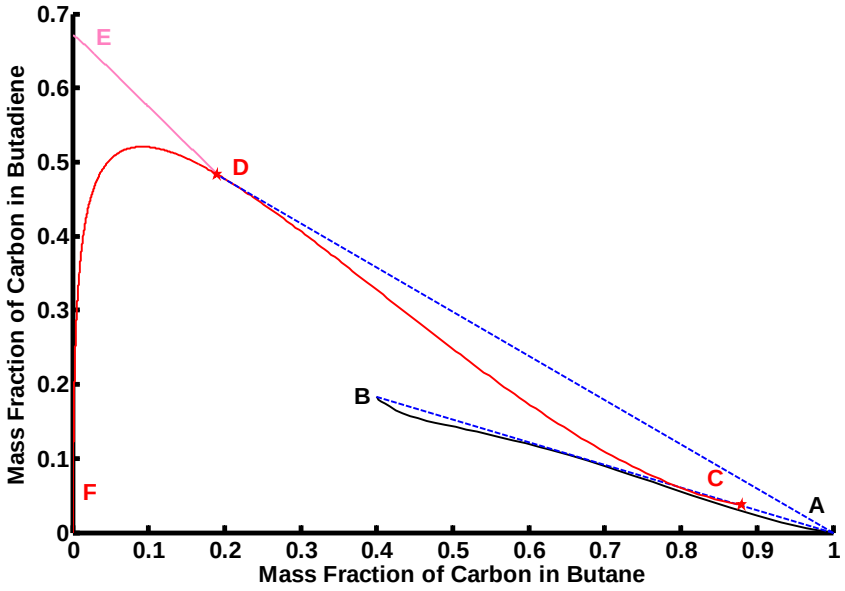


Figure 7.16. A PFR followed by two IMRs in series. Butane:butadiene concentration profiles. Values of *q1* and *q2* are 0.2 and 1.0 respectively.

In Figure 7.16, AB represents the butane-butadiene profile from the FBR. The dashed line AB is the locus of all butane-butadiene concentrations resulting from taking feed from the FBR after a residence time of 41 seconds and mixing this with fresh butane. This line also removes the concave sections of the FBR profile.

7.3.1 Reduction of Oxygen Partial Pressure in Feed to Third Reactor

Point C in Figure 7.16 gives the butane-butadiene concentrations for a *q1* value of 0.2, i.e. a mixture of fresh butane and feed from the PFR in the ratio of 0.2:0.8. These concentrations (and other products with residual reactants) are fed to IMR1 but with the oxygen concentration reduced to

1 % of its initial value at Point C. CDF is the concentration profile for butane-butadiene along the length of IMR1.

The concave region of this profile is removed by the tangent from Point A (fresh butane) to the IMR1 profile at Point D. The reactants and products are removed from IMR1 at Point D, the oxygen concentration in this stream is reduced to 1 % of its initial value at Point D and the stream then is fed to the second IMR, IMR2. DE shows the butane-butadiene concentration profile for IMR2 with the maximum butadiene yield of 0.670 shown at Point E.

Figure 7.15 and Table 7.9 show that the maximum yields of butadiene fall inside a narrow spectrum from 0.534 to 0.670 and that the associated residences time, in all instances, exceed 138 seconds.

A breakdown of the individual reactor residence times is given in Table 7.10. The residence times for the second IMR, IMR2, are those necessary to attain the maximum yield of butadiene.

Mixing Ratio, *q2*	**Residence Time, Seconds**			
	PFR	**IMR1**	**IMR2**	**Total**
1.00	41	119	2 600	2 760
0.90	41	107	429	577
0.80	41	95	304	440
0.70	41	83	253	377
0.60	41	71	223	335
0.50	41	60	202	303
0.40	41	48	185	274
0.30	41	36	172	249
0.20	41	24	160	225

Mixing Ratio, *q2*	Residence Time, Seconds			
	PFR	IMR1	IMR2	Total
0.10	41	12	149	202
0	0	0	138	138

Table 7.10. Individual reactor residence times for values of mixing ratio, *q2*. Value of mixing ratio, *q1*, 0.2. Oxygen partial pressure in reactants to IMR2 is 1 % of that in the combined off-take from IMR1 and fresh feed.

Table 7.11 shows the ranking of the various reactor configurations considered in this chapter according to their closeness to the maximum theoretical yield of butadiene of 0.800 (see Chapter 3) carbon mass fraction.

Source	Max. Butadiene Yield	Assoc. Butane Yield	Residence Time, Seconds	% of Theoretical Butadiene Yield	Oxygen Partial Pressure, kPa	Reactor Con-figuration
Table 7.9	0.670	0.001	2 760	84 %	0.005	A *
Table 7.2	0.665	0.042	322	83 %	0.25	IMR
Table 7.7	0.643	0.011	577	80 %	0.056	A *
Table 7.2	0.534	0.112	138	67 %	0.70	IMR
Table 7.3	0.526	0.012	676	66 %	0.06	B **
Table 7.6	0.521	0.091	206	65 %	0.53	B **
Table 7.1	0.183	0.399	41	23 %	70.0	PFR

Table 7.11. Best butadiene yields from the various reactor configurations ranked according to their closeness to the theoretical maximum yield of butadiene.

A * A PFR followed by two IMRs in series (Figure 7.9)

B ** A PFR followed by an IMR in series (Figure 7.5)

In Table 7.11, the oxygen partial pressures are those constant pressures in the final IMR. The figure of 70 kPa shown against the source Table 7.1 is the initial (and depleting) oxygen partial pressure in the feed to the PFR.

Figure 7.15 showed the greatest yields of butadiene of all reactor configurations examined in this chapter. In Chapter 3, Figure 3.25 showed the profile of the Candidate Attainable Region (AR^C) for the system butane –butadiene. It remains to be seen whether the boundaries of this region have been extended as a consequence of deploying a PFR followed by two IMRs in series.

Figure 7.17 shows the superimposition of the Candidate Attainable Region (AR^C) shown in Figure 3.25 upon Figure 7.15.

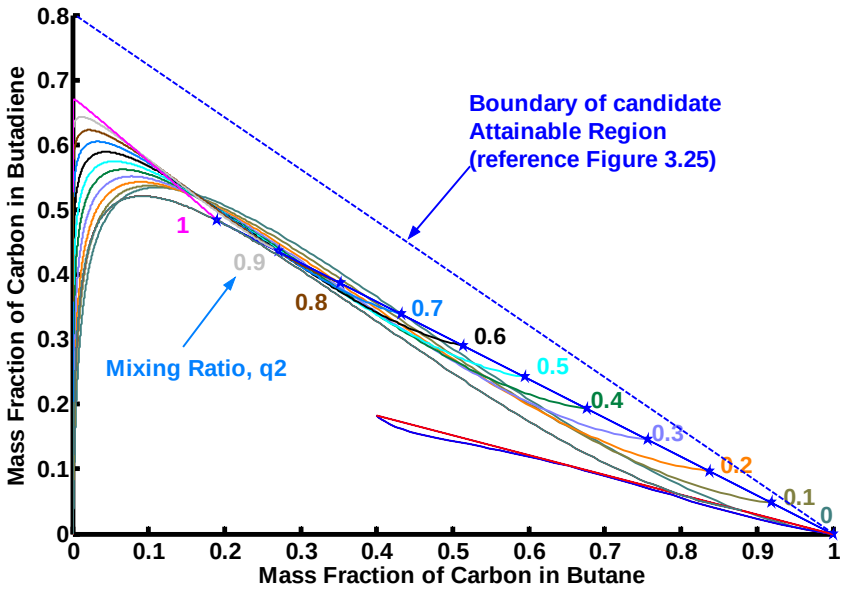


Figure 7.17. Superimposition of Candidate Attainable Region (AR^C) upon Figure 7.15.

Figure 7.17 shows that the best yields of butadiene identified in this chapter all lie within the boundaries of the candidate Attainable Region (AR^C) and as a consequence no grounds have been identified to disprove the validity of this candidate Attainable Region (AR^C).

7.4 Conclusions

Examination of Table 7.11 shows that a maximum butadiene yield of 0.670, 84 % of the theoretical maximum, is attainable from a PFR followed by two IMRs in series. However, the large residence time of 2 760 seconds required for this yield of butadiene plus the capital costs of three reactors would tend to relegate this reactor configuration to the realm of impracticality.

Consequently, it is concluded from Table 7.11 that an IMR with a residence time of 322 seconds operating under a fixed oxygen partial pressure of 0.25 kPa gives a maximum butadiene yield of 0.665 which is 83 % of the theoretical maximum yield of 0.800.

The next highest yield of 0.643, 80 % of the theoretical maximum, is from a PFR followed by two IMRs in series. Required total residence time is 577 seconds. Despite the significant reduction of this residence time compared to the 2 760 seconds for a similar reactor configuration, the capital costs of three reactors cannot justify this configuration when acceptable yields can be obtained from a single IMR.

The next highest yield also is from a single IMR. The butadiene yield of 0.534 (67 % of the theoretical maximum yield) was achieved at a constant oxygen partial pressure of 0.70 kPa and at a total residence time of 138 seconds.

The reactor configuration of a PFR followed by two IMRs cannot be justified because of the better yields of butadiene from a single IMR, the lengthy residence times required or because of the capital costs associated with two additional reactors in the process flow sheet.

In none of the reactor configurations studied was it possible to extend the boundaries of the candidate Attainable Region any further.

7.5 Literature Cited

Assabumrungrat, S. Rienchalanusarn, T. Praserthdam, P. and Goto, S. (2002) Theoretical study of the application of porous membrane reactor to oxidative dehydrogenation of *n*-butane, *Chemical Engineering Journal*, vol. 85, pp. 69-79.

Glasser, D. Hildebrandt, D. and Crowe, C. (1987) A geometric approach to steady flow reactors: the attainable region and optimisation in concentration space, *American Chemical Society*, pp. 1803-1810.

Milne, D. Glasser, D. Hildebrandt, D. Hausberger, B. (2006c) The Oxidative Dehydrogenation of *n*-Butane in a Fixed Bed Reactor and in an Inert Porous Membrane Reactor - Maximising the Production of Butenes and Butadiene, *Industrial and Engineering Chemistry Research* vol. 45, pp. 2661-2671.

Téllez, C. Menéndez, M. Santamaría, J. (1999a) Kinetic study of the oxidative dehydrogenation of butane on V/MgO catalysts, *Journal of Catalysis*, vol. 183, pp. 210-221.

Téllez, C. Menéndez, M. Santamaría, J. (1999b) Simulation of an inert membrane reactor for the oxidative dehydrogenation of butane, *Chemical Engineering Science*, vol. 54, pp. 2917-2925.

CHAPTER 8

Two Reactors in Series – The Effect of Oxygen Partial Pressure and Configuration upon Yield

---

8.1 Introduction

In this thesis I have used the two acronyms FBR (fixed bed reactor) and PFR (plug flow reactor) to describe a reactor in which the initial oxygen partial pressure is permitted to wane in accordance with the ODH process. In this chapter, the acronym FBR is used.

In Chapter 7 of this thesis, I discussed the maximum yields of butadiene from the ODH of *n*-butane when a FBR is followed by one or more IMRs and the oxygen control parameters associated with these yields. The FBR in all these instances was one in which the initial oxygen partial pressure was 70 kPa, this being the value that ensured the greatest yield of butadiene, 0.1828 carbon mass fraction, over the entire spectrum of partial pressures from 85 kPa to 0.25 kPa.

Chapter 7, in effect, was a specific case from a wide range of possibilities. Apart from its discussing only the yields of butadiene from the ODH of *n*-butane, it addressed neither the yields of butenes from *n*-butane nor the yields of butadiene from the ODH of *1*-butene. Furthermore, in Chapter 7 the reactor configuration was restricted to a FBR with an initial oxygen partial pressure of 70 kPa. The possibility of FBRs with other initial oxygen

partial pressures was not considered nor was the effect of reversing the sequence of reactors such that an IMR was followed by a FBR.

This chapter addresses these omissions and the following scenarios are examined.

- A FBR followed by an IMR.
- An IMR followed by a FBR.
- The variance of oxygen partial pressures to the first reactor over the range of 0.25 kPa to 85 kPa.
- The ODH of *n*-butane to produce butenes (all three isomers)
- The ODH of *n*-butane to produce butadiene
- The ODH of *1*-butene to produce butadiene

From these detailed analyses I shall find for each value of the oxygen partial pressure the reactor configuration that provided the best yield of hydrocarbon product as well as the associated residence time for each reaction.

In effect, this chapter should be regarded as an extension of its predecessor and it utilises the findings of Chapter 2 and Chapter 3 in developing the six case studies considered here.

8.2 Background Discussion

It is first necessary to review the profiles in mass concentration sub-space for a FBR and an IMR when each is deployed for the ODH of *n*-butane and *1*-butene.

For this chapter of my thesis it was imperative to decide when an ODH reaction was perceived to have ended. So long as there was a trace of oxygen present, so long was there was a small amount of hydrocarbon reactant in the gas stream, the ODH reaction would continue with the consequence of increasing the residence time with but a marginal increase in the yield of the desired hydrocarbon product. Another effect of a protracted residence time was the undesirable deep oxidation of hydrocarbons to carbon monoxide, carbon dioxide and water.

It was decided, therefore, that the ODH reaction would be deemed to have ended in a FBR once the earlier of two conditions was attained. These conditions were :

- The oxygen partial pressure had been reduced to less than 1e-5 kPa.
- A residence time of 2 500 seconds had elapsed.

The ODH reaction would be deemed to have ended in an IMR once the concentration of the hydrocarbon in the feed stream had fallen below 0.0001 carbon mass fraction. The FBR criterion for oxygen depletion clearly would not apply here as the reactor control policy for the IMRs' being studied is to maintain the oxygen partial pressure steady at its initial feed value.

A final condition for reaction cessation in an IMR was to cater for the situation where the residence time ran its full course of 2 500 seconds with but insignificant gains in the yield of hydrocarbon product. The criterion applied was that if the difference between the minimum and maximum yields of hydrocarbon product were less than 0.0001 carbon mass fraction, the reaction was deemed to have been of no benefit whatsoever in as much as no increase in residence time resulted in any meaningful gain in yield in excess of that in the feed stream.

8.2.1 The ODH of *n*-butane to butadiene in an IMR.

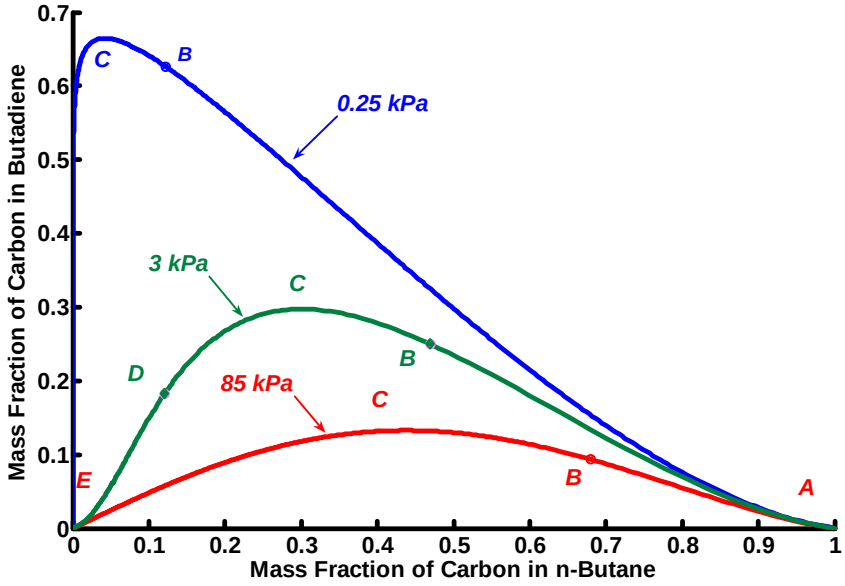


Figure 8.1. Mass concentration profiles for n-butane and butadiene from an IMR. Oxygen partial pressure range 0.25 kPa to 85 kPa.

The data used to derive Figure 8.1 were taken from Chapter 3.

For all values of oxygen partial pressure between 0.25 kPa and 85 kPa as represented in Figure 8.1, the following eight characteristics are applicable.

- The start point, representing in two-dimensional mass fraction space the feed composition, is shown by Point A.

- There is a maximum yield of hydrocarbon product at Point C.

- The composition at the conclusion of the reaction is shown by Point E.

- All the profiles for this reaction between Point A and Point B are concave.

- The concentration of product (butadiene) at Point C is greater than that at Point E.

- The concentration of product (butadiene) at Point E is not greater than that at Point A.

- A second concave region for all profiles exists extending backwards from the termination point, E. At high values of oxygen partial pressure, the concave region, though present, is minimal. An example of this second concave region is exhibited by the mass concentration profile for 3 kPa in Figure 8.1. The concave region is bounded by the profile and a line from Point E to Point D.

- The concentration of butadiene on completion of the reaction effectively is nil as deep oxidation to CO, CO_2 and H_2O has occurred.

The significance of Point B is that it is the point on the profile where the selectivity of *n*-butane to butadiene is a maximum. This means that a straight line between Point A and Point B, the tangent to the profile, represents the locus of all concentrations of *n*-butane and butadiene achievable through mixing hydrocarbons from Point B with fresh feed from Point A in various ratios. The line AB, in addition, has the effect of extending the AR^C for that oxygen partial pressure.

Similarly, Point D is that point on the mass concentration profile where the selectivity of *n*-butane to butadiene is a minimum and the straight line between Point D and Point E, the tangent to the profile, represents the locus of all concentrations of *n*-butane and butadiene achievable through mixing hydrocarbons from Point D with hydrocarbons from Point E in various ratios. The line DE, in addition, has the effect of extending the AR^C for that oxygen partial pressure.

8.2.2 The ODH of *n*-butane to butadiene in a FBR.

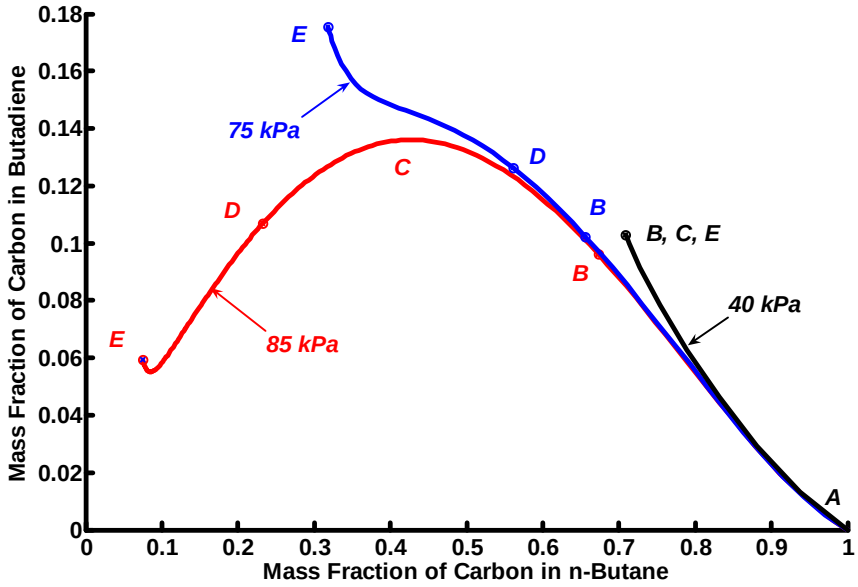


Figure 8.2. Mass concentration profiles for *n*-butane and butadiene from a FBR. Oxygen partial pressures 85 kPa, 75 kPa and 40 kPa.

The data used to derive Figure 8.2 were taken from Chapter 3.

Three characteristic mass concentration profiles exist for the ODH of *n*-butane to butadiene in a FBR. Consider the profile where the initial oxygen partial pressure is 85 kPa.

- The concentration of butadiene at Point B, the maximum selectivity of *n*-butane to butadiene, is less than the maximum concentration of butadiene, Point C.

- The concentration of butadiene on termination of the reaction, Point E, is less than the maximum yield of butadiene, Point C.

- The profile is concave between Point A and Point B.

- The profile is concave between Point D and Point E.

These characteristics are applicable to all profiles between oxygen partial pressures of 81 kPa and 85 kPa.

Consider the mass concentration profile for an initial oxygen partial pressure of 75 kPa.

The characteristics of this profile are :

- The concentration of butadiene on termination of the reaction, Point E, is greater than the concentration at the point of maximum selectivity, B.

- The concentration of butadiene on termination of the reaction is equal to the maximum yield of butadiene from the reaction.

- The profile is concave between Point A and Point B.

- The profile is concave between Point D and Point E.

These characteristics are applicable to all profiles between oxygen partial pressures of 80 kPa and 71 kPa.

Finally, consider the profile for an initial oxygen partial pressure of 40 kPa. The characteristics of this profile are :

- The concentration of butadiene on termination of the reaction, Point E, coincides with that of maximum concentration of butadiene, Point C, and with the point of maximum selectivity of *n*-butane to butadiene, Point B. Only one concave region exists unlike the previous two profiles where two separate such regions were identified.

- The profile is concave between Point A and Points B, C and E, the coordinates of these latter three points being identical.

These characteristics are applicable to all profiles between oxygen partial pressures of 70 kPa and 0.25 kPa.

8.2.3 The ODH of *n*-butane to butenes in an IMR.

Figure 8.3 shows the mass concentration profiles for the ODH of *n*-butane to butenes in an IMR in which the oxygen partial pressure is maintained at a constant value. The profiles are shown for the two extreme partial pressure values of 0.25 kPa and 85 kPa.

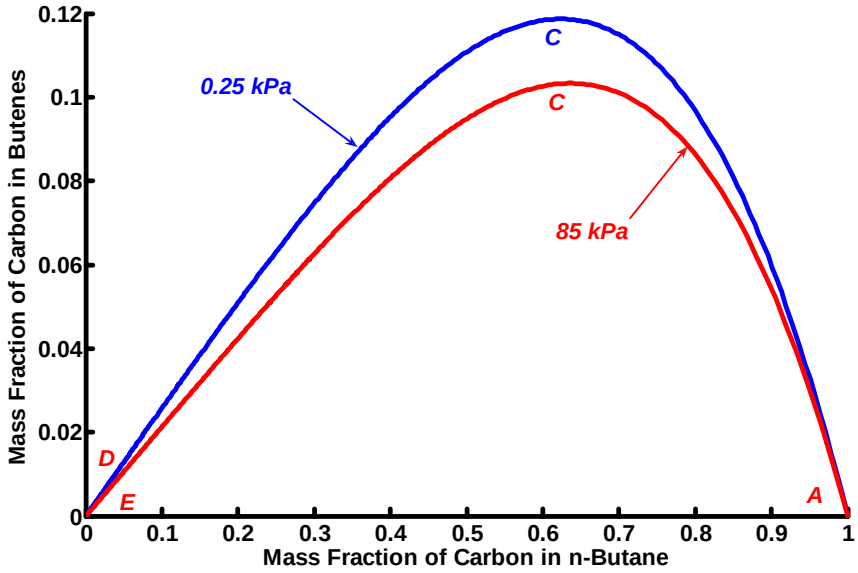


Figure 8.3 Mass concentration profiles for *n*-butane and butenes from an IMR. Oxygen partial pressure range 0.25 kPa to 85 kPa.

The data used to derive Figure 8.3 were taken from Chapter 3.

Figure 8.3 has eight characteristics common to all oxygen partial pressures between 0.25 kPa and 85 kPa.

- The start point, representing in two-dimensional mass fraction space the feed composition, is shown by Point A.

- There is a maximum yield of hydrocarbon product at Point C.

- The composition at the conclusion of the reaction, when all the feed has been oxidised, is shown by Point E.

- All the profiles for this reaction between Point A and Point C are convex.

- All the profiles have a miniscule concave region stretching backwards from the termination point, E to Point D.

- The concentration of product (butenes) at Point C is greater than that at Point E.

- The concentration of product (butenes) at Point E is not greater than that at Point A.

- The concentration of butenes at the end of the reaction effectively is nil as deep oxidation to CO, CO_2 and H_2O has occurred.

8.2.4 The ODH of *n*-butane to butenes in an FBR.

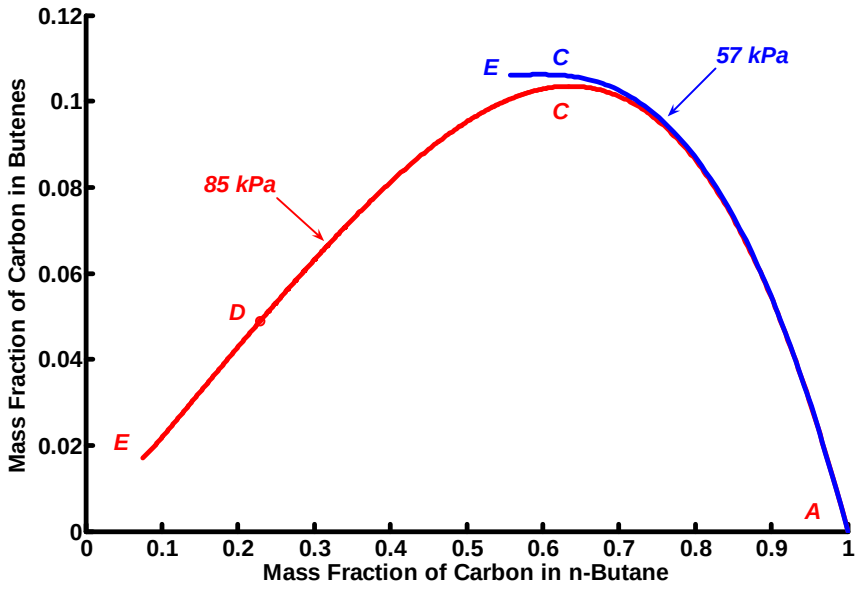


Figure 8.4. Mass concentration profiles for *n*-butane and butenes from a FBR. Oxygen partial pressure range 57 kPa to 85 kPa.

The data used to derive Figure 8.4 were taken from Chapter 3.

Over the range of oxygen partial pressures from 57 kPa to 85 kPa, there are seven characteristics common to these profiles and for all intermediary values of partial pressure.

- The start point, representing in two-dimensional mass fraction space the feed composition, is shown by Point A.

- There is a maximum yield of hydrocarbon produce at Point C.

- The composition at the conclusion of the reaction, when all the oxygen effectively has been depleted, is shown by Point E.

- All the profiles for this reaction between Point A and Point C are convex.

- The concentration of product (butenes) at Point C is greater than that at Point E.

- The concentration of product (butenes) at Point E is greater than that at Point A due to the effective depletion of oxygen.

- A concave region exists stretching back from the termination point, E, to Point D.

At oxygen partial pressures from 56 kPa to 0.25 kPa, the following seven characteristics are applicable.

- The start point, representing in two-dimensional mass fraction space the feed composition, is shown by Point A.

- There is a maximum yield of hydrocarbon produce at Point C.

- The composition at the conclusion of the reaction, when all the oxygen effectively has been depleted, is shown by Point E.

- All the profiles for this reaction between Point A and Point C are convex.

- The concentration of product (butenes) at Point C is equal to that at Point E.

- The concentration of product (butenes) at Point E is greater than that at Point A.

- There are no concave regions.

8.2.5 The ODH of *1*-butene to butadiene in an IMR.

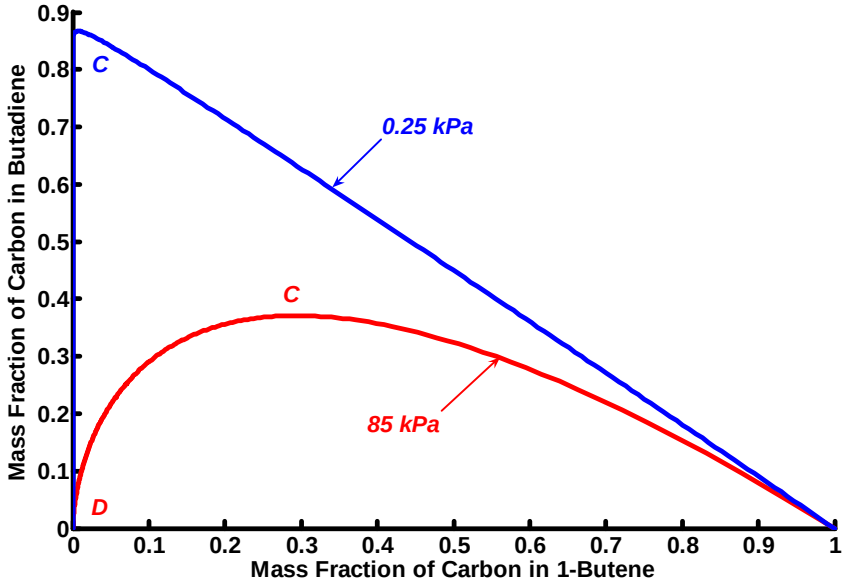


Figure 8.5. Mass concentration profiles for *1*-butene and butadiene from an IMR. Oxygen partial pressures 85 kPa and 0.25 kPa.

The data used to derive Figure 8.5 were taken from Chapter 2.

In the ODH of *1*-butene to butadiene in an IMR, for all values of oxygen partial pressure between 85 kPa and 0.25 kPa, the relevant mass concentration profiles exhibit the same characteristics. These are :

- The maximum yields of butadiene, as indicated by Point C, are greater than the yields of butadiene upon completion of the reaction.

- The yields of butadiene upon completion of the reaction are effectively nil as deep oxidation of this hydrocarbon to CO, CO_2 and H_2O has occurred.

- The mass concentration profiles are convex over their entire lengths.

8.2.6 The ODH of *1*-butene to butadiene in a FBR.

In the ODH of *1*-butene to butadiene in a FBR, there are three characteristic mass concentration profiles over the range of oxygen partial pressures from 85 kPa to 0.25 kPa.

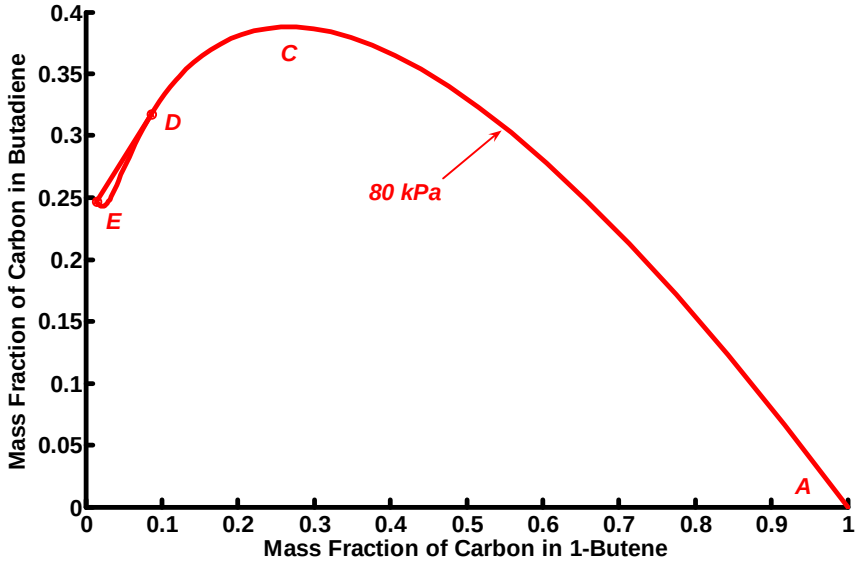


Figure 8.6. Mass concentration profile for *1*-butene and butadiene from a FBR. Oxygen partial pressure 80 kPa.

The data used to derive Figure 8.6 were taken from Chapter 2.

In Figure 8.6, the profile for 80 kPa is typical of all profiles for partial pressures from 85 kPa to 78 kPa. The features of this profile are :

- The feed point in two-dimensional mass fraction sub-space is shown by Point A.

- The maximum yields of butadiene occur at Point C of the respective profiles.

- A single concavity exists extending backwards from the termination point, Point E, to a point, Point D.

- The concave region is to the left of the point of maximum yield of butadiene, Point C.

- The butadiene concentration when the reaction is ended, Point E, is less than the maximum butadiene concentration from the reaction, Point C.

- The profile is convex between the feed concentration, Point A, and Point C, the maximum butadiene yield.

- As the oxygen partial pressure is reduced from 85 kPa to 78 kPa, the upper limit of the concave region, Point D, moves closer to the point of maximum yield of butadiene, Point C.

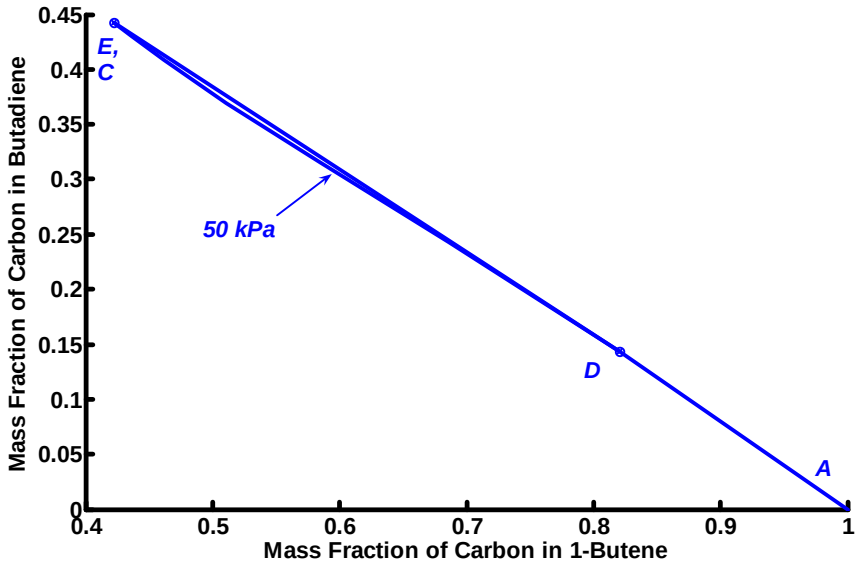


Figure 8.7. Mass concentration profile for *1*-butene and butadiene from a FBR. Oxygen partial pressure 50 kPa.

The profile in Figure 8.7 for an oxygen partial pressure of 50 kPa is representative of all profiles for oxygen partial pressures from 77 kPa to 39 kPa. Its features are :

- The points of reaction cessation, Point E, and of maximum yield of butadiene, Point C, coincide.
- A single concavity exists extending backwards from the termination point, E, to a point, Point D, between the termination point and the feed point, Point A.
- The concave region is to the right of the point of maximum yield of butadiene, Point C.
- As the oxygen partial pressure decreases, the lower point of the concave region, Point D, moves closer to the feed point, Point A.

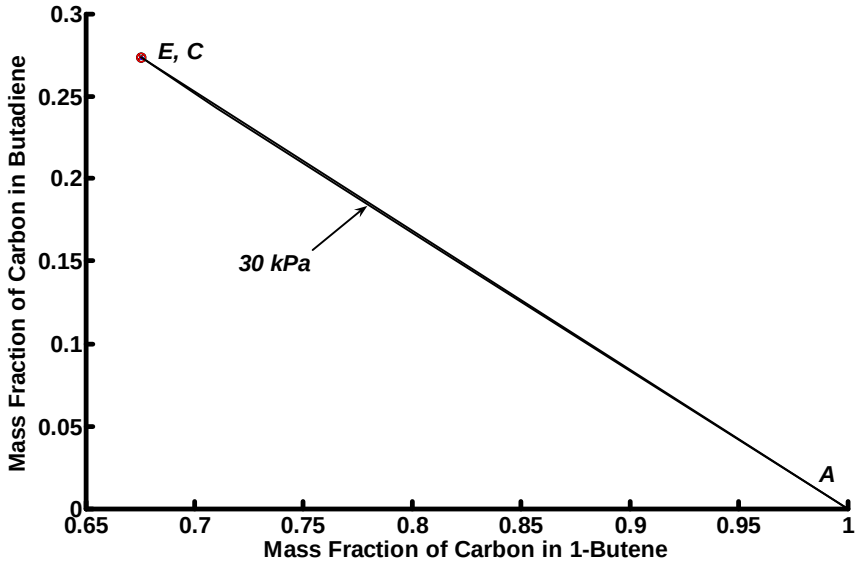


Figure 8.8. Mass concentration profile for *1*-butene and butadiene from a FBR. Oxygen partial pressure 30 kPa.

The profile in Figure 8.8 for an oxygen partial pressure of 30 kPa is representative of all profiles for oxygen partial pressures from 38 kPa to 0.25 kPa. Its features are :

- A single concavity exists extending from the feed point, Point A, over the entire profile.

- The butadiene concentration on cessation of the reaction, Point E, equals the maximum concentration of butadiene, Point C.

8.2.7 Conclusions

In each of the six scenarios discussed, we have shown that there can be significant changes to the mass concentration geometrical profiles. As shall be explained later in this chapter, the geometrical profile has a profound influence upon the residence time necessary to maximise the yield of hydrocarbon product.

8.3 Results

We shall now discuss the results from the six examples reviewed in Section 8.2 but instead of a single reactor two reactors in series shall be investigated.

The procedure adopted was to develop the relevant hydrocarbon mass concentration profile for each oxygen partial pressure and to determine the maximum yield of hydrocarbon product in incremental steps of one second (IMR) and 0.2 seconds (FBR) along the periphery. The second step was to take reactants and products from points along this periphery and use these mixtures as feed to a downstream reactor, be it a FBR or an IMR. Again, the maximum hydrocarbon yields from this succeeding reactor were noted. Finally, where concave regions existed in the original mass concentration profile, the AR^C was extended by convexifying these regions through a policy of by-pass and mixing in various ratios and the resulting mixtures again supplied to the same downstream reactor.

The maximum yield of hydrocarbon product from these three scenarios was identified as was/were the reactor configuration(s) necessary for its attainment. The residence times associated with these maxima were recognised.

8.3.1 Case 1 - The ODH of *n*-butane to butadiene; an IMR followed by a FBR

In Case 1 we shall answer now the following questions in relation to the ODH of *n*-butane to butadiene :

- What is the maximum yield of butadiene at each oxygen partial pressure from 0.25 kPa to 85 kPa when an IMR is followed by a FBR?

- What are the associated configuration arrangements necessary for this maximum production of butadiene, i.e. is it necessary to mix product from the IMR with fresh feed to the IMR and, if so, in what ratio, to attain this maximum? At what stage of the ODH reaction should this mixing occur?

- What is the total residence time for this maximum yield of butadiene?

The general reactor configuration studied is shown in Figure 8.9.

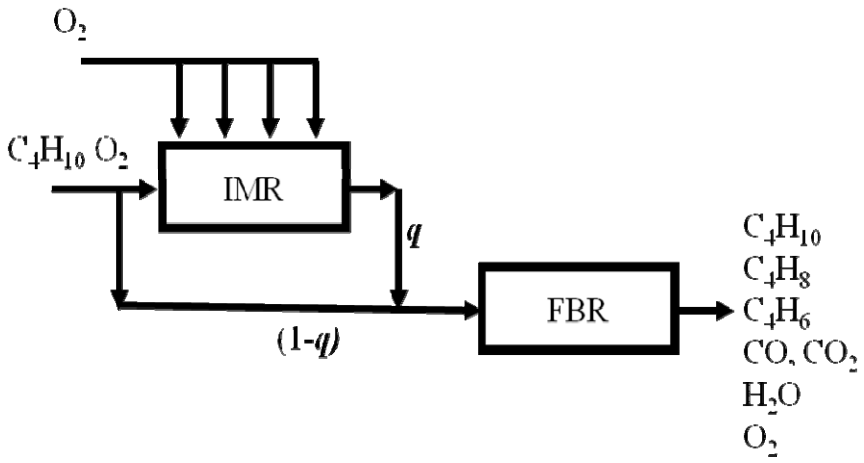


Figure 8.9. IMR:FBR configuration for the ODH of *n*-butane to butadiene.

A mixture of butane and oxygen, the latter at a defined partial pressure, is fed to an IMR. Additional oxygen is supplied along the length of the reactor so as to maintain the partial pressure of the oxygen in the mixture of reactants and products constant at the same partial pressure as in the feed. In addition a bleed is taken from the feed and by-passed around the IMR and mixed with the products from the IMR. The factor *q* represents the ratio of products from the reactor to the bleed stream. A factor of unity represents no bleed stream and a factor of zero signifies the total by-passing of the IMR. The combination of bleed stream and output from the IMR is then supplied to a FBR where the oxygen present is allowed to wane as dictated by the normal ODH process.

In this example (and the subsequent ones), no by-pass and mixing policy was applied to the downstream reactor, this principle being confined to the initial reactor.

Such a rector configuration is represented graphically in the following figure (where the initial and constant oxygen partial pressure is 65 kPa).

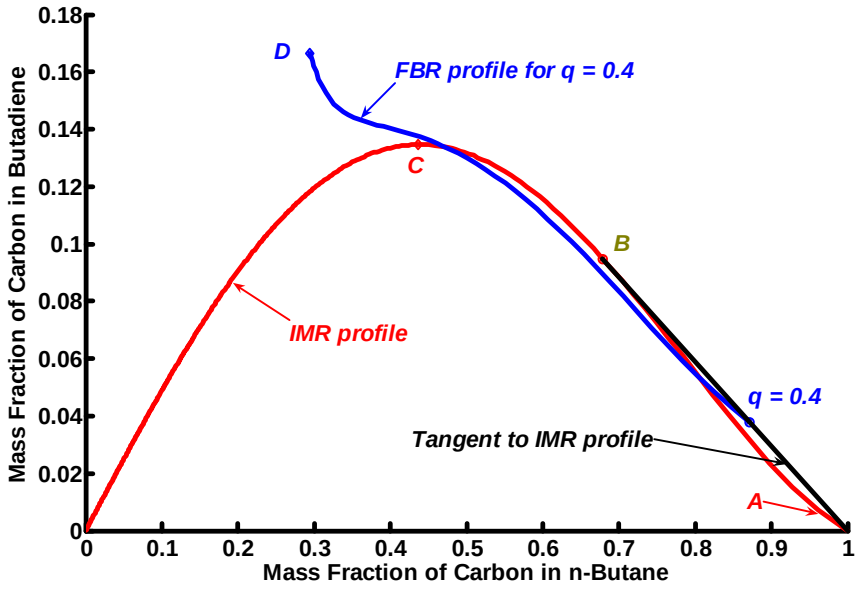


Figure 8.10. Geometrical representation of the ODH of *n*-butane to butadiene in an IMR followed by a FBR. Feed to FBR is a mixture of output from the IMR to fresh feed to IMR in the ratio 0.4:0.6.

In Figure 8.10 the normal butane:butadiene profile is shown for the IMR. As discussed above in 8.2.1, there is a pronounced concavity in that part of the profile from the feed point, point A, to point B as well as a lesser one at the end of the profile. Consequently, line AB represents the tangent from the feed point to the profile and the presence of the line effectively removes the concavity and extends the geometrical area within which all residual products and reactants can be found. How do we know that point B represents the tangency point for this profile ? It was identified by using the graphical technique described in Chapter 4 of this thesis, namely the identification of the point on the IMR profile where the selectivity of *n*-butane is a maximum.

One of the features of AR theory is that mass fraction variables, unlike partial pressures, obey linear mixing rules. The line AB, as a consequence, is the locus of all combinations of feed to the reactor and products from the reactor at point B. In effect, line AB models the by-passing of fresh feed around the IMR and mixing it with the output from point B. Furthermore, line AB represents the locus of all mixed feed streams to the FBR linked to the IMR in series. The same argument, of course, applies to the second concave region but the latter, being miniscule, cannot easily be illustrated at an oxygen partial pressure of 65 kPa.

Figure 8.10 shows geometrically this reactor configuration where the initial oxygen partial pressure to the IMR is 65 kPa. This geometrical representation is valid for all oxygen partial pressures from 85 kPa to 0.25 kPa for the ODH of *n*-butane and the discussion that follows, though in the context of an oxygen partial pressure of 65 kPa is relevant to the full gamut of oxygen partial pressures.

From Figure 8.10 we can see that the maximum yield of butadiene from an isothermal IMR with a controlled oxygen partial pressure of 65 kPa is 0.1346 carbon mass fraction (Point C). Consequently, the purpose of this discussion is to assess whether this yield can be increased further were at any point on the IMR profile the mixture of reactants and products to be removed and fed to a FBR.

Firstly, we can disregard that part of the IMR profile to the left of the maximum point C where the yield of butadiene is decreasing. Why ? Because any point on this portion of the profile the butadiene value has its identical value on the section of the profile to the right of point C and because our objective is to maximise the yield of butadiene we need only

focus our attention to that part of the profile between the feed Point A and Point C. In addition, the concentration of *n*-butane to the right of the maximum yield of butadiene (Point C) for any concentration of butadiene is greater than that to the left of Point C, thus providing more *n*-butane for oxidation.

Again to maximise the yield of butadiene, in taking reactants and products from the IMR it makes sense to follow the line AB in addition to following the concave profile. Again, this is because for any butane concentration projection between point A and point B, there exists a greater butadiene concentration along line AB than there is when the normal profile is followed.

In Figure 8.10, to illustrate our subsequent discussion, we have assumed a value for the mixing ratio, *q*, of 0.4. This means that we have taken a stream of reactants and products from the IMR at point B and mixed this stream with a mixture of butane and oxygen from point A in the ratio of 0.4:0.6.

When this mixture is supplied to the FBR the resultant *n*-butane:butadiene profile is from the feed point (q = 0.4) to point D. The maximum yield from the FBR for a mixing ratio q of 0.4 is 0.167 (point D). This is an increase in butadiene yield of 24 % relative to that for the IMR at Point C, 0.1346 carbon mass fraction.

The conclusion to be made from this is that for an oxygen partial pressure of 65 kPa in the feed to an IMR, a higher yield of butadiene over that from the IMR is possible if the feed to a downstream FBR from the IMR consists of a 40:60 ratio of output from the IMR at the point of maximum selectivity of

butane and fresh butane and oxygen feed to the IMR. The yield from the FBR is 24 % better than from the IMR.

However, as the saying goes, one swallow doth not a Summer make. If values of the mixing ratio, q, other than 0.4 were used, would the yield from the FBR also be an improvement over the maximum possible from the IMR? What would be the result were we to take the feed to the FBR from that part of the IMR profile between the tangency Point B and Point C ? Why not explore the second concave area even though our instincts tell us that there can be no benefit from taking a feed to the second reactor from a stage of the first reactor where the hydrocarbon product concentration already has been grievously depleted? Furthermore, we have considered only the case where the control parameter, oxygen partial pressure, has a value of 65 kPa. What is the effect of partial pressures both greater and less than 65 kPa?

To resolve this matter, the following approach was adopted. For each oxygen partial pressure from 85 kPa to 0.25 kPa, the IMR butane:butadiene profile was prepared. The two concave areas were identified and removed by the respective tangents. For each such area, using the spectrum of mixing ratios from nought to unity, the compositions of the mixed feeds were calculated and used as feeds to the downstream FBR. The maximum butadiene yields were noted for each value of the mixing ratio, q, for each convexified area. In addition, for the whole of the IMR concave profile from the feed point to the termination point, in residence time increments of one second, a stream of reactants and products was taken from the IMR and delivered to the FBR. For each such stream taken from the IMR, the resulting maximum yield from the FBR was calculated.

The results are summarised in Figure 8.11 and in Figure 8.12. Figure 8.11 shows the maximum yield of butadiene from the IMR:FBR combination for each partial pressure value. This maximum value represents the highest obtainable from the two reactors when all feed possibilities are taken into account i.e. when using by-pass and mixing and when taking the feed from the convex portions of the IMR curve after a by-pass and mixing policy. As a comparison, this figure also shows the butadiene concentrations in the mix from the initial IMR to the down-stream FBR at each oxygen partial pressure value.

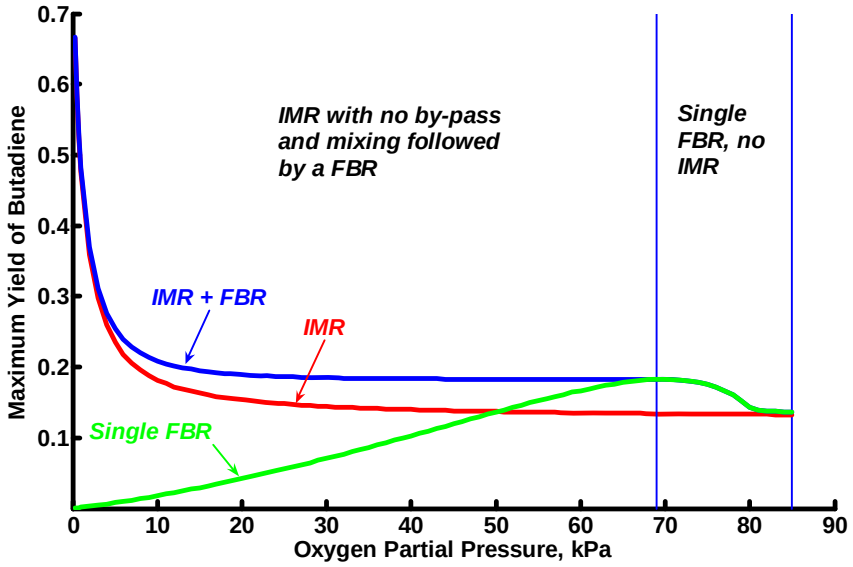


Figure 8.11. Profiles of maximum yields of butadiene and reactor configurations as functions of oxygen partial pressures from a series combination of an IMR followed by a FBR.

As a comparison, Figure 8.11 shows the profile of maximum butadiene yields from a single FBR. It can be seen that over the range of oxygen partial pressures from 85 kPa to 69 kPa, the single FBR profile matches exactly the profile of the series combination of an IMR and a FBR. Below 69 kPa, the FBR profile of maximum butadiene yields falls below that of the series combination. In Figure 8.11, the butadiene yields from the FBR and

the IMR are not additive, i.e. the butadiene yields from the series combination are not the sum of those from the FBR and the IMR.

Examination of Figure 8.11 throws up the presence of two reactor configurations. For oxygen partial pressures from 85 kPa to 69 kPa the maximum yields of butadiene are obtained from a single FBR without a preceding IMR. In other words, the mixing ratio, q, required for these maxima was zero over this range of oxygen partial pressures (see Figure 8.9).

For oxygen partial pressures below 69 kPa, maximum yields of butadiene were derived without any butane and oxygen feeds' being by-passed around the IMR, mixed with output from the IMR and then supplied to the sequential FBR. Over this range of partial pressures, the values of the mixing ratio, q, and necessary for these maxima all were 1.0. Referring to Figure 8.10, the feed to the FBR lay along the segment of the profile between Point B, the tangent point and Point C, the zenith of the mass concentration profile.

All the enhanced yields from the downstream FBR were obtained as a result of the respective feed streams being taken directly from the IMR without any by-pass and mixing whatsoever. The conclusion to be made is that neither of the two concave regions was of any consequence in securing the necessary feed stream to the FBR for maximising the production of butadiene.

A final observation can be made from Figure 8.11. The butane:butadiene profiles cross at 50 kPa. Above this value of oxygen partial pressure a FBR

produces greater yields of butadiene than an IMR. Below 50 kPa, the situation is reversed.

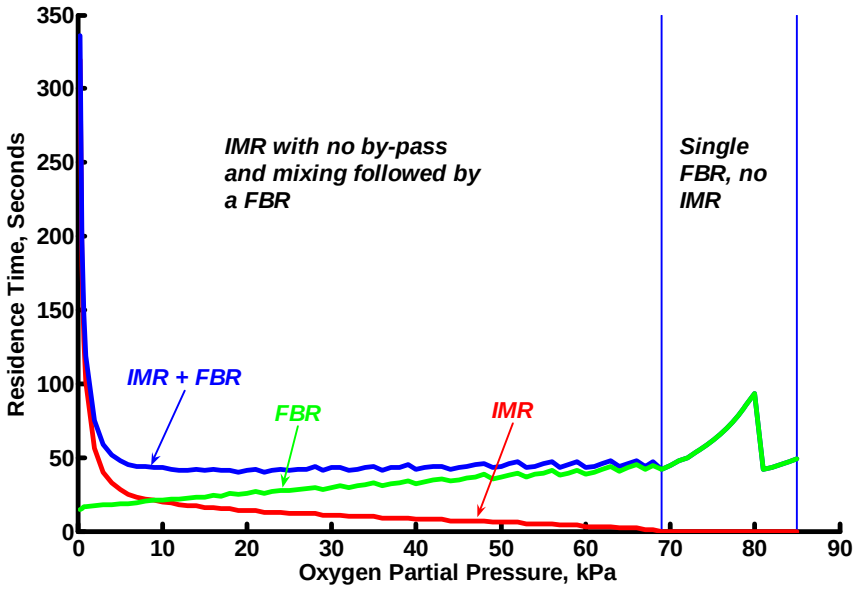


Figure 8.12. Residence times for the maximum yields of butadiene from an IMR:FBR series configuration.

In Figure 8.12, residence times are plotted as functions of oxygen partial pressure for each of the two reactors and also for the combined residence time.

The residence times for the initial IMR are nil between 81 kPa and 69 kPa because between these two oxygen partial pressure values it proved better for maximising the yield of butadiene to by-pass the IMR completely and to use only the FBR. At oxygen partial pressures less than 69 kPa, the IMR residence times increased slowly and below 10 kPa steeply.

FBR residence times show a spike at 80 kPa. This is explained by reference to 8.2.2 above where it was shown that at this oxygen partial pressure value the characteristic mass concentration profile for the ODH of *n*-butane to butadiene in a FBR underwent a significant change, one where the maximum yield of butadiene no longer was greater than but was equal to the yield on cessation of the reaction. Thereafter there is a steep decline in FBR residence times between 80 kPa and 69 kPa. Over this range of oxygen partial pressures the initial IMR still is not required for the best yield of butadiene but at an oxygen partial pressure of 69 kPa, it becomes advantageous to introduce the IMR. The FBR residence times below an oxygen partial pressure of 69 kPa decline gradually with a concomitant gradual increase in IMR residence times until an oxygen partial pressure of 10 kPa when the IMR residence times increase sharply.

The effective total residence time for the two rectors shows the same initial spike and steep decline to an oxygen partial pressure of 69 kPa. Below this partial pressure, the combined residence time is fairly static until an oxygen partial pressure of 10 kPa is reached. At this value and below this value, the residence time of the IMR increases significantly and consequently the sum of the residence times from the two reactors.

Figure 8.13 shows the percentage improvement in FBR butadiene yields over those from an IMR as functions of oxygen partial pressure.

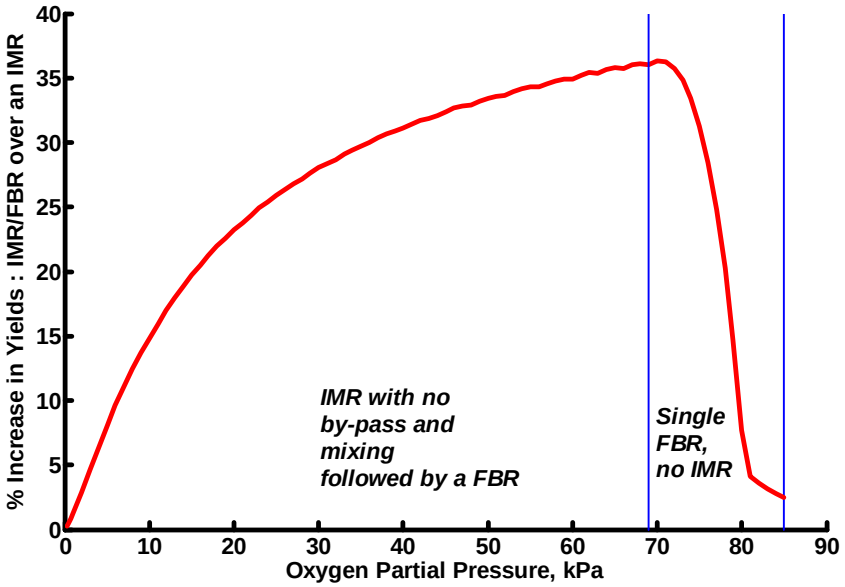


Figure 8.13. Percentage improvement in butadiene production from an IMR:FBR series combination over that from a single IMR.

Initially, the percentage improvement in butadiene yields from an IMR:FBR combination over an IMR rises steeply with a maximum of 36.3 % at an oxygen partial pressure of 70 kPa. This is associated with employing a single FBR, in effect by-passing completely the IMR. In Chapter 7 a FBR with an initial partial pressure of 70 kPa was selected as the first reactor to be followed by an IMR. The choice of a FBR with an oxygen partial pressure of 70 kPa was deliberate as this resulted in the highest yield of butadiene from a FBR over the entire sweep of oxygen partial pressures.

Below an oxygen partial pressure of 69 kPa, the percentage advantage declines with the introduction of the IMR as the first reactor and this pattern continues until the oxygen partial pressure is 0.25 kPa. Over this range of oxygen partial pressures, the feed from the IMR to the FBR is taken from that segment of the mass concentration profile between Point B and Point C (Figure 8.10) and the initial advantage of the IMR:FBR combination over a

single IMR wanes further as a result of the negligible contribution from the FBR towards increasing further the yield of butadiene from the IMR.

The results of this investigation into the use of an IMR:FBR combination in the ODH of *n*-butane to butadiene are shown in Table 8.1.

Oxygen Partial Pressure, kPa	Residence Time, Seconds	Max. IMR Butadiene Yield	Max. IMR:FBR Butadiene Yield	% Increase in IMR:FBR Butadiene Yield over IMR Yield
85	49	0.1328	0.1361	2.5
84	47	0.1328	0.1366	2.8
83	45	0.1329	0.1372	3.2
82	43	0.1330	0.1378	3.6
81	42	0.1331	0.1386	4.1
80	94	0.1332	0.1434	7.7
79	86	0.1332	0.1528	14.6
78	78	0.1333	0.1604	20.3
77	72	0.1334	0.1665	24.8
76	66	0.1335	0.1715	28.5
75	62	0.1336	0.1754	31.3
74	57	0.1337	0.1783	33.4
73	53	0.1338	0.1804	34.8
72	50	0.1339	0.1818	35.8
71	48	0.1340	0.1826	36.3
70	44	0.1341	0.1828	36.3
69	42	0.1342	0.1826	36.0
68	45	0.1343	0.1828	36.1
67	43	0.1344	0.1828	36.0
66	47	0.1345	0.1826	35.7
65	45	0.1346	0.1828	35.8
64	43	0.1347	0.1828	35.6
63	47	0.1349	0.1826	35.4
62	45	0.1350	0.1828	35.4
61	43	0.1352	0.1828	35.2
60	42	0.1353	0.1826	34.9
59	46	0.1355	0.1828	34.9

Oxygen Partial Pressure, kPa	Residence Time, Seconds	Max. IMR Butadiene Yield	Max. IMR:FBR Butadiene Yield	% Increase in IMR:FBR Butadiene Yield over IMR Yield
58	43	0.1356	0.1828	34.8
57	42	0.1358	0.1828	34.6
56	46	0.1360	0.1826	34.3
55	44	0.1361	0.1829	34.3
54	43	0.1363	0.1829	34.2
53	42	0.1365	0.1828	33.9
52	45	0.1367	0.1827	33.6
51	44	0.1369	0.1829	33.6
50	43	0.1371	0.1829	33.4
49	42	0.1374	0.1829	33.2
48	45	0.1376	0.1828	32.9
47	44	0.1378	0.1830	32.8
46	43	0.1381	0.1831	32.6
45	42	0.1383	0.1831	32.4
44	41	0.1386	0.1831	32.1
43	43	0.1389	0.1832	31.9
42	43	0.1392	0.1833	31.7
41	41	0.1395	0.1833	31.4
40	40	0.1398	0.1834	31.1
39	43	0.1402	0.1834	30.9
38	42	0.1405	0.1836	30.7
37	41	0.1409	0.1837	30.4
36	40	0.1413	0.1837	30.0
35	43	0.1417	0.1839	29.7
34	41	0.1422	0.1841	29.4
33	41	0.1427	0.1842	29.1
32	40	0.1432	0.1843	28.7
31	42	0.1438	0.1845	28.4
30	41	0.1443	0.1848	28.1
29	40	0.1450	0.1850	27.6
28	42	0.1457	0.1853	27.2
27	41	0.1464	0.1856	26.8
26	40	0.1472	0.1860	26.4
25	40	0.1480	0.1863	25.9
24	41	0.1489	0.1868	25.4

Oxygen Partial Pressure, kPa	Residence Time, Seconds	Max. IMR Butadiene Yield	Max. IMR:FBR Butadiene Yield	% Increase in IMR:FBR Butadiene Yield over IMR Yield
23	40	0.1499	0.1873	24.9
22	39	0.1510	0.1878	24.3
21	41	0.1522	0.1884	23.8
20	40	0.1535	0.1892	23.2
19	39	0.1550	0.1900	22.5
18	40	0.1566	0.1910	21.9
17	39	0.1585	0.1921	21.2
16	40	0.1605	0.1934	20.5
15	39	0.1629	0.1949	19.7
14	40	0.1655	0.1967	18.9
13	39	0.1686	0.1989	17.9
12	40	0.1722	0.2015	17.0
11	41	0.1765	0.2047	16.0
10	41	0.1816	0.2086	14.9
9	42	0.1878	0.2135	13.7
8	42	0.1954	0.2198	12.4
7	42	0.2052	0.2279	11.1
6	44	0.2180	0.2390	9.6
5	46	0.2354	0.2543	8.0
4	51	0.2600	0.2766	6.4
3	58	0.2973	0.3111	4.6
2	73	0.3590	0.3694	2.9
1	118	0.4763	0.4821	1.2
0.75	145	0.5235	0.5280	0.9
0.50	196	0.5838	0.5868	0.5
0.25	334	0.6648	0.6663	0.2

Table 8.1. Maximum yields of butadiene from an IMR and a FBR in series as functions of oxygen partial pressure.

In Table 8.1, the oxygen partial pressure (kPa) is that in the feed to the initial IMR (where it is maintained at this constant value) and that in the

feed to the succeeding FBR where it is permitted to wane through the normal ODH process.

A value in the second column connotes the combined residence time (seconds) from the IMR and the FBR that resulted in the maximum yield of butadiene shown in column 4.

The maximum IMR butadiene yield in column 3 of Table 8.1 is that from the initial IMR where the oxygen partial pressure is held constant at the indicated value.

In column 4 the maximum IMR:FBR butadiene yield is that from a FBR preceded by an IMR and after the combined residence time shown in column 2.

The last column of Table 8.1 shows the percentage increase in butadiene yield from the IMR:FBR series combination relative to the IMR. It should be noted that the maximum percentage increase of 36.3 % is when the oxygen partial pressure is 70 kPa.

Conclusions.

At oxygen partial pressures greater than or equal to 50 kPa, a single FBR produces greater yields of butadiene than does a single IMR operated under a constant oxygen partial regime. Below 50 kPa, the converse applies.

For oxygen partial pressures less than 70 kPa, an IMR followed by a FBR always results in higher yields of butadiene than does either a single IMR or a single FBR. Above 70 kPa, a single FBR is superior to the series combination of an IMR and a FBR.

The maximum percentage differential, 36.3 %, between the best butadiene yield from an IMR followed by a FBR and the greatest concentration of butadiene from a single IMR occurs at an oxygen partial pressure of 70 kPa.

The percentage advantage of an IMR and a FBR over a single IMR declines as the oxygen partial pressure is reduced below 70 kPa. At an oxygen partial pressure of 0.25 kPa, the percentage differential is 0.23 %.

The strategy of by-pass and mixing applied to the two concave sections of the IMR mass concentration profile is ineffectual towards maximising the production of butadiene.

8.3.2 Case 2 – The ODH of *n*-butane to butadiene; a FBR followed by an IMR

In Case 2 the reactor configuration is shown in Figure 8.14.

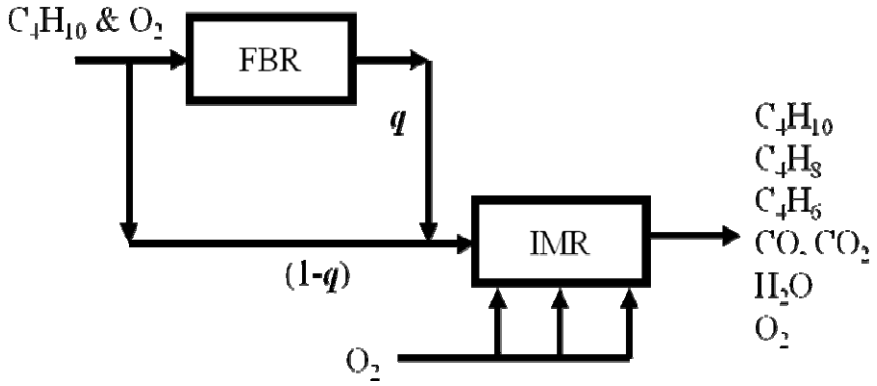


Figure 8.14. FBR:IMR configuration for the ODH of *n*-butane to butadiene.

We noted in 8.2.2 above that for all oxygen partial pressures, the mass concentration profile for the ODH of *n*-butane to butadiene in a FBR shows a concave region emanating from the feed point. In addition, for oxygen partial pressures in excess of 70 kPa a second concave region exists extending backwards from the point of reaction cessation. As a result, in assessing the maximum yields of butadiene from this reactor configuration, we shall take into account the possible benefits from bypassing and mixing reactants and products to extend both of these two concave areas.

The results for the ODH of *n*-butane to butadiene in a FBR followed by an IMR are shown in Figure 8.15.

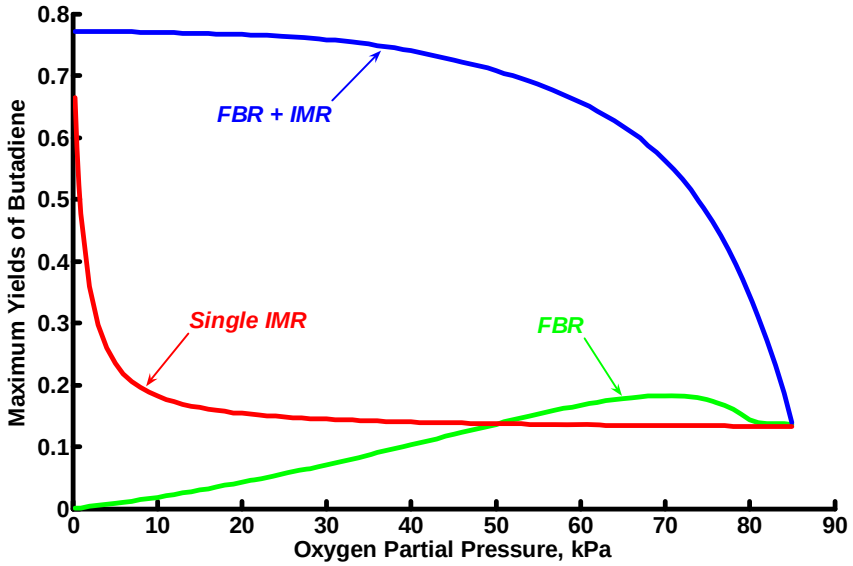


Figure 8.15. Profiles of maximum yields of butadiene as functions of oxygen partial pressures from a series combination of a FBR followed by an IMR.

In Figure 8.15, the FBR profile indicates the maximum yield of butadiene possible from the initial FBR for each value of the oxygen partial pressure. The profile designated FBR + IMR shows the actual butadiene maxima attainable from the down-stream IMR. As a comparison, the butadiene maxima from a stand-alone IMR are shown in Figure 8.15. As mentioned previously, the butadiene maxima from the FBR and the single IMR are not additive.

Over the full range of oxygen partial pressures from 84 kPa to 0.25 kPa, the maximum yields of butadiene are derived when a FBR is followed by an IMR. These maxima are greater than can be obtained from a single FBR as can be seen in Figure 8.15. The maximum yield of butadiene from a single FBR is 0.1828 carbon mass fraction and this occurs when the inlet oxygen partial pressure to the FBR is 70 kPa.

At 85 kPa the maximum butadiene yield from a FBR is 0.1361 carbon mass fraction. When an IMR is connected to this FBR so as to follow it in series the resulting yields of butadiene all are less than that in the stream from the FBR into the IMR. Consequently, the maximum yield of butadiene from the FBR:IMR series combination is to be found in the stream entering the IMR i.e. the same as in that leaving the FBR. This is why Figure 8.15 shows identical yields of butadiene for an oxygen partial pressure of 85 kPa from the single FBR and from the series combination of a FBR followed by an IMR. Along the full profile (in mass concentration space) of this FBR, the profiles for the IMR all fall within the FBR profile.

The maximum yield of butadiene from the series combination of a FBR and an IMR is 0.7738 carbon mass fraction when the oxygen partial pressure to the FBR is 0.25 kPa.

At oxygen partial pressures from 84 kPa to 0.25 kPa, the maximum yields of butadiene from the FBR:IMR series combination are all obtained when the feed to the IMR is taken from the FBR profile without any mixing process undertaken to eliminate the two concave regions. The use of an extended convexified region to produce a mixed feed from the FBR does not result in a butadiene yield from the down-stream IMR greater than that emanating from the original concave profiles of the FBR profile.

As was noticed in 8.3.1, the FBR and IMR mass concentration profiles for butane and butadiene intersect at an oxygen partial pressure of 50 kPa. Above 50 kPa, a FBR produces butadiene concentration maxima greater than an IMR and *vice versa*.

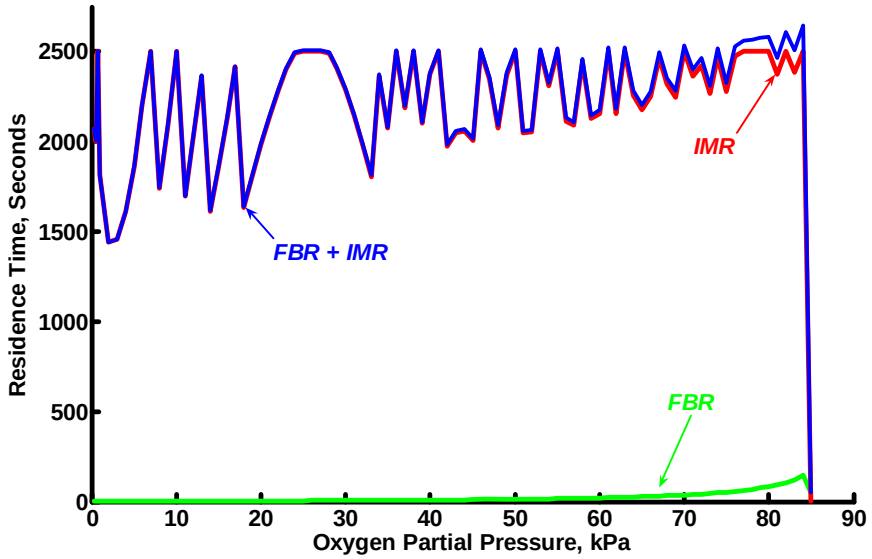


Figure 8.16. Residence times for the maximum yields of butadiene from a FBR:IMR series configuration.

Figure 8.16 shows the total residence time for the FBR and the IMR required for the maximum concentrations of butadiene for each value of oxygen partial pressure in the feed to the initial FBR. The total residence time is the sum of the respective times for the FBR and the succeeding IMR. As a reference, the residence time for the FBR also is plotted in Figure 8.16 but this residence time is relatively insignificant when contrasted with the overall time. Clearly, the residence time associated with the IMR is the controlling step.

A clearer exposition of the two residence time profiles is shown in Figure 8.17 where the FBR and total residence times are plotted on a linear-log scale. The maximum FBR residence time of 145 seconds at an oxygen partial pressure of 84 kPa is less than 6 % of the total residence time.

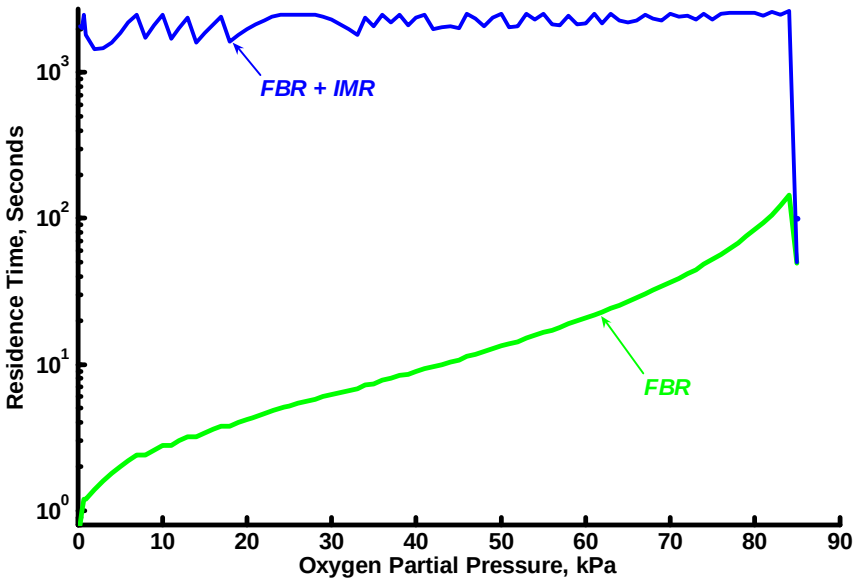


Figure 8.17. Residence times for the maximum yields of butadiene from a FBR:IMR series configuration (linear:log scale).

The characteristic of the total residence time profile in Figure 8.16 is its apparent randomness albeit there is a semblance of a repetitive pattern to be seen. This randomness is at variance with other profiles shown in this thesis where a smooth, regular and mathematically-identifiable curve invariably resulted. At first, the residence time randomness of Figure 8.16 was believed to be the outcome either of the Matlab® ordinary differential equation (ODE) operator used for integration or of a general instability in the mathematical model employed but after exhaustive checking both these two likelihoods were discarded. A reversal to fundamental principles then was adopted and this approach produced an explanation for the random profile shown in Figure 8.16.

Examination of the kinetic data (Table 1.7) shows that the rate of reaction, r, for each of the nine species associated with the ODH reaction is proportional to the selective (θ_0) and non-selective (λ_0) oxidation catalyst

sites each of which, in turn, is a function of the partial pressure of oxygen, i.e.

$$r_i = f\left(p_{O2}\right) \tag{1}$$

The rate of reaction, r_i, in turn is inversely proportional to residence time, i.e. the faster the reaction the smaller is the residence time required to attain a specific yield of product. Consequently, the rate of reaction is a function of the inverse of the residence time,

$$r_i = f\left(\frac{1}{\tau}\right) \tag{2}$$

From equations (1) and (2), we deduce that

$$\tau = f\left(\frac{1}{p_{O2}}\right) \tag{3}$$

i.e. the residence time is a function of the reciprocal of the oxygen partial pressure.

To test this observation, the residence time in the IMR is plotted in Figure 8.18 for each oxygen partial pressure in the feed to the FBR. Also plotted is the reciprocal of the inlet (and constant) oxygen partial pressure to the IMR from the FBR.

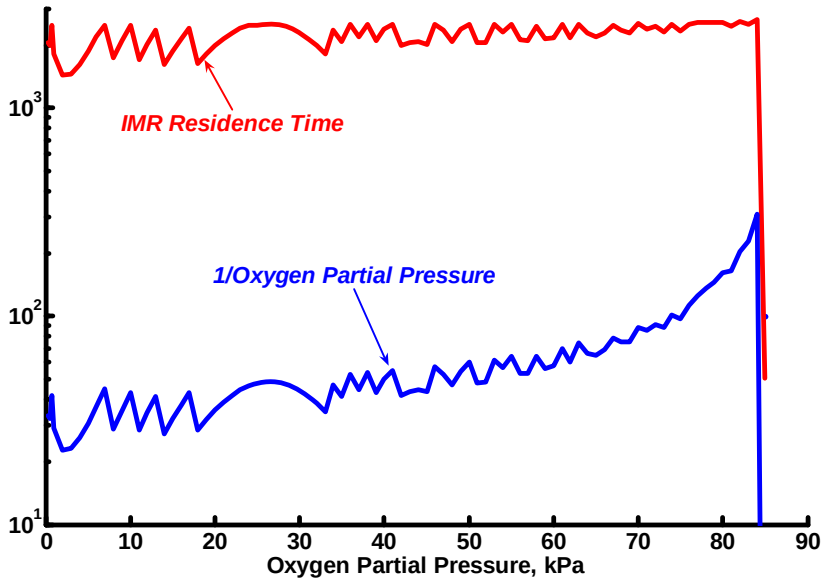


Figure 8.18. IMR residence times and reciprocal of IMR oxygen partial pressures against oxygen partial pressure in feed to the initial FBR (linear:log scale).

There is a marked commonality in the two profiles. Firstly, the nadirs and zeniths of each align exactly and at the same oxygen partial pressure. Secondly, there is a pronounced similarity in the two profiles particularly at oxygen partial pressures less than 70 kPa.

It should be noted that the *y*-axis of Figure 8.18 neither shows a title nor an indication of the relevant units. What I wish to show is that the noted similarities between the two profiles are so evident that the element of coincidence has to be excluded and what must emerge from a study of Figure 8.18 is the causal effect of the inverse of oxygen partial pressure upon the residence time in the down-stream IMR.

Upon reflection this conclusion is not as absurd as initially it might have been supposed to be. In the initial FBR, the residence time at which the mixture of reactants and products is fed to the IMR cannot be greater than the minimum associated with (a) 2 500 seconds and (b) an oxygen partial pressure less than 1e-5 kPa. Equally in the FBR, the larger the residence time the smaller is the oxygen partial pressure in the products from the ODH reaction as more of it is consumed as the oxidation process continues. Hence therein lies the inverse relationship between residence time and oxygen partial pressure. In effect, the FBR inlet oxygen partial pressure influences both the subsequent FBR residence time and the oxygen partial pressure in the feed to the IMR.

Whatever then the oxygen partial pressure in the stream from the FBR to the IMR, once the mixture enters the IMR the control policy is to keep that oxygen partial pressure constant by the judicious addition of fresh oxygen along the length of the IMR. In this circumstance, the IMR residence time to maximise the yield of butadiene again is a function of the constant oxygen partial pressure as was shown earlier in this thesis (see Figure 3.20). In Chapter 3 and Figure 3.20 I showed that over the range of oxygen partial pressures from 85 kPa to 15 kPa the required residence time decreased. Below 15 kPa the residence time began to increase slowly and below 1 kPa rapidly and asymptotically. Consequently, the link between oxygen partial pressure and residence time existed but mathematically was fairly complex.

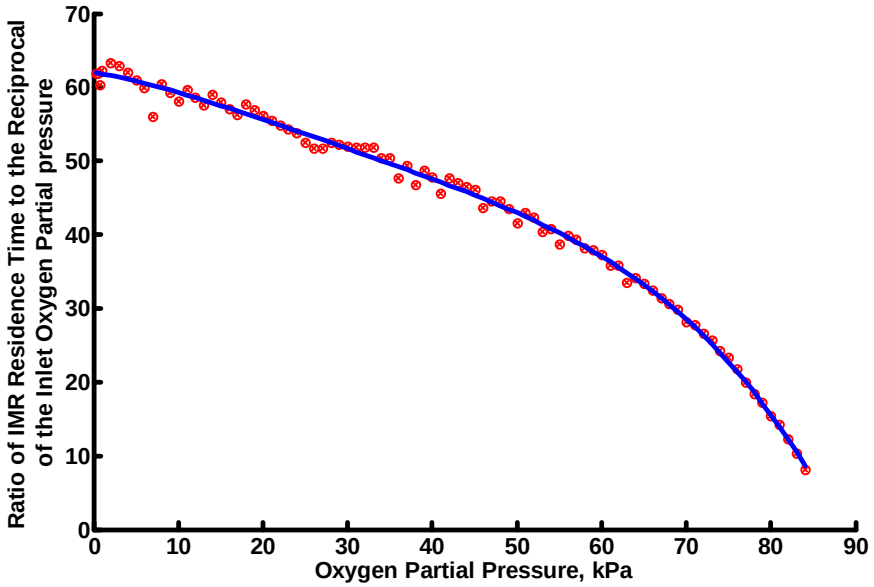


Figure 8.19. Ratio of IMR residence time and reciprocal of oxygen partial pressure as a function of oxygen partial pressure.

In Figure 8.19 I have plotted the ratio of the IMR residence time and the inverse of the IMR oxygen partial pressure (in reality, the product of the residence time and partial pressure) against the inlet oxygen partial pressure to the FBR. The respective values are shown in red and the lack of randomness (as discussed earlier) together with the regularity of the disposition of these points immediately suggested that a mathematical equation to describe the relationship would not be too difficult to derive.

A fourth-order polynomial expression was found to give the best fit and is plotted in blue in Figure 8.19.

The equation of this polynomial curve is ;

$$Y = - 2.0079e\text{-}6X^4 + 224.8130e\text{-}6X^3 - 9.9632e\text{-}3X^2 - 193.5993e\text{-}3X + 61.9908 \quad (4)$$

where

X = the oxygen partial pressure (kPa) in the feed to the initial FBR.

Y = ratio of oxygen partial pressure leaving the FBR (and entering the IMR) and the reciprocal of the residence time (seconds) required to obtain the maximum yield of butadiene from the IMR.

From this mathematical expression can be obtained for each value of oxygen partial pressure in the inlet feed to the FBR either the residence time in the IMR to maximise the yield of butadiene or the required oxygen partial pressure in the stream from the FBR provided one of the latter two is known.

A word of caution nevertheless is necessary. The fourth-order polynomial expression describes a relationship existing in a two-dimensional projection from a ten-dimensional surface, the ten dimensions being the nine chemical species plus residence time. The relationship required to take account of all ten dimensions would not be as simple and as neat as that that characterises Equation 4 above.

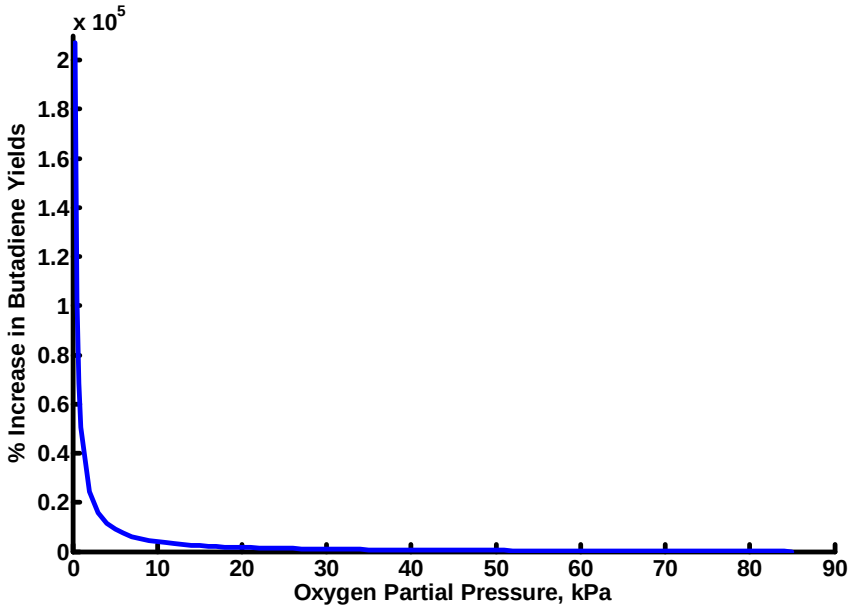


Figure 8.20. Percentage improvement in butadiene production from an FBR:IMR series combination over that from a single FBR.

Figure 8.20 shows the percentage increase in butadiene yields from the series combination of a FBR and an IMR relative to those from a single FBR as a function of the initial oxygen partial pressure to the FBR.

The gain in butadiene yields from 85 kPa to 20 kPa is not readily apparent due to the relative size of the *y*-axis against the *x*-axis. By plotting the same data, but this time using a log scale for the *y*-axis, the effect of oxygen partial pressure on the improvement in butadiene yield is easier to discern.

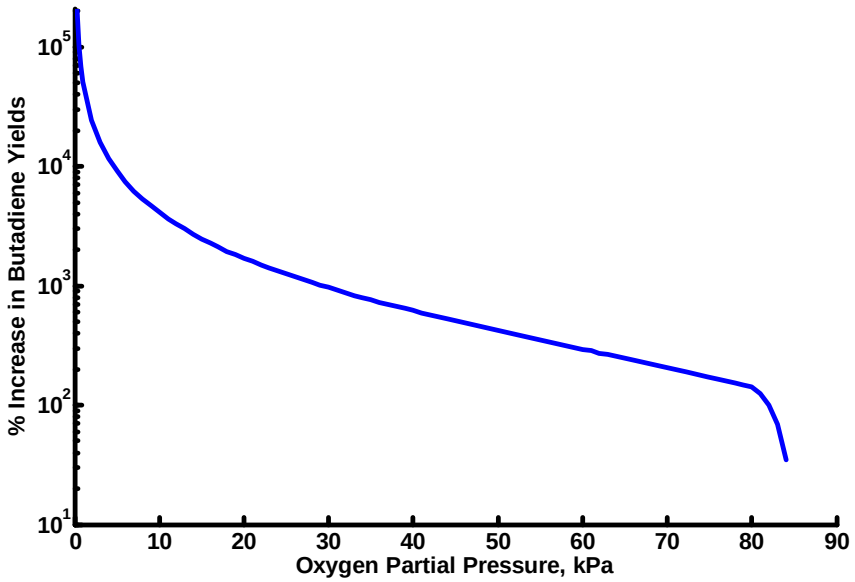


Figure 8.21. Percentage improvement in butadiene production from an FBR:IMR series combination over that from a single FBR (linear/log scale).

Figure 8.21 shows that a 100 % improvement in yield can be obtained if the oxygen partial pressure in the feed to the FBR is 82 kPa. Below this pressure, the gain continues to increase. At 50 kPa the gain is 420 %, at 30 kPa 1 000 %. At partial pressures less than 10 kPa the gain increases asymptotically and at 0.25 kPa a gain in excess of 200 000 % is obtained. However, to put the latter into perspective, at this value of oxygen partial pressure the maximum yield of butadiene from a single FBR is less than 0.0005 carbon mass fraction and the yield from the succeeding IMR is 0.7738 carbon mass fraction.

The results of this study into the use of a FBR:IMR series combination for the ODH of *n*-butane to butadiene are shown in Table 8.2.

Oxygen Partial Pressure, kPa	Residence Time, Seconds	Max. FBR Butadiene Yield	Max. FBR:IMR Butadiene Yield	% Increase in FBR:IMR Butadiene Yield over FBR Yield
85	50	0.1361	0.1361	0
84	2645	0.1366	0.1840	35
83	2505	0.1372	0.2318	69
82	2606	0.1378	0.2750	100
81	2466	0.1386	0.3129	126
80	2583	0.1434	0.3473	142
79	2575	0.1528	0.3787	148
78	2568	0.1604	0.4062	153
77	2562	0.1665	0.4322	160
76	2530	0.1715	0.4558	166
75	2328	0.1754	0.4761	171
74	2517	0.1783	0.4967	179
73	2313	0.1804	0.5136	185
72	2465	0.1818	0.5310	192
71	2401	0.1826	0.5460	199
70	2537	0.1828	0.5609	207
69	2281	0.1826	0.5727	214
68	2354	0.1820	0.5854	222
67	2494	0.1810	0.5976	230
66	2281	0.1796	0.6069	238
65	2205	0.1780	0.6163	246
64	2282	0.1762	0.6261	255
63	2524	0.1741	0.6348	265
62	2181	0.1719	0.6421	274
61	2522	0.1694	0.6520	285
60	2177	0.1669	0.6569	294
59	2147	0.1642	0.6633	304
58	2460	0.1614	0.6719	316
57	2108	0.1584	0.6753	326
56	2132	0.1555	0.6811	338
55	2517	0.1524	0.6873	351
54	2326	0.1493	0.6929	364
53	2515	0.1461	0.6983	378
52	2067	0.1428	0.7000	390
51	2061	0.1396	0.7042	404

Oxygen Partial Pressure, kPa	Residence Time, Seconds	Max. FBR Butadiene Yield	Max. FBR:IMR Butadiene Yield	% Increase in FBR:IMR Butadiene Yield over FBR Yield
50	2513	0.1363	0.7097	421
49	2383	0.1330	0.7145	437
48	2090	0.1297	0.7158	452
47	2357	0.1264	0.7213	471
46	2511	0.1230	0.7237	488
45	2020	0.1197	0.7247	506
44	2070	0.1163	0.7281	526
43	2058	0.1130	0.7307	547
42	1986	0.1097	0.7326	568
41	2509	0.1063	0.7364	593
40	2381	0.1030	0.7408	619
39	2110	0.0997	0.7408	643
38	2508	0.0965	0.7424	670
37	2197	0.0932	0.7457	700
36	2508	0.0900	0.7465	730
35	2083	0.0867	0.7483	763
34	2373	0.0836	0.7525	800
33	1813	0.0804	0.7487	831
32	1988	0.0773	0.7523	873
31	2149	0.0742	0.7553	918
30	2295	0.0711	0.7579	966
29	2410	0.0681	0.7602	1016
28	2498	0.0651	0.7621	1071
27	2506	0.0621	0.7622	1127
26	2505	0.0592	0.7625	1188
25	2505	0.0563	0.7647	1258
24	2495	0.0535	0.7665	1333
23	2407	0.0507	0.7668	1414
22	2289	0.0479	0.7667	1501
21	2146	0.0452	0.7663	1596
20	1989	0.0425	0.7654	1702
19	1815	0.0398	0.7641	1817
18	1637	0.0373	0.7621	1946
17	2419	0.0347	0.7716	2123
16	2138	0.0322	0.7697	2289

Oxygen Partial Pressure, kPa	Residence Time, Seconds	Max. FBR Butadiene Yield	Max. FBR:IMR Butadiene Yield	% Increase in FBR:IMR Butadiene Yield over FBR Yield
15	1868	0.0298	0.7673	2477
14	1617	0.0274	0.7641	2692
13	2368	0.0250	0.7734	2990
12	2017	0.0227	0.7706	3289
11	1699	0.0205	0.7668	3640
10	2503	0.0183	0.7759	4134
9	2095	0.0162	0.7726	4669
8	1743	0.0141	0.7685	5335
7	2502	0.0121	0.7663	6214
6	2205	0.0102	0.7746	7494
5	1867	0.0083	0.7710	9160
4	1615	0.0065	0.7673	11669
3	1459	0.0048	0.7644	15885
2	1440	0.0031	0.7641	24425
1	1817	0.0015	0.7707	50559
0.75	2501	0.0011	0.7776	68474
0.50	2004	0.0008	0.7731	102777
0.25	2069	0.0004	0.7738	207132

Table 8.2. Maximum yields of butadiene from a FBR and an IMR in series as functions of oxygen partial pressures

In Table 8.2, the oxygen partial pressure (kPa) is that to the initial FBR and where it is permitted to wane through the normal ODH process.

A value in the second column connotes the combined residence time (seconds) from the FBR and the IMR that resulted in the maximum yield of butadiene shown in column 4.

The maximum FBR butadiene yield in column 3 of Table 8.2 is that from a FBR where the initial oxygen partial pressure is that shown in the first column.

In column 4 the maximum FBR:IMR butadiene yield is that from an IMR preceded by a FBR and after the combined residence time shown in column 2.

The last column of Table 8.2 shows the percentage increase in butadiene yield from the FBR:IMR series combination relative to the FBR. The maximum percentage advantage occurs at an oxygen partial pressure of 0.25 kPa.

Conclusions.

At oxygen partial pressures greater than or equal to 50 kPa, a single FBR produces greater yields of butadiene than does a single IMR operated under a constant oxygen partial regime. Below 50 kPa, the converse applies.

For the ODH of *n*-butane to butadiene with one exception, a FBR followed by an IMR always produces better yields of butadiene than can be obtained from a single FBR. The one exception to this occurs at an oxygen partial pressure of 85 kPa where the down-stream IMR fails to produce a better yield of butadiene than that in the feed from the FBR.

The maximum yield of butadiene, 0.7738 carbon mass fraction, is obtained when the oxygen partial pressure in the feed to the FBR is 0.25 kPa. This yield of butadiene requires a total residence time of 2 069 seconds.

The relationship between the inlet oxygen partial pressure to the FBR and the product of IMR residence time and constant IMR oxygen partial pressure can be expressed in two-dimensional mass fraction concentration space by a fourth-order polynomial equation.

The convexification of two concave regions in the FBR profiles for *n*-butane and butadiene did not improve the yield of butadiene either from the single FBR or from the down-stream IMR.

8.3.3 Case 3 – The ODH of *n*-butane to butenes; an IMR followed by a FBR

In Case 3 the reactor configuration is as was shown in Figure 8.9.

In 8.2.3 above, we identified the characteristics in mass concentration space of the profile for the ODH of *n*-butane to butenes (all three isomers) in an IMR. For all oxygen partial pressures from 85 kPa to 0.25 kPa, the profiles all have a concave area extending backwards from the termination point of the mass concentration profile.

As a result, in assessing the maximum yields of butenes from this reactor configuration, the opportunity to avail of the advantages that might accrue through a policy of by-pass and mixing across this concave area was taken.

The results for the ODH of *n*-butane to butenes in an IMR followed by a FBR are shown in Figure 8.22.

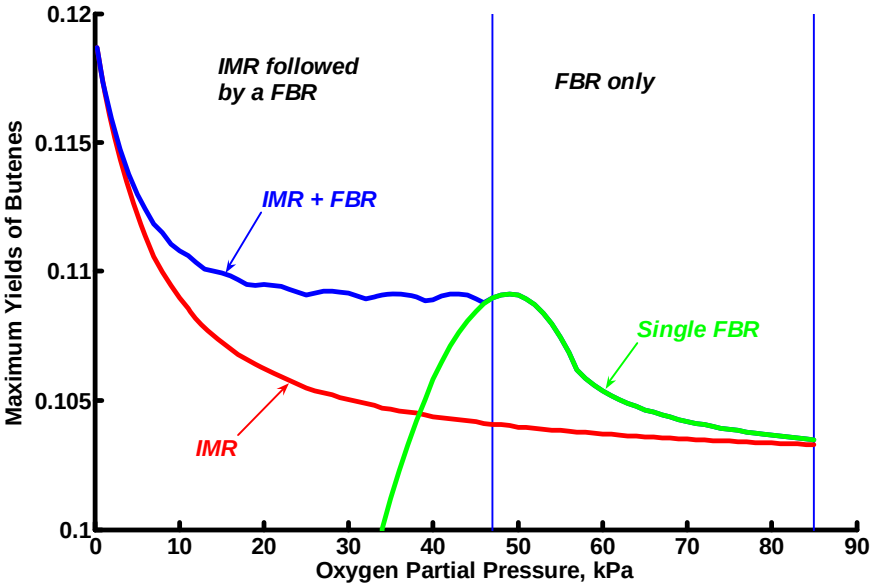


Figure 8.22. Profiles of maximum yields of butenes and reactor configurations as functions of oxygen partial pressures from a series combination of an IMR followed by a FBR.

Figure 8.22 shows the maximum yields of butenes from the initial IMR and when the IMR is followed by a FBR. For oxygen partial pressures from 85 kPa to 47 kPa, the IMR was by-passed and the initial feed stream of *n*-butane and oxygen was supplied directly to a FBR in this way obtaining better yields of butenes than could have been derived from an IMR followed by a FBR. This means that for oxygen partial pressures equal to or greater than 47 kPa, the yields of butenes from a single FBR are greater than those from an IMR when the constant oxygen partial pressure policy in the latter reactor is adopted.

At oxygen partial pressures from 46 kPa to 0.25 kPa, the best yields of butenes were when an IMR preceded the FBR and the feed to the FBR was taken from the IMR after the ODH reaction had been allowed to proceed for some time. For example, at an oxygen partial pressure of 30 kPa, the ODH

reaction in the IMR was discontinued after three seconds and the mixture of reactants and products then fed to the FBR. In the FBR, the initial oxygen partial pressure was allowed to wane and the maximum yield of butenes, 0.1092 carbon mass fraction, was when the ODH reaction in the FBR had run for fifteen seconds. The combined residence time for both reactors was 18 seconds.

The FBR and IMR mass concentration profiles for *n*-butane and butenes intersect at an oxygen partial pressure of 38 kPa. Above 38 kPa, a FBR yields greater butenes maxima than an IMR. Below this partial pressure, the opposite ensues.

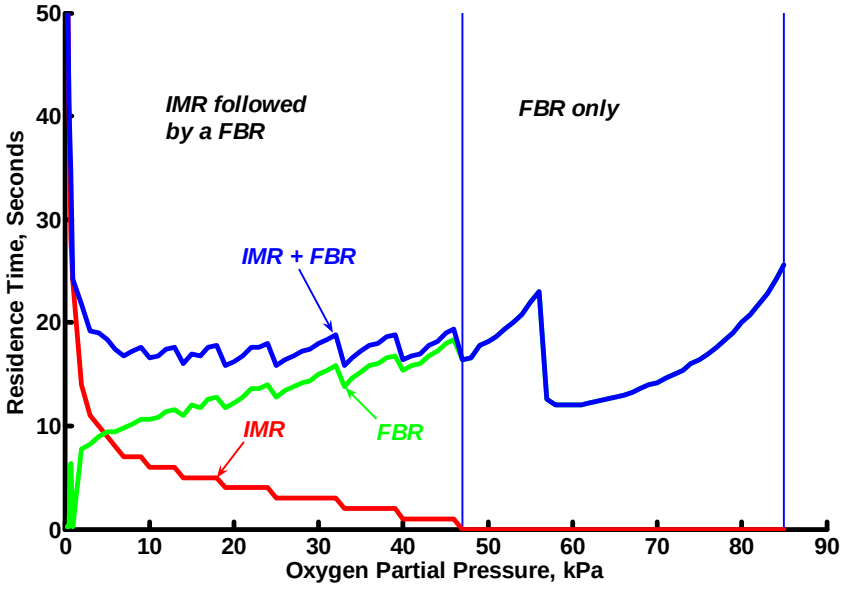


Figure 8.23. Residence times for the maximum yields of butenes from an IMR:FBR series configuration.

Figure 8.23 shows the residence times for the individual reactors and their totals as functions of oxygen partial pressure. For oxygen partial pressures from 85 kPa to 47 kPa, the IMR residence times are nil as the best yields of butenes were when the IMR was by-passed and only the downstream FBR

was employed. At oxygen partial pressures of 46 kPa to 0.25 kPa, the IMR was introduced, initially slowly, i.e. with small residence times, but at a monotonically increased rate. At 46 kPa, the IMR residence time was one second, at 0.25 kPa, it was seventy-five seconds. As the residence times in the IMR increased, the FBR residence times decreased at a steady rate. The FBR residence time at 46 kPa was eighteen seconds, at 0.25 kPa it was less than a second.

The abrupt increase in the FBR residence time from an oxygen partial pressure of 57 kPa to 56 kPa is explained by reference to section 8.2.4 where it was shown that at a partial pressure of 56 kPa, the yield of butenes on cessation of the reaction no longer was less than but became equal to the maximum yield thus mandating a longer residence time.

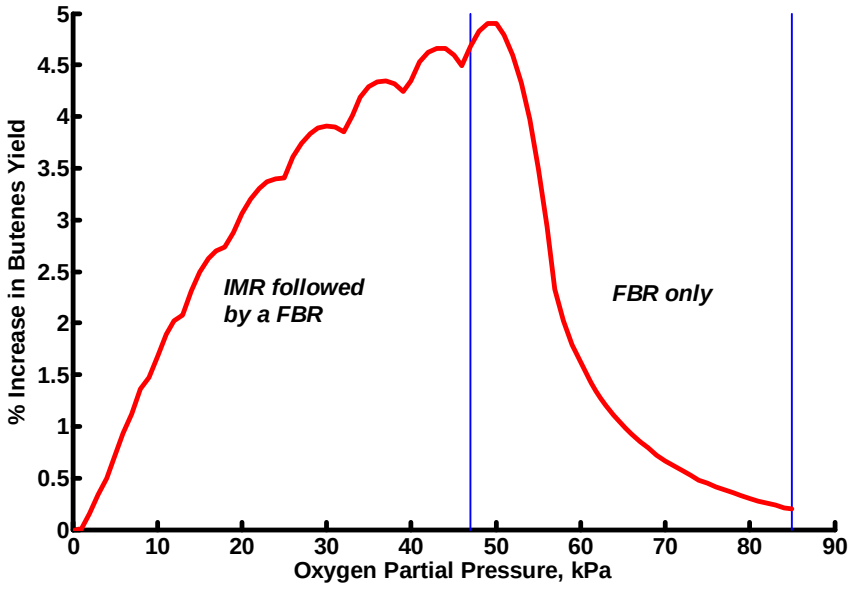


Figure 8.24. Percentage improvement in butenes production from an IMR:FBR series combination over that from a single IMR.

Figure 8.24 shows the percentage improvements in yields of butenes from the IMR:FBR combination relative to those from a single IMR as functions

of oxygen partial pressure. The maximum percentage improvement was 4.9 % at an oxygen partial pressure of 50 kPa. As can be seen from Figure 8.24, this maximum improvement occurred when a single FBR was used. With the introduction of an IMR at 46 kPa, the percentage improvement in yields from the combined reactors decreased and effectively disappeared at 0.25 kPa.

The results of this investigation into the use of an IMR:FBR combination in the ODH of *n*-butane to butenes are shown in Table 8.3.

Oxygen Partial Pressure, kPa	Residence Time, Seconds	Maximum IMR Butenes Yield	Maximum IMR:FBR Butenes Yield	% Increase in IMR:FBR Butenes Yield over IMR Yield
85	26	0.1033	0.1035	0.2
84	24	0.1033	0.1035	0.2
83	23	0.1033	0.1036	0.2
82	22	0.1033	0.1036	0.3
81	21	0.1033	0.1036	0.3
80	20	0.1034	0.1037	0.3
79	19	0.1034	0.1037	0.3
78	18	0.1034	0.1037	0.4
77	18	0.1034	0.1038	0.4
76	17	0.1034	0.1038	0.4
75	16	0.1034	0.1039	0.4
74	16	0.1034	0.1039	0.5
73	15	0.1035	0.1040	0.5
72	15	0.1035	0.1041	0.6
71	15	0.1035	0.1041	0.6
70	14	0.1035	0.1042	0.7
69	14	0.1035	0.1043	0.7
68	14	0.1035	0.1044	0.8
67	13	0.1036	0.1044	0.9
66	13	0.1036	0.1045	0.9
65	13	0.1036	0.1046	1.0
64	13	0.1036	0.1048	1.1
63	12	0.1036	0.1049	1.2

Oxygen Partial Pressure, kPa	Residence Time, Seconds	Maximum IMR Butenes Yield	Maximum IMR:FBR Butenes Yield	% Increase in IMR:FBR Butenes Yield over IMR Yield
62	12	0.1037	0.1050	1.3
61	12	0.1037	0.1052	1.5
60	12	0.1037	0.1054	1.6
59	12	0.1037	0.1056	1.8
58	12	0.1038	0.1059	2.0
57	13	0.1038	0.1062	2.3
56	23	0.1038	0.1069	2.9
55	22	0.1038	0.1075	3.5
54	21	0.1038	0.1080	4.0
53	20	0.1039	0.1084	4.3
52	19	0.1039	0.1087	4.6
51	19	0.1039	0.1089	4.8
50	18	0.1040	0.1091	4.9
49	18	0.1040	0.1091	4.9
48	17	0.1041	0.1091	4.8
47	16	0.1041	0.1090	4.7
46	19	0.1041	0.1088	4.5
45	19	0.1042	0.1090	4.6
44	18	0.1042	0.1091	4.7
43	18	0.1043	0.1091	4.7
42	17	0.1043	0.1091	4.6
41	17	0.1043	0.1090	4.5
40	16	0.1044	0.1089	4.3
39	19	0.1044	0.1089	4.2
38	19	0.1045	0.1090	4.3
37	18	0.1046	0.1091	4.3
36	18	0.1046	0.1091	4.3
35	17	0.1047	0.1091	4.3
34	17	0.1047	0.1091	4.2
33	16	0.1048	0.1090	4.0
32	19	0.1049	0.1089	3.9
31	18	0.1050	0.1091	3.9
30	18	0.1050	0.1092	3.9
29	17	0.1051	0.1092	3.9
28	17	0.1052	0.1092	3.8

Oxygen Partial Pressure, kPa	Residence Time, Seconds	Maximum IMR Butenes Yield	Maximum IMR:FBR Butenes Yield	% Increase in IMR:FBR Butenes Yield over IMR Yield
27	17	0.1053	0.1092	3.7
26	16	0.1054	0.1092	3.6
25	16	0.1055	0.1091	3.4
24	18	0.1056	0.1092	3.4
23	18	0.1058	0.1093	3.4
22	18	0.1059	0.1094	3.3
21	17	0.1061	0.1095	3.2
20	16	0.1062	0.1095	3.1
19	16	0.1064	0.1095	2.9
18	18	0.1066	0.1095	2.7
17	18	0.1068	0.1097	2.7
16	17	0.1070	0.1098	2.6
15	17	0.1073	0.1099	2.5
14	16	0.1075	0.1100	2.3
13	18	0.1078	0.1101	2.1
12	17	0.1082	0.1104	2.0
11	17	0.1086	0.1106	1.9
10	17	0.1090	0.1108	1.7
9	18	0.1095	0.1111	1.5
8	17	0.1100	0.1115	1.4
7	17	0.1106	0.1118	1.1
6	17	0.1114	0.1124	0.9
5	18	0.1122	0.1130	0.7
4	19	0.1132	0.1138	0.5
3	19	0.1144	0.1148	0.3
2	22	0.1158	0.1159	0.2
1	24	0.1173	0.1173	0
0.75	34	0.1178	0.1178	0
0.50	41	0.1182	0.1182	0
0.25	75	0.1187	0.1187	0

Table 8.3. Maximum yields of butenes from an IMR and a FBR in series as functions of oxygen partial pressures

In Table 8.3, the oxygen partial pressure (kPa) is that of the initial IMR (where it is maintained at this constant value) and that in the feed to the succeeding FBR where it is permitted to wane through the normal ODH process.

The second column gives the combined residence time (seconds) from the IMR and the FBR that resulted in the maximum yield of butenes shown in column 4.

The maximum yield of butenes in column 3 of Table 8.3 is that from an IMR where the initial and constant oxygen partial pressure is that shown in the first column.

In column 4 the maximum IMR:FBR yield of butenes is that from the IMR:FBR series combination, the combined residence times being shown in column 2.

The last column of Table 8.3 shows the percentage increase in yield of butenes from the IMR:FBR series combination relative to the IMR. The maximum percentage advantage occurs at an oxygen partial pressure of 50 kPa.

Conclusions.

At oxygen partial pressures greater than or equal to 38 kPa, a single FBR produces greater yields of butadiene than does an IMR operated under a constant oxygen partial regime. Below 38 kPa, the converse applies.

For oxygen partial pressures above 46 kPa in the ODH of *n*-butane, a single FBR provides better yields of butenes than does a single IMR. For oxygen partial pressure less than 47 kPa, an IMR:FBR series combination provides better yields of butenes than does a single IMR.

The maximum percentage differential, 4.9 %, between the best butenes yield relative to a single IMR comes from a single FBR and occurs at an oxygen partial pressure of 50 kPa.

The greatest concentration of butenes, 0.1187 carbon mass fraction, is at an oxygen partial pressure of 0.25 kPa from an IMR with a residence of 75 seconds followed by a FBR with a residence time less than one second.

The convexification of the IMR concave areas through a strategy of by-pass and mixing failed to produce yields of butenes from the down-stream FBR better than otherwise could have been obtained.

8.3.4 Case 4 – The ODH of *n*-butane to butenes; a FBR followed by an IMR

In Case 4 the reactor configuration is as was shown in Figure 8.14.

In 8.2.4 above, we identified the characteristics in mass concentration space of the profile for the ODH of *n*-butane to butenes (all three isomers) in a FBR. For all oxygen partial pressures from 85 kPa to 0.25 kPa, the profiles all were convex. The other distinguishing feature of the profile was that for all oxygen partial pressures less than 57 kPa the concentration of butenes when the ODH reaction ended was the same as the maximum yield attained from the reaction.

The results for the ODH of *n*-butane to butenes in a FBR followed by an IMR are shown in Figure 8.25.

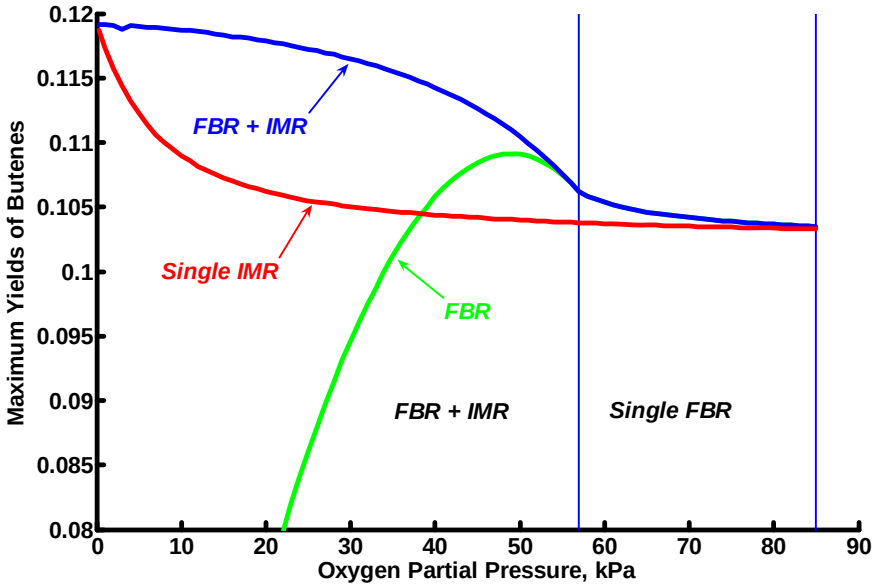


Figure 8.25. Profiles of maximum yields of butenes and reactor configurations as functions of oxygen partial pressures from a series combination of a FBR followed by an IMR.

The interpretation of Figure 8.25 is that a single FBR over the range of oxygen partial pressures from 85 kPa to 57 kPa resulted in greater yields of butenes than did the series combination of a FBR followed by an IMR. The reason for this is to be found in the criteria for reaction termination described at the start of this chapter. For all oxygen partial pressures over this range when the feeds from the FBR were supplied to the downstream IMR and when the IMR ODH reaction was permitted to run for 2 500 seconds, it was found that the differences between the minimum and maximum yields of butenes from the IMR all were less than 0.0001 carbon mass fraction. This meant that over this range of residence time the profile of butenes yields from the IMR was flat and that these yields varied but insignificantly relative to those in the feed streams. Consequently, it was concluded that the addition of an IMR resulted in no benefit and, accordingly, the best yields of butenes emanated from a single FBR.

Referring again to Figure 8.25, there is a change in the profile of maximum yields of butenes at an oxygen partial pressure of 56 kPa. The increase of 0.0007 carbon mass fraction in butenes' yields from 0.1062 (57 kPa) to 0.1069 (56 kPa), an increase of 0.0007 in itself may seem insignificant but when considered in the context of previous maximum increments of 0.0003 deserves an explanation. This can be done through an analysis of Figure 8.26 and Figure 8.27.

The FBR and IMR mass concentration profiles for *n*-butane and butenes intersect at an oxygen partial pressure of 38 kPa. Above 38 kPa, a FBR yields greater butenes maxima than an IMR. Below this partial pressure, the opposite ensues.

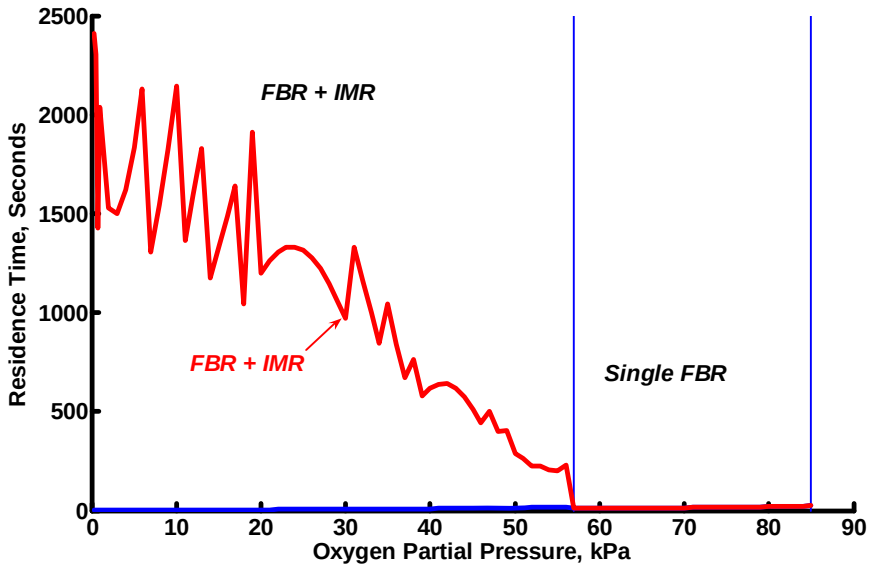


Figure 8.26. Residence times for the maximum yields of butenes from a FBR:IMR series configuration.

The residence time profile for the FBR, difficult to ascertain in Figure 8.26, can be shown more clearly if Figure 8.26 is redrawn with the *y*-axis plotted on a log scale. See Figure 8.27.

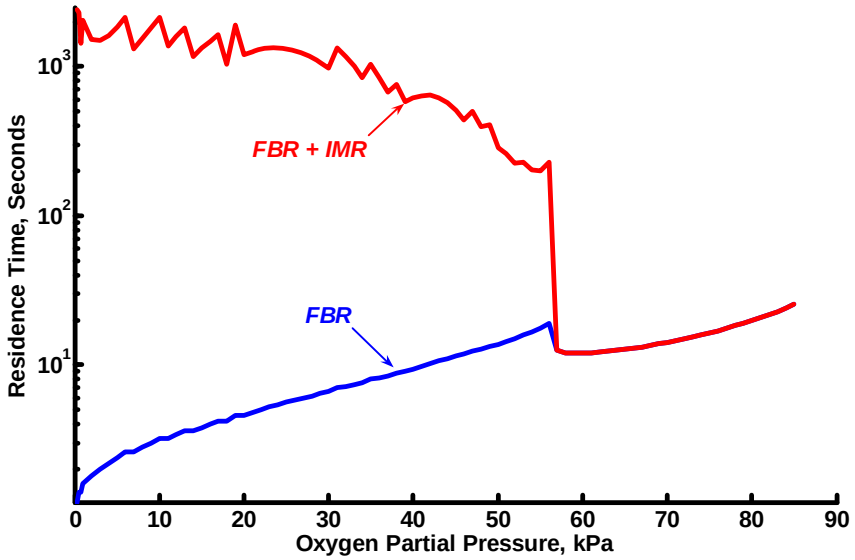


Figure 8.27 Residence times for the maximum yields of butenes from a FBR:IMR series configuration (linear:log scale).

The residence time profile for the maximum yields of butenes from a FBR shows a steady decline from 26 seconds at 85 kPa to 13 seconds at 57 kPa. The residence time for 56 kPa is 19 seconds, an increase of 6 seconds or 46 %. Why?

In 8.2.4 above, I remarked upon the mass concentration profile change for the ODH of *n*-butane to butenes below an oxygen partial pressure of 57 kPa. For oxygen partial pressures from 85 kPa to 57 kPa, the maximum yield of butenes is greater than the yield upon reaction termination and the residence time for maximum yield is less than that at termination. At a partial pressure of 57 kPa the maximum yield coincides with the yield at termination and as the partial pressure is reduced below 57 kPa, the maximum yield and the

yield at reaction termination are one and the same. Simply expressed, this means that the residence time for maximum yield of butenes at 56 kPa is greater than that at 57 kPa because the reaction has to run for a longer time.

For the FBR and IMR series, the combined residence time is 228 seconds at 56 kPa and it then increases to 2 409 seconds at 0.25 kPa.

As was noticed in Case 2, the ODH of *n*-butane to butadiene in a FBR followed by an IMR, the total residence time profile in Figure 8.26 exhibits a similar degree of randomness. This randomness was explained by adopting the same analytical process as in Case 2, namely the causal relationship between oxygen partial pressure and residence time.

The residence time in the IMR is plotted in Figure 8.28 for each oxygen partial pressure in the feed to the FBR. Also plotted is the reciprocal of the inlet (and constant) oxygen partial pressure to the IMR from the FBR.

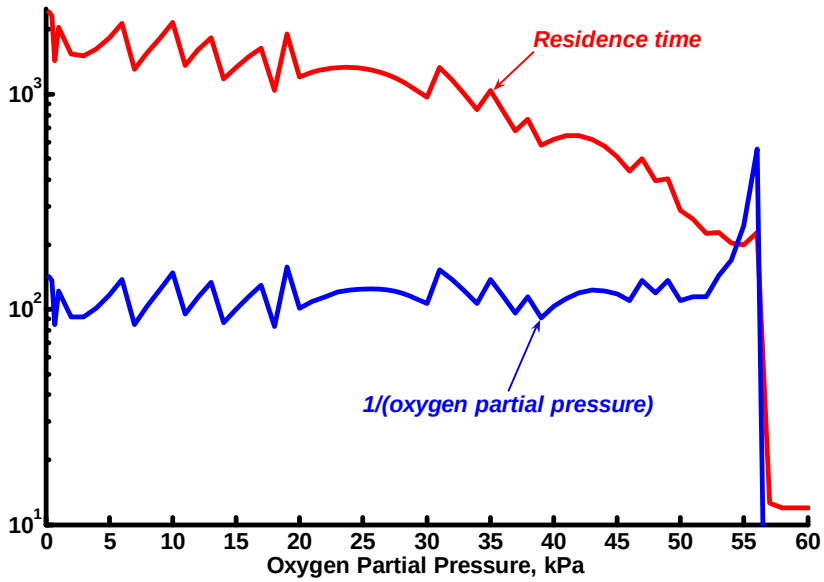


Figure 8.28. Representation of the influence of oxygen partial pressure upon residence time for the maximum yields of butenes from a FBR:IMR series configuration (linear:log scale).

There is a marked commonality in the two profiles in that the nadirs and zeniths of each align exactly and at the same oxygen partial pressure. The *y*-axis of Figure 8.28 neither shows a title nor an indication of the relevant units, the purpose of Figure 8.28 being to draw attention to the causal link between the inverse of oxygen partial pressure and residence time.

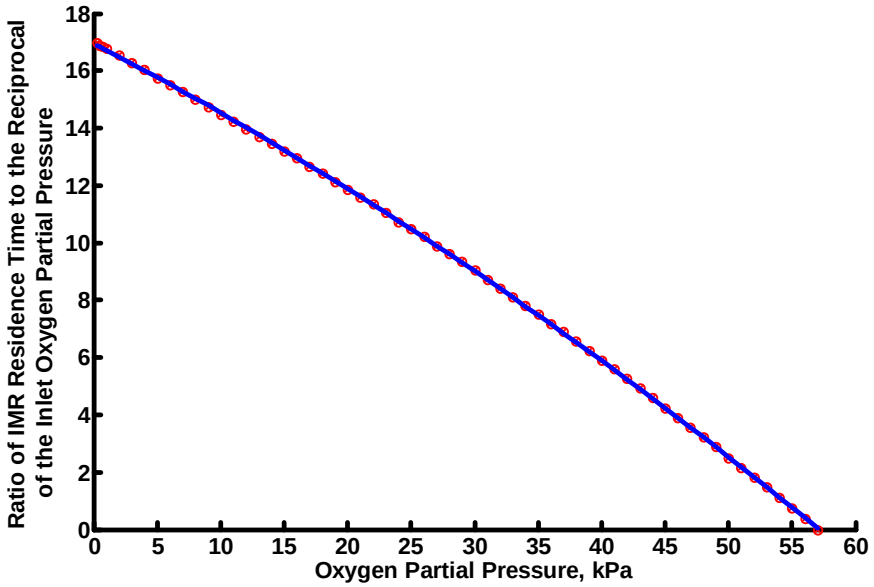


Figure 8.29. Ratio of IMR residence time and reciprocal of oxygen partial pressure as a function of oxygen partial pressure.

Figure 8.29 shows the ratio of the IMR residence time and the inverse of the IMR oxygen partial pressure (in reality, the product of the residence time and partial pressure) against the inlet oxygen partial pressure to the FBR. The respective values are shown in red.

In Figure 8.29, a second-order polynomial curve (shown in blue) was found to give the best fit to the results (shown in red).

The equation of this polynomial curve is ;

$$Y = -1.1690e\text{-}3X^2 - 229.7525e\text{-}3X + 16.9514 \quad (5)$$

where

X = the oxygen partial pressure (kPa) in the feed to the initial FBR.

Y = Ratio of oxygen partial pressure leaving the FBR (and entering the IMR) and the reciprocal of the residence time (seconds) required to obtain the maximum yield of butenes from the IMR.

From this mathematical expression, for each value of oxygen partial pressure in the inlet feed to the FBR either the residence time in the IMR to maximise the yield of butenes or the required oxygen partial pressure in the stream from the FBR can be obtained provided one of the latter two is known.

Another word of caution nevertheless is necessary. The second-order polynomial expression describes a relationship existing in a two-dimensional projection from a ten-dimensional surface, the ten dimensions being the nine chemical species plus residence time. The relationship required to take account of all ten dimensions would not be as simple and as neat as that that characterises Equation 5 above.

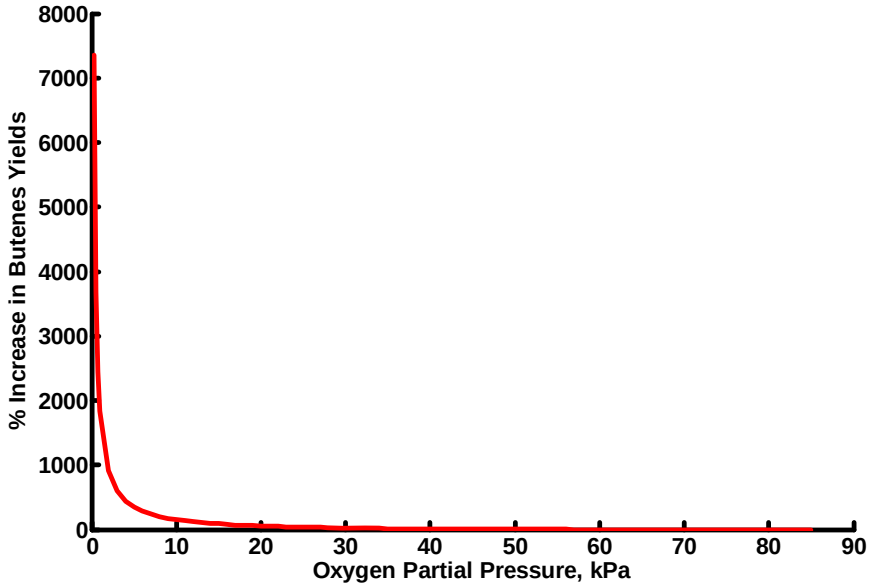


Figure 8.30. Percentage improvement in butenes production from a FBR:IMR series combination over that from a single FBR.

Figure 8.30 shows the percentage benefit in butenes' yields from an IMR:FBR series combination over that from a single FBR. When Figure 8.30 is redrawn on a linear-log scale, the percentage improvement in yields of butenes is easier to observe. See Figure 8.31.

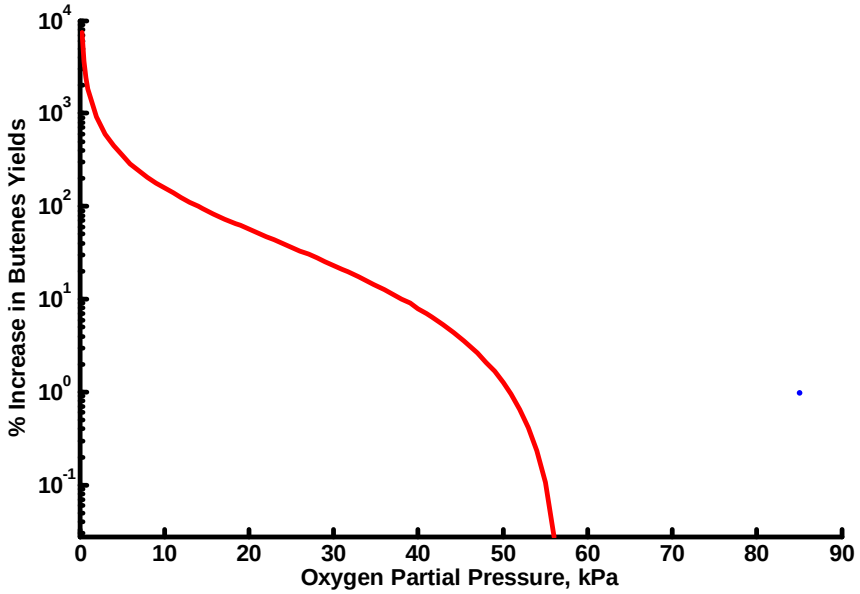


Figure 8.31. Percentage improvement in butenes production from a FBR:IMR series combination over that from a single FBR (linear:log scale).

There is no real benefit in enhanced yields of butenes from the series combination of a FBR and an IMR relative to a single FBR over the range from 85 kPa to 57 kPa. The advantage only begins to be manifested below this lower oxygen partial pressure. Over the range of partial pressures from 56 kPa to 0.25 kPa the percentage improvement in butenes' yields from the FBR:IMR series combination over those from a single FBR increases monotonically and reaches its maximum of 7 346 % at an oxygen partial pressure of 0.25 kPa.

The results of this study into the use of a FBR:IMR series combination for the ODH of *n*-butane to butenes are shown in Table 8.4.

Oxygen Partial Pressure, kPa	Residence Time, Seconds	Maximum FBR Butenes Yield	Maximum FBR:IMR Butenes Yield	% Increase in FBR:IMR Butenes Yield over FBR Yield
85	26	0.1035	0.1035	0
84	24	0.1035	0.1035	0
83	23	0.1036	0.1036	0
82	22	0.1036	0.1036	0
81	21	0.1036	0.1036	0
80	20	0.1037	0.1037	0
79	19	0.1037	0.1037	0
78	18	0.1037	0.1037	0
77	18	0.1038	0.1038	0
76	17	0.1038	0.1038	0
75	16	0.1039	0.1039	0
74	16	0.1039	0.1039	0
73	15	0.1040	0.1040	0
72	15	0.1041	0.1041	0
71	15	0.1041	0.1041	0
70	14	0.1042	0.1042	0
69	14	0.1043	0.1043	0
68	14	0.1044	0.1044	0
67	13	0.1044	0.1044	0
66	13	0.1045	0.1045	0
65	13	0.1046	0.1046	0
64	13	0.1048	0.1048	0
63	12	0.1049	0.1049	0
62	12	0.1050	0.1050	0
61	12	0.1052	0.1052	0
60	12	0.1054	0.1054	0
59	12	0.1056	0.1056	0
58	12	0.1059	0.1059	0
57	13	0.1062	0.1062	0
56	228	0.1069	0.1069	0
55	200	0.1075	0.1076	0
54	204	0.1080	0.1082	0
53	227	0.1084	0.1088	0
52	224	0.1087	0.1094	1
51	263	0.1089	0.1100	1

Oxygen Partial Pressure, kPa	Residence Time, Seconds	Maximum FBR Butenes Yield	Maximum FBR:IMR Butenes Yield	% Increase in FBR:IMR Butenes Yield over FBR Yield
50	287	0.1091	0.1105	1
49	406	0.1091	0.1109	2
48	398	0.1091	0.1114	2
47	501	0.1090	0.1118	3
46	441	0.1088	0.1122	3
45	511	0.1085	0.1126	4
44	574	0.1081	0.1130	5
43	617	0.1076	0.1133	5
42	641	0.1071	0.1136	6
41	639	0.1065	0.1139	7
40	618	0.1058	0.1142	8
39	578	0.1050	0.1145	9
38	763	0.1042	0.1148	10
37	673	0.1033	0.1150	11
36	840	0.1023	0.1153	13
35	1043	0.1012	0.1155	14
34	844	0.1000	0.1157	16
33	1000	0.0988	0.1159	17
32	1159	0.0975	0.1161	19
31	1332	0.0961	0.1163	21
30	969	0.0946	0.1165	23
29	1063	0.0931	0.1166	25
28	1146	0.0915	0.1168	28
27	1221	0.0897	0.1170	30
26	1277	0.0880	0.1171	33
25	1313	0.0861	0.1173	36
24	1329	0.0841	0.1174	40
23	1329	0.0820	0.1175	43
22	1307	0.0799	0.1176	47
21	1262	0.0777	0.1178	52
20	1200	0.0754	0.1179	56
19	1913	0.0729	0.1180	62
18	1043	0.0704	0.1181	68
17	1640	0.0678	0.1182	74
16	1487	0.0651	0.1183	82

Oxygen Partial Pressure, kPa	Residence Time, Seconds	Maximum FBR Butenes Yield	Maximum FBR:IMR Butenes Yield	% Increase in FBR:IMR Butenes Yield over FBR Yield
15	1329	0.0622	0.1184	90
14	1174	0.0593	0.1184	100
13	1831	0.0562	0.1185	111
12	1592	0.0530	0.1186	124
11	1363	0.0497	0.1187	139
10	2145	0.0462	0.1187	157
9	1824	0.0426	0.1188	179
8	1545	0.0389	0.1189	206
7	1305	0.0349	0.1189	241
6	2129	0.0308	0.1190	287
5	1836	0.0264	0.1190	350
4	1622	0.0218	0.1190	445
3	1498	0.0170	0.1191	602
2	1528	0.0118	0.1191	912
1	2038	0.0062	0.1191	1835
0.75	1429	0.0047	0.1191	2448
0.50	2304	0.0032	0.1191	3674
0.25	2409	0.0016	0.1191	7346

Table 8.4. Maximum yields of butenes from a FBR and an IMR in series as functions of oxygen partial pressures

In Table 8.4, the oxygen partial pressure (kPa) is that to the initial FBR and where it is permitted to wane through the normal ODH process.

A value in the second column connotes the combined residence time (seconds) from the FBR and the IMR that resulted in the maximum yield of butenes shown in column 4.

The maximum FBR yield of butenes in column 3 of Table 8.4 is that from a FBR where the initial oxygen partial pressure is that shown in the first column.

In column 4 the maximum FBR:IMR yield of butene is that from an IMR preceded by a FBR and after the combined residence time shown in column 2.

The last column of Table 8.4 shows the percentage increase in yield of butenes from the FBR:IMR series combination relative to the FBR. The maximum percentage advantage occurs at an oxygen partial pressure of 0.25 kPa.

Conclusions

At oxygen partial pressures greater than or equal to 38 kPa, a single FBR produces greater yields of butadiene than does an IMR operated under a constant oxygen partial regime. Below 38 kPa, the converse applies.

For the ODH of *n*-butane to butenes over the range of 85 kPa to 57 kPa, a single FBR produces maximum yields of butenes better than can be obtained from a series combination of a FBR and an IMR. Below 57 kPa, the converse applies.

The best yield of butenes from a single FBR is 0.1091 carbon mass fraction at an oxygen partial pressure of 49 kPa and with a residence time of 16 seconds. Residual concentration of *n*-butane is 0.6337 carbon mass fraction (see Chapter 3 and Figure 3.3 of this thesis).

The maximum yield of butenes, 0.1191 carbon mass fraction, is obtained when the oxygen partial pressure in the feed to the FBR is 0.25 kPa. This yield of butenes requires a total residence time of 2 409 seconds.

The relationship between the inlet oxygen partial pressure to the FBR and the product of IMR residence time and constant oxygen partial pressure can be expressed in two-dimensional mass fraction concentration space by a second-order polynomial equation.

The convexification of the concave region in the FBR profiles for *n*-butane and butenes did not improve the yield of butenes either from the single FBR or from the down-stream IMR.

8.3.5 Case 5 – The ODH of *1*-butene to butadiene; an IMR followed by a FBR

In Case 5 the reactor configuration is as was shown in Figure 8.9.

In 8.2.5 above, we identified the characteristics in mass concentration space of the profile for the ODH of *1*-butane to butadiene in an IMR. For all oxygen partial pressures from 85 kPa to 0.25 kPa, the profiles all were convex.

The results for the ODH of *1*-butane to butadiene in an IMR followed by a FBR are shown in Figure 8.32.

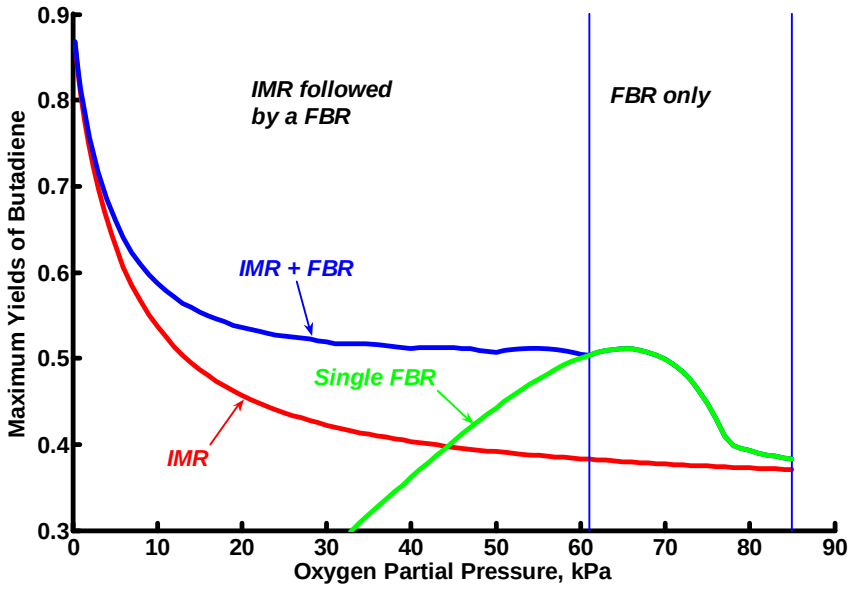


Figure 8.32. Profiles of maximum yields of butadiene and reactor configurations as functions of oxygen partial pressures from a series combination of an IMR followed by a FBR.

Examination of Figure 8.32 shows that there are two distinct regions each with its characteristic reactor configuration required to give the maximum yields of butadiene from the ODH of *1*-butene in a series combination of an IMR followed by a FBR.

The first region encompasses oxygen partial pressures from 85 kPa to 61 kPa. Within this region a single FBR provided greater yields of butadiene than a single IMR and the series combination of an IMR and a FBR in itself does not result in maximum yield of butadiene in excess of those derived from a single FBR. In this region, the IMR effectively was bypassed and the initial feed of *1*-butene and oxygen supplied directly to the FBR.

The second region spans oxygen partial pressures from 60 kPa to 0.25 kPa. In this region, the series combination of an IMR followed by a FBR gives butadiene maxima better than a single IMR. The butadiene profile for the two reactors is fairly flat over the partial pressure range of 60 kPa to approximately 15 kPa below which it begins to climb steeply, attaining its greatest value of 0.8686 carbon mass fraction at 0.25 kPa.

The FBR and IMR mass concentration profiles for *n*-butane and butadiene intersect at an oxygen partial pressure of 44 kPa above which pressure maximum yields of butadiene from a FBR greater than those from an IMR are possible. Below 44 kPa the opposite happens.

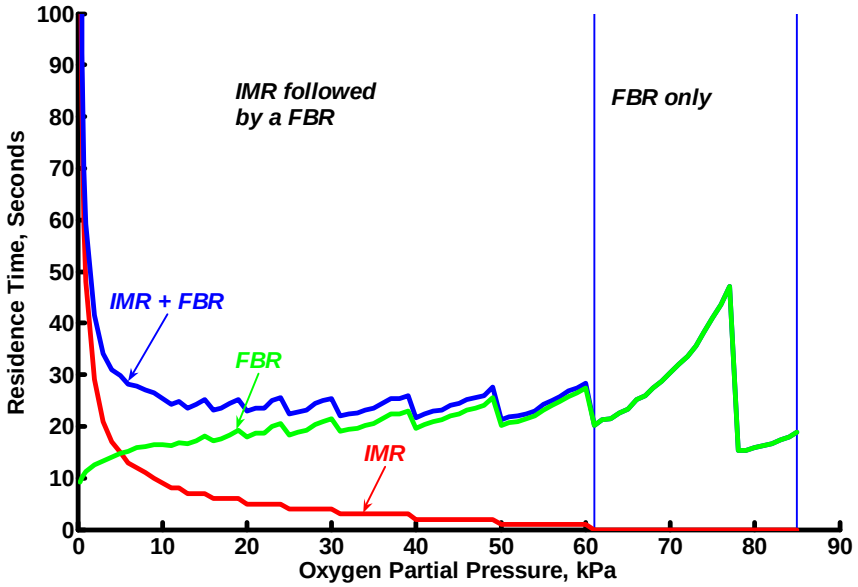


Figure 8.33. Residence times for the maximum yields of butadiene from an IMR:FBR series configuration.

A feature of Figure 8.33 is the "saw-toothed" profile of the FBR residence time. The maximum "jump" from 20 seconds to 28 seconds occurs between 61 kPa and 60 kPa and represents a 40 % increase in residence time. It is surmised that this is caused by insensitivity in the mathematical model in assessing when the FBR reaction is completed, i.e. the residence time at which the imposed constraint upon the initial oxygen partial pressure has been effected. This constraint deemed the reaction to have been ended once the oxygen partial pressure in the FBR had fallen to less than 0.00001 kPa. This "saw-toothed" pattern repeated itself between 51 kPa and 50 kPa also with a 40 % increase in residence time. Similar increases occurred at below 50 kPa at intervals of 10 kPa but with diminishing amplitudes.

Figure 8.33 shows the various residence times as functions of oxygen partial pressure. From a partial pressure of 85 kPa to 61 kPa, the IMR residence time is nought. The relevant time for the FBR (and the series combination of

the two reactors) shows a spike at an oxygen partial pressure of 77 kPa. Reference to 8.2.5 provides the explanation for this abrupt change. This partial pressure marks the point where the butadiene concentration on termination of the ODH reaction in a FBR ceases to be less than the maximum concentration and instead becomes equal to it and where previously a relative short residence time was required to reach the maximum point on the profile now the length of the profile is greater and with it a greater residence time than at 78 kPa. The FBR residence time then decreases over the range from 77 kPa to 61 kPa but in an irregular manner.

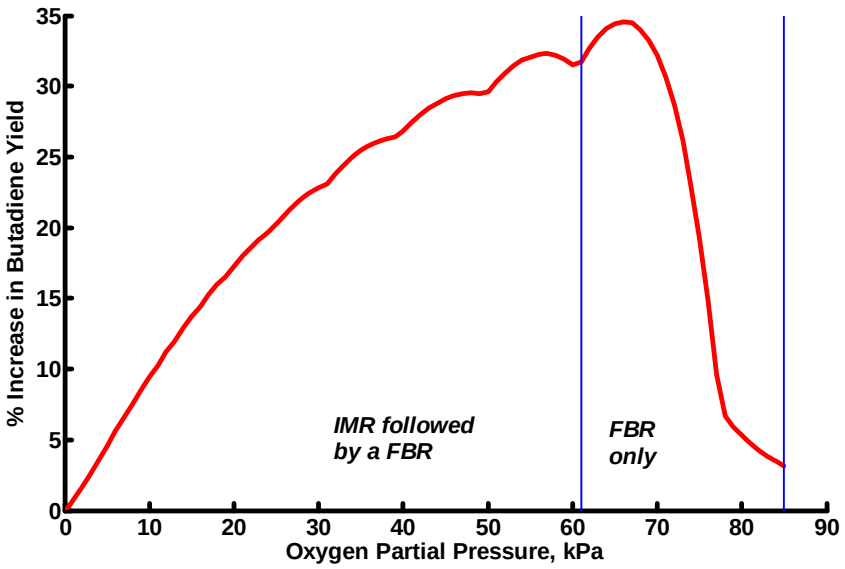


Figure 8.34. Percentage improvement in butadiene production from an IMR:FBR series combination over that from a single IMR.

Figure 8.34 shows the percentage increase in yields of butadiene from the IMR:FBR series combination over those from a FBR. The maximum increase of 34.6 % occurs at an oxygen partial pressure of 66 kPa. Over the range of oxygen partial pressures from 85 kPa to 61 kPa maxima butadiene yields from a FBR exceed those from an IMR. Below 61 kPa, the resultant percentage declines and at 0.25 kPa is less than 1 %.

The results of this investigation into the use of an IMR:FBR series combination for the ODH of *1*-butene to butadiene are shown in Table 8.5.

Oxygen Partial Pressure, kPa	Residence Time, Seconds	Max. IMR Butadiene Yield	Max. IMR:FBR Butadiene Yield	% Increase in IMR:FBR Butadiene Yield over IMR Yield
85	19	0.3709	0.3826	3.2
84	18	0.3713	0.3843	3.5
83	17	0.3717	0.3861	3.9
82	17	0.3721	0.3881	4.3
81	16	0.3724	0.3902	4.8
80	16	0.3728	0.3927	5.3
79	15	0.3732	0.3954	6.0
78	15	0.3736	0.3986	6.7
77	47	0.3740	0.4100	9.6
76	44	0.3744	0.4302	14.9
75	41	0.3749	0.4474	19.3
74	38	0.3754	0.4619	23.1
73	36	0.3758	0.4740	26.1
72	34	0.3763	0.4841	28.6
71	32	0.3768	0.4922	30.6
70	30	0.3773	0.4986	32.2
69	29	0.3778	0.5036	33.3
68	27	0.3784	0.5071	34.0
67	26	0.3789	0.5095	34.5
66	25	0.3796	0.5108	34.6
65	23	0.3801	0.5111	34.4
64	23	0.3807	0.5104	34.1
63	21	0.3814	0.5090	33.4
62	21	0.3820	0.5067	32.7
61	20	0.3827	0.5039	31.7
60	28	0.3834	0.5041	31.5
59	27	0.3840	0.5067	31.9
58	27	0.3848	0.5086	32.2
57	26	0.3855	0.5100	32.3
56	25	0.3862	0.5109	32.3
55	24	0.3871	0.5112	32.1

Oxygen Partial Pressure, kPa	Residence Time, Seconds	Max. IMR Butadiene Yield	Max. IMR:FBR Butadiene Yield	% Increase in IMR:FBR Butadiene Yield over IMR Yield
54	23	0.3879	0.5113	31.8
53	22	0.3887	0.5109	31.4
52	22	0.3896	0.5100	30.9
51	22	0.3906	0.5088	30.3
50	21	0.3915	0.5074	29.6
49	28	0.3925	0.5081	29.5
48	26	0.3934	0.5097	29.5
47	26	0.3946	0.5109	29.5
46	25	0.3957	0.5118	29.3
45	24	0.3969	0.5125	29.1
44	24	0.3981	0.5128	28.8
43	23	0.3993	0.5129	28.5
42	23	0.4006	0.5127	28.0
41	22	0.4020	0.5123	27.4
40	22	0.4035	0.5117	26.8
39	26	0.4050	0.5120	26.4
38	25	0.4066	0.5134	26.3
37	25	0.4082	0.5147	26.1
36	24	0.4099	0.5157	25.8
35	24	0.4117	0.5164	25.4
34	23	0.4136	0.5169	25.0
33	23	0.4157	0.5172	24.4
32	22	0.4178	0.5173	23.8
31	22	0.4202	0.5172	23.1
30	25	0.4226	0.5190	22.8
29	25	0.4251	0.5207	22.5
28	24	0.4278	0.5222	22.1
27	23	0.4307	0.5235	21.6
26	23	0.4337	0.5246	21.0
25	22	0.4370	0.5255	20.3
24	26	0.4405	0.5268	19.6
23	25	0.4442	0.5294	19.2
22	24	0.4482	0.5317	18.6
21	24	0.4525	0.5339	18.0
20	23	0.4571	0.5360	17.2

Oxygen Partial Pressure, kPa	Residence Time, Seconds	Max. IMR Butadiene Yield	Max. IMR:FBR Butadiene Yield	% Increase in IMR:FBR Butadiene Yield over IMR Yield
19	25	0.4622	0.5385	16.5
18	24	0.4677	0.5422	15.9
17	24	0.4736	0.5458	15.3
16	23	0.4800	0.5492	14.4
15	25	0.4870	0.5539	13.7
14	24	0.4951	0.5592	12.9
13	24	0.5040	0.5642	11.9
12	25	0.5137	0.5714	11.2
11	24	0.5244	0.5784	10.3
10	25	0.5370	0.5876	9.4
9	26	0.5507	0.5975	8.5
8	27	0.5667	0.6092	7.5
7	28	0.5852	0.6234	6.5
6	28	0.6065	0.6404	5.6
5	30	0.6319	0.6606	4.6
4	31	0.6621	0.6856	3.5
3	34	0.6991	0.7170	2.6
2	42	0.7452	0.7571	1.6
1	59	0.8050	0.8108	0.7
0.75	70	0.8234	0.8277	0.5
0.50	92	0.8437	0.8465	0.3
0.25	154	0.8672	0.8686	0.2

Table 8.5. Maximum yields of butadiene from an IMR and a FBR in series as functions of oxygen partial pressures

In Table 8.5, the oxygen partial pressure (kPa) is that of the initial IMR (where it is maintained at this constant value) and that in the feed to the succeeding FBR where it is permitted to wane through the normal ODH process.

The second column gives the combined residence time (seconds) from the IMR and the FBR that resulted in the maximum yield of butadiene shown in column 4.

The maximum butadiene yield in column 3 of Table 8.5 is that from an IMR where the initial oxygen partial pressure is that shown in the first column.

In column 4 the maximum IMR:FBR yield of butadiene is that from the IMR:FBR series combination, the combined residence times being shown in column 2.

The last column of Table 8.5 shows the percentage increase in yield of butadiene from the IMR:FBR series combination relative to the IMR. The maximum percentage advantage occurs at an oxygen partial pressure of 66 kPa.

Conclusions

At oxygen partial pressures greater than or equal to 44 kPa, a single FBR produces maximum yields of butadiene greater than does an IMR operated under a constant oxygen partial regime. Below 44 kPa, the converse applies.

For the ODH of *1*-butene to butadiene over the range of 85 kPa to 61 kPa, a single FBR produces maximum yields of butadiene better than can be

obtained from a series combination of a FBR and an IMR. Below 61 kPa, the converse applies.

The maximum yield of butadiene, 0.8686 carbon mass fraction, is obtained when the oxygen partial pressure in the feed to the initial IMR is 0.25 kPa. This yield of butadiene requires a total residence time of 154 seconds.

8.3.6 Case 6 – The ODH of *1*-butene to butadiene; a FBR followed by an IMR

In Case 6 the reactor configuration is as was shown in Figure 8.14.

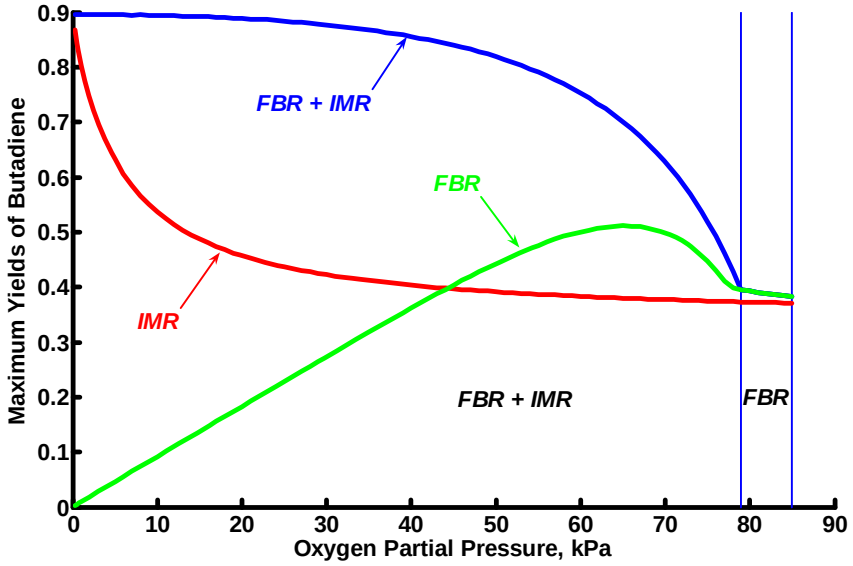


Figure 8.35. Profiles of maximum yields of butadiene and reactor configurations as functions of oxygen partial pressures from a series combination of a FBR followed by an IMR.

The results for the ODH of *1*-butene to butadiene in a FBR followed by an IMR are shown in Figure 8.35.

The interpretation of Figure 8.35 is that a single FBR over the range of oxygen partial pressures from 85 kPa to 79 kPa resulted in greater yields of butadiene than did the series combination of a FBR followed by an IMR. The reason for this is to be found in the criteria for reaction termination described at the start of this chapter. For all oxygen partial pressures over

this range when the feeds from the FBR were supplied to the downstream IMR and when the IMR ODH reaction was permitted to run for 2 500 seconds, it was found that the differences between the minimum and maximum yields of butadiene from the IMR all were less than 0.0001 carbon mass fraction. This meant that over this range of residence time the profile of butadiene yields from the IMR was flat and that these yields varied but insignificantly relative to those in the feed streams. Consequently, it was concluded that the addition of an IMR resulted in no benefit and, accordingly, the best yields of butadiene emanated from a single FBR.

Figure 8.36 shows the residence times for the FBR and the combined FBR and IMR at each value of oxygen partial pressure. These residence times are those required to maximise yields of butadiene.

The FBR and IMR mass concentration profiles for *n*-butane and butadiene intersect at an oxygen partial pressure of 44 kPa above which pressure maximum yields of butadiene from a FBR greater than those from an IMR are possible. Below 44 kPa the opposite happens.

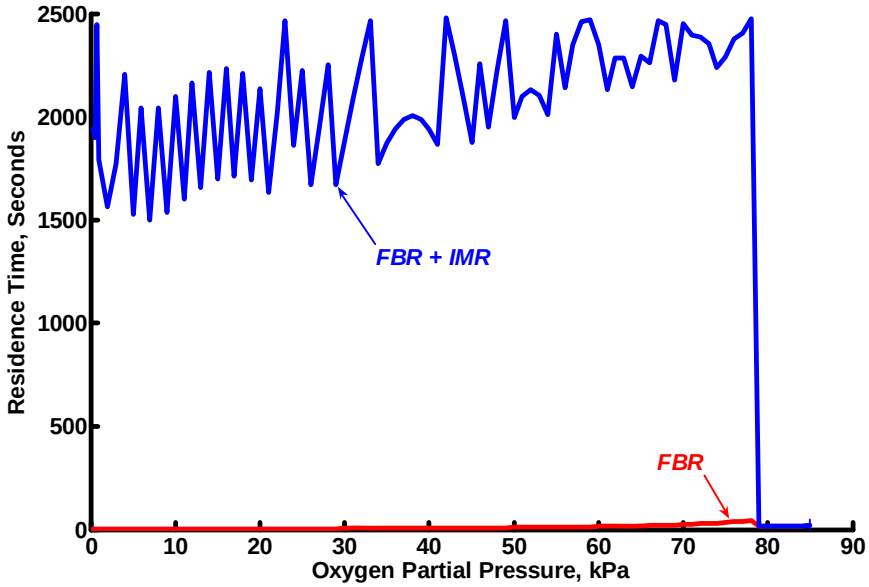


Figure 8.36. Residence times for the maximum yields of butadiene from a FBR:IMR series configuration.

Again, as was noticed in Case 2 and in Case 4, the residence time profile for the combined FBR and IMR displays an apparently haphazard pattern. Nevertheless, an underlying rationale for this pattern emerged through application of the same relationship between oxygen partial pressure and residence time as was found to exist in Case 2 and in Case 4.

Before developing this relationship, Figure 8.36 needs to be discussed further. The FBR residence time profile is difficult to behold as its maximum is but a slight percentage of that for the combined FBR and IMR. Secondly, the residence time profile for the down-stream IMR also is hard to espy because it lies so close to the combined profile as to be well-nigh collinear with it. Figure 8.37 addresses these matters by using a linear-log scale to compress the scale of the *y*-axis.

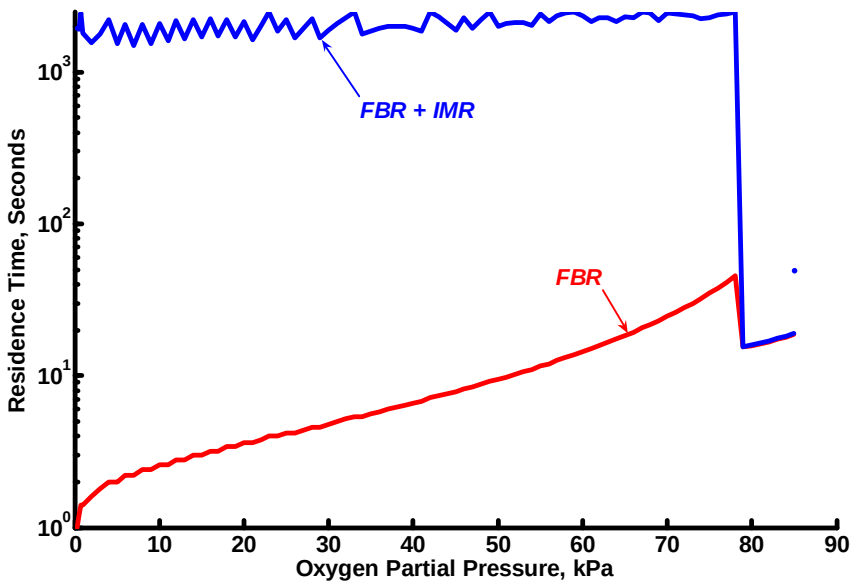


Figure 8.37. Residence times for the maximum yields of butadiene from a FBR:IMR series configuration (linear:log scale).

The residence time profile for the down-stream IMR, despite the use of a log scale for the *y*-axis, is occluded by that for the combined FBR and IMR.

Figure 8.38 shows the residence time profile for the FBR that is required to attain the maximum yield of butadiene from the down-stream IMR.

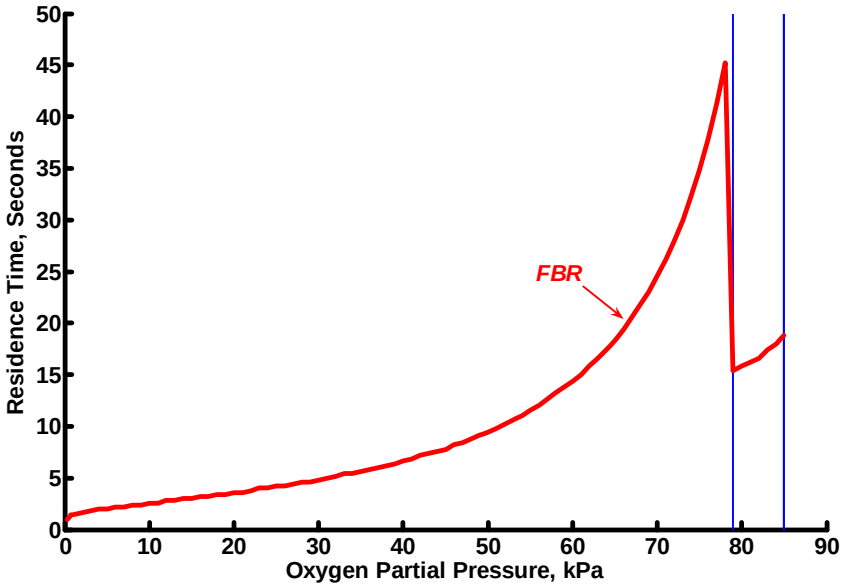


Figure 8.38. Residence times for the maximum yields of butadiene from a FBR.

The maximum FBR residence time is 45 seconds at an oxygen partial pressure of 78 kPa. Earlier in this chapter (8.2.6) it was explained that the mass concentration profile for *1*-butene and butadiene underwent a significant change at an oxygen partial pressure of 77 kPa when the butadiene concentration on termination of the ODH reaction and the maximum yield of butadiene were identical. Above 77 kPa the yield on completion of the reaction had been less than the maximum.

In Figure 8.38, the increase in the FBR residence time occurred at an oxygen partial pressure of 78 kPa and not at 77 kPa as discussed in 8.2.6. The reason for this is that the FBR residence time shown in Figure 8.38 is the residence time at which the maximum yield of butadiene was possible from an IMR when connected to the FBR after this residence time for the latter had elapsed. To put this into its proper context, the maximum yield of butadiene from a stand-alone FBR with an initial oxygen partial pressure of

78 kPa is 0.3986 carbon mass fraction and has an associated residence time of 15 seconds. When an IMR is linked to the FBR the maximum yield of butadiene from the IMR (0.4290) is not after a FBR residence time of 15 seconds but occurs after a FBR residence time of 45 seconds. Referring to Figure 8.6, for the greatest yield of butadiene the IMR has to be connected to the FBR at that part of the FBR profile between Point D and Point E and to attain this section of the FBR profile requires a greater residence time than that required for Point C.

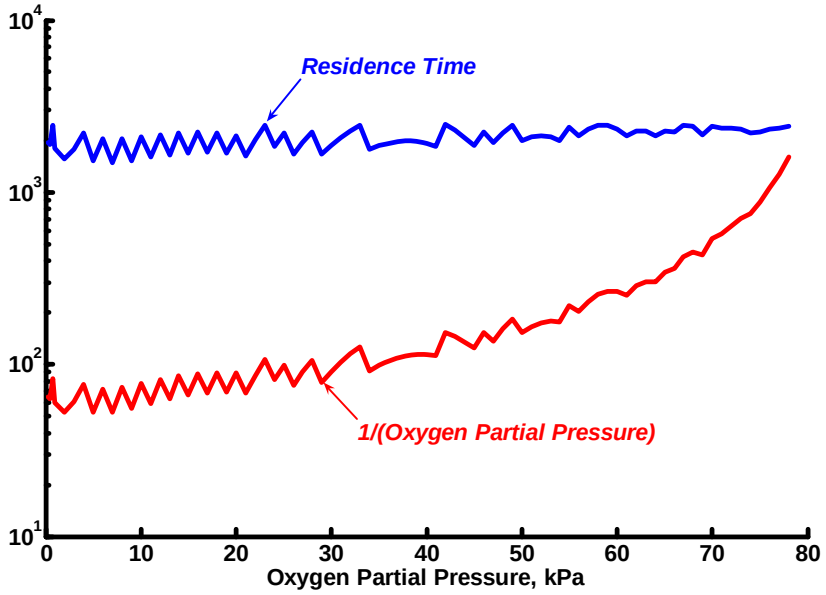


Figure 8.39. Profiles of IMR residence times and reciprocal of oxygen partial pressures.for the maximum yields of butadiene.

Figure 8.39 shows the residence time from the IMR for each value of oxygen partial pressure as well as the inverse of the (constant) oxygen partial pressure in the IMR. The data is plotted on a log-linear scale and, for the reasons specified previously, neither a title nor units are shown for the *y*-axis.

The sequence of peaks and troughs in Figure 8.39 coincide as does the pattern, the latter more noticeable at partial pressures below 70 kPa.

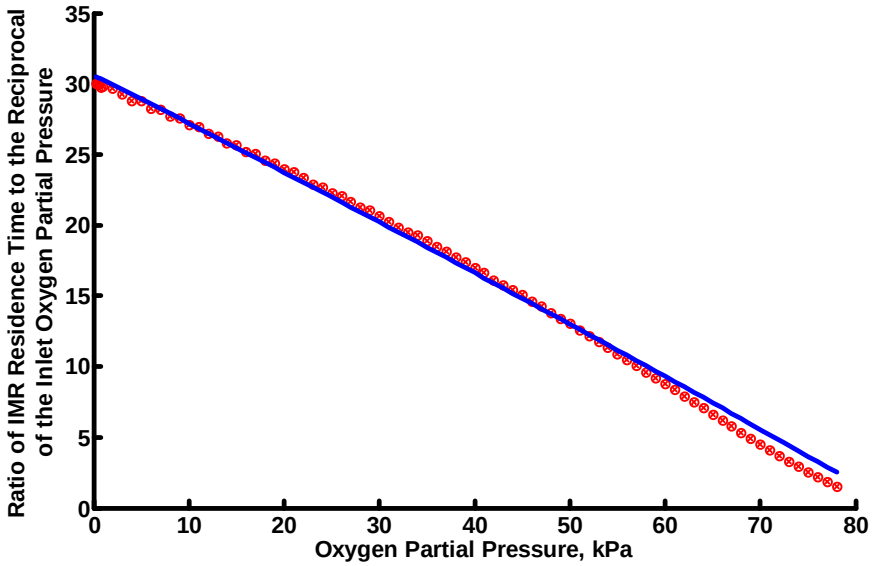


Figure 8.40. Ratio of IMR residence time and reciprocal of oxygen partial pressure as a function of oxygen partial pressure.

In Figure 8.40 the ratio of the IMR residence time and the inverse of the IMR oxygen partial pressure (in reality, the product of the residence time and partial pressure) are shown against the inlet oxygen partial pressure to the FBR. The respective values are shown in red.

A second-order polynomial curve (shown in blue) was found to give the best fit to the results (shown in red).

The equation of this polynomial curve is ;

$$Y = - 290.6662e\text{-}6X^2 - 337.4219e\text{-}3X + 30.6000 \qquad (6)$$

where

X = the oxygen partial pressure (kPa) in the feed to the initial FBR.

Y = Ratio of oxygen partial pressure leaving the FBR (and entering the IMR) and the reciprocal of the residence time (seconds) required to obtain the maximum yield of butadiene from the IMR.

From this mathematical expression, for each value of oxygen partial pressure in the inlet feed to the FBR either the residence time in the IMR to maximise the yield of butadiene or the required oxygen partial pressure in the stream from the FBR can be obtained provided one of the latter two is known.

Another word of caution nevertheless is necessary. The second-order polynomial expression describes a relationship existing in a two-dimensional projection from a seven-dimensional surface, the seven dimensions being the sixe chemical species plus residence time. The relationship required to take account of all seven dimensions would not be as simple and as neat as that that characterises Equation 6 above.

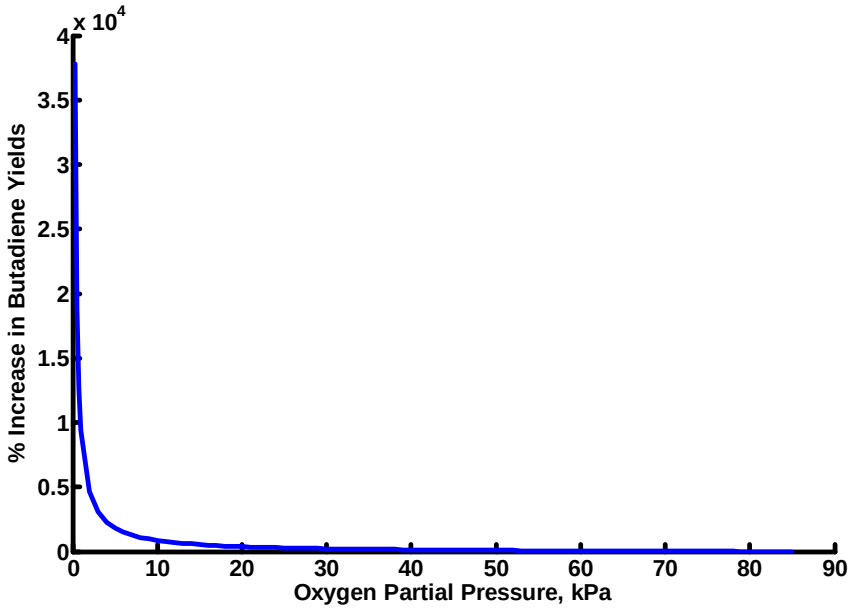


Figure 8.41. Percentage improvement in butadiene production from a FBR:IMR series combination over that from a single FBR.

Figure 8.41 shows the percentage benefit in yields of butadiene from an IMR:FBR series combination over that from a single FBR. When Figure 8.41 is redrawn on a linear-log scale, the percentage improvement in the yields of butadiene is easier to observe.

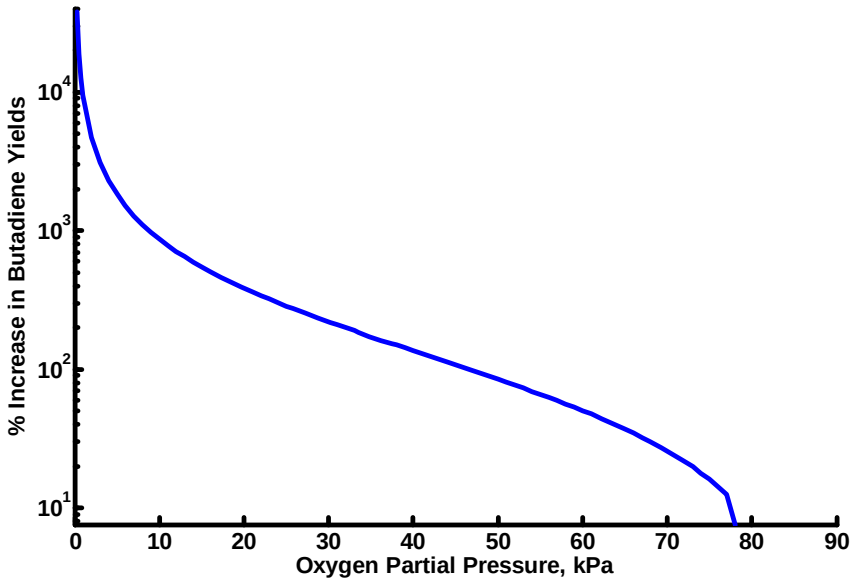


Figure 8.42. Percentage improvement in butadiene production from a FBR:IMR series combination over that from a single FBR (linear:log scale).

There is no real benefit in enhanced yields of butadiene from the series combination of a FBR and an IMR relative to a single FBR over the range from 85 kPa to 79 kPa. The advantage only begins to be manifested below this lower oxygen partial pressure. Over the range of partial pressures from 78 kPa to 0.25 kPa the percentage improvement in yields of butadiene from the FBR:IMR series combination over those from a single FBR increases monotonically and reaches its maximum of 37 828 % at an oxygen partial pressure of 0.25 kPa. Putting this enormous percentage increase into perspective, the concentration of butadiene in the stream exiting the FBR and entering the IMR is 0.0024 carbon mass fraction. In the down-stream IMR this concentration is boosted to 0.8959 carbon mass fraction, an increase of 37 828 %.

The results of this investigation into the use of a FBR:IMR series combination for the ODH of *1*-butene to butadiene are shown in Table 8.6.

Oxygen Partial Pressure, kPa	Residence Time, Seconds	Max. FBR Butadiene Yield	Max. FBR:IMR Butadiene Yield	% Increase in FBR:IMR Butadiene Yield over FBR Yield
85	19	0.3826	0.3826	0
84	18	0.3843	0.3843	0
83	18	0.3861	0.3861	0
82	17	0.3881	0.3881	0
81	16	0.3902	0.3902	0
80	16	0.3927	0.3927	0
79	16	0.3954	0.3954	0
78	2472	0.3986	0.4290	8
77	2403	0.4100	0.4620	13
76	2378	0.4302	0.4921	14
75	2287	0.4474	0.5196	16
74	2237	0.4619	0.5448	18
73	2354	0.4740	0.5681	20
72	2386	0.4841	0.5895	22
71	2394	0.4922	0.6092	24
70	2451	0.4986	0.6275	26
69	2176	0.5036	0.6444	28
68	2446	0.5071	0.6602	30
67	2464	0.5095	0.6748	32
66	2261	0.5108	0.6884	35
65	2295	0.5111	0.7010	37
64	2145	0.5104	0.7128	40
63	2286	0.5090	0.7240	42
62	2282	0.5067	0.7343	45
61	2132	0.5039	0.7440	48
60	2349	0.5005	0.7532	50
59	2469	0.4964	0.7617	53
58	2462	0.4920	0.7698	56
57	2349	0.4870	0.7772	60
56	2140	0.4816	0.7842	63
55	2401	0.4759	0.7910	66
54	2011	0.4698	0.7971	70
53	2102	0.4634	0.8031	73
52	2130	0.4567	0.8087	77

Oxygen Partial Pressure, kPa	Residence Time, Seconds	Max. FBR Butadiene Yield	Max. FBR:IMR Butadiene Yield	% Increase in FBR:IMR Butadiene Yield over FBR Yield
51	2098	0.4497	0.8139	81
50	1994	0.4426	0.8188	85
49	2465	0.4353	0.8238	89
48	2223	0.4277	0.8281	94
47	1949	0.4199	0.8320	98
46	2258	0.4120	0.8362	103
45	1875	0.4040	0.8397	108
44	2090	0.3958	0.8434	113
43	2292	0.3875	0.8468	119
42	2479	0.3791	0.8501	124
41	1866	0.3706	0.8527	130
40	1939	0.3621	0.8556	136
39	1987	0.3534	0.8582	143
38	2003	0.3447	0.8608	150
37	1985	0.3359	0.8631	157
36	1938	0.3271	0.8654	165
35	1868	0.3183	0.8675	173
34	1773	0.3093	0.8694	181
33	2464	0.3004	0.8719	190
32	2284	0.2915	0.8736	200
31	2087	0.2825	0.8751	210
30	1879	0.2735	0.8765	221
29	1669	0.2644	0.8778	232
28	2251	0.2554	0.8798	244
27	1952	0.2464	0.8809	258
26	1670	0.2373	0.8819	272
25	2225	0.2282	0.8836	287
24	1863	0.2191	0.8844	304
23	2464	0.2101	0.8861	322
22	2020	0.2010	0.8866	341
21	1634	0.1919	0.8870	362
20	2136	0.1829	0.8886	386
19	1692	0.1738	0.8889	411
18	2208	0.1647	0.8902	440
17	1715	0.1557	0.8903	472

Oxygen Partial Pressure, kPa	Residence Time, Seconds	Max. FBR Butadiene Yield	Max. FBR:IMR Butadiene Yield	% Increase in FBR:IMR Butadiene Yield over FBR Yield
16	2233	0.1466	0.8916	508
15	1700	0.1376	0.8916	548
14	2212	0.1285	0.8928	595
13	1659	0.1194	0.8926	647
12	2165	0.1103	0.8937	710
11	1599	0.1013	0.8933	782
10	2098	0.0922	0.8945	870
9	1536	0.0831	0.8940	976
8	2041	0.0740	0.8950	1110
7	1497	0.0649	0.8944	1279
6	2041	0.0557	0.8955	1508
5	1525	0.0465	0.8948	1823
4	2204	0.0373	0.8960	2301
3	1773	0.0281	0.8956	3090
2	1564	0.0188	0.8953	4668
1	1793	0.0094	0.8957	9407
0.75	2449	0.0071	0.8965	12575
0.50	1898	0.0047	0.8959	18881
0.25	1940	0.0024	0.8959	37828

Table 8.6. Maximum yields of butadiene from a FBR and an IMR in series as functions of oxygen partial pressures

In Table 8.6, the oxygen partial pressure (kPa) is that to the initial FBR and where it is permitted to wane through the normal ODH process.

A value in the second column connotes the combined residence time (seconds) from the FBR and the IMR that resulted in the maximum yield of butadiene shown in column 4.

The maximum FBR yield of butadiene in column 3 of Table 8.6 is that from a FBR where the initial oxygen partial pressure is that shown in the first column.

In column 4 the maximum FBR:IMR butadiene yield is that from an IMR preceded by a FBR and after the combined residence time shown in column 2.

The last column of Table 8.6 shows the percentage increase in butadiene yield from the FBR:IMR series combination relative to the FBR. The maximum percentage advantage occurs at an oxygen partial pressure of 0.25 kPa.

Conclusions.

At oxygen partial pressures greater than or equal to 44 kPa, a single FBR produces greater yields of butadiene than does an IMR operated under a constant oxygen partial regime. Below 44 kPa, the converse applies.

A single FBR produces greater butadiene concentration maxima than do a series combination of a FBR and an IMR over the range of oxygen partial pressures from 85 kPa to 79 kPa. At oxygen partial pressures from 78 kPa to 0.25 kPa a series combination of a FBR and an IMR results in greater butadiene maxima than either a single FBR or a single IMR.

The maximum yield of butadiene, 0.8959 carbon mass fraction, is obtained when the oxygen partial pressure in the feed to the FBR is 0.25 kPa. This yield of butadiene requires a total residence time of 1 940 seconds.

The relationship between the inlet oxygen partial pressure to the FBR and the product of IMR residence time and constant IMR oxygen partial pressure can be expressed in two-dimensional mass fraction concentration space by a second-order polynomial equation.

The convexification of the single concave region in the FBR profiles for *1*-butene and butadiene did not improve the yield of butadiene either from the single FBR or from the down-stream IMR.

8.3.7 Overall Conclusions.

The geometrical mass concentration profiles for a hydrocarbon reactant and the desired hydrocarbon product affects the series configuration of reactors and the residence time required to maximise yields of product.

Convexifying concave areas and feeding the mixtures to a down-stream reactor failed to produce higher yields of hydrocarbon than could be obtained when the feed was taken from the non-concave sections of the mass concentration profiles.

In all six cases reviewed, for maximising the yield of the desired hydrocarbon, a single FBR was found to be superior to series combinations

of a FBR and an IMR irrespective of the sequencing of the two reactors. This superiority was apparent at the higher end of the oxygen partial pressure spectrum. The following Table 8.7 shows the lower end of the oxygen partial pressure range over which a FBR has an advantage over any series combination of a FBR and an IMR.

Reactor Sequence	**Reaction**	**Lower Limit of Oxygen Partial Pressure Range**
IMR and FBR	*n*-Butane - Butadiene	69 kPa
FBR and IMR	*n*-Butane - Butadiene	85 kPa
IMR and FBR	*n*-Butane - Butenes	47 kPa
FBR and IMR	*n*-Butane - Butenes	57 kPa
IMR and FBR	*1*-Butene - Butadiene	61 kPa
FBR and IMR	*1*-Butene - Butadiene	79 kPa

Table 8.7. Lower limit of oxygen partial pressure range over which a FBR is superior to a FBR and an IMR.

Table 8.7 the lower limit for the range of oxygen partial pressures over which a FBR is superior to any of the reactor sequences shown in Column 1 is presented. In all instances, the upper limit is 85 kPa.

For all cases where a FBR was the initial reactor, a causal relationship between the inlet oxygen partial pressure to the FBR and the product of the IMR constant oxygen partial pressure and the IMR residence time was found. This relationship could be described mathematically by a polynomial equation.

For each of the three reactions studied, a single FBR was found to be superior to a single IMR embodying a constant oxygen partial pressure

policy when the criterion was the maximisation of hydrocarbon product. This predominance exists over a range of oxygen partial pressures, the upper limit being 85 kPa with the lower limit shown in Table 8.8.

Reaction	Lower Limit of Oxygen Partial Pressure Range
n-Butane - Butadiene	50 kPa
n-Butane - Butenes	38 kPa
1-Butene - Butadiene	44 kPa

Table 8.8. Lower limit of oxygen partial pressure range for superiority of a single FBR over a single IMR for maximum yields of hydrocarbon product.

CHAPTER 9
Conclusions of this Thesis

9.1 Yields of Hydrocarbons

The principal objective of this thesis was to use the Attainable Region (AR) concept to obtain an understanding of the factors influencing the yields of butenes and butadiene from the oxidative dehydrogenation (ODH) of *n*-butane. To evaluate and rank any assessment of yields scientifically it was necessary to determine the kinetic limitations of the ODH process, i.e. what the theoretical maximum outputs were. In all instances these theoretical limitations were obtained.

The Attainable Region (AR) concept is used to assist in the design of the process flow sheet for a chemical reaction, specifically to select the items of equipment (reactors) necessary to achieve a particular objective function. In this thesis, the objective function used was the maximisation of product, be it butenes or butadiene commensurate with the smallest residence time.

In this thesis, the reactors investigated were a PFR (FBR) and in an IMR (DSR). For each reactor three scenarios were considered. These were the ODH of *n*-butane to butenes, the ODH of *1*-butene to butadiene and the ODH of *n*-butane to butadiene.

For each of the six cases the conclusions are :

9.1.1 The ODH of *n*-Butane to Butenes in an IMR.

Chapter 3 refers.

A candidate Attainable Region was identified for the system *n*-butane:butenes (Figure 3.13).

The maximum theoretical yield of butenes from the ODH of *n*-butane in an IMR is 0.119 carbon mass fraction (Figure 3.13). The reactor configuration for this yield is a very large IMR operating at a very low constant oxygen partial pressure. The required residence time for this maximum yield is 1.7 x 10^7 seconds (Figure 3.14). The associated selectivity of butane is 0.316.

99.7 % of this theoretical maximum yield of butenes can be obtained from an IMR operating at a constant oxygen partial pressure of 0.25 kPa at a residence time of 75 seconds (Figure 3.15). The butane selectivity is 0.314 (Table 3.2) for this maximum yield of butenes.

For feed concentrations of *n*-butane less than 0.76 carbon mas fraction, an increase in temperature reduces the maximum yield of butenes. A reduction in temperature increases the maximum yield of butenes (Figure 3.16). Over the *n*-butane concentration range of 0.76 to 0.90, both an increase and a decrease in temperature results in slightly lower yields of butenes (Figure 3.17).

9.1.2 The ODH of *n*-Butane to Butenes in a PFR.

Chapter 3 refers.

Over the range of oxygen partial pressures studied, there was insufficient oxygen to complete the ODH process resulting in residual *n*-butane on effective completion of the reaction (Figure 3.3). The effective completion of the reaction occurred at higher concentrations of the *n*-butane feed as the oxygen partial pressure was reduced. Consequently, no candidate Attainable Region emerged from this study that encompassed the full spectrum of reactant and product concentrations.

The maximum yield of butenes from the ODH of *n*-butane in a PFR is 0.119 carbon mass fraction. The reactor configuration for this yield is a PFR operating at an initial oxygen partial pressure of 49 kPa (Figure 3.3). The required residence time for this maximum yield is 16 seconds (Figure 3.4 and Table 3.2). The reduction of the oxygen partial pressure in the PFR below 49 kPa resulted only in the cessation of the oxidation process at yields of butenes less than 0.119.

9.1.3 The ODH of *1*-Butene to Butadiene in an IMR.

Chapter 2 refers.

A candidate Attainable Region was identified for the system *1*-butene:butadiene (Figue 2.10).

The maximum theoretical yield of butadiene from the ODH of *1*-butene in an IMR is 0.899 carbon mass fraction (Figure 2.10). The reactor configuration for this yield is a very large IMR operating at a very low constant oxygen partial pressure. The required residence time for this maximum yield is 2.93 x 10^7 seconds (Figure 2.11). The selectivity of *1*-butene is 0.899 for this maximum yield of butadiene.

A butadiene yield of 0.87, 96 % of the theoretical maximum yield, can be obtained from an IMR operating at a constant oxygen partial pressure of 0.25 kPa at a residence time of 147 seconds (Figure 2.8 and Figure 2.12).

The maximum yield of butadiene increases when the operating temperature is increased from 773K to 823K. Reducing the temperature from 773K to 748K reduces the maximum yield of butadiene (Figure 2.13).

9.1.4 The ODH of *1*-Butene to Butadiene in a PFR.

Chapter 2 refers.

Over the range of oxygen partial pressures studied, there was insufficient oxygen to complete the ODH process resulting in residual *1*-butene on effective completion of the reaction (Figure 2.3). The effective completion of the reaction occurred at higher concentrations of the *1*-butene feed as the oxygen partial pressure was reduced. Consequently, no candidate Attainable

Region emerged from this study that encompassed the full spectrum of reactant and product concentrations.

The maximum yield of butadiene from the ODH of *1*-butene in a PFR is 0.51 carbon mass fraction. The reactor configuration for this yield is a PFR operating at an initial oxygen partial pressure of 65 kPa (Figures 2.2 and 2.3). The required residence time for this maximum yield is 20 seconds (Figure 2.4). The reduction of the oxygen partial pressure in the PFR below 65 kPa resulted only in the cessation of the oxidation process at yields of butadiene less than 0.51.

9.1.5 The ODH of *n*-Butane to Butadiene in an IMR.

Chapter 3 and Chapter 7 refer.

A candidate Attainable Region was identified for the system *n*-butane:butadiene (Figure 3.25).

The maximum theoretical yield of butadiene from the ODH of *n*-butane in an IMR is 0.800 carbon mass fraction (Figure 3.22). The reactor configuration for this yield is a very large IMR operating at a very low constant oxygen partial pressure. The required residence time for this maximum yield is 5.6×10^7 seconds (Figure 3.23). The selectivity of butane is 0.800 for this maximum yield of butadiene.

83 % of this theoretical maximum yield of butadiene can be obtained from an IMR operating at a constant oxygen partial pressure of 0.25 kPa at a

residence time of 322 seconds (Table 3.5). The butane selectivity is 0.694 for this maximum yield of butadiene (Table 7.2).

The maximum yield of butadiene increases when the operating temperature is increased from 773K to 823K. Reducing the temperature from 773K to 748K reduces the maximum yield of butadiene (Figure 3.26).

9.1.6 The ODH of *n*-Butane to Butadiene in a PFR.

Chapter 3 and Chapter 7 refer.

Over the range of oxygen partial pressures studied, there was insufficient oxygen to complete the ODH process resulting in residual *n*-butane and butadiene on effective completion of the reaction (Figure 3.6). The effective completion of the reaction occurred at higher concentrations of the *n*-butane feed as the oxygen partial pressure was reduced. Consequently, no candidate Attainable Region emerged from this study that encompassed the full spectrum of reactant and product concentrations.

The maximum yield of butadiene from the ODH of *n*-butane in a PFR is 0.183 carbon mass fraction. The reactor configuration for this yield is a PFR operating at an initial oxygen partial pressure of 70 kPa (Figure 3.6). The required residence time for this maximum yield is 41 seconds (Figure 3.7). The reduction of the oxygen partial pressure in the PFR below 70 kPa resulted only in the cessation of the oxidation process at yields of butadiene

below 0.183. The selectivity of butane for this maximum yield of butadiene is 0.304 (Table 7.1).

9.2 Graphical Technique for Assessing a Reactor's Characteristics

Chapter 4 refers.

A graphical technique is proposed to illustrate the interplay between the feed concentration, the desired product yield and the residence time in a reactor.

This technique offers a simple yet effective method to assess the effect of any two of the variables, reactant concentration, desired product yield and residence time upon the third and in so doing contributes to a better understanding of the kinetic process underpinning a chemical reaction.

9.3 Maximum Selectivity of a Reactant

Chapter 4 refers.

A graphical technique is proposed to determine the operating characteristics necessary for the maximum selectivity of a reactant.

This extremely simple method permits the determination of the residence time required for the most efficient utilisation of a reactant in a chemical reaction. Efficiency in this context is defined as the maximum yield of product with the minimum consumption of reactant.

9.4 Residence Time Ratio

Chapter 5 refers.

A technique is proposed for assessing at what stage of the ODH of *n*-butane and *1*-butene it would be advantageous to switch from an IMR to a CSTR. The perceived advantage lies in a lesser overall residence time from the two reactors in series than is applicable to a single reactor.

The Levenspiel concept, one based upon the reaction rate expression for a reactant or product, is a tool that has been used for many years to demarcate the interface between a CSTR and a PFR. The Residence Time Ratio (RTR) concept is another technique for the same purpose but one which could justify a series arrangement of a CSTR and a PFR to achieve a combined residence time less than is required from a single reactor. This concept also permits the analysis of reactions more complex than can be evaluated by a Levenspiel plot.

Whereas the RTR concept has been demonstrated only on the oxidative dehydrogenation of *n*-butane, nevertheless it is applicable to any chemical reaction for which reliable kinetic information is available.

9.5 Recursive Convex Control Policy

Chapter 6 refers.

The Recursive Convex Control (RCC) algorithm has confirmed the maximum yields of hydrocarbon products identified in Chapter 2 and in Chapter 3. The reactor configurations identified in these earlier chapters for the maximum yields of hydrocarbon product, namely an IMR with a controlled oxygen partial pressure, was corroborated but with a significant difference. The starting premise in Chapter 2 and in Chapter 3 was an IMR in which the oxygen partial pressure was held at a constant value along the length of the reactor. The RCC algorithm made no such assumption but from the range of possible reactor configurations concluded that an IMR in which the oxygen partial pressure was controlled in accordance with a specified regimen was the preferred reactor choice. (Author's note. The acronym IMR is referred elsewhere as a DSR, a differential side-stream reactor).

The RCC algorithm has been confirmed as a valuable tool for the analysis of complex chemical reactions for which reliable kinetic data are available.

9.6 Practical Application of Reactors

Chapter 7 refers.

For the ODH of *n*-butane to butadiene, the best yield of butadiene, 84 % of the theoretical maximum was obtained from a PFR followed by two IMRs in series (Table 7.11). The constant oxygen partial pressure in the final IMR was 0.005 kPa. The total residence time was 2 760 seconds.

83 % of the theoretical maximum yield of butadiene can be obtained from a single IMR operating at a constant oxygen partial pressure of 0.25 kPa with a required residence time of 322 seconds (Table 7.11).

It is concluded that the marginally higher yield of butadiene from the PFR and two IMRs represents a disproportionate benefit considering the capital costs and excessive residence time and, as a result, a single IMR always is to be advocated for maximising the yield of butadiene.

For the oxidative dehydrogenation of *n*-butane, the best practical reactor configuration to attain maximum yield of product was an IMR operating at a low constant oxygen partial pressure of 0.25 kPa. Lower partial pressures were not considered other than that adopted (0.000001 kPa) to establish the theoretical maximum yields (Table 7.11).

9.7 Two Reactors in Series

Chapter 8 refers.

The shape of the geometrical profile for a hydrocarbon feed stock and the desired hydrocarbon product for both a FBR and an IMR profoundly influences the reactor series configurations and the residence times for maximising yield of product.

A FBR in which the oxygen partial pressure is permitted to wane by the ODH process is found to be superior to any combination of a FBR and an IMR with a constant oxygen partial pressure policy when the objective function is to maximise yields of hydrocarbon product. This superiority extends over a range of decreasing oxygen partial pressures beginning at 85 kPa and applies to all three chemical reactions (Table 8.7).

A single FBR always produces higher yields of hydrocarbon product than does a single IMR with a constant oxygen partial pressure policy. This predominance extends over a range of decreasing oxygen partial pressures beginning at 85 kPa and applies to all three chemical reactions (Table 8.8).

Convexifying the concave regions of the two-dimensional mass concentration sub-space profiles for a hydrocarbon feed stock and the desired hydrocarbon product failed to achieve better yields of product than could be obtained from the non-concave sections of the profile.

In all instances where a FBR was the initial reactor, a mathematical relationship, expressed as a polynomial equation, exists between the initial oxygen partial pressure to the FBR and the product of the inlet (and constant) partial pressure to the down stream IMR and the residence time in that IMR to attain the maximum yield of hydrocarbon product.

CHAPTER 10

Recommendations for Future Research

10.1 Relevance of Kinetic Expressions

Dixon (1999) commented that that for a reactor where a reactant is added to the stream of reactants and products the apparently-favourable kinetics quoted in the literature might well be unfavourable at the lower partial pressures of the added reactant that seem necessary for the maximisation of the desired product. The reactor configurations studied in this thesis, with the exception of a plug flow reactor, all belong to this category.

It is recommended that the relevance of the kinetic expressions used in this thesis, specifically those reported by Téllez (1999a and 1999b) and Assabumrungrat (2002) and shown in Table 1.7 and Table 1.8, be examined for their relevance at low values of oxygen partial pressure.

10.2 Ratio of Butene Isomers

Several authors {Frey and Huppke (1933), Chaar *et al*. (1987), Soler *et al*. (1999),} reported upon the relative ratios of *1*-butene, trans-*2*-butene and cis-*2*-butene formed by the oxidative dehydrogenation of *n*-butane.

It is recommended that the data reported in this thesis be examined for agreement with these earlier results.

10.3 The Residence Time Ratio and the Levenspiel Concept

The Levenspiel (1972) concept is used to identify the interface between a plug flow reactor (PFR) and a continually-stirred tank reactor (CSTR) and assumes that the stoichiometric ratio between the residual reactants at the exit from a CSTR is the same as that in the feed. It does not cater for a reaction where this ratio is not constant and where multiple parallel and complex reactions occur. The Levenspiel concept, in identifying separate reactor residence times for a PFR and a CSTR does not address the issue of minimising the overall residence time by a different reactor configuration, i.e. a possible series combination of a PFR and a CSTR.

It is the belief of this author that the Residence Time Ratio (RTR) concept presented in this thesis overcomes these apparent deficiencies in the Levenspiel concept. It is recommended that this supposition by this author be investigated.

10.4 Application of the Residence Time Ratio to Other Chemical Reactions

The Residence Time Ratio (RTR) concept presented in this thesis was developed by studying the ODH of *1*-butene to butadiene. Its development was facilitated by access to reliable and comprehensive kinetic data for this reaction.

Because of the potential usefulness of this concept, it is recommended that it be applied to other reactions for which reliable kinetic data are available.

10.5 The Recursive Convex Control Policy

The Recursive Convex Control (RCC) Policy was used in this thesis to confirm the results for the ODH of *n*-butane derived from the application of a more constrained scenario in as much as the initial reactor configuration had been assumed, the RCC policy not being subject to such limitations. The RCC policy has been used to derive candidate attainable regions and flow sheets for the synthesis of ammonia and methanol to the water-gas shift reaction {Seodigeng (2006, 2007)}.

It is recommended that the RCC policy be applied to the study of other chemical reactions of industrial significance.

10.6 Graphical Technique for assessing a Reactor's Characteristics

The graphical techniques described in Chapter 4 of this thesis presented in an easily understood two-dimensional format the interplay between feed concentration, yield of product and residence time for a chemical reaction.

It is recommended that this graphical technique .by used to study other chemical reactions of industrial significance, in particular, the synthesis of ammonia and methanol and the water-gas shift reaction.

REFERENCES

Abraham, T.K., Feinberg, M., (2004), Kinetic bounds on attainability in the reactor synthesis problem, *Industrial and Engineering Chemistry Research*, vol. 43, pp. 449-457.

Alfonso, M.J., Menéndez, M., Santamaría, J., (2002), *Chemical Engineering Journal*, vol. 90, pp. 131-138.

Assabumrungrat, S., Rienchalanusarn, T., Praserthdam, P., and Goto, S., (2002), Theoretical study of the application of porous membrane reactor to oxidative dehydrogenation of *n*-butane, *Chemical Engineering Journal*, vol. 85, pp. 69-79.

Burri, J. F., Wilson, S. D., Manousiouthakis, V. I., (2000), Infinite Dimensional State-space approach to reactor network synthesis: application to attainable region construction, *Computers and Chemical Engineering*, **26**, no. 6, pp. 849 – 862.

Cavini, F., Trifirò, F., (1997), Some aspects that affect the selective oxidation of paraffins, *Catalysis Today*, vol 36, pp. 431-439.

Chaar, M.A., Patel, D., Kung, M.C., Kung, H.H., (1987), Selective oxidative dehydrogenation of butane over V/MgO catalysts, *Journal of Catalysis*, vol. 105, pp. 483-498.

Chambers (1966), *Chambers's Twentieth Century Dictionary*, Edited by William Geddie, W. & R. Chambers, Edinburgh and London

Cortés, I., Rubio, O., Herguido, J., Menéndez, M., (2004), Kinetics under dynamic conditions of the oxidative dehydrogenation of butane with doped V/MgO, *Catalysis Today,* vol. 91-92, pp. 281-284.

Dejoz, A., LópezNieto, J.M., Melo, F., Vázquez, I., (1997), Kinetic study of the oxidation of *n*-butane on vanadium oxide supported on Al/Mg mixed oxide, *Industrial and Engineering Chemistry Research*, vol. 36, pp. 2558-2596.

Dixon, A.G., (1999), Innovations in Catalytic Inorganic Membrane Reactors, *Catalysis, vol. 14, The Royal Society of Chemistry,* pp. 40-92

Feinberg, M., (1999), Recent results in optimal reactor synthesis via attainable region theory, *Chemical Engineering Science*, vol. 54, pp. 2535-2543.

Feinberg, M., (2000a), Optimal reactor design from a geometric viewpoint II: Critical side-stream reactors, *Chemical Engineering Science*, **55**, pp. 2455 – 2479.

Feinberg, M., (2000b), Optimal reactor design from a geometric viewpoint III: Critical CFSTRs, *Chemical Engineering Science*, **55**, pp. 3553 – 3565.

Feinberg, M., and Hildebrandt, D., (1997), Optimal reactor design from a geometric viewpoint – I. Universal properties of the attainable region, *Chemical Engineering Science*, vol. 52, no. 10, pp. 1637-1665.

Frey, F.E., Huppke, W.F., (1933), Equilibrium dehydrogenation of ethane, propane and the butanes, *Industrial and Engineering Chemistry*, vol. 25, no. 1, pp. 54-59.

Ge, S., Liu, C., Zhang, S., Li, Z., (2003), Effect of carbon dioxide on the reaction performance of oxidative dehydrogenation of *n*-butane over a V/MgO catalyst, *Chemical Engineering Journal*, vol. 94, pp. 121-126.

Ge, S.H., Liu, C.H., Wang, L.J., (2001), Oxidative dehydrogenation of butane using inert membrane reactor with non-uniform permeation pattern, *Chemical Engineering Journal*, vol. 84, pp. 497-502.

Glasser, D., Hildebrandt, D. (1997), Reactor and Process Synthesis, *Computers and Chemical Engineering*, vol 21, Suppl., S775-S783.

Glasser, D., Hildebrandt, D., Crowe, C., (1987), A geometric approach to steady flow reactors: the attainable region and optimisation in concentration space, *American Chemical Society*, pp. 1803-1810.

Godorr, S., Hildebrandt, D., Glasser, D., McGregor, C., (1999), Choosing optimal control policies using the attainable region approach, *Industrial and Engineering Chemistry Research*, vol. 38, no. 3, pp. 639-651.

Happel, J., Blanck, H., Hamill, T.D., (1966), Dehydrogenation of butane and butenes over chrome-alumina catalyst, *Industrial and Engineering Chemistry Fundamentals*, vol. 5, no. 3, pp. 289-294.

Hildebrandt, D., Glasser, D., (1990), The attainable region and optimal reactor structures, *Chemical Engineering Science*, vol. 45, no. 8, pp. 2161-2168.

Hildebrandt, D., Glasser, D., and Crowe, C., (1990), Geometry of the attainable region generated by reaction and mixing: with and without constraints, *Industrial and Engineering Chemistry Research*, vol. 29, no. 49, pp. 49-58.

Horn, F.J.M., (1964), Attainable and non-attainable regions in chemical reaction technique, *Proceedings of the Third European Symposium on Chemical Reaction Engineering*, Amsterdam, The Netherlands, Pergamon Press, Oxford, UK, pp. 293-303.

Hou, K., Hughes, R., Ramos, R., Menéndez, M., Santamaría, J., (2001), Simulation of a membrane reactor for oxidative dehydrogenation of propane, incorporating radial concentration and temperature profiles, *Chemical Engineering Science*, vol. 56, pp. 57-67.

International Network for Environmental Compliance and Enforcement, Washington, DC, USA, Anon, Industrial Processes. Web site www.inece.org/mmcourse/chapt1.pdf.

Itoh, N., Govind, R., (1989), Combined oxidation and dehydrogenation in a palladium membrane reactor, *Industrial and Engineering Chemistry Research*, vol. 28, pp. 1554-1557.

Kauchali, S., Rooney, W.C., Biegler, L.T., Glasser, D., Hildebrandt, D., (2002), Linear programming formulations for attainable region analysis, *Chemical Engineering Science*, **57** (11), pp. 2015-2228.

Kearby, K.K., (1950), Catalytic dehydrogenation of butenes, *Industrial and Engineering Chemistry*, vol. 42, no. 2, pp. 295-300.

Khumalo, N., Glasser, D., Hildebrandt, D., Hausberger, B., (2007), An experimental validation of a specific energy-based approach for comminution, *Chemical Engineering Science*, vol. 62, pp. 2765-2776.

Khumalo, N., Glasser, D., Hildebrandt, D., Hausberger, B., Kauchali, S., (2006), The application of the attainable region analysis to comminution, *Chemical Engineering Science*, vol. 61, pp. 5969-5980.

Kung, H.H., Kung, M.C., (1997), Oxidative dehydrogenation of alkanes over vanadium-magnesium oxides, *Applied Catalysis A:General*, vol. 157, pp. 105-116.

Lemonidou, A.A., Tjatjopoulos, G.J., Vasalos, I.A., (1998), Investigations on the oxidative dehydrogenation of *n*-butane over V/MgO-type catalysts, *Catalysis Today*, vol. 45, pp. 65-71.

Levenspiel, O., (1972), *Chemical Reaction Engineering Second Edition*, Wiley International, Singapore, Chapters 6-7.

Manousiouthakis V. I., Justanieah A. M., Taylor L. A., (2004), The Shrink-Wrap algorithm for the construction of the attainable region: an application of the IDEAS framework, *Computers and Chemical Engineering*, **28**, pp. 1563 – 1575.

McGregor, C., Glasser, D., Hildebrandt, D., (1999), The attainable region and Pontryagin's maximum principle, *Industrial and Engineering Chemistry Research*, vol. 38, no. 3, pp. 652-659.

Milne, D., Glasser, D., Hildebrandt, D., Hausberger, B., (2006a), Graphical Technique for Assessing a Reactor's Characteristics, *Chemical Engineering Progress,* vol. 102, no. 3, pp. 46-51.

Milne, D., Glasser, D., Hildebrandt, D., Hausberger, B., (2006b), Reactor Selection : Plug Flow or Continuously Stirred Tank?, *Chemical Engineering Progress*. vol. 102, no. 4, pp. 34-37.

Milne, D., Glasser, D., Hildebrandt, D., Hausberger, B., (2006c), The Oxidative Dehydrogenation of *n*-Butane in a Fixed Bed Reactor and in an Inert Porous Membrane Reactor - Maximising the Production of Butenes and Butadiene, *Industrial and Engineering Chemistry Research* vol. 45, pp. 2661-2671.

Milne, D., Glasser, D., Hildebrandt, D., Hausberger, B., (2004), Application of the Attainable Region Concept to the Oxidative Dehydrogenation of *1*-Butene in Inert Porous Membrane Reactors, *Industrial and. Engineering Chemistry Research*, vol. 43, pp. 1827-1831 with corrections subsequently published in *Industrial and Engineering Chemistry Research*, vol. 43, p. 7208.

Milne, D., Seodigeng, T., Glasser, D., Hildebrandt, D., Hausberger, B., (2008), The Application of the Recursive Convex Control (RCC) policy to the Oxidative Dehydrogenation of *n*-Butane and *1*-Butene, *Industrial and Engineering Chemistry Research,* (submitted for publication).

Nicol, W., Hernier, M., Hildebrandt, D., Glasser, D., (2001), The attainable region and process synthesis: reaction systems with external cooling and heating. The effect of relative cost of reactor volume to heat exchange area on the optimum process layout, *Chemical Engineering Science*, vol. 56, pp. 173-191.

Nisoli, A., Malone, M.F., Doherty, M.F., (1997), Attainable regions for reaction with separation, *American Institute of Chemical Engineers Journal*, vol. 43, no. 2, pp. 374-387.

Omtveit, T., Tanskanen, J., Lien, K.M., (1994), Graphical targeting procedures for reactor systems, *Computers in Chemical Engineering*, vol. 18, Suppl., pp. S113-S118.

Oyama, S.T., Middlebrook, A.M., Somorjai, G.A., (1990), Kinetics of ethane oxidation on vanadium oxide, *Journal of Physical Chemistry*, vol. 94, no. 12, pp. 5029-5033.

Pedernera, M., Alfonso, M.J., Menéndez, M., Santamaría, J., (2002), Simulation of a catalytic membrane reactor for the oxidative dehydrogenation of butane, *Chemical Engineering Science*, vol. 57, pp. 2531-2544.

Reid, R., Prausnitz, J., Poling, B., (1987), The properties of gases and liquids, fourth edition, McGraw-Hill, New York.

Rezac, M.E., Koros, W.J., Miller, S.J., (1994), Membrane-assisted dehydrogenation of *n*-butane. Influence of membrane properties on system performance, *Journal of Membrane Science*, vol. 93, pp. 193-201

Rezac, M.E., Koros, W.J., Miller, S.J., (1995), Membrane-assisted dehydrogenation of *n*-butane, *Industrial and Engineering Chemistry Research*, vol. 34, pp. 862-868.

Rooney, W.C., Hausberger, B.P., Biegler, L.T., Glasser, D., (2000), Convex attainable region projections for reactor network synthesis, *Computers and Chemical Engineering*, **24**, no. 2-7, pp. 225 – 229.

Rubio, O., Herguido, J., Menéndez, M., (2003), Oxidative dehydrogenation of *n*-butane on V/MgO catalysts – kinetic study in anaerobic conditions, *Chemical Engineering Science*, vol. 58, pp. 4619-4627.

Rubio, O., Mallada, R., Herguido, J., Menéndez, M., (2002), Experimental study on the oxidation of butane to maleic anhydride in a two-zone fluidised bed reactor, *Industrial and Engineering Chemistry Research*, vol. 41, pp. 5181-5186.

Seodigeng, T.G., (2006), Numerical Formulations for Attainable Region Analysis, Ph.D. thesis, University of the Witwatersrand, Johannesburg, South Africa.

Seodigeng T., Hausberger B., Hildebrandt D., Glasser D., (2007), Recursive constant control policy algorithm for attainable region analysis, *Computers and Chemical Engineering,* (submitted for publication).

Smith, R., (2005), Chemical Process Design and Integration, John Wiley and Sons Ltd., Table 3, p. 100.

Smith, R.L., Malone, M.F., (1997), Attainable regions for polymerisation reaction systems, *Industrial and Engineering Chemistry Research*, vol. 36, no. 4, pp. 1076-1084.

Soler, J., LópezNieto, J.M., Herguido, J., Menéndez, M., Santamaría, J., (1998), Oxidative dehydrogenation of *n*-butane on V/MgO catalysts. Influence of the type of contactor, *Catalysis Letters*, vol. 50, pp. 25-30

Soler, J., LópezNieto, J.M., Herguido, J., Menéndez, M., Santamaría, J., (1999), Oxidative dehydrogenation of *n*-butane in a two-zone fluidised-bed reactor, *Industrial and Engineering Chemistry Research*, vol. 38, pp. 90-97.

Soler, J., Téllez, C., Herguido, M., Menéndez, M., Santamaría, J., (2001), Modelling of a two-zone fluidised-bed reactor for the oxidative dehydrogenation of *n*-butane, *Powder Technology*, vol. 120, pp. 88-96.

Téllez, C., Abon, A., Dalmon, J.A., Mirodatos, C., Santamaría, J., (2000), Oxidative dehydrogenation of butane over V/MgO catalysts, *Journal of Catalysis*, vol. 195, pp. 113-124.

Téllez, C., Menéndez, M., Santamaría, J., (1997), Oxidative dehydrogenation of butane using membrane reactors, *American Institute of Chemical Engineers Journal*, vol. 43, no. 3, pp. 777-784.

Téllez, C., Menéndez, M., Santamaría, J., (1999a), Kinetic study of the oxidative dehydrogenation of butane on V/MgO catalysts, *Journal of Catalysis*, vol. 183, pp. 210-221.

Téllez, C., Menéndez, M., Santamaría, J., (1999b), Simulation of an inert membrane reactor for the oxidative dehydrogenation of butane, *Chemical Engineering Science*, vol. 54, pp. 2917-2925.

Videl-Michel, R., Hohn, K.L., (2004), Effect of crystal size on the oxidative dehydrogenation of butane on V/MgO catalysts, *Journal of Catalysis*, vol. 221, pp. 127-136.

Zhao, W., Zhao, C., Zhang, Z., Han, F., (2002), Strategy of an attainable region partition for reactor network synthesis, *Industrial and Engineering Chemistry Research*, vol. 41, pp. 190-195.

Zhou Wen, Manousiouthakis Vasilios I., (2006), Non-ideal reactor network synthesis through IDEAS: Attainable region construction, *Chemical Engineering Science*, **61**, pp. 6936-6945.

Zhou Wen, Manousiouthakis, Vasilios I., (2008), On dimensionality of Attainable Region Construction for Isothermal Reactor Networks, *Computers and Chemical Engineering,* vol. 32, 3, pp. 439-450.

Zhou, W. Manousiouthakis, V.I. (2007) Variable density fluid reactor network synthesis – construction of the attainable region through the IDEAS approach, *Chemical Engineering Journal*, vol. 129, pp. 91-103.

PUBLICATIONS

Milne, D., Glasser, D., Hildebrandt, D., Hausberger, B., (2004), Application of the Attainable Region Concept to the Oxidative Dehydrogenation of *1*-Butene in Inert Porous Membrane Reactors, *Industrial and. Engineering Chemistry Research*, vol. 43, pp. 1827-1831.

Milne, D., Glasser, D., Hildebrandt, D., Hausberger, B., (2006a), Graphical Technique for Assessing a Reactor's Characteristics, *Chemical Engineering Progress,* vol. 102, no. 3, pp. 46-51.

Milne, D., Glasser, D., Hildebrandt, D., Hausberger, B., (2006b), Reactor Selection : Plug Flow or Continuously Stirred Tank?, *Chemical Engineering Progress*. vol. 102, no. 4, pp. 34-37.

Milne, D., Glasser, D., Hildebrandt, D., Hausberger, B., (2006c), The Oxidative Dehydrogenation of *n*-Butane in a Fixed Bed Reactor and in an Inert Porous Membrane Reactor - Maximising the Production of Butenes and Butadiene, *Industrial and Engineering Chemistry Research* vol. 45, pp. 2661-2671.

Milne, D., Seodigeng, T., Glasser, D., Hildebrandt, D., Hausberger, B., (2008), The Application of the Recursive Convex Control (RCC) policy to the Oxidative Dehydrogenation of *n*-Butane and *1*-Butene, *Industrial and Engineering Chemistry Research,* (submitted for publication).